Development of Colloids for Cell and Tissue Targeting

Bisphosphonate-Functionalized Gold Nanoparticles for the Investigation of Bone Targeting

Dissertation to obtain the Degree of Doctor of Natural Sciences

(Dr. rer. nat.)

from the Faculty of Chemistry and Pharmacy

University of Regensburg

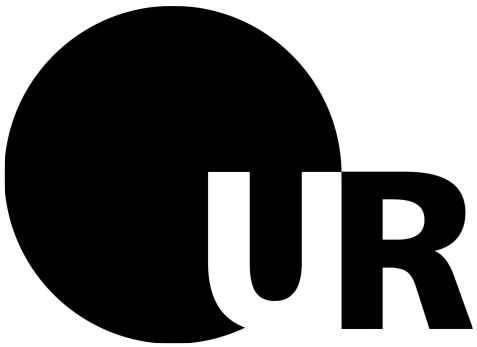

Presented by

Gamal Zayed

from Bany-Ady, Assiut, Egypt

February 2009

To

my Family,

my Wife and

my Children

This work was carried out from December 2004 until February 2009 at the Department of Pharmaceutical Technology of the University of Regensburg.

The thesis was prepared under the supervision of Prof. Dr. Achim Göpferich.

Submission of the PhD application:	23.01.2009	
Date of examination:	13.02.2009	
Examination board:	Chairman:	Prof. Dr. S. Elz
	1. Expert:	Prof. Dr. A. Göpferich
	2. Expert:	Prof. Dr. J. Heilmann
	3. Examiner:	Prof. Dr. F.-M. Matysik

Table of Contents

Chapter 1

Introduction and Goals of the Thesis

Gamal Zayed[1], Jörg Teßamr[1], Achim Göpferich[1]

[1]Department of Pharmaceutical Technology, University of Regensburg,

93040 Regensburg, Germany

1. Targeted Drug Delivery

The pharmacological response of an organism or tissue to an applied drug substance is, in general, directly linked to the drug concentration at the site where it is supposed to act. Due to this fact, many of the active ingredients in currently available medicines and drug therapies are not as efficient in vivo as they have already proven to be in cell cultures. Specifically, in many cases, the applied substances are not available in the optimum concentration and can therefore not exhibit the desirable effect [1]. Still, the majority of today's applied drugs are delivered systematically, which leads to them being evenly distributed throughout the body. Their specific mode of action is mediated by localized receptor distributions or by certain physicochemical parameters of the target, which lead to an accumulation at the target site. This conventional method of drug delivery, however, results often in non-optimal drug efficacy and can often be associated with negative side effects, resulting from the use of large doses of the active ingredients that must be used. Moreover, there is drug resistance at the target originating from cellular drug elimination that further reduces the concentration of the active substances at the site of action. Finally, many current drugs have very poor water solubility or low bioavailability, making them very difficult to apply, especially if they are very rapidly cleared from the body by reticuloendothelial system due to their particulate character.

Because of the difficulties associated with current drugs, targeted delivery of drug molecules or small particulate drug carriers to organs or certain tissue sites, an idea initiated by Paul Ehrlichs's magic bullet concept, represents one of the most challenging research areas in pharmaceutical sciences today. For all drug therapies, the most important goal is to get the drugs exactly where they are needed in the body without affecting other tissues. Targeted drug delivery can be defined as the attempt to deliver drugs to a specific target site in the body where they have greatest pharmacological effects, and additionally, to not allow them to diffuse to other sites where they may cause damage or trigger side effects.

In principle, successful drug targeting can be achieved by specific physical, biological or molecular interactions, which result in the accumulation of the pharmacologically active agents at the relevant sites of action. Based on the chosen mechanism of interaction two kinds of targeted drug delivery exist. The first kind is passively targeted drug delivery, which is mainly based on the physical characteristics of the diseased target tissue, such as the enhanced permeability and retention of tumor tissues with leaky blood vessels and imperfect lymph drainage (EPR-effect). Additionally, local properties, such as the pH or the presence of certain enzymes or the activity of bacteria can be used to achieve passive targeting to a certain site.

The second type of accumulation is mediated via active mechanisms of targeting, which rely on the expression of certain disease specific markers including certain antigens or receptors, which can be targeted using corresponding antibodies or ligands. The different types of drug targeting principles that can be found in literature are summarized in Scheme 1 [2-8].

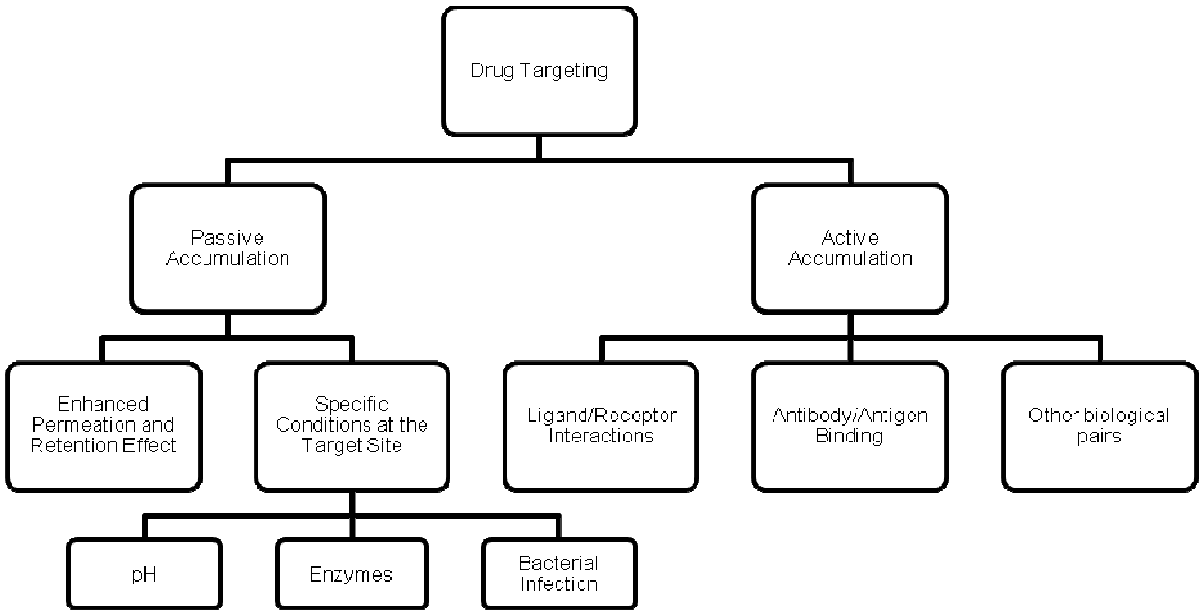

Scheme 1: Schematic representation of different types of drug targeting

Successful drug targeting to specific tissues, however, is a very complicated process. It demands the control over various distribution and absorption processes as well as drug metabolism and disposition. Therefore, a number of important parameters have to be considered for the design of each drug targeting system. These include the nature of biological and cellular membranes of the target tissues, distribution and presence of specific receptors, as well as the activity of enzymes responsible for the subsequent drug metabolism and also the local blood flow, which is responsible for the transport to and from the target tissue.

2. Nanoparticles as Targeted Drug Delivery System

For drug targeting approaches, particulate delivery systems of different sizes can be used as transport vehicles without affecting the activity of the drug ingredient by chemical modification. Due to limitations of tissue permeation and the necessary transport in the blood stream, particles for drug delivery systems must be nanometer sized and highly biocompatible with blood components and tissues in order to obtain long blood circulation times in the patient without immunological reactions.

The nanoparticles (NPs) used for drug delivery applications are part of a rapidly developing field within material science. This field is nanotechnology, and it has many potential applications in clinical medicine and research. Due to their unique size- dependent optical and physicochemical properties, which include the specific absorption of electromagnetic waves, nanoparticles offer unique potential for the development of both therapeutic and diagnostic tools based on the absorption and emission of light [9].

Furthermore, nanoparticles used for the purpose of drug delivery can be designed in a variety of different systems such as micellar solutions, liquid filled vesicles or liquid crystal dispersions as well as solid polymeric or metallic nanoparticle dispersions [10]. Further modifications of these drug carriers with ligands or other targeting molecules, specific for the intended site of action, allow the design of personalized medicines, which reduce the side effects of the drug while maximizing the therapeutic effects. Such local action is mainly achieved with very small nanoparticles, which sufficiently penetrate across barriers through small capillaries and finally into individual cells [11].

Based on their aforementioned properties, there are several important technological advantages of nanoparticles, which make them suitable for application as drug carriers:

1) *Small particle size*; Nanoparticles less than 100 nm are in a similar size-range as biological materials like viruses, DNA and proteins.

2) *Inert surface modification*; The surface of nanoparticles can be decorated with various molecules in order to avoid being recognized by the immune system enabling them to reach their target more efficiently.

3) *Targeted surface modification*; The surface can be easily manipulated to achieve both active and passive targeting by attaching suitable targeting ligands.

4) *High carrier capacity*; Drug molecules can be adsorbed, dissolved or dispersed in the particle matrix.

5) *Flexible loading*; Based on the nanoparticle matrix material both hydrophilic and hydrophobic drug substances can be delivered.

6) *Flexible route of administration*; Nanoparticles can be used for various routes of administration including oral, pulmonary, parenteral, intraocular, for mention just a few [12-15].

Several types of nanoparticles have been extensively studied as vehicles to target drug molecules to specific sites with optimal drug release profiles. Such nanoparticulate delivery systems can be used to treat cancer and a wide range of other diseases [9,16,17]. Some of the most important therapeutic applications of nanoparticles that are currently in use are described below.

2.1. Therapeutic Applications of Nanoparticles

2.1.1. Cancer Therapy

Nanotechnological approaches promise broad applicability for therapies against cancer, which include molecular imaging of tumor cells, molecular diagnosis as well as targeted drug therapy. Moreover, continuous developments in nanotechnology hold the promise of more personalized oncology, in which identified genetic or protein biomarkers of one patient can be used to diagnose and treat cancer based on the molecular profile of the individual patient [18].

For an effective anticancer treatment, applied nanoparticulate drug delivery systems should first be able to reach the desired tumor tissues through penetration of biological barriers, which are naturally present in the body as well as those barriers developed during tumor growth and progression. This transport should be achieved with a minimal loss of number and activity in the blood circulation. Second, after reaching the respective tumor tissues, the released drugs should have the ability to selectively kill the tumor cells without affecting normal cells around the tumor. Fulfillment of these two basic requisites is associated with significant improvement of patient survival and quality of life because local concentration of drugs is increased and dose-limiting toxicity of drugs is reduced. Overall, successful achievement of these requisites shows that targeted nanoparticles seem to have high potential to satisfy all the requirements for effective drug carrier systems against cancer [19-23].

In today’s cancer therapy, the occurrence of drug resistance is a major obstacle for the successful treatment of tumors. Poly(alkyl cyanoacrylate) nanoparticles have been found to provide a useful alternative at a cellular level to overcome multidrug resistance mediated by P-glycoprotein by increasing the intracellular concentration of the drug [24]. Similarly, methotrexate conjugated to gold nanoparticles is more effective in the treatment of lung

cancer than methotrexate alone. This finding can be attributed to the increased drug concentration due to the accumulation of gold nanoparticles carrying methotrexate inside the tumor cells [23]. More interestingly, multifunctional nanotherapeutic systems based on gold nanoparticles have been developed to target solid tumor carrying multiple therapeutic agents in order to increase the overall efficacy and also to overcome the limitations of using a single drug [22,25].

Alternative therapeutic approaches, like photodynamic cancer therapy, are based on the destruction of cancer cells by laser generated atomic oxygen without the use of cytotoxic substances. For these applications, a large amount of photosensitizer is required to generate enough atomic oxygen, and this is mainly achieved by targeted accumulation in cancer cells. This leads to only the targeted cancer cells being killed when the tumor area is exposed to the laser radiation. Unfortunately, remaining photosensitizer later migrates to the skin and eyes and renders patients sensitive to daylight exposure. To avoid these side effects, photosensitizers have been enclosed inside porous nanoparticles, which trap the dye and limited diffusion to other parts of the body. At the same time, the oxygen generating ability of the photosensitizers and therefore therapeutic efficiency is not affected [26].

2.1.2. Treatment of Respiratory Diseases

Other therapeutic approaches using nanoparticles make use of the pulmonary route of administration, which is of increasing interest for the development of new medicines, not only for the treatment of lung diseases (e.g. asthma and chronic obstructive pulmonary disease), but also for a fast and efficient delivery of drugs into the systemic blood circulation avoiding parenteral application. The advantages of direct delivery to the lungs for treatment of respiratory diseases include the potential to reduce systemic toxicity and to achieve higher drug concentrations at the site of action. Additionally first-pass metabolism can be avoided, which mainly occurs after conventional oral administration [27,28]. Theophylline is a drug that reduces the inflammatory effect of allergic asthma, but it is difficult to administer it in appropriate dosage without causing systemic side effects. It was found that, intranasal inhalation of theophylline complexed with thiolated chitosan nanoparticles augmented the anti-inflammatory effect of the drug in relation to theophylline administered alone in a mouse model of allergic asthma. The beneficial effects of theophylline in treating asthma may be enhanced through the use of this novel drug delivery system by increasing the local concentration or by a slower release rate in the lung after nasal inhalation of nanoparticles containing theophylline [29]. It has also been reported that, the encapsulation of three

antitubercular drugs, isoniazid, rifampicin and pyrazinamide in alginate nanoparticles administered by inhalation resulted in an increase in the relative bioavailability and therapeutic efficacy of these drugs when compared with oral administration of the same free drugs, This was attributed to increased local concentration of drugs at the main site of action [30].

2.1.3. Treatment of Cardiovascular Diseases

One of the most recent therapeutic applications of nanoparticles is their use for the local delivery of active substances for the treatment of cardiovascular disorders. Targeted perfluorocarbon nanoparticles have been applied in animal models for the treatment of various cardiovascular disorders such as ruptured plaque, atherosclerotic plaque or the delivery of antirestenotic therapy following balloon angioplasty. Nanoscaled particles can be synthetically designed to potentially intervene in the lipoprotein matrix retention and lipoprotein uptake in cells, a process central to atherosclerosis. Nanoengineered systems molecules called nanolipoblockers can be used to attack the atherosclerotic plaque due to raised local levels of low density lipoproteins [31]. Nanotechnology here may facilitate the repair and replacement of blood vessels, myocardium and myocardial valves. It may also be used to stimulate regenerative processes, such as therapeutic angiogenesis for the treatment of ischemic heart disease [15].

2.1.4. Treatment of Neurological Disorders

The potential benefits of nanoparticles for the treatment of both peripheral and CNS disorders are tremendous and may also offer both the patient and clinician novel therapeutic choices. The central nervous system (CNS), including the brain, has attracted a lot of research attention due to the multitude of diseases linked to disorders of signal transport and degeneration, such as Alzheimer’s or Parkinson’s disease. Most of the therapies are limited due to difficulties in overcoming the blood-brain barrier (BBB). The use of nanoparticles to deliver drugs to the brain across the BBB may provide significant advantages over current strategies, since particles can be used to mask the transport limiting properties of the drug substances to protect drugs from chemical or enzymatic degradation in the blood stream and also to provide the opportunity for a sustained release, which can additionally reduce the peripheral toxicity of the free drug substances. It has been reported that nanoparticles coated with polysorbate 80 have the ability to penetrate the BBB and deliver drugs of various chemical structures (including peptides, hydrophilic and lipophilic compounds) to the brain

[32,33]. When a suspension of polysorbate-coated nanoparticles is introduced into blood, apolipoproteins of the plasma adsorb on the particle surfaces, which then interact with receptors of low-density lipoproteins in the endothelial cells of cerebral blood vessels and subsequently stimulate the endocytosis of the particles [34,35]. Drugs that have been successfully transported to the brain using this delivery system include loperamide [36], dalagrin (a short peptide, Leu enkephalin analogue), kyotorphin [37], nerve growth factor [38], tubocurarine [39] and doxorubicin [40].

Other therapeutic approaches with nanoparticles utilize free radical mediated damages, which is known to play a major role in ischemic and degenerative disorders of the CNS. For example, water soluble derivatives of buckminsterfullerene C60 are used as a unique class of nanoparticles with potent antioxidant properties. Furthermore, it has been reported that nanoparticles composed of cerium oxide or yttrium oxide protect nerve cells from oxidative stress and their observed neuroprotection is also independent of particle size. The ceria and yttria nanoparticles act as direct antioxidants, which limit the amount of reactive oxygen, which is known to kill cells. Consequently, it can be surmised that this group of nanoparticles can modulate many kinds of oxidative stress in biological systems in addition to in the central nervous system [41].

2.1.5. Ocular Drug Delivery

For more accessible organs, like the eye, nanoparticles offer advantages over presently known therapies. Conventional eye drops represent about 90% of all ophthalmic drug formulations, and it is well known that up to 95% of the applied drug is lost through immediate tear drainage. This mechanism is useful for protecting our eyes against the exposure of noxious substances. For these applications, nanocarriers such as nanoparticles, liposomes or high molecular weight dendrimers, can be easily administered as eye droplets. These nanocarriers may provide prolonged residence time due to interactions with the ocular surface after instillation, which enable them to avoid the natural clearance mechanism of the eye. In combination with controlled drug release from these particles, it should be possible to develop ocular formulations that provide local therapeutic concentrations for long periods of time, thereby reducing the dose administered as well as the necessary instillation frequency. For intraocular drug delivery, the same mechanisms can be used to release the drug in a controlled way, reducing the number of intraocular injections required to maintain therapeutically active concentrations [15]. Another potential advantage of these systems is the targeting to specific sites of action, which can lead to a necessary dose decrease and

consequently a decrease of side effects [15]. For all of these applications, the formulation of biodegradable polymers as colloidal systems allows enhanced ocular drug delivery by immobilization of the particles inside and on the eye for long periods of time, while additionally avoiding the need to remove the empty delivery systems from the patient due to the degradation of the polymer carrier.

In recent investigations, chitosan based nanoparticles have been investigated for the delivery of drugs to the ocular mucosa using the immunosuppressive peptide cyclosporine A as a model drug. The expected advantage of these systems in ocular drug delivery is their ability to contact intimately with the corneal and conjunctival surfaces, thereby prolonging and increasing the delivery of the drug substance to external ocular tissues without compromising the inner ocular structures and avoiding systemic drug exposure [42]. Consequently, these nanoparticulate systems show great promise with regard to the circumvention of the present limitations for the treatment of external inflammatory or autoimmune ocular diseases such as keratoconjuctivitis sicca, or dry eye disease. The described local application and immobilization of nanoparticles inside the eye is completely different from the systemic administration of nanoparticles, where the particles are designed to circulate inside the body until reaching the site of action. This extended range of application reflects and confirms the usefulness of nanoparticles as a versatile drug delivery system.

2.1.6. Treatment of Infections

A final example for the application of nanoparticulate delivery systems are colloidal drug carriers, such as liposomes and nanoparticles, which are easily taken up by phagocytic cells and accumulate in the organs of the reticuloendothelial system, which make them useful for the treatment of intracellular infections with antibiotics that would normally not sufficiently access the intracellular sites. Consequently, in vitro and in vivo experiments with drug substances incorporated in liposomes and nanoparticles did demonstrate the increased therapeutic efficacy of substances, such as amphotericin B, dihydrostreptomycin, amikacin and ampicillin, against a number of microorganisms, including *Leishmania donovani, Candida albicans, Staphylococcus aureus, Mycobacterium avium, Listeria monocytogenes*, and *Salmonella typhimurium* [43,44]. Furthermore, polymeric nanoparticles have also been applied to develop an oral delivery system of the otherwise only injectable streptomycin. The results of the biodistribution and activity studies of particle-loaded antibiotic suggested that nano-encapsulation of streptomycin might be useful in the development of an oral dosage

form of streptomycin and perhaps other injectable antibiotics, since encapsulated drugs showed a significant increased bioavailability after oral administration. The enhanced bioavailability is attributed to the intestinal absorption of antibiotic-loaded nanoparticles by the intestinal epithelium and sustained drug release after reaching the systemic circulation [45].

The continuing increase in microbial drug resistance has led to widespread problems in the treatment of conventional bacterial infections. Of particular concern are those illnesses caused by methicillin or multiple resistances *staphylococcus aureus* (MRSA), which are responsible for the majority of all hospital-acquired infections. Clinical complications and nearly 100,000 deaths each year are attributed to these infections in the United States alone. Since penicillin and other β-lactam antibiotics have been the basis in the clinical treatment of bacterial infections, their effectiveness is now significantly compromised in bacteria that produce β-lactamase enzymes, which efficiently hydrolyzes the β-lactam ring to an inactive ring-opened product. An additional incorporation of these antibiotics into nanoparticle matrices may successfully shield them from bacterial penicillinase degradation and render them effective against penicillinase producing bacteria [46,47].

2.2. Imaging and Diagnosis

Nanoparticles targeted to certain structures give us the ability to identify individual cells within organs or find molecular changes within tissues that we otherwise cannot detect through conventional imaging because of these nanoparticles have high sensitivity and photostability, which allow imaging for prolonged periods [48]. Several types of nanoparticles have been specifically designed for diagnostic and imaging purposes: the most frequently used are gold nanoparticles (GNPs), quantum dots (QDs) and magnetic nanoparticles. GNPs are known for their high electron contrast, this is why they are used as markers for all kinds of electron microscopy.

QDs are nanometer sized inorganic fluorophores that are based on different types of semiconductors. They offer significant advantages over conventionally used organic fluorescent markers. They are much brighter than conventional fluorescent dyes and can be tuned by alteration of their size to shine at different emission wavelengths. Due to their high photostability they can be used for much longer observation times in comparison to organic dyes, which are often very sensitive to photobleaching. This increased length of observation time is crucial to study slower cellular process. Fluorescent particles can moreover help to identify new cellular receptors as targets for new drug candidates and a more detailed

understanding of the behavior of these receptors, including their activation or internalization. This understanding can open up new treatment options for nanoparticulate delivery systems [13,49].

Superparamagntic iron oxide nanoparticles (SPIONs), measuring 2-3 nm, have been used in conjunction with magnetic resonance imaging (MRI) to reveal small and otherwise undetectable lymph-node metastases. Ultrasmall SPIONs also enhance MRI contrast for successful imaging of cerebral ischemic lesions. Surface modified dextran-coated iron oxide nanoparticles also enhanced MRI visibility of intracranial tumors for longer time [50].

Early diagnosis of Type I diabetes (insulin-dependent diabetes mellitus, IDDM) is very important for the treatment of this disease. The early and sensitive diagnosis depends on the detection of autoantibodies, which are present before clinical onset. Supramolecular protein nanoparticles have been applied by Lee et al. [51] for ultrasensitive early detection of antibodies of IDDM. The principles of detection depend on the formation of supramolecular protein nanoparticles by the self-assembly of the antigenic protein expressed in bacteria. Each nanoparticle has many binding sites for the specific antibody (the early marker of type I diabetes). After complexation with further nanoparticles that carry polylysine residues suitable for the binding of DNA, the nanoparticles-antibodies complexes are detected by using highly sensitive PCR. Similar supramolecular protein nanoparticles would also be useful in the diagnosis of infectious diseases, such as such as AIDS and hepatitis C during the early phase of infection, when the concentration of antibodies is very low.

Nanoparticles are also attracting considerable interest as contrast agents for other types of medical imaging. Hainfeld et al. [52] showed that, gold nanoparticles are useful X-ray contrast agents that offer novel physical and pharmacokinetic advantages over the currently used agents. They, for example, enable higher contrast and also longer imaging times than the currently standard iodine-based agents.

The overproduction of hydrogen peroxide is linked to many different diseases and there is consequently a great interest in the development of contrast agents that can image hydrogen peroxide production in vivo. It has been demonstrated that nanoparticles formulated from peroxalate ester and fluorescent dye image hydrogen peroxide with specificity and sensitivity. The peroxalate nanoparticles image hydrogen peroxide by undergoing a three-component chemiluminescent reaction between hydrogen peroxide, peroxalate esters and a fluorescent dye. First hydrogen peroxide diffuses into the nanoparticles and reacts with peroxalate ester groups, generating a high energy-dioxetanedione that chemically excites encapsulated fluorescent dyes through the chemically initiated electron-exchange

luminescence mechanism and leads to the chemiluminescence. Peroxalate nanoparticles have great potential for imaging of hydrogen peroxide-associated diseases, given their high specificity and sensitivity and their capability for deep-tissue-imaging [53].

3. Gold Nanoparticles

Among the colloids of metallic and semiconductor origin, gold nanoparticles stand out as one of the most extensively investigated systems. This is mainly due to the fact that colloidal gold has well defined chemical, physical electronic and optical properties with respect to shape and size [54]. Also, gold nanoparticles are of special interest for research due to their potential applications in biomedical, electronic and optical materials [55]. In biomedical applications, gold nanoparticles are used for rapid and sensitive diagnostic assays [56], for radiotherapy and imaging [57,58] and as the basis for drug and gene delivery systems [59-61].

3.1. Advantages of gold nanoparticles

Gold nanoparticles (GNPs) play a special role in nanoscience and nanotechnology due to the following facts;

1. Gold is most stable at the nanoscale [62].
2. GNPs have unique optical properties. GNPs exhibit strong absorption of electromagnetic waves in the visible range due to surface plasmon resonance (SPR). SPR is caused by the oscillation of the conductive electrons on the metal surfaces upon irradiation by electromagnetic waves. The wavelength of the peak absorption here depends on many factors like particle size, dielectric constant of the surrounding media, and the inter-particle distance. Spherical nanoparticles have a single plasmon resonance extinction peak at around 520 nm, which does not shift extensively by change in the size and refractive index of the surrounding medium [63-65].
3. GNPs can be synthesized in different sizes and in different media according to the desired application.
4. GNPs provide a versatile nanoscale platforms that can easily be functionalized with small drug molecules, polymers and biomaterials for many potential applications [66].

3.2. Synthesis of gold nanoparticles

Different methods have been developed and optimized to prepare and subsequently characterize gold nanoparticles. For the preparation of nanoparticles, special precautions must be taken to avoid uncontrolled growth and aggregation, because single particles tend to be unstable in solution. The most frequent synthesis method for gold nanoparticles in aqueous medium is the chemical reduction of gold salts such as ($HAuCl_4$) by tri-sodium citrate. In this method, the citrate salt acts initially as the reducing agent to reduce Au $(III)^{3+}$ ions to Au(0) and later also functions as stabilizing agent by forming a layer of citrate anions on top of the nanoparticle surface. The adsorption of citrate anions on the particle surface charges the particles negatively and induces enough electrostatic repulsion forces between individual particles to keep them separately dispersed in the synthesis medium [67-72]. Particles synthesized by citrate reduction can be obtained as almost monodisperse spheres, the sizes of which are controlled by the initial reagent concentrations and the chosen reaction conditions. The particles in aqueous dispersion are characterized by a deep red color with surface plasmon resonance peak at about 524 nm as shown in Figure 1 [73].

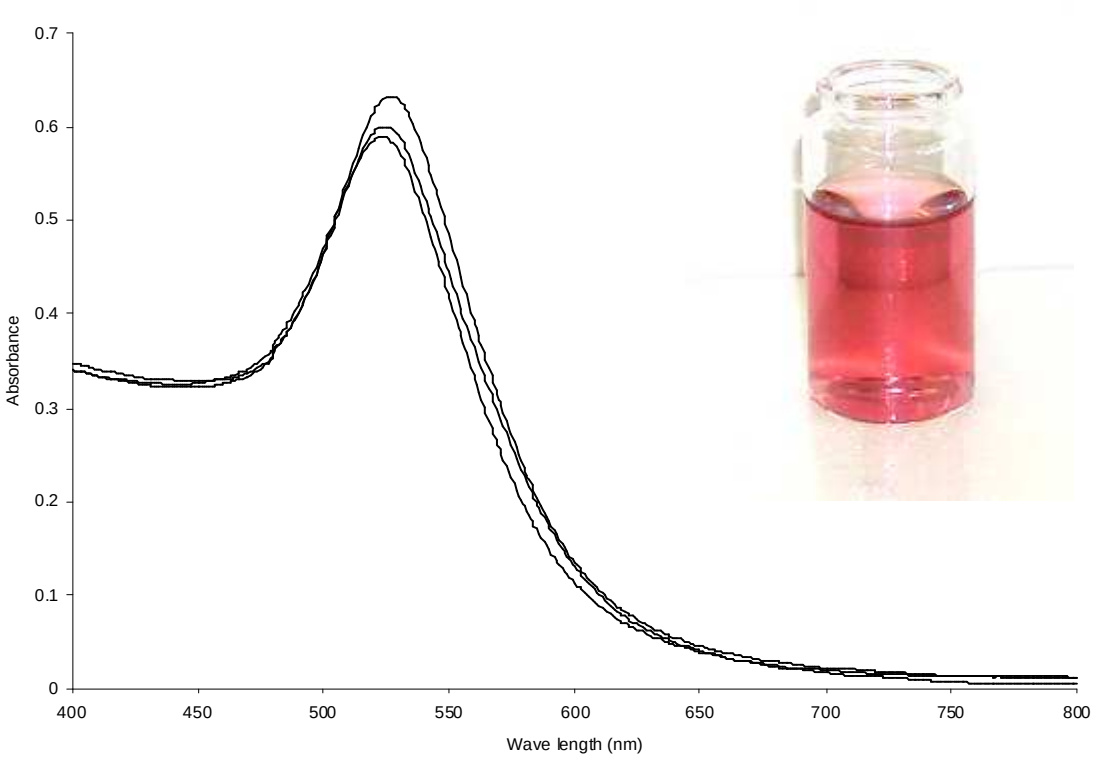

Figure 1: UV-Vis absorption spectra of different gold nanoparticles preparations Insert: Flask with freshly prepared gold nanoparticles

3.3. Stabilization and functionalization of gold nanoparticles

For successful application of GNPs, they must be stabilized in order to maintain their individuality upon the changing of the dispersion medium. For this task, self assembled monolayers (SAMs) of polymers are frequently used as sterically stabilizing agents. SAMs are ordered molecular arrangements that are formed by spontaneous adsorption to a surface with specific affinity of its head group to the underlying substrate [74]. In other words, SAMs are thin monolayers of organic molecules that have end groups that spontaneously and selectively interact with metal or semiconductor substrates [75]. Recently, the synthesis, functionalization and assembly of monolayer-protected gold nanoparticles have been extensively studied, and particles have been designed that are suitable for application in many fields such as discovery of biomarkers [50], molecular imaging and radiotherapy [57,58], and DNA delivery [60]. For all of these particles, thiol groups and disulfides have a very strong tendency to spontaneously react with the gold surfaces, explaining the high popularity of modifying gold surfaces. Such adsorption in general results in the formation of well-organized SAMs due to the strong chemical bond formed between gold and sulfur [76].

For all biomedical applications, the surface functionalization of gold nanoparticles is the essential prerequisite for applying them to cell cultures or allowing selective interactions with organs, tissues, cells or even biomolecules. For many different applications, it has been reported that poly(ethylene glycol) (PEG) surface modification of gold nanoparticles significantly improves their dispersion stability, especially, in the presence of high electrolyte concentrations, which would furthermore lead to the breakdown of the electrostatic repulsion of the citrate coating. Additionally, PEG layers inhibit unspecific protein adsorption to the particle surfaces due to steric repulsion effects of the tethered PEG strands. PEG-modification (PEGylation) of nanoparticles imparts a stealth-shielding of these particles and prevents unspecific opsonins from recognizing the particles, thereby limiting the phagocytosis by the RES cells and increasing the systemic circulation time from minutes to hours or even days [77]. The protective action of PEG is mainly grounded in the formation of a dense, hydrophilic cloud of long flexible polymer chains on the surface of the colloidal particle that reduces the adsorption of opsonins and thus also reduces the hydrophobic interaction with the RES. The tethered or chemically anchored PEG chains protect the surface in different spatial conformations depending on their molecular weights, thus preventing the opsonization of the gold particles, which usually leads to the uptake by macrophages of the RES and causes preferential accumulation in the liver and spleen. Attached PEG is non-toxic, non-immunogenic and approved by the FDA for internal use in humans. Furthermore, it is

included in the list of inactive ingredients for oral and parenteral administration [78-81]. The mechanism of steric hindrance of PEG modified surface coated nanoparticles was proposed by Gref et al. [82]. The water molecules included in the PEG layers form a structured shell through hydrogen bonding with the ether oxygen's of PEG. The tightly bound water then forms a hydrated film around the particles and consequently repels all interactions with proteins and other nanoparticles.

Besides surface bound or conjugated PEG, amphiphilic block co-polymers such as poloxamers and poloxamine, consisting of blocks of hydrophilic PEG and hydrophobic poly(propylene oxide) (PPO) have been applied to impart nanoparticles with stealth-shielding properties. The hydrophobic section of the polymers, which contains the PPO units, can be used to adsorb and anchor the polymer molecules onto the particle surface, while the hydrophilic PEG section can extend into the solution and shield the particle surfaces. This method is simple to achieve and can also impart increased RES avoidance of the particles. Conversely, it has the drawback that surface adsorbed polymers can desorb again, leaving spaces in the surface coating where proteins can subsequently bind. Beyond this, proteins may also be adsorbed to the hydrophobic part of the polymers, and this has detrimental effects on colloid stability [83]. Accordingly, several trials have been done to increase the strength of the polymer attachment to the gold surfaces. Many publications report the utilization of thiol-terminated poly(ethylene glycol) for the preparation of water soluble and stable gold nanoparticles, which is very important for the biologically applied particles [84-89]. Other organosulphur compounds, such as aliphatic or aromatic thiols and disulfides, also form self-assembled monolayers (SAMs) on gold surfaces due to the chemisorptive Au-S bond, which forms very strong links due to the high affinity of thiols for the gold surface [90]. In addition to the stabilization of nanoparticles, functionalization of the second terminal end of thioalkylated poly(ethylene glycol)s with certain functional groups, such as amine groups, provides valuable versatile polymers for the preparation of surface functionalized gold nanoparticles. Therefore, a coating of nanoparticles with such bifunctional polymers produces fairly stable nanoparticles and at the same time provides terminal functionality for the installation of targeting ligands, which can later interact with the specific receptor or target tissue [54].

4. The Need for Bone Tissue Targeting

Many chronic bone diseases, such as osteoporosis and osteoarthritis, are closely associated with the natural aging process and consequently gain more importance in aging societies. Osteoporosis, for example, is a bone debilitating disease that causes nearly 1.3 million bone fractures each year. In addition to the chronic and destructive diseases, bone is also affected by various types of cancers, originating from bone tissue or as metastases from other tissues (90% of patients that died of breast cancer or prostate cancer also have skeletal metastases). Bone cancer and cancer metastases are often associated with significant pain, and their therapy is generally very difficult since the tissue is very difficult to reach with irradiation.

A number of currently known therapeutic agents are beneficial for the treatment of different bone diseases. However, because bone tissue is distributed throughout the body, the systemic drug concentration needs to be maintained at a level such that the drugs exhibit pharmacological activity sufficiently also at the peripheral site. This often causes unfavorable systemic effects, leaving a very narrow therapeutic window for the treatment of bone diseases. The incorporation of osteotropicity to a bone therapeutic agent may, therefore, dramatically alter the pharmacokinetic profile to favor skeletal deposition [91-95].

Apart from the treatment of osteoporosis or cancer, delivery systems for bone targeting could significantly improve other treatment opportunities. Bone targeting could increase the efficacy and reduce toxicity or the side effects of new and already applied drugs by altering their pharmacokinetics and biodistribution by restricting their biological action to the skeletal system [95].

To develop successful drug delivery systems for treatment of bone diseases, a sound rationale based on the bone biology is needed. To this end, an overview on the structure and biological functions of the bone tissue will be presented [95].

5. Structure of Bone Tissue

Bone tissue is a specialized form of connective tissue and is the main element of the skeletal tissues. It is composed of cells and a calcified extracellular matrix, in which stabilizing fibers are embedded. Bone is a rather unique tissue that performs several functions in addition to contributing to body shape and form. It is the major attachment site for tendons and muscles, essential for locomotion and other movements of the body. In some parts of the body, bones also provide the protective structures for vital tissues, such as brain, heart, lung, bladder and pelvis viscera. Bone also serves as the main source and depot for minerals and

corresponding anions, mainly calcium and phosphate, and as such is intimately involved in the mineral homeostasis of the body. In addition, the bone marrow is the place where most of the blood components, such as blood or immune cells, are formed. Finally, there are also mineralized tissues that have very specialized functions, such as for example the bones of the inner ear, which are responsible for the transmission of sound. The actual composition of bone varies strongly with age, anatomical location, and the general health and nutritional state. In general, the bone mineral accounts for about 50-70% of adult bone mass, the organic matrix for about 20-40%, water for about 5-10% and embedded lipids for about 1-5% [95-97].

Bone in human and other mammalian bodies is generally classified into two types. The dense outer shell is termed “cortical bone”, and is also known as compact bone. The inside contains a much finer network of bone, which more resembles a sponge, and is termed spongy or cancellous bone. Cortical bone is much denser with a porosity ranging between 5% and 10% and is found primarily in the shaft of long bones, but it also forms the outer shell around cancellous bone at the end of joints and in the vertebrae as shown in Figure 2 [97,98].

Bone has the ability to repair itself without leaving behind scar tissue. It also rapidly removes and replaces mineral storage based on metabolic demand, and it structurally reshapes in response to alterations in the mechanical stimului (e.g. following fractures or degenerative diseases). Four distinct cell types are responsible for carrying out the local formation, resorption, and maintenance of bone. These are osteoblasts, osteoclasts, osteocytes and the bone lining cells. Osteoblasts are the cells that synthesize the bone matrix and participate in bone mineralization. The functions of osteoblasts are influenced by a number of endocrine and cytokine mediators such as parathyroid hormone, prostaglandins, estrogens, vitamin D and some cytokines. Osteoclasts on the other hand, are multinucleated giant cells mainly responsible for resorption of bone, which also takes place during regular remodelling of the bone tissue. There are numerous factors that play a role in the regulation of osteoclast functions and bone resorption, which include parathyroid hormone (PTH), PTH related peptide, calcitonin, glucocorticoids, vitamin D, prolactin, interleukine-1 (IL-1), interleukine-6 (IL-6), tumor necrosis factor (TNF), prostaglandins, interferon-gamma, and members of the transforming growth factors beta superfamily, including bone morphogenetic proteins and others. Osteocytes are cells, which are buried within mature bone and are formed from osteoblasts that have been entrapped during bone formation. Several important roles are attributed to these cells, one of the most important being the maintenance of mineral homeostasis by permitting the diffusion of fluids and minerals through the cannicular system. Osteocytes may also serve as a mechanical damage sensor responsible for initiating bone

remodelling or repair. Finally, the bone lining cells are formed by inactivation of osteoblasts or perhaps other mesenchymal type cells and they are mainly present on the surfaces of adult bone. The role of bone lining cells includes the partitioning of bone fluid compartment from interstitial fluids, the nutritional and metabolic support of osteocytes, and the initiation of osteoclast mediated resorption of bone [96,97,99-102].

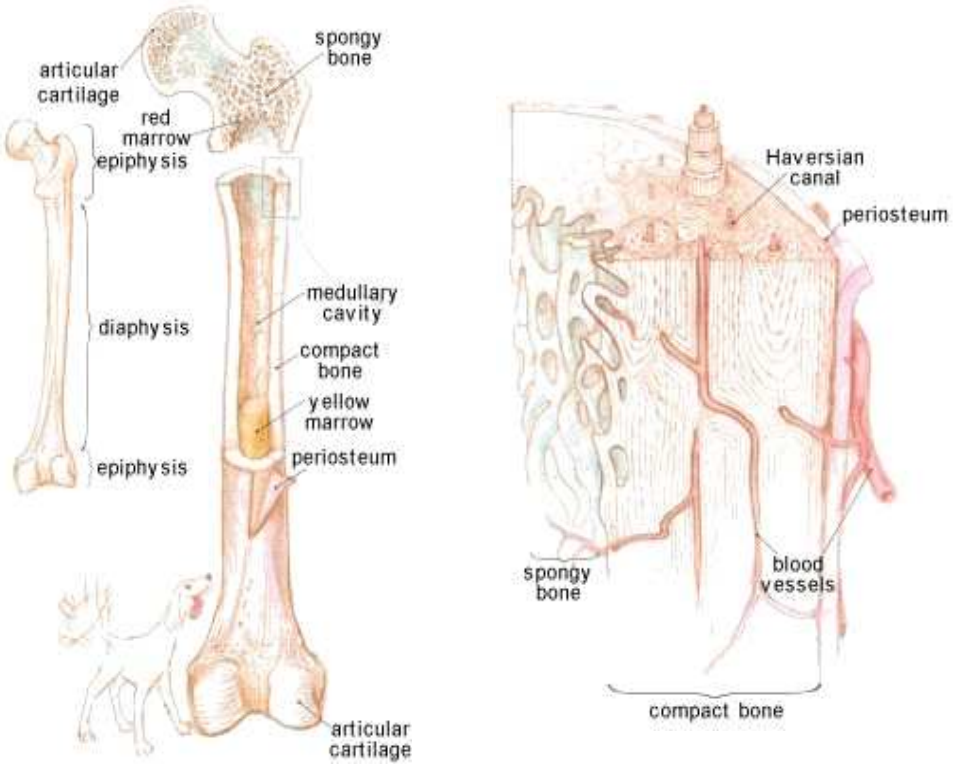

Figure 2: Diagram represents the structure of different types of bone.

Besides the metabolically active cellular portion of bone, it also contains the non-living but very important bone matrix. It is the major constituent of bone and it is a well organized composite material consisting of an organic and an inorganic component [103]. About 90% of the organic matrix of bone is composed of type I collagen, which is synthesized by the osteoblasts and deposited in distinct layers known as lamellae in mature bones. The organic component of the matrix gives the bone its outer shape and contributes to its ability to resist tensional load. Bone also contains a variety of noncollagenous proteins that may be important in the organization of the matrix, the mineralization of the bone, and the behavior of the bone cells. These proteins include osteocalcin, osteonectin, bone sialoprotein, bone phosphoproteins and small proteoglycans. Living bone matrix obviously also contains many

different growth factors that can influence the function of bone cells and thereby regulation the function of this tissue [97,98].

The inorganic matrix, or mineral phase of bone, constitutes about 75% of the bone tissue mass and it is composed principally of calcium ions and phosphate, which are combined to form specific hydroxyapatite crystals of the composition **$[Ca_{10}(PO_4)_6(OH)_2]$**. The hydroxyapatite in bone consists of very small crystals and contains many minute impurities, including carbonate or magnesium. Bone apatite is usually referred to as a "poorly crystalline, carbonate-substituted apatite" because of the impurities in the crystals, which are important in rendering bone apatite more soluble, thus permitting the apatite to release ions when needed for homeostasis or for the remodeling of bone [104]. The inorganic matrix of bone performs two essential functions: it serves as ion reservoir, and it gives bone most of its stiffness and strength. Approximately 99% of the body calcium, approximately 85% of the phosphorous and between 40% and 60% of the total body sodium and magnesium are associated with the bone mineral crystals [97].

6. Ligands for Bone Targeting

The bone's most distinguishing property from the rest of the human body is the presence of bone mineral, hydroxyapatite, which is not present in any other tissue under normal circumstances. A very practical approach for the design of bone targeting systems is to synthesize drugs or drug conjugates that have a very high affinity for hydroxyapatite, which consequently leads to an accumulation in bone after systemic administration. Although, a number of drug targeting systems showed promising improvements of the therapeutic index by increasing efficacy and minimizing adverse side effects, a true bone-specific delivery system still remains to be developed. To attain this goal, there are several molecules and moieties that can be used as selective-bone targeting ligands. Ideally, a bone-targeting moiety should have the following properties: it must possess a strong affinity for hydroxyapatite, the targeting moiety must be chemically modifiable to allow conjugation to the biomaterials used to construct the delivery system, the introduction of bone-targeting ligands must not render the delivery system toxic, and the biological effects of the targeting moiety itself should be minimal, or at least it should not interfere with the biological activity of the payload [95]. Several bone targeting moieties that possess these characteristics are known, and these are now described briefly.

6.1. Bisphosphonates

Bisphosphonates (BPs) are synthetic analogues of the inorganic pyrophosphate (PPi), a naturally occurring polyphosphate present in serum and urine, which can prevent calcification of bone by binding to newly forming crystals of hydroxyapatite [105]. Bisphosphonates consist of two phosphonate groups linked by phosphoether bonds to a central (geminal) carbon atom (Figure 3; P–C–P structure). Unlike the unstable nature of P–O–P bonds, the P–C–P structure is highly resistant to hydrolysis under acidic conditions as well as to cleavage by pyrophosphatases. Two additional covalent bonds to the geminal carbon atom of bisphosphonate can be formed with carbon, oxygen, halogen, sulphur, or nitrogen atoms giving rise to a wide range of possible chemical structures of bisphosphonates [105-108].

The P–C–P structure of bisphosphonates imparts the ability to bind divalent metal ions, such as Ca^{2+}. For this reason, after being administered, bisphosphonates are rapidly cleared from the circulation and localize to the bone surface at sites of active bone remodeling, particularly areas undergoing osteoclastic resorption [109].

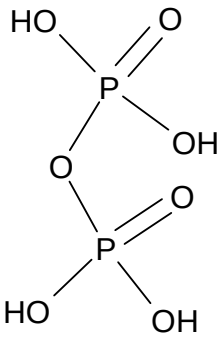

Pyrophosphoric acid

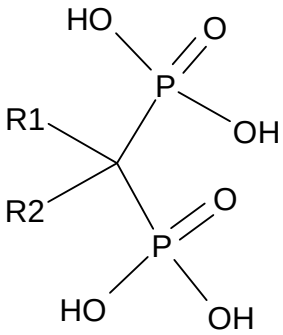

Bisphosphonic acid

Figure 3: The structure of pyrophosphate and bisphosphonate

The ability of bisphosphonates to bind to bone mineral, preventing both crystal growth and dissolution, was enhanced when the R1 side chain was a hydroxyl group rather than a halogen atom. The presence of a hydroxyl group at the R1 position increases the affinity for calcium owing to the ability of the bisphosphonates to chelate calcium ions by tridentate instead of bidentate binding. In addition to antimineralization properties, bisphosphonates are also capable of inhibiting bone resorption in vitro and in vivo. This property requires the P–C–P structure and could not be achieved by the monophosphonate or with P–C–C–P or

P–N–P compounds. Furthermore, the antiresorptive effect seems not to depend on the adsorption of bisphosphonate to bone mineral and the subsequent prevention of hydroxyapatite dissolution, because some bisphosphonate derivatives with less affinity for hydroxyapatite are even more potent antiresorptive agents, despite not being bound to the hydroxyapatite. Bisphosphonates inhibit bone resorption by their cellular effect on osteoclasts, rather than by a purely physicochemical mechanism [105,110-112].

Bisphosphonates are nowadays used for the treatment of patients with various disorders affecting the skeleton including osteoporosis [113], metastatic bone diseases [114-116] and Paget's disease [117]. The pharmacological action of bisphosphonates is mediated through their action on osteoclasts with four different postulated mechanisms: inhibition of osteoclast recruitment, inhibition of osteoclast adhesion, shortening of osteoclast life span (apoptosis) and inhibition of osteoclast activity. However, it also has been shown that bisphosphonates have an inhibitory action also on osteoblasts, macrophages and certain tumor cells [105,118]. Therefore, the major concern for using bisphosphonates as bone-targeting moieties is their possible pharmacological effect on the bone cells. Particle conjugated bisphosphonates may thus still be capable to induce apoptosis in osteoclasts, and if a controlled release mechanism is used, caution must be taken that free bisphosphonate may counteract the activity of intended payload drug. In addition, one should avoid using bisphosphonates as a bone targeting ligand, if an osteoclast-mediated release mechanism of the active material is applied [95].

In order to attempt bone targeting of other molecules than bisphosphonates, suitable conjugates must be developed. The main limitation of this approach is the fact that osseous tissues in contrast to other tissues, have a very low blood flow rate, because they mainly consist of inorganic hydroxyapatite mineral. Since this hydroxyapatite and the calcified tissues are the main targets for accumulation of bisphosphonates and their conjugates, long blood circulation times before the drugs reach their targets must be expected. Successful osteotropic drug-delivery systems based on this bisphosphonic prodrug concept as a novel method for site-specific delivery of other drugs to the osseous tissues have been developed making use of the adsorption of the prodrug to the mineral component of the bone [119]. To prove this concept, Erez et al. [120] demonstrated two chemical options to construct hydrolytically activated chemotherapeutic prodrugs containing the bisphosphonate bone-targeting ligand. The first option is applicable for any drug molecules that possess a hydroxyl group. Here, the drug is attached to the bisphosphonate component through a labile ester linkage. The second option is suitable for drug molecules with amine functional groups. In

this case, a degradable linker is used to attach the drug to bisphosphonate component through a carbonate-labile linkage. This concept was demonstrated using camptothecin (containing hydroxyl group) and tryptophan (a model molecule for drug with amine functionalities). Both prodrugs bound successfully to pure hydroxyapatite, a model substance resembling bone, and were hydrolytically activated under physiological conditions.

Bisphosphonate-coupled radiopharmaceuticals are already widely used in clinics for imaging and pain palliation of the skeleton. Ogawa et al. [121] developed a novel ^{99m}Tc-chelate-conjugated bisphosphonate as a bone scintigraphic agent. The obtained results showed that the radiopharmaceutical conjugated-bisphosphonate was selectively distributed to the skeleton, specifically favoring sites of high bone turnover. In this case, bone-specificity was mediated by the bisphosphonate affinity for the apatite surface.

For this thesis, bisphosphonate moieties were selected as the bone targeting ligand, because they are chemically very stable synthetic compounds that resist chemical and enzymatic hydrolysis induced by osteoclasts and therefore seem to possess the capability for modifying a previously-developed delivery system without affecting the chemical integrity of the targeting ligand [122].

6.2. Acidic oligopeptides.

Recently, another drug delivery system using acidic compounds, namely oligopeptides, was developed to target bone. This unique approach is based on the well known structures of several non-collagenous bone proteins that have a repetitive sequence of several acidic amino acids (L-aspartic acid or L-glutamic acid) that makes them adhesive to hydroxyapatite. Osteopontin and bone sialoproteins, two major non-collagenous proteins of bone, have L-Asp and L-Glu repetitive sequences and rapidly bind to hydroxyapatite after addition to osteoblastic cell culture [123,124]. Studies indicated that the minimum number of amino acids in the sequence should not be less than six in order to obtain high binding to hydroxyapatite. There is no effect of either the chemical nature of the acidic amino acid (aspartic or glutamic) or the optical isomer form (L or D) on the in-vitro binding to bone mineral [125-127]. The affinity of acidic oligopeptides to hydroxyapatite is due to ionic interactions between the negatively charged acid groups of these peptides and the positively charged calcium ions within the mineral component of bone at physiological pH [128]. The structure of commonly used acidic oligopeptides is indicated in Figure 4.

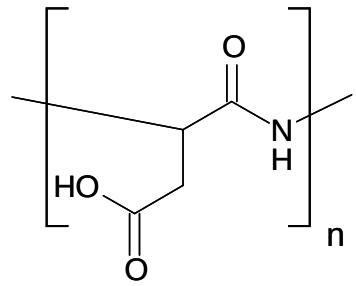

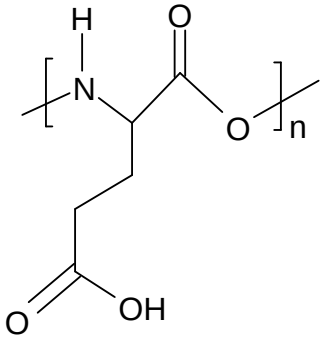

Polyaspartic acid	Polyglutamic acid

Figure 4: The structure of commonly used acidic oligopeptides

Because of the unique features of these compounds, much effort has been directed to conjugate non-specific bone agents with small acidic peptides in order to obtain osteotropicity. A prodrug conjugate consisting of β-estradiol (E_2) and L-Asp-hexapeptide has been prepared and was used to target bone tissue for the treatment of postmenopausal osteoporosis. The clinical use of E_2 alone is limited by adverse effects, due to the fact that E_2 easily penetrates biological membranes. By conjugating estradiol with the hydrophilic peptide, the prodrug was designed to improve patient compliance. In the in-vivo study, the prodrug conjugate was selectively delivered to the bone and it was eliminated very slowly after injection into mice. This finding also confirmed the usefulness of acidic polypeptides as selective bone targeting ligands [129].

6.3- Tetracyclines.

Other acidic components with known bone-targeting ability include the tetracyclines, yellow crystalline substances from the metabolites of the actinomycete *Streptomyses rimosus* with a wide range of antibiotic activities. While tetracyclines possess a wide range of biological activity, they all have a similar basic molecular structure as shown in Figure 5.

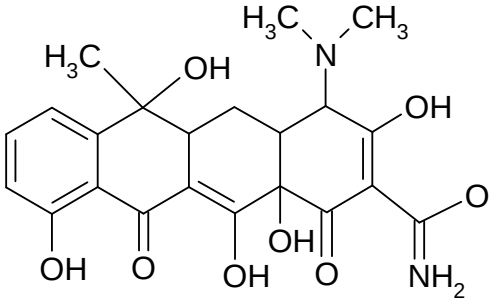

Figure 5: The basic structure of tetracycline

Tetracyclines are mainly deposited in the newly-formed bone after injection into the living organism. This is due to the direct reaction between tetracycline and one or more of inorganic components of the mineralized tissue, the most likely species being hydoxyapatite. The affinity of tetracycline for hydroxyapatite is due to its chelation capacity for calcium ions present at the surface of the mineral bone matrix [95,130].

Due to their high affinity for bone, tetracyclines have been conjugated with some therapeutic agents for improved diagnosis and treatment of skeletal diseases. They have been conjugated with synthetic polymers to develop water soluble polymeric bone-targeting drug delivery system based on PEG and HPMA copolymer. These systems may be used as universal vehicles for the targeted delivery of bone therapeutics [131]. Because of the uptake of tetracycline in vivo by the centers of active bone formation, Frost et al. [132] applied it as a marker to measure the rate of bone formation at the level of osteoblast. However, the complicated structure of tetracyclines and their poor chemical stability seems to hinder further utilization of tetracyclines as bone targeting moieties.

6.4. Miscellaneous.

In addition to all of the above mentioned compounds, a few other molecules have been applied as bone-targeting moieties. These chemical groups include polymalonic acid, sialic acid, N-methacrylamido salicylic acid, N-acryloyl aspartic acid, phosphonylated polyphenylene oxide, and non-ionic polymers such as glucan. The structures of some of these compounds are presented below in Figure 6 [95].

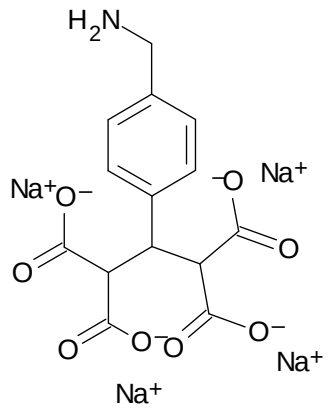

Polymalonic acid

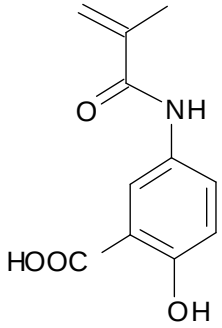

N-methacrylamido salicylic acid

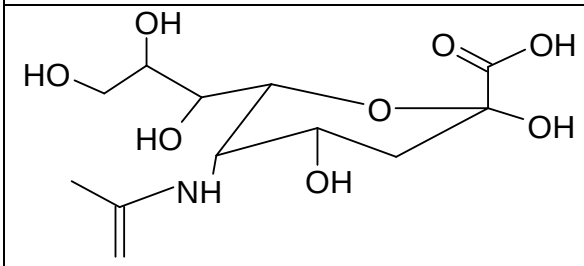

Sialic acid

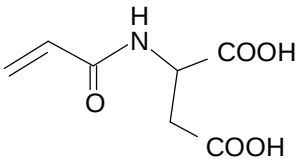

N-acrylol aspartic acid

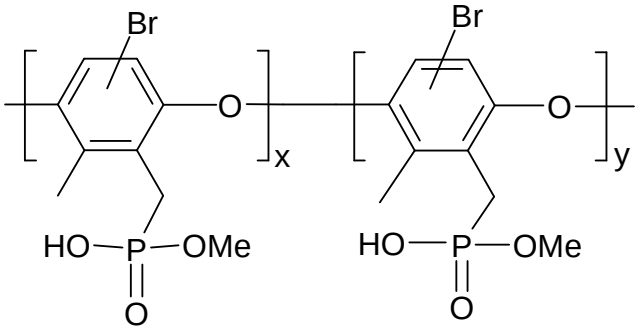

Phosphonylated polyphenylene oxide

Figure 6: The structure of miscellaneous bone-targeting ligands

7. Goals of the Thesis

The main objective of this work was the preparation, optimization and investigation of nanoparticulate bone targeted drug delivery systems using the well known gold nanoparticles as model system for the investigation and basis for the versatile production of the particles.

The chosen gold nanoparticles represent an excellent model candidate in the field of nanoparticle-based targeted drug delivery because they can be easily obtained in the desired size, they are easy to manufacture, and they can be easily modified to impart various functionalities by conjugation with various biomaterials and other molecules without altering the biological activity of the conjugated compounds. Additionally, gold nanoparticles can be easily detected by UV-Vis spectroscopy due to their unique optical properties such as distinctive extension band in the visible region (SPR) due to the surface plasmon oscillation of the free electrons [133-135].

One of the essential requirements for this design of nanoparticles is long blood circulation time to allow them to reach the specific target sites. In order to achieve this, the nanoparticle surfaces must be coated with a layer of hydrophilic polymers such as poly(ethylene glycol) to avoid rapid uptake by the reticuloendothelial system (RES). At the same time, the polymer could act as platform for further functionalization of the nanoparticles with targeting ligands [136].

Along these lines **chapter 2** describes the synthesis of poly(ethylene glycol)-undecyl mercaptane, either methoxy or amine terminated used for the functionalization of the gold. The synthesized polymers are characterized by their high affinity for gold surfaces and the formation of a well ordered self assembled monolayer due to the presence of the alkanethiol parts. Amine terminated poly(ethylene glycol)-undecyl mercaptane was also functionalized with bisphosphonate as a bone targeting ligand and successfully proved its affinity for hydroxyapatite.

The necessary optimization of polymer synthesis using retrosynthesis approaches was used to establish suitable methods to obtain highly pure derivatives of poly(ethylene glycol)-undecyl mercaptane. Various experiments using other synthesis schemes were used to determine the optimal reaction conditions for the synthesis of the required polymers (**Chapter 3**).

Chapter 4 outlines the preparation and optimization of the gold nanoparticles suitable for intravenous administration by citrate reduction. The obtained nanoparticles were coated with methoxy poly(ethylene glycol)-undecyl mercaptane and amino poly(ethylene glycol)-undecyl mercaptane. The prepared nanoparticles were characterized by size determination (using photon correlation spectroscopy and TEM), zeta potential measurements and UV-Vis spectroscopy. Furthermore, the stability of polymer modified nanoparticles was tested in the presence of sodium chloride, BSA and serum to simulate the later in vivo conditions.

The objective of the further work was the evaluation of the in vitro binding of bisphosphonate-functionalized gold nanoparticles to hydroxyapatite (HA). The effect of coating with different concentrations of bisphosphonate on the in vitro affinities of nanoparticles for hydroxyapatite at room temperature was investigated. In order to simulate the in vivo conditions, in vitro binding of bisphosphonate-functionalized gold nanoparticles to endobone was also studied in the presence of calcium chloride, BSA and serum (**Chapter 5**).

The final goal of the thesis was to test bisphosphonate functionalized gold nanoparticles in vivo. Nanoparticles were labeled with radioactive indium in order to track them after intravenous injection. The biodistribution in different organs and the pharmacokinetics of functionalized and control gold nanoparticles in mice were investigated (**Chapter 6**).

8. References

1. C. Destree, J. Ghijsen, and J. B. Nagy, "Preparation of Organic Nanoparticles Using Microemulsions: Their Potential Use in Transdermal Delivery," Langmuir **23,** 1965-1973 (2007).

2. Rajni Sinha, Gloria J. Kim, Shuming Nie, and Dong M. Shin, "Nanotechnology in cancer therapeutics: bioconjugated nanoparticles for drug delivery," Mol Cancer Ther **5,** 1909-1917 (2006).

3. Lisa M. Bareford and Peter W. Swaan, "Endocytic mechanisms for targeted drug delivery," Advanced Drug Delivery Reviews **59,** 748-758 (2007).

4. K. Maruyama, O. Ishida, T. Takizawa, and K. Moribe, "Possibility of active targeting to tumor tissues with liposomes," Advanced Drug Delivery Reviews **40,** 89-102 (1999).

5. Robert A. Freitas, Jr., "Pharmacytes: an ideal vehicle for targeted drug delivery," Journal of Nanoscience and Nanotechnology **6,** 2769-2775 (2006).

6. S. S. Dharap, Y. Wang, P. Chandna, J. J. Khandare, B. Qiu, S. Gunaseelan, P. J. Sinko, S. Stein, A. Farmanfarmaian, and T. Minko, "Tumor-specific targeting of an anticancer drug delivery system by LHRH peptide," Proceedings of the National Academy of Sciences of the United States of America **102,** 12962-12967 (2005).

7. Jaspreet K. Vasir, Maram K. Reddy, and Vinod D. Labhasetwar, "Nanosystems in drug targeting: opportunities and challenges," Current Nanoscience **1,** 47-64 (2005).

8. Hideya Kimura, Tsutomu Yasukawa, Yasuhiko Tabata, and Yuichiro Ogura, "Drug targeting to choroidal neovascularization," Advanced Drug Delivery Reviews **52,** 79-91 (2001).

9. David A. Groneberg, Michael Giersig, Tobias Welte, and Ulrich Pison, "Nanoparticle-based diagnosis and therapy," Current Drug Targets **7,** 643-648 (2006).

10. Costas Kaparissides, Sofia Alexandridou, Katerina Kotti, and Sotira Chaitidou, "Recent advances in novel drug delivery systems," Online Journal of Nanotechnology **2,** No (2006).

11. C. Medina, M. J. Santos-Martinez, A. Radomski, O. Corrigan, I, and M. W. Radomski, "Nanoparticles: pharmacological and toxicological significance," Br J Pharmacol **150,** 552-558 (2007).

12. Jayanth Panyam and Vinod Labhasetwar, "Biodegradable nanoparticles for drug and gene delivery to cells and tissue," Advanced Drug Delivery Reviews **55,** 329-347 (2003).

13. Kalevi Kairemo, Paola Erba, Kim Bergstrom, and Ernest K. J. Pauwels, "Nanoparticles in cancer," Current Radiopharmaceuticals **1,** 30-36 (2008).

14. Sha Jin and Kaiming Ye, "Nanoparticle-Mediated Drug Delivery and Gene Therapy," Biotechnology Progress **23,** 32-41 (2007).

15. K. K. Jain, "Nanomedicine: application of nanobiotechnology in medical practice," Med Princ Pract **17,** 89-101 (2008).

16. Ulrich Pison, Tobias Welte, Michael Giersig, and David A. Groneberg, "Nanomedicine for respiratory diseases," European Journal of Pharmacology **533,** 341-350 (2006).

17. O. Kayser, A. Lemke, and N. Hernandez-Trejo, "The impact of nanobiotechnology on the development of new drug delivery systems," Current Pharmaceutical Biotechnology **6,** 3-5 (2005).

18. Weibo Cai, Ting Gao, Hao Hong, and Jiangtao Sun, "Application of gold nanoparticles in cancer nanotechnology," Nanotechnology, Science and Applications **1,** 17-31 (2008).

19. G. Ramachandra Reddy, Mahaveer S. Bhojani, Patrick McConville, Jonathan Moody, Bradford A. Moffat, Daniel E. Hall, Gwangseong Kim, Yong Eun Koo, Michael J. Woolliscroft, James V. Sugai, Timothy D. Johnson, Martin A. Philbert, Raoul Kopelman, Alnawaz Rehemtulla, and Brian D. Ross, "Vascular Targeted Nanoparticles for Imaging and Treatment of Brain Tumors," Clinical Cancer Research **12,** 6677-6686 (2006).

20. Kwangjae Cho, Xu Wang, Shuming Nie, Zhuo Chen, and Dong M. Shin, "Therapeutic Nanoparticles for Drug Delivery in Cancer," Clinical Cancer Research **14,** 1310-1316 (2008).

21. Irene Brigger, Catherine Dubernet, and Patrick Couvreur, "Nanoparticles in cancer therapy and diagnosis," Advanced Drug Delivery Reviews **54,** 631-651 (2002).

22. Giulio F. Paciotti, David G. I. Kingston, and Lawrence Tamarkin, "Colloidal gold nanoparticles: a novel nanoparticle platform for developing multifunctional tumor-targeted drug delivery vectors," Drug Development Research **67,** 47-54 (2006).

23. Yu Hung Chen, Chiau Yuang Tsai, Pon Yu Huang, Meng Ya Chang, Pai Chiao Cheng, Chen Hsi Chou, Dong Hwang Chen, Chrong Reen Wang, Ai Li Shiau, and Chao Liang Wu, "Methotrexate Conjugated to Gold Nanoparticles Inhibits Tumor Growth in a Syngeneic Lung Tumor Model," Molecular Pharmaceutics **4,** 713-722 (2007).

24. C. Vauthier, C. Dubernet, C. Chauvierre, I. Brigger, and P. Couvreur, "Drug delivery to resistant tumors: the potential of poly(alkyl cyanoacrylate) nanoparticles," Journal of Controlled Release **93,** 151-160 (2003).

25. Masaaki Hidaka, Takashi Kanematsu, Kazutoshi Ushio, and Junzo Sunamoto, "Selective and effective cytotoxicity of folic acid-conjugated cholesteryl pullulan hydrogel nanoparticles complexed with doxorubicin in in vitro and in vivo studies," Journal of Bioactive and Compatible Polymers **21,** 591-602 (2006).

26. Indrajit Roy, Tymish Y. Ohulchanskyy, Haridas E. Pudavar, Earl J. Bergey, Allan R. Oseroff, Janet Morgan, Thomas J. Dougherty, and Paras N. Prasad, "Ceramic-based nanoparticles entrapping water-insoluble photosensitizing anticancer drugs: a novel drug-carrier system for photodynamic therapy," Journal of the American Chemical Society **125,** 7860-7865 (2003).

27. Rajesh Pandey, Anjali Sharma, A. Zahoor, Sadhna Sharma, G. K. Khuller, and B. Prasad, "Poly (DL-lactide-co-glycolide) nanoparticle-based inhalable sustained drug

delivery system for experimental tuberculosis," Journal of Antimicrobial Chemotherapy **52,** 981-986 (2003).

28. Svetlana Gelperina, Kevin Kisich, Michael D. Iseman, and Leonid Heifets, "The potential advantages of nanoparticle drug delivery systems in chemotherapy of tuberculosis," Am J Respir Crit Care Med **172,** 1487-1490 (2005).

29. Dong Won Lee, Shawna A. Shirley, Richard F. Lockey, and Shyam S. Mohapatra, "Thiolated chitosan nanoparticles enhance anti-inflammatory effects of intranasally delivered theophylline," Respiratory Research **7,** No (2006).

30. A. Zahoor, Sadhna Sharma, and G. K. Khuller, "Inhalable alginate nanoparticles as antitubercular drug carriers against experimental tuberculosis," International Journal of Antimicrobial Agents **26,** 298-303 (2005).

31. Evangelia Chnari, Jessica S. Nikitczuk, Kathryn E. Uhrich, and Prabhas V. Moghe, "Nanoscale Anionic Macromolecules Can Inhibit Cellular Uptake of Differentially Oxidized LDL," Biomacromolecules **7,** 597-603 (2006).

32. Barnabas Wilson, Malay Kumar Samanta, Kumaraswamy Santhi, Kokilampal Perumal Sampath Kumar, Nallupillai Paramakrishnan, and Bhojraj Suresh, "Poly(n-butyl cyanoacrylate) nanoparticles coated with Polysorbate 80 for the targeted delivery of rivastigmine into the brain to treat Alzheimer's disease," Brain Research **1200,** 159-168 (2008).

33. Barnabas Wilson, Malay Kumar Samanta, Kumaraswamy Santhi, Kokilampal Perumal Sampath Kumar, Nallupillai Paramakrishnan, and Bhojraj Suresh, "Targeted delivery of tacrine into the brain with polysorbate 80-coated poly(n-butylcyanoacrylate) nanoparticles," European Journal of Pharmaceutics and Biopharmaceutics **70,** 75-84 (2008).

34. K. K. Jain, "Nanobiotechnology-based drug delivery to the central nervous system," Neurodegenerative Diseases **4,** 287-291 (2007).

35. Sandip B. Tiwari and Mansoor M. Amiji, "A review of nanocarrier-based CNS delivery systems," Current Drug Delivery **3,** 219-232 (2006).

36. Giovanni Tosi, Luca Costantino, Barbara Ruozi, Flavio Forni, and Maria Angela Vandelli, "Polymeric nanoparticles for the drug delivery to the central nervous system," Expert Opinion on Drug Delivery **5,** 155-174 (2008).

37. Ulrike Schroeder, Petra Sommerfeld, Sven Ulrich, and Bernhard A. Sabel, "Nanoparticle Technology for Delivery of Drugs Across the Blood-Brain Barrier," Journal of Pharmaceutical Sciences **87,** 1305-1307 (1998).

38. Basel A. Abdel Wahab, Petrov V. Evgenivetch, and Renad N. Alyautdin, "Brain targeting of nerve growth factor using poly(butylcyanoacrylate) nanoparticles," Internet Journal of Pharmacology **3,** No (2005).

39. R. N. Alyautdin, E. B. Tezikov, P. Ramge, J. Kroiter, D. Begli, and D. A. Kharkevich, "Poly(butyl cyanoacrylate) nanoparticles coated with Polysorbate-80 for the transport of tubocurarine to brain," Eksperimental'naya i Klinicheskaya Farmakologiya **61,** 23-26 (1998).

40. Joerg Kreuter, "Application of nanoparticles for the delivery of drugs to the brain," International Congress Series **1277,** 85-94 (2005).

41. David Schubert, Richard Dargusch, Joan Raitano, and Siu Wai Chan, "Cerium and yttrium oxide nanoparticles are neuroprotective," Biochemical and Biophysical Research Communications **342,** 86-91 (2006).

42. A. M. De Campos, A. Sanchez, and M. J. Alonso, "Chitosan nanoparticles: a new vehicle for the improvement of the delivery of drugs to the ocular surface. Application to cyclosporin A," International Journal of Pharmaceutics **224,** 159-168 (2001).

43. Elias Fattal, Mohammad Youssef, Patrick Couvreur, and Antoine Andremont, "Treatment of experimental salmonellosis in mice with ampicillin-bound nanoparticles," Antimicrobial Agents and Chemotherapy **33,** 1540-1543 (1989).

44. J. Kreuter, "Liposomes and nanoparticles as vehicles for antibiotics," Infection (Munich, Germany) **19,** S224-S228 (1991).

45. Rajesh Pandey and Gopal K. Khuller, "Nanoparticle-based oral drug delivery system for an injectable antibiotic - streptomycin," Chemotherapy (Basel, Switzerland) **53,** 437-441 (2007).

46. Edward Turos, Jeung Yeop Shim, Yang Wang, Kerriann Greenhalgh, G. Suresh Kumar Reddy, Sonja Dickey, and Daniel V. Lim, "Antibiotic-conjugated polyacrylate nanoparticles: New opportunities for development of anti-methicillin-resistant Staphylococcus aureus agents," Bioorganic & Medicinal Chemistry Letters **17,** 53-56 (2007).

47. Edward Turos, G. Suresh Kumar Reddy, Kerriann Greenhalgh, Praveen Ramaraju, Sampath C. Abeylath, Seyoung Jang, Sonja Dickey, and Daniel V. Lim, "Penicillin-bound polyacrylate nanoparticles: Restoring the activity of b-lactam antibiotics against methicillin-resistant Staphylococcus aureus," Bioorganic & Medicinal Chemistry Letters **17,** 3468-3472 (2007).

48. J. Botsoa, V. Lysenko, A. Geloen, O. Marty, J. M. Bluet, and G. Guillot, "Application of 3C-SiC quantum dots for living cell imaging," Applied Physics Letters **92,** 173902-1-173902/3 (2008).

49. Kewal K. Jain, "The role of nanobiotechnology in drug discovery," Drug Discovery Today **10,** 1435-1442 (2005).

50. Kewal K. Jain, "Applications of nanobiotechnology in clinical diagnostics," Clinical Chemistry (Washington, DC, United States) **53,** 2002-2009 (2007).

51. Sung Hyun Lee, Hyewon Lee, Jin Seung Park, Hyoung Choi, Kyung Yeon Han, Hyuk Seong Seo, Keum Young Ahn, Sung Sik Han, Yunjung Cho, Kee Hyoung Lee, and Jeewon Lee, "A novel approach to ultrasensitive diagnosis using supramolecular protein nanoparticles," FASEB Journal **21,** 1324-1334 (2007).

52. J. F. Hainfeld, D. N. Slatkin, T. M. Focella, and H. M. Smilowitz, "Gold nanoparticles: a new X-ray contrast agent," British Journal of Radiology **79,** 248-253 (2006).

53. Dongwon Lee, Sirajud Khaja, Juan C. Velasquez-Castano, Madhuri Dasari, Carrie Sun, John Petros, W. Robert Taylor, and Niren Murthy, "In vivo imaging of hydrogen peroxide with chemiluminescent nanoparticles," Nature Materials **6,** 765-769 (2007).

54. Weili Shi, Y. Sahoo, and Mark T. Swihart, "Gold nanoparticles surface-terminated with bifunctional ligands," Colloids and Surfaces, A: Physicochemical and Engineering Aspects **246,** 109-113 (2004).

55. Tony Azzam and Adi Eisenberg, "Monolayer-protected gold nanoparticles by the self-assembly of micellar poly(ethylene oxide)-b-poly(e-caprolactone) block copolymer," Langmuir **23,** 2126-2132 (2007).

56. Koutarou Idegami, Miyuki Chikae, Kagan Kerman, Naoki Nagatani, Teruko Yuhi, Tatsuro Endo, and Eiichi Tamiya, "Gold nanoparticle-based redox signal enhancement for sensitive detection of human chorionic gonadotropin hormone," Electroanalysis **20,** 14-21 (2007).

57. K. V. Katti, R. Kannan, K. Katti, V. Kattumori, R. Pandrapraganda, V. Rahing, C. Cutler, E. J. Boote, S. W. Casteel, C. J. Smith, J. D. Robertson, and S. S. Jurrison, "Hybrid gold nanoparticles in molecular imaging and radiotherapy," Czechoslovak Journal of Physics **56,** d23-d34 (2006).

58. James F. Hainfeld, Daniel Slatkin, and Henry M. Smilowitz, "The use of gold nanoparticles to enhance radiotherapy in mice," Physics in Medicine & Biology **49,** N309-N315 (2004).

59. Giulio F. Paciotti, Lonnie Myer, David Weinreich, Dan Goia, Nicolae Pavel, Richard E. McLaughlin, and Lawrence Tamarkin, "Colloidal gold: a novel nanoparticle vector for tumor directed drug delivery," Drug delivery **11,** 169-183 (2004).

60. David A. Giljohann, Dwight S. Seferos, Pinal C. Patel, Jill E. Millstone, Nathaniel L. Rosi, and Chad A. Mirkin, "Oligonucleotide Loading Determines Cellular Uptake of DNA-Modified Gold Nanoparticles," Nano Letters **7,** 3818-3821 (2007).

61. Nathaniel L. Rosi, David A. Giljohann, C. Shad Thaxton, Abigail K. R. Lytton-Jean, Min Su Han, and Chad A. Mirkin, "Oligonucleotide-Modified Gold Nanoparticles for Intracellular Gene Regulation," Science (Washington, DC, United States) **312,** 1027-1030 (2006).

62. Jun Shan and Heikki Tenhu, "Recent advances in polymer protected gold nanoparticles: synthesis, properties and applications," Chemical Communications (Cambridge, United Kingdom) 4580-4598 (2007).

63. Min Hu, Jingyi Chen, Zhi Yuan Li, Leslie Au, Gregory V. Hartland, Xingde Li, Manuel Marquez, and Younan Xia, "Gold nanostructures: engineering their plasmonic properties for biomedical applications," Chemical Society Reviews **35,** 1084-1094 (2006).

64. Raja Gopal Rayavarapu, Wilma Petersen, Constantin Ungureanu, Janine N. Post, Ton G. van Leeuwen, and Srirang Manohar, "Synthesis and bioconjugation of gold nanoparticles as potential molecular probes for light-based imaging techniques," International Journal of Biomedical Imaging 29817-1-29817/10 (2007).

65. Patrick Rooney, Asad Rezaee, Songbo Xu, Touraj Manifar, Abdollah Hassanzadeh, Ganna Podoprygorina, Volker Bohmer, Chitra Rangan, and Silvia Mittler, "Control of surface plasmon resonances in dielectrically coated proximate gold nanoparticles immobilized on a substrate," Physical Review B: Condensed Matter and Materials Physics **77,** 235446-1-235446/9 (2008).

66. Peter J. Roth and Patrick Theato, "Versatile Synthesis of Functional Gold Nanoparticles: Grafting Polymers From and Onto," Chemistry of Materials **20,** 1614-1621 (2008).

67. Tao Yang, Zhuang Li, Li Wang, Cunlan Guo, and Yujing Sun, "Synthesis, characterization, and self-assembly of protein lysozyme monolayer-stabilized gold nanoparticles," Langmuir **23,** 10533-10538 (2007).

68. G. Frens, "Controlled nucleation for the regulation of the particle size in monodisperse gold suspensions," Nature (London), Physical Science **241,** 20-22 (1973).

69. Boon Kin Pong, Hendry I. Elim, Jian Xiong Chong, Wei Ji, Bernhardt L. Trout, and Jim Yang Lee, "New insights on the nanoparticle growth mechanism in the citrate reduction of gold(III) salt: Formation of the Au nanowire intermediate and its nonlinear optical properties," Journal of Physical Chemistry C **111,** 6281-6287 (2007).

70. A. Sugunan, C. Thanachayanont, J. Dutta, and J. G. Hilborn, "Heavy-metal ion sensors using chitosan-capped gold nanoparticles," Science and Technology of Advanced Materials **6,** 335-340 (2005).

71. Andrew N. Shipway, Eugenii Katz, and Itamar Willner, "Nanoparticle arrays on surfaces for electronic, optical, and sensor applications," ChemPhysChem **1,** 18-52 (2000).

72. Marie Christine Daniel and Didier Astruc, "Gold Nanoparticles: Assembly, Supramolecular Chemistry, Quantum-Size-Related Properties, and Applications toward Biology, Catalysis, and Nanotechnology," Chemical Reviews (Washington, DC, United States) **104,** 293-346 (2004).

73. Sanjeev Kumar, K. S. Gandhi, and R. Kumar, "Modeling of formation of gold nanoparticles by citrate method," Industrial & Engineering Chemistry Research **46,** 3128-3136 (2007).

74. Touraj Manifar, Asad Rezaee, Mehdi Sheikhzadeh, and Silvia Mittler, "Formation of uniform self-assembly monolayers by choosing the right solvent: OTS on silicon wafer, a case study," Applied Surface Science **254,** 4611-4619 (2008).

75. Hideyuki Ogawa, Takumi Takamura, and Yuhei Shimoyama, "Self-assembly process of alkanethiol monolayers," Japanese Journal of Applied Physics, Part 1: Regular Papers, Short Notes & Review Papers **38,** 6019-6023 (1999).

76. Qingwen Li, Gao Hong, Yiming Wang, Guoan Luo, and Jie Ma, "Studies on self-assembly monolayers of cysteine on gold by XPS, QCM, and electrochemical techniques," Electroanalysis **13,** 1342-1346 (2001).

77. R. Gref, M. Luck, P. Quellec, M. Marchand, E. Dellacherie, S. Harnisch, T. Blunk, and R. H. Muller, "'Stealth' corona-core nanoparticles surface modified by polyethylene glycol (PEG): influences of the corona (PEG chain length and surface density) and of

the core composition on phagocytic uptake and plasma protein adsorption," Colloids and Surfaces, B: Biointerfaces **18,** 301-313 (2000).

78. Wei Fu, Dinesh Shenoy, Jane Li, Curtis Crasto, Graham Jones, Charles Dimarzio, Srinivas Sridhar, and Mansoor Amiji, "Biomedical applications of gold nanoparticles functionalized using hetero-bifunctional poly(ethylene glycol) spacer," Materials Research Society Symposium Proceedings **845,** 223-228 (2005).

79. Motoi Oishi, Junpei Nakaogami, Takehiko Ishii, and Yukio Nagasaki, "Smart PEGylated gold nanoparticles for the cytoplasmic delivery of siRNA to induce enhanced gene silencing," Chemistry Letters **35,** 1046-1047 (2006).

80. Lilian E. van Vlerken, Tushar K. Vyas, and Mansoor M. Amiji, "Poly(ethylene glycol)-modified Nanocarriers for Tumor-targeted and Intracellular Delivery," Pharmaceutical Research **24,** 1405-1414 (2007).

81. Zhuang Liu, Corrine Davis, Weibo Cai, Lina He, Xiaoyuan Chen, and Hongjie Dai, "Circulation and long-term fate of functionalized, biocompatible single-walled carbon nanotubes in mice probed by Raman spectroscopy," Proc Natl Acad Sci U S A **105,** 1410-1415 (2008).

82. R. Gref, A. Domb, P. Quellec, T. Blunk, R. H. Mueller, J. M. Verbavatz, and R. Langer, "The controlled intravenous delivery of drugs using PEG-coated sterically stabilized nanospheres," Advanced Drug Delivery Reviews **16,** 215-233 (1995).

83. Donald E. Owens and Nicholas A. Peppas, "Opsonization, biodistribution, and pharmacokinetics of polymeric nanoparticles," International Journal of Pharmaceutics **307,** 93-102 (2006).

84. Robert Knerr, Barbara Weiser, Sigrid Drotleff, Claudia Steinem, and Achim Goepferich, "Measuring cell adhesion on RGD-modified, self-assembled PEG monolayers using the quartz crystal microbalance technique," Macromolecular Bioscience **6,** 827-838 (2006).

85. Barbara Menz, Robert Knerr, Achim Goepferich, and Claudia Steinem, "Impedance and QCM analysis of the protein resistance of self-assembled PEGylated alkanethiol layers on gold," Biomaterials **26,** 4237-4243 (2005).

86. Fajun Zhang, Donald G. Dressen, Maximilian W. A. Skoda, Robert M. J. Jacobs, Stefan Zorn, Richard A. Martin, Christopher M. Martin, Graham F. Clark, and Frank Schreiber, "Gold nanoparticles decorated with oligo(ethylene glycol) thiols: kinetics of colloid aggregation driven by depletion forces," European Biophysics Journal **37,** 551-561 (2008).

87. Fajun Zhang, Maximilian W. A. Skoda, Robert M. J. Jacobs, Stefan Zorn, Richard A. Martin, Christopher M. Martin, Graham F. Clark, Guenter Goerigk, and Frank Schreiber, "Gold nanoparticles decorated with oligo(ethylene glycol) thiols: protein resistance and colloidal stability," Journal of Physical Chemistry A **111,** 12229-12237 (2007).

88. Ming Zheng, Zhigang Li, and Xueying Huang, "Ethylene Glycol Monolayer Protected Nanoparticles: Synthesis, Characterization, and Interactions with Biological Molecules," Langmuir **20,** 4226-4235 (2004).

89. Ming Zheng and Xueying Huang, "Nanoparticles Comprising a Mixed Monolayer for Specific Bindings with Biomolecules," Journal of the American Chemical Society **126,** 12047-12054 (2004).

90. J. Christopher Love, Lara A. Estroff, Jennah K. Kriebel, Ralph G. Nuzzo, and George M. Whitesides, "Self-Assembled Monolayers of Thiolates on Metals as a Form of Nanotechnology," Chemical Reviews (Washington, DC, United States) **105,** 1103-1169 (2005).

91. T. A. Abbott, III, B. J. Lawrence, and S. Wallach, "Osteoporosis: the need for comprehensive treatment guidelines," Clin Ther **18,** 127-149 (1996).

92. Hideki Hirabayashi and Jiro Fujisaki, "Bone-specific drug delivery systems: Approaches via chemical modification of bone-seeking agents," Clinical Pharmacokinetics **42,** 1319-1330 (2003).

93. R. E. Coleman, "Skeletal complications of malignancy," Cancer **80,** 1588-1594.

94. M. J. Goblirsch, P. Zwolak, and D. R. Clohisy, "Advances in understanding bone cancer pain," Journal of Cellular Biochemistry **96,** 682-688 (2005).

95. Dong Wang, Scott C. Miller, Pavla Kopeckova, and Jindrich Kopecek, "Bone-targeting macromolecular therapeutics," Advanced Drug Delivery Reviews **57,** 1049-1076 (2005).

96. J. Fanghanel, T. Bayerlein, T. Gedrange, E. Kauschke, E. Rumpel, W. Gerike, V. Bienengraber, and P. Proff, "Bone functions and the requirements for bone grafts and substitutes in the orofacial region," Folia Morphol (Warsz) **65,** 56-58 (2006).

97. Jill E. Shea and Scott C. Miller, "Skeletal function and structure: implications for tissue-targeted therapeutics," Advanced Drug Delivery Reviews **57,** 945-957 (2005).

98. J. A. Buckwalter, M. J. Glimcher, R. R. Cooper, and R. Recker, "Bone biology. I: Structure, blood supply, cells, matrix, and mineralization" 1996).

99. S. Mori and D. B. Burr, "Increased intracortical remodeling following fatigue damage," Bone **14,** 103-109 (1993).

100. S. C. Manolagas, "Birth and death of bone cells: basic regulatory mechanisms and implications for the pathogenesis and treatment of osteoporosis," Endocr Rev **21,** 115-137 (2000).

101. H. C. Blair, "How the osteoclast degrades bone," Bioessays **20,** 837-846 (1998).

102. Juliet E. Compston, "Sex steroids and bone," Physiological Reviews **81,** 419-447 (2001).

103. N. C. Rath, J. M. Balog, W. E. Huff, G. R. Huff, G. B. Kulkarni, and J. F. Tierce, "Comparative differences in the composition and biomechanical properties of tibiae of seven- and seventy-two-week-old male and female broiler breeder chickens," Poultry Science **78,** 1232-1239 (1999).

104. A. S. POSNER, "The structure of bone apatite surfaces," J Biomed Mater Res **19,** 241-250 (1985).

105. M. J. Rogers, J. C. Frith, S. P. Luckman, F. P. Coxon, H. L. Benford, J. Monkkonen, S. Auriola, K. M. Chilton, and R. G. G. Russell, "Molecular mechanisms of action of bisphosphonates," Bone (New York) **24,** 73S-79S (1999).

106. Anke J. Roelofs, Keith Thompson, Sharon Gordon, and Michael J. Rogers, "Molecular Mechanisms of Action of Bisphosphonates: current Status," Clinical Cancer Research **12,** 6222s-6230s (2006).

107. M. J. Rogers, S. Gordon, H. L. Benford, F. P. Coxon, S. P. Luckman, J. Monkkonen, and J. C. Frith, "Cellular and molecular mechanisms of action of bisphosphonates," Cancer **88,** 2961-2978 (2000).

108. Wafaa M. Abdou and Abeer A. Shaddy, "The development of bisphosphonates for therapeutic uses, and bisphosphonate structure-activity consideration," ARKIVOC (Gainesville, FL, United States) 143-182 (2008).

109. J. H. Lin, "Bisphosphonates: A review of their pharmacokinetic properties," Bone (New York) **18,** 75-85 (1996).

110. R. Graham Russell, "Determinants of structure-function relationships among bisphosphonates," Bone (San Diego, CA, United States) **40,** S21-S25 (2007).

111. Robert G. G. Russell, R. C. Muehlbauer, Silvia Bisaz, D. A. Williams, and Herbert Fleisch, "Influence of pyrophosphate, condensed phosphates, phosphonates, and other phosphate compounds on the dissolution of hydroxyapatite in vitro and on bone resorption induced by parathyroid hormone in tissue culture and in thyroparathyroidectomised rats," Calcified Tissue Research **6,** 183-196 (1970).

112. Jon B. Catterall and Tim E. Cawston, "Drugs in development: bisphosphonates and metalloproteinase inhibitors," Arthritis Res Ther **5,** 12-24 (2003).

113. J. A. Batch, J. J. Couper, C. Rodda, C. T. Cowell, and M. Zacharin, "Use of bisphosphonate therapy for osteoporosis in childhood and adolescence," J Paediatr Child Health **39,** 88-92 (2003).

114. Dominique Heymann, Benjamin Ory, Francois Gouin, Jonathan R. Green, and Francoise Redini, "Bisphosphonates: new therapeutic agents for the treatment of bone tumors," Trends in Molecular Medicine **10,** 337-343 (2004).

115. J. R. Ross, Y. Saunders, P. M. Edmonds, S. Patel, D. Wonderling, C. Normand, and K. Broadley, "A systematic review of the role of bisphosphonates in metastatic disease," Health Technol Assess **8,** 1-176 (2004).

116. Verena Stresing, Florence Daubine, Ismahene Benzaid, Hannu Monkkonen, and Philippe Clezardin, "Bisphosphonates in cancer therapy," Cancer Letters (Amsterdam, Netherlands) **257,** 16-35 (2007).

117. J. P. Walsh, R. Attewell, B. G. A. Stuckey, M. J. Hooper, J. D. Wark, S. Fletcher, V. Ferrari, and J. A. Eisman, "Treatment of Paget's disease of bone: A survey of clinical practice in Australia," Bone (San Diego, CA, United States) **42,** 1219-1225 (2008).

118. Samuel D. Vasikaran, "Bisphosphonates: an overview with special reference to alendronate," Annals of Clinical Biochemistry **38,** 608-623 (2001).

119. A. Ezra and G. Golomb, "Administration routes and delivery systems of bisphosphonates for the treatment of bone resorption," Advanced Drug Delivery Reviews **42,** 175-195 (2000).

120. Rotem Erez, Sharon Ebner, Bernard Attali, and Doron Shabat, "Chemotherapeutic bone-targeted bisphosphonate prodrugs with hydrolytic mode of activation," Bioorganic & Medicinal Chemistry Letters **18,** 816-820 (2008).

121. Kazuma Ogawa, Takahiro Mukai, Yasuyuki Inoue, Masahiro Ono, and Hideo Saji, "Development of a novel 99mTc-chelate-conjugated bisphosphonate with high affinity for bone as a bone scintigraphic agent," Journal of Nuclear Medicine **47,** 2042-2047 (2006).

122. R. Graham Russell, Michael J. Rogers, Julie C. Frith, Steven P. Luckman, Fraser P. Coxon, Helena L. Benford, Peter I. Croucher, Claire Shipman, and Herbert A. Fleisch, "The pharmacology of bisphosphonates and new insights into their mechanisms of action," Journal of Bone and Mineral Research **14,** 53-65 (1999).

123. W. T. Butler, "The nature and significance of osteopontin," Connect Tissue Res **23,** 123-136 (1989).

124. Aake Oldberg, Ahnders Franzen, and Dick Heinegaard, "The primary structure of a cell-binding bone sialoprotein," Journal of Biological Chemistry **263,** 19430-19432 (1988).

125. Matthew B. Murphy, Jeffrey D. Hartgerink, Achim Goepferich, and Antonios G. Mikos, "Synthesis and in Vitro Hydroxyapatite Binding of Peptides Conjugated to Calcium-Binding Moieties," Biomacromolecules **8,** 2237-2243 (2007).

126. Shohei Kasugai, Ryuichi Fujisawa, Yoshihiro Waki, Ken Ichi Miyamoto, and Keiichi Ohya, "Selective drug delivery system to bone: small peptide (Asp)6 conjugation," Journal of Bone and Mineral Research **15,** 936-943 (2000).

127. Tatsuo Takahashi-Nishioka, Koichi Yokogawa, Shunji Tomatsu, Masaaki Nomura, Shinjiro Kobayashi, and Kenichi Miyamoto, "Targeted drug delivery to bone: pharmacokinetic and pharmacological properties of acidic oligopeptide-tagged drugs," Current Drug Discovery Technologies **5,** 39-48 (2008).

128. Sara Sarig, "Aspartic acid nucleates the apatite crystallites of bone: a hypothesis," Bone (San Diego, CA, United States) **35,** 108-113 (2004).

129. Koichi Yokogawa, Kazuhiro Miya, Tohru Sekido, Yasuhiko Higashi, Masaaki Nomura, Ryuichi Fujisawa, Keiko Morito, Yukito Masamune, Yoshihiro Waki, Shohei Kasugai, and Ken Ichi Miyamoto, "Selective delivery of estradiol to bone by aspartic acid oligopeptide and its effects on ovariectomized mice," Endocrinology **142,** 1228-1233 (2001).

130. D. D. Perrin, "Binding of tetracyclines to bone," Nature (London, United Kingdom) **208,** 787-788 (1965).

131. Dong Wang, Scott Miller, Monika Sima, Pavla Kopeckova, and Jindrich Kopecek, "Synthesis and Evaluation of Water-Soluble Polymeric Bone-Targeted Drug Delivery Systems," Bioconjugate Chem. **14,** 853-859 (2003).

132. H. M. Frost, "Tetracycline bone labeling in anatomy," Am J Phys Anthropol **29,** 183-195 (1969).

133. Ganeshchandra Sonavane, Keishiro Tomoda, Akira Sano, Hiroyuki Ohshima, Hiroshi Terada, and Kimiko Makino, "In vitro permeation of gold nanoparticles through rat skin and rat intestine: Effect of particle size," Colloids and Surfaces, B: Biointerfaces **65,** 1-10 (2008).

134. Hsuen Li Chen, Hsu Chun Cheng, Tsung Shine Ko, Shang Yu Chuang, and Tien Chi Chu, "Characterizing optical properties of self-assembled gold nanoparticles for surface plasmon resonance device applications," Japanese Journal of Applied Physics, Part 1: Regular Papers, Brief Communications & Review Papers **45,** 6984-6986 (2006).

135. Xiaohua Huang, Prashant K. Jain, Ivan H. El Sayed, and Mostafa A. El Sayed, "Gold nanoparticles: Interesting optical properties and recent applications in cancer diagnostics and therapy," Nanomedicine (London, United Kingdom) **2,** 681-693 (2007).

136. A. Beletsi, Z. Panagi, and K. Avgoustakis, "Biodistribution properties of nanoparticles based on mixtures of PLGA with PLGA-PEG diblock copolymers," International Journal of Pharmaceutics **298,** 233-241 (2005).

Chapter 2

Synthesis of Bifunctional Polyethylene Glycol Derivatives for Simultaneous Gold Surface Coating and Binding of Hydroxyapatite

Gamal Zayed[1], Achim Göpferich[1], Jörg Teßmar[1,*]

[1] Department of Pharmaceutical Technology,
University of Regensburg,
93040 Regensburg, Germany

Email of corresponding author:
joerg.tessmar@chemie.uni-regensburg.de

to be submitted

Keywords: bifunctional polymers, poly(ethylene glycol), gold surface modification, drug targeting, bisphosphonate, hydroxyapatite

Abstract

Heterobifunctional poly(ethylene glycol) derivatives have a wide range for biomedical applications ranging from the modulation of the solubility of badly soluble compounds to the surface modification of implants. For the modification of variously shaped gold surfaces thioalkylated poly(ethylene glycol)s are well established, since they form very stable self assembled monolayers (SAMs). For a more sophisticated functionalization, the polymers should furthermore provide functional groups, which can be used for the attachment of other molecules. For this study two different polymers (methoxy poly(ethylene glycol)-undecyl mercaptane and amino poly(ethylene glycol)-undecyl mercaptane) were synthesized applying a new synthetic strategy. Subsequently, a suitable bone targeting ligand, bisphosphonate, well soluble in non aqueous media was synthesized and reacted with the amine terminus of the polymer using standard DCC/NHS chemistry. The obtained polymers were characterized by ^{1}H-NMR, HPLC and mass spectroscopy and demonstrated a high degree of purity. Furthermore, it was demonstrated that the bisphosphonate-modified polymers bind to gold surfaces and to hydroxyapatite, which indicated the successful linkage of the two functionalities. Consequently, the synthesized polymers seem to be promising for the preparation of functionalized gold nanoparticles, which additionally exhibit a high affinity for the bone mineral hydroxyapatite.

1. Introduction

In order to modify biomaterial surfaces, like polymers or metals, bifunctional derivatives of poly(ethylene glycol) play an important role due to their unique properties, like high water solubility, good biocompatibility, low cytotoxicity, low immunogenicity, low protein binding and subsequent poor cell adhesion [1-4]. An additionally introduced bifunctionality furthermore allows for the selective attachment to surfaces and the presentation of specific groups suitable to introduce further functions into the polymers, like for example controlled cellular adhesion, immobilization of bioactive compounds or also the targeting to a certain cell type or tissue. The so far most prominent applications of functionalized PEG molecules include: PEGylation of peptide and protein drugs [5-9], preparation of hydrogels for drug delivery applications [10,11], as well as the surface modification of materials in order to control cellular adhesion [12] or the surface stabilization and functionalization of different nanoparticles [13-15].

For all of these applications, thiol functionalized or thioalkylated poly(ethylene glycol)s are known to binds strongly to gold surfaces due to their spontaneous and very specific adsorption of the thiol or disulfide derivatives to the gold surfaces, leading to the formation of very stable self assembled monolayers (SAMs). For these applications, the alkanethiol part of the polymers is essential to form a highly stable, highly ordered and well oriented monolayer film due to the present Van der Waals interactions between neighboring alkyl chains, which almost form crystal structures during their assembly [16]. Also, the binding of the sulfur head group to the gold substrate occurs in the form of the metal thiolate, which is an extremely strong bond and subsequently the resulting monolayer are quite stable [17-19]. It is reported in literature that the minimum length of used alkyl chain should be 11 carbon atoms in order to obtain a densely packed almost crystalline like assembly of the chains. Shorter aliphatic parts (less than 11) consequently produce less ordered structures with a lower packing density and also weaker coverage of the underlying gold surfaces [20-22].

The application of poly(ethylene glycol) as surface coating is well known to prevent non specific adsorption of proteins to the modified surfaces. The PEG mediated protein resistance also of SAMs is due to the formation of stable interfacial aqueous layer, which prevents a direct contact between the underlying biomaterial surface and the proteins, and furthermore exhibits also no interactions between the uncharged PEG and the protein molecules [23]. It is described in literature that the inhibition of the unspecific protein adsorption to PEG modified surfaces is almost independent on the chain length of the PEG

coating, but a minimum chain length of PEG is required to diminish cellular adhesion, which is found to be about 2000 Da [24,25].

The functionalization of PEG for surface coatings is already described in literature to achieve specific interactions with cells. Knerr and et al. [12] reported the modification of gold coated quartz surfaces with alkanethiol PEG modified with RGD containing adhesion sequences in order to measure the cellular adhesion using the quartz crystal microbalance. Functionalized gold nanoparticles have been also used to target specific organs in the body via the surface receptors of certain cells. Here, folic acid modified poly(ethylene glycol) coated nanoparticles were used to target folate receptor on cancer cells [26] or PEG-thiol coated gold nanoparticles were used as a platform to optimize hepatocyte-targeted delivery in vivo using galactose targeting moieties [27]

In order to achieve bone targeting of nanoparticles, we chose bisphosphonates, organic analogues of pyrophosphate, due to their exceptional high affinity to bone mineral, which already led to their exploration for targeting different pharmacological agents to bone tissues [28]. Currently, bisphosphonates are the most important class of antiresorptive drugs used in the treatment of metabolic bone diseases, including osteoporosis, tumor-associated osteolysis and also subsequent hypercalcemia. All these compounds have a very high affinity for calcium ions and therefore mainly target the bone mineral, where they are as primarily adsorbed drugs internalized by the bone resorbing osteoclasts and subsequently inhibit their physiological function [29]. Bisphosphonates have also been studied as tool to achieve a high bone mineral affinity for various other materials. Functional nanoparticles for the treatment of bone disease were designed by surface modification of PLGA particles using alendronate as targeting moiety. The observed HA affinity assay suggested that the alendronate-modified PLGA nanoparticles have the potential to the targeted these drug delivery systems to bone [30].

Additionally, protein-based therapeutic agents intended for treatment of bone diseases have been prepared by direct chemical conjugation with bisphosphonate. It was demonstrated by several experiments that conjugation of bone-seeking bisphosphonate with various bigger proteins improved their localized delivery to mineralized tissues [31-36]. Also the delivery of an antineoplastic agent, methotrexate, to bone through chemical ligation with bisphosphonate has been achieved and demonstrated an over five times greater antineoplastic activity against osteosarcoma compared to methotrexate alone [37]. Hirabayashi et al. [38] described the development of diclofenac prodrugs linked to bisphosphonate (DIC-BP) creating an osteotropic drug delivery system (ODDS). Their results demonstrated that the synthesized

prodrug provides a localized and prolonged release of diclofenac, while at the same time preventing adverse side effects in the stomach. In an attempt to achieve higher drug loading per molecule alendronate and an also bone targeting aspartic acid peptide were conjugated to water-soluble polymers as polymer based bone targeting system. Alendronate and aspartic acid were introduced in the polymers either by direct conjugation or by copolymerization with the corresponding monomers. The obtained results for their bone targeting affinities also showed that these novel delivery systems were accumulated in the bone tissue [39].

The main drawbacks for conjugating bisphosphonates to polymers or other compounds are the limited abilities to detect their binding due to the lack of a sufficient chromophore and the limited solubility in non aqueous media due to their high polarity.

The goal of this study was the establishment of a synthesis providing a bisphosphonate labeled poly(ethylene glycol) suitable for the surface functionalization of differently sized gold particles in order to provide systems for the investigation of bone targeting of nanoparticles. In order to achieve this, an organic soluble bisphosphonate with an aromatic ring as chromophore was chosen to conjugate to thiol alkane modified poly(ethylene glycol). The polymers should, furthermore, be provided with a high purity in order to estimate the surface composition on the later used gold particles based on the polymer amounts used for their assembly.

2. Materials and Methods

Tetraethyl methylenebisphosphonate, diethylamine, 11-bromo-1-undecene, sodium hydride, N-hydroxysuccinimide (NHS), N,N\-dicyclohexylcardodiimide (DCC), ethylene oxide, and ammonium persulfate, were obtained from Fluka (Buchs, Switzerland). P-toluene sulfonic acid monohydrate, 3,5-diaminobenzoic acid, poly(ethylene glycol) monomethyl ether (mPEG, M_w 2000 Da), α,α´ azoisobutyronitrile (AIBN), thioacetic acid, potassium bis(trimethylsilyl) amide, di-t-butyl dicarbonate (BOC), tetramethylsilane (TMS), bromotrimethylsilane, amylamine, DEAE-sephadex A25 and dialysis tubing with a molecular weight cut-off (MWCO) of 1000 Da were acquired from Sigma-Aldrich Chemical Company (Steinheim, Germany). Paraformaldeyde, calcium hydride, methanol, toluene, dichloromethane, chloroform, acetonitrile, tetrahydrofuran (THF), acetone, 1,4-dioxane, sodium sulphate, hydrochloric acid, sulfuric acid, acetic acid, sodium acetate, ammonium carbonate, zinc powder, ammonium heptamolybdate tetrahydrate, diethyl ether, ascorbic acid and hydroxyapatite (HA) were purchased from Merck (Darmstadt, Germany). Deuterated

chloroform was from Deutero GmbH (Kastellaun, Germany). Ibandronate as standard substance was a generous gift from Boehringer (Mannheim, Germany).

2.1. Synthesis of 3,5-Di(ethylamino-2,2-bisphosphono)benzoic Acid:

3,5-Di(ethylamino-2,2-bisphosphono)benzoic acid as bisphosphonate carrying label for the polymers was synthesized according to a procedure described by Bansal et al. [40] (Scheme 1). Briefly, dietylamine (0.580 g, 8 mmol) and paraformaldeyde (1.212 g, 40 mmol) were added to 25 ml of methanol and the mixture was slightly warmed until a clear solution was obtained. Tetramethyl methylenebisphosphonate **(1)** (2.326 g, 8 mmol) was added and the mixture was refluxed for 24 h, and methanol was removed under vacuum and subsequent addition and evaporation of toluene. This last step was repeated to ensure complete removal of methanol from the solution of the product. This reaction leads to the formation of tetraethyl 2-methoxyethylene-bisphosphonate **(2),** which was finally dissolved in 100 ml of toluene. Catalytic amounts of p-toluenesulfonic acid monohydrate (5 mg) were added and the solution was refluxed for 14 h using a Soxhlet apparatus containing calcium hydride for the complete removal of methanol and water. After the reaction toluene was evaporated and the obtained product was dissolved in chloroform (50 ml) and washed three times with 30 ml of water. The organic layer was subsequently dried with anhydrous sodium sulphate and concentrated to yield an oily residue. The crude product was purified by fractional distillation to a produce a clear liquid of the boiling point 115-116 °C, which is characteristic for the tetraethyl ethenylidenebis(phosphonate) intermediate **(3)** [41]. The intermediate **(3)** (0.96 g, 3.2 mmol) and 3,5-diaminobenzoic acid (**4**, 0.24 g, 1.6 mmol) were subsequently heated in 30 ml of tetrahydrofuran at 60 °C for 5 h to produce 3,5-di(tetraethyl ethylamino-2,2-bisphosphonate) benzoic acid (**5**). Tetrahydrofuran was removed under vacuum and the product **(5)** (0.9 g, 1.18 mmol) was dissolved in dry dichloromethane (10 ml) and bromotrimethylsilane (4.02 g, 26.2 mmol) was added drop wise at 0 °C. The obtained mixture was then stirred at room temperature for two days. Finally, dichloromethane was evaporated and 3,5-di(ethylamino-2,2-bisphosphono)benzoic acid **(6)** was obtained and purified by anion exchange chromatography using DEAE-sephadex A25.

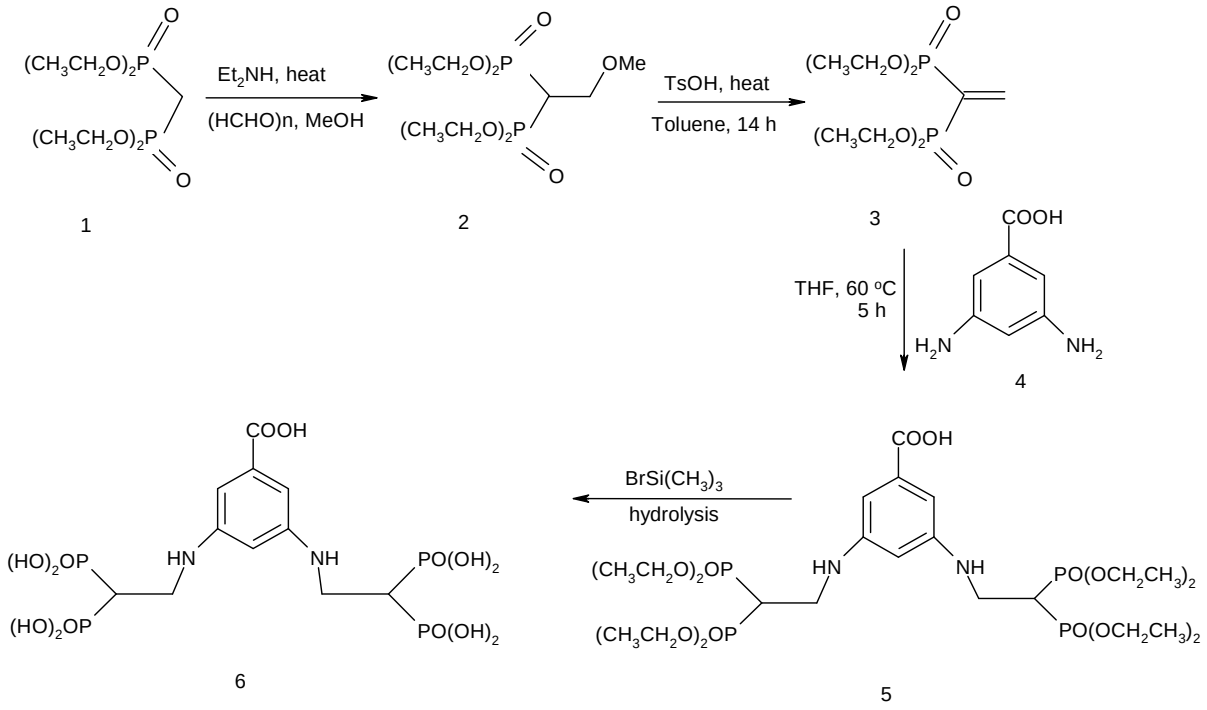

Scheme 1: Synthesis of targeting ligand for hydroxyapatite binding

2.2. Purification of bisphosphonate by DEAE-sephadex A25

A weak anion exchange material, DEAE-sephadex A25, was used for the purification of the hydrolyzed bisphosphonate. The sephadex was swollen in acetate buffer (pH=4) for two days; the dissolved bisphosphonate was than loaded in the same buffer onto the swollen column material. Resin loaded with bisphosphonate was washed two times with the loading buffer using Buchner funnel to remove the impurities. Bisphosphonate was eluted from the resin by using 0.2 M ammonium carbonate. The ammonium carbonate solution was then freeze dried giving dry product. The pure final product was characterized by ^{1}H, ^{13}C, ^{31}P-NMR, ion pair chromatography, and mass spectroscopy

2.3. Bisphosphonate characterization

2.3.1. NMR analysis

^{1}H-NMR (nuclear magnetic resonance spectroscopy) spectra were recorded on a Bruker Avance 600 spectrometer (Bruker Biospin, Rheinstetten, Germany).

2.3.2. Ion-pair chromatography

Samples with hydrolyzed bisphosphonate group were investigated by high pressure liquid chromatography (HPLC) using a setup consisting of a DGU-14A degasser, LC-10-AT pump, SIL-10 AD autosampler, RF-10A XL fluorescence detector, SPD-10A VP UV-Vis

detector and SCL-10A VP controller (Shimadzu, Duisburg, Germany). The samples were separated on C_{18} column (25 cm × 4.6 mm I.D., 5 µm) purchased from Supleco (Deisenhofen, Germany). The mobile phase used was a mixture of 18 mM *n*-amylamine aqueous solution (adjusted to pH 7.0 with acetic acid) and acetonitrile (95%:5% (V/V)). The flow rate was kept constant at 1 ml/min and the experiments were conducted at room temperature [42,43].

2.3.3. ESI-Mass

Mass spectra of the synthesized compounds were obtained using the TSQ7000 electrospray- mass spectrometer (ThermoQuest, San Jose, CA, USA) with the detection range of 1-1000 Da.

2.4. Synthesis of poly(ethylene glycol)-undecyl mercaptane derivatives:

2.4.1. Methoxy poly(ethylene glycol)-undecyl mercaptane ($mPEG_{2000}C_{11}H_{22}SH$)

To synthesize thioalkylated poly(ethylene glycol) monomethyl ether, the synthetic Scheme 2 was applied. 5 g (2.5 mmol) of methoxy poly(ethylene glycol) **(7)** were melted in an oil bath under argon atmosphere. 600 mg (25 mmol) of sodium hydride were added to the molten mPEG and stirred at 110-120 ^{o}C until the evolution of hydrogen abated (about 20 minutes). 11-bromo-1-undecene **(8)** (2.33 ml, 10 mmol) was added to the reaction flask and the mixture was stirred at the same temperature overnight to form the ether product. At the end of the reaction, the remaining hydride was quenched by the addition of 30 ml of methanol. After evaporation of methanol, the residue was dissolved in toluene, filtered to remove inorganic salts precipitated in toluene. Finally, toluene was evaporated and the obtained residue was dissolved in acetone and precipitated in cold diethyl ether to yield the product methoxy poly(ethylene glycol)-undecene **(9)**. For the addition of thioacetic acid to the terminal double bond, 4.4 g (2 mmol) of the intermediate **9** and 0.480 g (3 mmol) of α,α'-azo-isobutyronitril (AIBN) were dissolved in 30 ml of dry methanol (dried by using a molecular sieve of 4Å). 2 ml of thioacetic acid were added and the reaction mixture was stirred under reflux for 72 h. Finally, remaining methanol was evaporated using the rotary evaporator, and the obtained polymer residue was dissolved in acetone and subsequently precipitated in cold diethyl ether yielding compound **10** [17]. The following hydrolysis of the thioacetate ester **10** to the free thiol group was carried out in methanolic HCl as described by Bain et al. [22] to give the methoxy poly(ethylene glycol)-undecyl mercaptane (**11 a),** which was purified by repeated precipitation in cold diethyl ether. The synthesized polymer was characterized by ^{1}H-NMR and HPLC to determine the conversion and the purity of the synthesized compound.

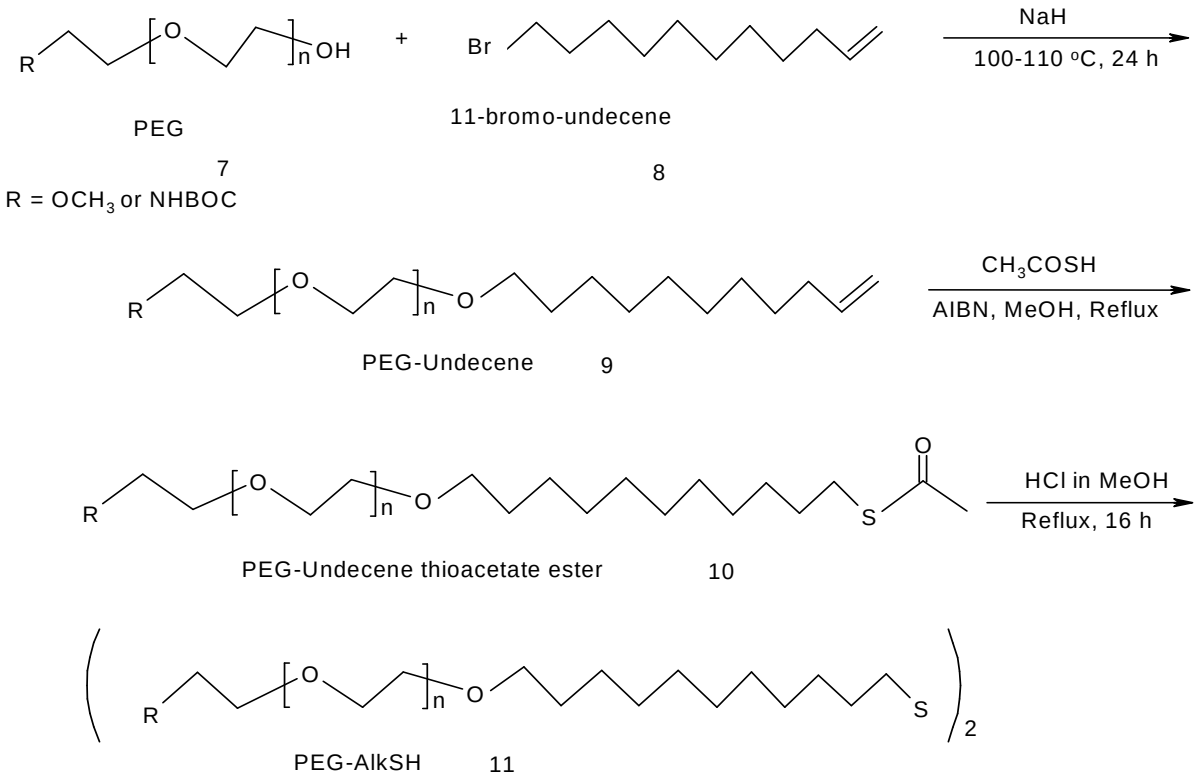

11a; R = OCH_3; methoxy poly(ethylene glycol)-undecyl mercaptane
11b; R = NH_2; amino poly(ethylene glycol)-undecyl mercaptane

Scheme 2: Synthesis of the bifunctional PEG-undecyl mercaptane

2.4.2. Amino poly(ethylene glycol)-undecyl mercaptane (H_2N-$PEG_{2000}C_{11}H_{22}SH$).

A similar reaction scheme (Scheme 2) was applied for the synthesis of the corresponding amine derivative of the polymer with some slight modifications due to the present amine group. Amine group protected t-butoxycarbonyl amino (polyethylene glycol) (BOC-NH-PEG) was used instead of methoxy poly(ethylene glycol) in order to prevent the alkylation of the amine group during the Williamson ether synthesis. The corresponding poly(ethylene glycol)-monoamine was synthesized by polymerization of ethylene oxide with potassium bis(trimethylsilyl) amide as anionic initiator according to methods described in literature [44,45]. The terminal amine group was then protected by di-t-butyl dicarbonate (BOC) by stirring it overnight in a mixture of dioxane and water in the presence of potassium hydroxide [46]. The efficiency of obtained amine protection was examined by measurement with the amine reactive fluorescamine [47,48]. After amine group protection, the reaction with 11-bromundecene was completed as described above for the methyl terminated poly(ethylene glycol). In the final step, the used methanolic HCl hydrolyzed not only the

thioacetate ester to free thiol, but also deprotected BOC protected amine to yield the free amino poly(ethylene glycol)-undecyl mercaptane **(11 b)**.

2.4.3. Conjugation of amino poly(ethylene glycol)-undecyl mercaptane with 3,5-di(tetraethyl ethylamino-2,2-bisphosphonate)benzoic acid.

The polymer was conjugated to the bisphosphonate carrying benzoic acid using standard carbodiimide chemistry as depicted in reaction Scheme 3. Briefly, 1.5 g (2 mmol) of the still ethyl protected bisphosphonate compound **5** were dissolved in 50 ml of dry dioxane (dried by 4Å molecular sieve). To this solution, 0.46 g of N-hydroxysuccinimide (4 mmol) and 0.824 g (4 mmol) of N,N'-dicyclohexylcardodiimid were added and the obtained solution was stirred for two hours at room temperature in order to activate the carboxyl group of the bisphosphonate for the reaction. After that, 2.2 g (1 mmol) of the amine terminated poly(ethylene glycol)-undecyl mercaptane (**11b**) were added and the flask was further stirred for two days. Afterwards the precipitated dicycloexylurea was filtered off, and the solvent dioxane was evaporated under vacuum, the obtained product was again dissolved in acetone and precipitated twice in cold diethyl ether, and finally collected by suction filtration and subsequently dried under vacuum. To obtain the final product bearing the free bisphosphonate group, the ethyl groups of the esters were removed by subsequent mild hydrolysis using bromotrimethylsilane as reagent. 3 g of the compound **13** were dissolved in 10 ml of dichloromethane and cooled to 0 °C. 5 ml of bromotrimethylsilane were added drop-wise to this solution and the mixture was further stirred at room temperature for two days. After evaporation of dichloromethane, 20 ml of methanol were added and the mixture was stirred overnight and subsequently methanol was removed by heat treatment. The dried final product was dissolved again in buffer and subsequently purified by DEAE-sephadex A25 similarly as described for the bisphosphonate and finally dried using freeze drying of the eluted buffer solution. Only, a further purification step was added, which is the dialysis of the freeze dried product for two days against de-ionized water using dialysis tubing of molecular weight cutoff (MWCO) 1000 Da in order to remove non-evaporated buffer salts and eventually free bisphosphonate also retained by the ion exchange column.

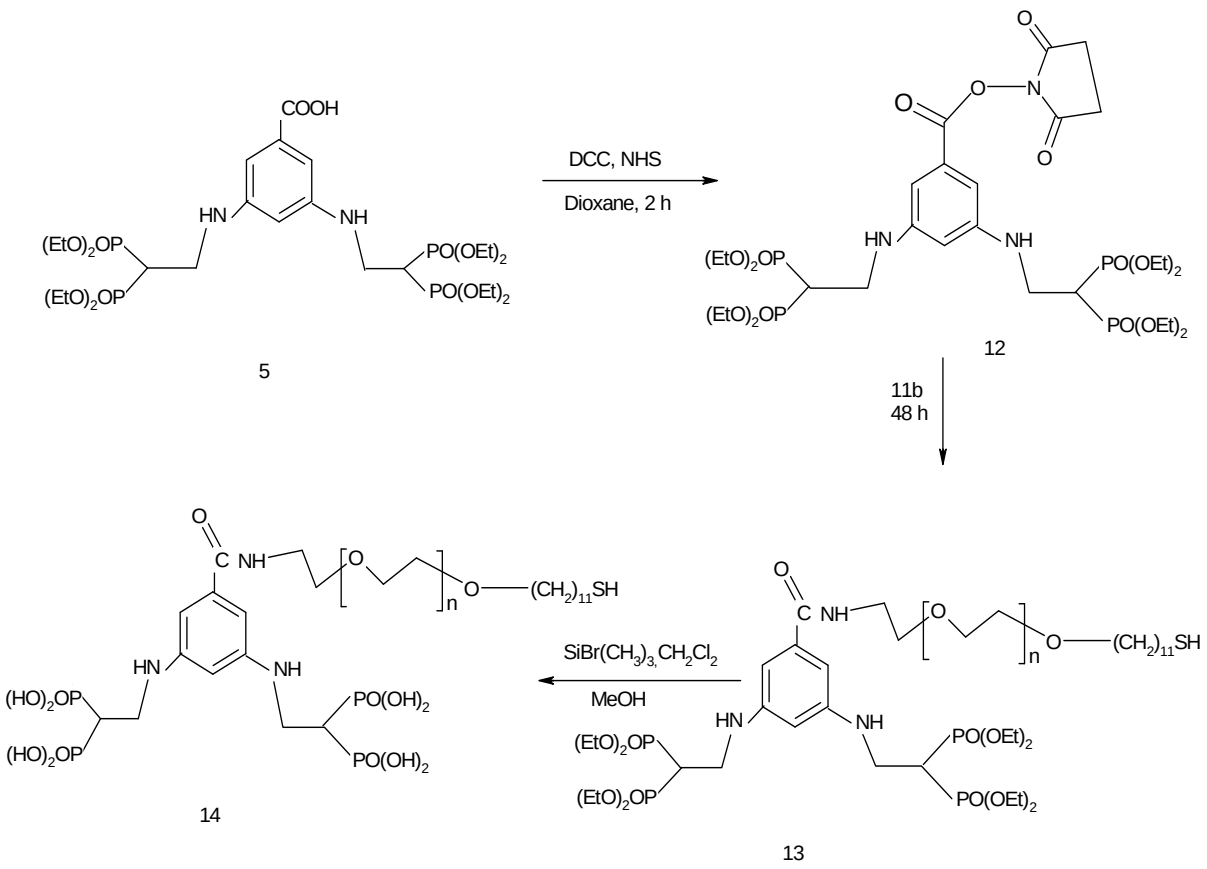

Scheme 3: Synthesis of bisphosphonate conjugated polymer

2.5. Polymer characterization

2.5.1. ^{1}H-NMR

For NMR spectra of the polymers, they were dissolved in $CDCl_3$ with tetramethyl-silane as internal standard, if applicable due to the solubility of the bisphosphonate, and subsequently measured using Bruker Avance 600 spectrometer (Bruker Biospin, Rheinstetten, Germany).

2.5.2. MADI-ToF mass Spectrometry

Matrix assisted laser desorption/ionization mass spectrometry (MALDI-ToF MS) data were acquired on a HP G2030A spectrometer using a positive ion mode. The polymers were analyzed using the molecular weight range of 0-6000 m/z, data were recorded for about 150 laser shot per spectrum using indoleacrylic acid dissolved in THF (0.15 mg/ml) as matrix component. The samples were prepared on the MALDI target by depositing 1 µl of a mixture of matrix solution and polymer solution (1 mg/ml) (3:1), which were subsequently dried under vacuum at room temperature.

2.5.3. RP-HPLC

HPLC analysis of the synthesized polymers was performed on the same HPLC system as used for analysis of the bisphosphonate. A linear gradient of 20% to 100% solvent B (90% acetonitrile in water) in solvent A (10% acetonitrile in water) over 30 min. was applied as mobile phase at a flow rate of 1 ml/min. 50 µl samples (5 mg/ml) were separated at 40 °C using a combination of two macroporous reversed phase columns, namely a PLRP-S guard column and an analytical column (PLRP-S 300 Å, 5 µm, Polymer Laboratories, Amherst/MA, USA). The samples were detected by a low temperature evaporative light scattering detector (ELSD–LT Shimadzu GmbH, Duisburg, Germany).

2.5.4. Phosphate assay

The phosphate content of the polymers modified with bisphosphonate was determined according to a reported test method [49]. For the phosphate detection organic bound bisphosphonates are oxidized to orthophosphate by ammonium persulfate followed by a reaction with molybdenum-ascorbate to yield the phosphomolybdate chromophore, which is detected at 820 nm using UV-Vis spectroscopy. A standard substance for bisphosphonate (ibandronate) was used for the preparation of a calibration curve. Briefly, 0.1 ml of a solution containing 1-10 µM of ibandronate were mixed with 0.1 ml of 50 µM ammonium persulfate and the samples were heated in a boiling water bath for 5 minutes. Then 1 ml of the molybdate-ascorbate reagent [50] was then added and the samples were heated for another 10 minutes in the boiling water bath. After cooling down to room temperature, the absorbance was measured at 820 nm using a plate reader (Shimadzu CS-9301 PC, Shimadzu, Duisburg, Germany). An amount of the final product equivalent to 2.5 µM phosphate was then taken and treated similar to ibandronate for the quantification of the incorporated bisphosphonate molecules.

2.6. Testing the polymer's binding functionalities (binding to hydroxyapatite or gold)

The dual functionalities of the polymer were explored by testing its affinity to hydroxyapatite (HA) powder (due to the presence of bisphosphonate groups) and gold surfaces (due to the presence of the alkanethiol part). For HA binding, 2 ml of the polymer modified with free bisphosphonate (1 mg/ml) were added to an Eppendorf centrifuge tube containing 10 mg of accurately weighed hydroxyapatite powder. The tube was agitated in a horizontal shaker adjusted to 200 rpm at room temperature overnight. After that, the tube was centrifuged at 3000 rpm and the liquid supernatant was subsequently analyzed by the above described ion pair HPLC [51].

Binding to gold surfaces was tested according to the following procedure: 1 ml of free bisphosphonate modified polymer solution (1mg/ml) was added to four glass cover slips coated by a thin layer of gold (18*18 mm) at room temperature. After one day of shaking, the solution was analyzed for the presence of the polymer by HPLC [12].

3. Results and Discussion

3.1. Synthesis of 3,5-Di(ethylamino-2,2-bisphosphono)benzoic Acid:

The two bisphosphonate compounds **5** and **6** were synthesized as targeting ligands, since they are suited to overcome problems associated with the commercially available bisphosphonates, like solubility in organic solvents or lack of possible conjugation schemes to the PEG derivatives. The used bisphosphonates have the following advantages: firstly, two bisphosphonate groups are contained in one attached molecule, which then consequently has a higher hydroxyapatite binding affinity compared to compounds containing only one bisphosphonate group. Secondly, the ease of detection due to the presence of an aromatic benzene ring, which can be either detected using its fluorescence or alternatively by UV absorption, which is sufficient to distinguish it from the unmodified PEG polymer. Furthermore, the compounds both provide a free carboxylic group for subsequent easy conjugation with primary amines using DCC chemistry. The synthesis of the ester 3,5-di(tetraethyl ethylamino-2,2-bisphosphonate)benzoic acid **5** and the free acid 3,5-di(ethylamino-2,2-bisphosphono)benzoic acid **6** are depicted in Scheme 1. The synthesis started with bisphosphonate compound **1,** which underwent methoxy methylation with methanol and paraformaldehyde in the presence of diethyl amine to yield the intermediate **2** (first step). [^{1}H-NMR spectrum for **2,** δ_H ($CDCl_3$): 4.19 (m, 8H, OCH_2CH_3), 3.63 (m, 2H, CH_3OCH_2), 3.2 (s, 3H, CH_3O), 2,52 (tt, 1H, PCHP) and 1,18 (t, 12H, CH_2CH_3)].

The unstable Intermediate **2** was then converted to the unsaturated compound **3** by elimination of methanol, catalyzed by refluxing it with trace amounts of p-toluenesulfonic acid in toluene. Methanol is thereby removed from the reaction mixture by calcium hydride using a Soxhlet apparatus (step 2). [^{1}H-NMR spectrum for **3,** δ_H ($CDCl_3$): 6.98 (dd, 2H, CH_2=), 4.15 (m, 8H, OCH_2CH_2), and 1.3 (m, 12H, CH_3CH_2)]. The chemical shifts of both compounds **2** and **3** are in a good agreement with that described in the literature [40,41].

Compound **5** was obtained by anti-Markovnikov addition of the amine groups of 3,5-diaminobenzoic acid, compound **4**, to the double bond of intermediate **3** (step 3). [^{1}H-NMR spectrum for **5,** δ_H ($CDCl_3$): 6.91 (s, 2H, ortho protons of benzene ring), 6.15 (s 1H, para proton of benzene ring), 4.15 (m, 16H, -O-C**H**$_2$-CH_3), 3.78 (m, 4H, -NH-C**H**$_2$-CH), 2.75 (tt,

2H, P-C**H**-P) and 1,37 (t, 24H, -O-CH_2-C$\mathbf{H}_3$). ESI-Mass spectrum for **5** is presented in Figure 1; MS: *m/z* 753.2 ($M+H^+$), 775.2 ($M+Na^+$) and 791.2 ($M+K^+$)].

Hydrolysis of the phosphonate esters of compound **5** was achieved by using the mild dealkylating agent also used for peptide synthesis, bromotrimethylsilane (step 4). Bromotrimethylsilane here firstly forms a silyl ester intermediate with replacing of the ethyl groups. This silyl ester is unstable and can subsequently be easily hydrolyzed by water or methanol yielding the free acid form (compound **6**). The ^{1}H-NMR spectrum for **6** demonstrated disappearance of the phosphonate esters due to the lack of any signals from the ethyl groups. [MS *m/z* 527.2 (M^-), 263.1 (M^{2-}) and 174.8 (M^{3-})].

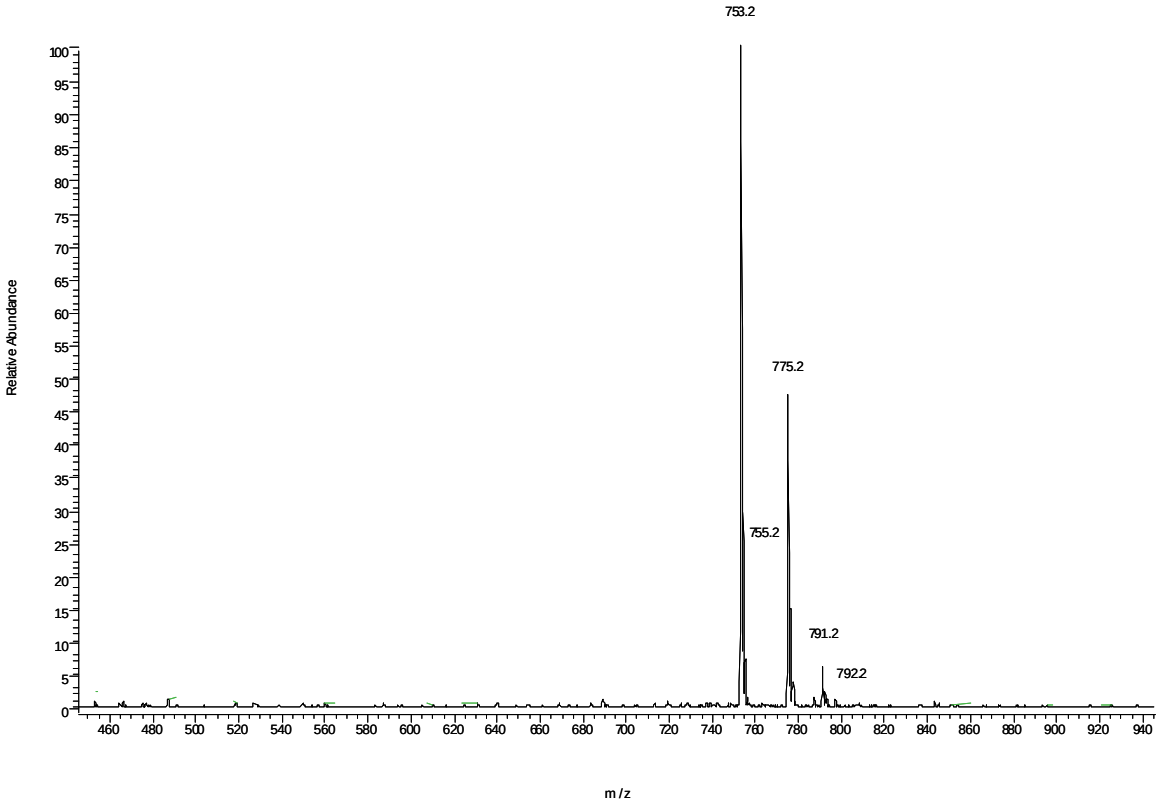

*Figure 1: ESI-Mass spectra of 3,5-di(tetraethyl ethylamino-2,2-bisphosphonate)benzoic acid(compound **5**)*

3.2. Synthesis of poly(ethylene glycol)-undecyl mercaptanes:

3.2.1. Methoxy poly(ethylene glycol)-undecyl mercaptane ($mPEG_{2000}C_{11}H_{22}SH$).

Alkanethiol terminated poly(ethylene glycol) monomethyl ether was obtained through a three-step synthesis as described in reaction Scheme 2. For the reaction the poly(ethylene glycol) monomethyl ether **(7)** was deprotonated by 10 equivalents of sodium hydride and subsequently reacted with an excess of the 11-bromo-1-undecene **(8)** in order to obtain a complete modification of the added PEG polymers to methoxy poly(ethylene glycol)-

undecene **(9)**. Subsequently the polymers were precipitated in cold ether, which is a good solvent for eventually residual alkene. The terminal double bond of the alkene part is not reactive under these conditions and therefore did not need any protection. [^{1}H-NMR spectrum for intermediate **(9),** δ_H ($CDCl_3$): 5.8 (m, 1H, -C**H**=), 4.95 (t, 2H, C**H**$_2$=), 3.5-3.9 (m, ~180 H, -OC**H**$_2$C**H**$_2$-), 3.45 (m, 2 H, -OC**H**$_2$-C-C-C), 3,3 (s, 3 H, CH_3O-), 2.0 (m, 2 H, -CH_2CH=) and 1.7-1.2 (m, 14 H, the remaining protons of the alkene part)].

Radical addition of thioacetic acid to the double bond of compound **9** was performed by applying heat in the presence of AIBN as radical initiator. This reaction follows anti-Markovnikov rule and yields acetate protected thiol derivatives (**10**) with a high conversion (above 95%). The ^{1}H-NMR spectrum of compound **10** is characterized by the disappearance of the signals attributed to the double bond of the alkene located at 5.8, 4.95 and 2,0 ppm and the appearance of new signals at δ_H ($CDCl_3$): 2,85 ppm (t, 2 H, -CH_2S) and 2.3 ppm (s, 3H, -$SCOCH_3$) for the thioacetic acid part. There were no obvious changes observed for other proton signals, which are related to mPEG chain and the aliphatic part of the molecule. The final deprotection of the of the thioacetate group of compound **10** to free thiol was carried out under acidic condition using anhydrous solution HCl in MeOH [52,53]. [^{1}H-NMR spectrum of the final product $mPEG_{2000}C_{11}H_{22}SH$ (**11a**)**,** (Figure 2, above spectrum)**,** δ_H ($CDCl_3$) 3.5-3.9 (m, 180 H, -OCH_2CH_2), 3.45 (m, 2 H, -OCH_2-), 3.3 (s, 3 H, CH_3O-), 2.55 (tt, 2 H, -CH_2SH) and 1.7-1.2 (m, 18 H, the remaining protons of the alkane part)].

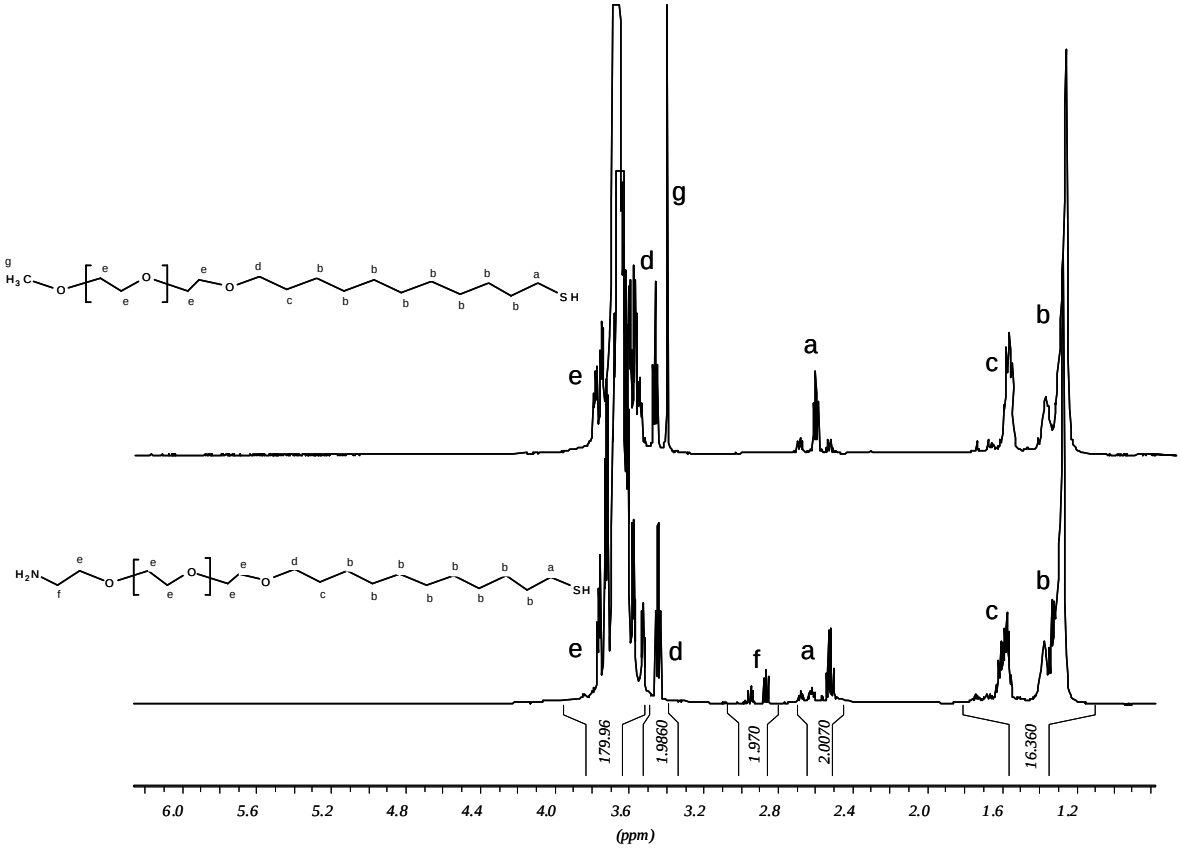

Figure 2: ^{1}H-NMR spectrum of methoxy poly(ethylene glycol)-undecyl mercaptane (above spectrum) and amino poly(ethylene glycol)-undecyl mercaptane (low spectrum)

3.2.2. Synthesis of amino poly(ethylene glycol)-undecyl mercaptane (NH_2PEG_{2000}-$C_{11}H_{22}SH$).

Poly(ethylene glycol) monoamine with a molecular weight of 2.000 Da was synthesized as reported earlier [45]. The actual molecular weight of the polymer was confirmed by MALDI-ToF and ^{1}H-NMR. The results indicated that the obtained average molecular weight of NH_2-PEG-OH was about 1960 Da. For the further reaction the primary amine of NH_2-PEG-OH was protected with an excess of BOC-anhydride in presence of potassium hydroxide solution. Under these alkaline conditions, BOC protection is only achieved for the amine group, since the diester formed with the hydroxyl group is again cleaved under these reaction conditions. Based on a standard fluorescamine assay, it was found that the protected polymer contains less than 1% free amine indicating a sufficient protection of the terminal amine with BOC. [^{1}H-NMR spectrum of BOC-NH-PEG-OH is characterized by the following signals; δ_H ($CDCl_3$): 3.5-3.9 ppm (m, 180 H, -OCH_2CH_2-) and 1.45 ppm (s, 9 H, -$C(CH_3)_3$)].

The BOC protected poly(ethylene glycol)-monoamine was then reacted with 11-bromo-1-undecene in the presence of sodium hydride as described for the methoxy derivative

to yield the protected poly(ethylene glycol) monoamine-undecene as described in Scheme 2. The use of the BOC-protected polymer prevented the possible alkylation of the amine group to take place. The reaction was then completed with the thiol addition and the hydrolysis of the protective groups as described for the synthesis of methoxy poly(ethylene glycol)-undecyl mercaptane. [^{1}H-NMR spectrum of pure amino poly(ethylene glycol)-undecyl mercaptane (**11 b**) is presented in Figure 1 (low spectrum). The spectrum is characterized by the following signals δ_H ($CDCl_3$) 3.5-3.9 (m, 180 H, OCH_2CH_2), 3.45 (m, 2 H, -OCH_2-), 2.8 (t,t, 2 H, -CH_2NH_2), 2.55 (tt, 2 H, -CH_2SH) and 1.7-1.2 (m, 18 H, the remaining protons of the alkane part)].

3.2.3. RP-HPLC:

HPLC chromatograms of the different synthesized and used polymers are presented in Figure 3, the chromatogram of the methoxy poly(ethylene glycol)-undecyl mercaptane (mPEG-AlkSH) is characterized by two neighboring peaks. The first peak eluted at about 20 minutes is related to the reduced (singly present) portion of the synthesized polymer and the second peak eluted at about 22 minutes is related to the oxidized, dimeric portion of the polymer. Both alkylated polymer species are retained longer on the solvent material, which is related to their increase hydrophobicity compared to methoxy poly(ethylene glycol) (mPEG), which is eluted at 16 minutes. The oxidized polymers are eluted at the later time point, because the oxidized form has a high molecular weight and at the same time it is less hydrophilic due to the presence of the disulfide bond.

The chromatogram of the corresponding poly(ethylene glycol) monoamine is also characterized by a single peak eluted at about 15 minutes, which is significantly broader than the methoxy derivative since it is obtained by custom synthesis. In case of the modified amino poly(ethylene glycol)-undecyl mercaptane (NH_2-PEG-AlkSH), also two peaks can be detected in the chromatogram. One peak eluting at 19 minutes due to the reduced portion and the other peak eluted at about 22 minutes, which is due to the oxidized portion of the polymer. The broad peaks obtained for these polymers are due to the wider molecular weight distribution of the poly(ethylene glycol) monoamine used for the synthesis of the thioalkylated polymer [54].

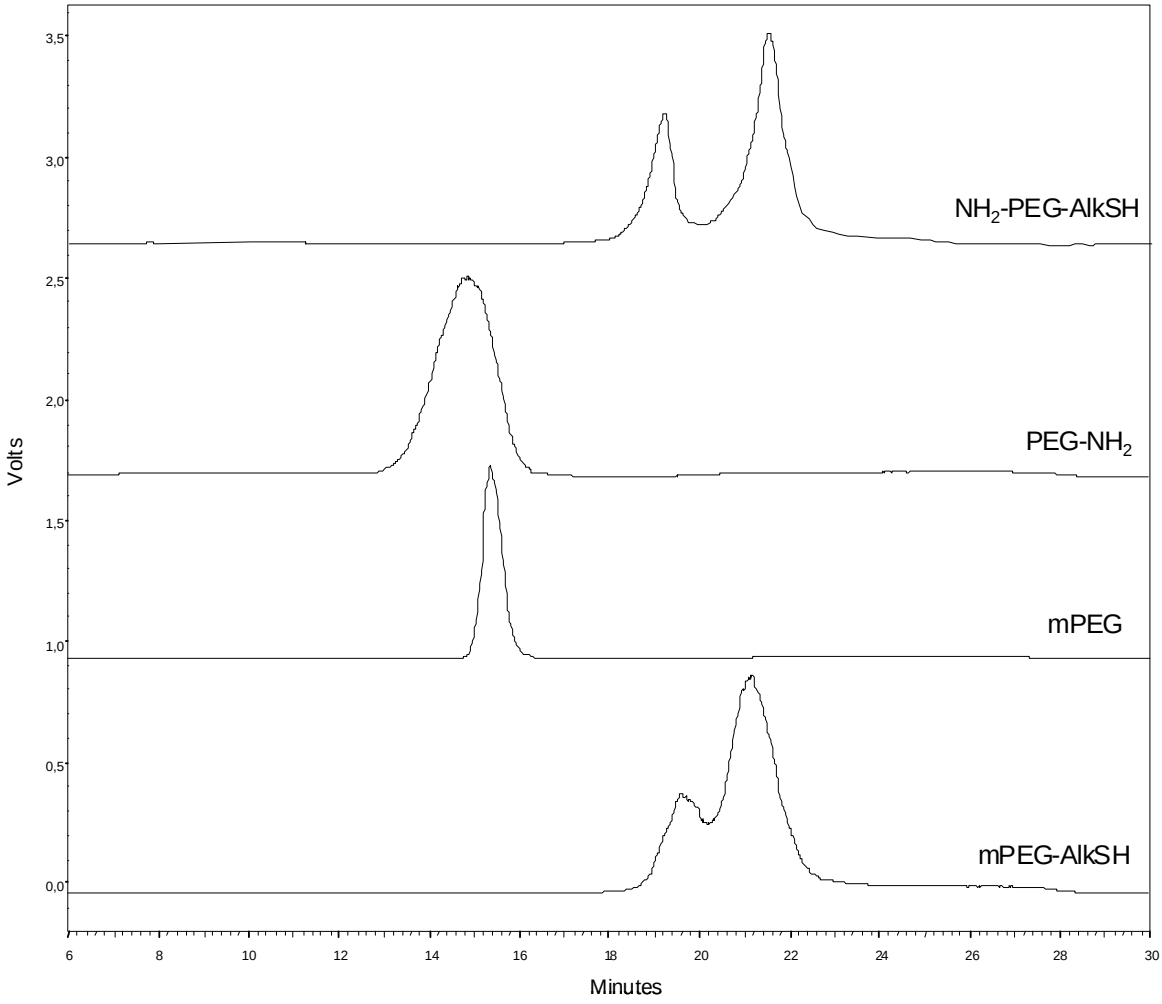

Figure 3: HPLC chromatograms of methoxy poly(ethylene glycol)-undecyl mercaptane (mPEG-AlkSH), methoxy poly(ethylene glycol) (mPEG), poly(ethylene glycol) monoamine (PEG-NH_2) and amino poly(ethylene glycol)-undecyl mercaptane(NH_2PEG-AlkSH)

3.2.4. MALDI-ToF mass spectrometry

For further characterization and elucidation of the obtained polymer structures, matrix-assisted laser desorption/ionization time-of-flight mass spectroscopy (MALDI-ToF-MS) was used. The peak molecular weight (M_p) of the synthesized poly(ethylene glycol) monoamine was found to be 1947 Da, which approximates the molecular weight calculated by ^{1}H-NMR. Adjacent peaks differing from each other by a mass difference of 44 Da represent the typical mass of one ethylene oxide unit, which is the repeating unit of the PEG chain. MALDI-ToF mass spectra of methoxy poly(ethylene glycol)-undecyl mercaptane and amino poly(ethylene glycol)-undecyl mercaptane proved that the polymers are obtained as mixtures of the reduced and oxidized form as demonstrated by the observed double molecular weights. The peak molecular weight of the reduced form of amino poly(ethylene glycol)-undecyl mercaptane

was 2148 Da, which agrees with the calculated value. The peak molecular weight of the oxidized form is about 4232 Da, which can be explained with the formation of disulfide form of two polymer chains. Similar values were measured for the molecular weights of the methoxy poly(ethylene glycol)-undecyl mercaptane, 2158 Da were observed for the monomer and 4431 Da for the dimer.

3.2.5. Polymer modified with bisphosphonate:

For the final modification of the amino poly(ethylene glycol)-undecyl mercaptane the unhydrolyzed bisphosphonate was linked to the polymer via an amide bond between the carboxylic group of the bisphosphonate and the primary amine terminus of the polymer. The reaction was carried out applying standard DCC and NHS chemistry in non aqueous media as depicted in Scheme 3. The molar ratio between the bisphosphonate and the polymer was kept at 2:1, which is low compared to the ratios used in literature, to avoid a modification of both ends of the polymers with bisphosphonate (thiol should be kept free for the binding to gold) [55]. The measured ^{1}H-NMR spectrum of the product showed the characteristic peaks of both parts of the polymer and of the bisphosphonate. Bromotrimethylsilane supported hydrolysis of the ester group of the bisphosphonate resulted in the free bisphosphonate modified polymer (compound 14).

Bisphosphonates and also the polymers conjugated to these molecules are highly hydrophilic compounds and it is consequently very difficult to retain them sufficiently on a reversed phase column. For this reason, ion-pair HPLC has been used for separation of these compounds. To form the ion pair, the polymers are combined with a lipophilic positively charged amyl amine contained in the mobile phase, which can then be retained on the non polar stationary phase and still allow detection with ELSD detector, which is necessary to identify the non UV adsorbing polymers [56]. The HPLC chromatogram of the final product is compared to that of the free bisphosphonate (compound 6) and also amino poly(ethylene glycol)-undecyl mercaptane in Figure 4. The hydrolyzed bisphosphonate (compound **6**) (BP), which contains two free bisphosphonate groups, is eluted at about 16 minutes (detected by fluorescence detector). The polymer alone (NH_2-PEG-AlkSH), which doesn't contain any acidic functionality to pair with the amyl amine, is not retained on the C18 RP column and is consequently eluted very early with the injection peak at about 5 minutes (detected by ELSD). The synthesized polymer, which is modified with the bisphosphonate (BP-PEG-AlkSH) is eluted at about 10 minutes in between the two other compounds, and can be detected with both the fluorescence detector and the ELSD, which also indicated the incorporation of

polymer and bisphosphonate. The increase of the polymer's retention time modified with bisphosphonate in comparison to the polymer alone indicates that it contains the free bisphosphonate group and consequently it is retained inside the column for a longer time. The decrease in the retention time compared to the bisphosphonate alone indicates that the modified polymer is more hydrophilic than bisphosphonate, due to the presence of PEG chain and the disappearance of the carboxylic group. The small peak eluted later at 12 minutes is most likely again due to the oxidized form of the polymer.

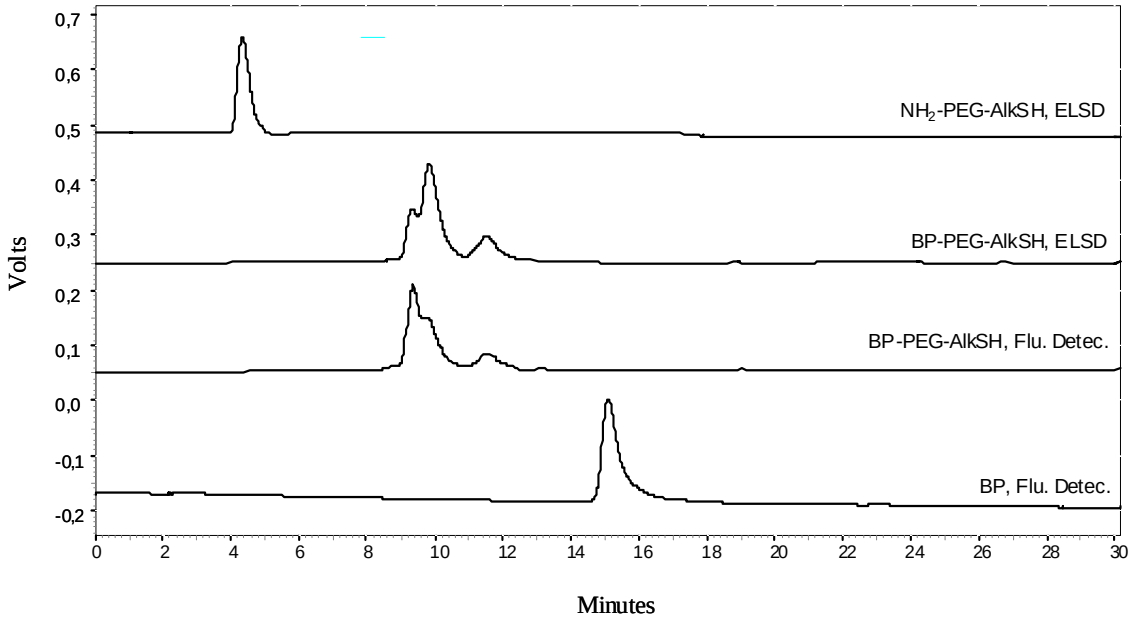

Figure 4: Ion-pair HPLC chromatograms of 3,5-Di(ethylamino-2,2-bisphosphono)benzoic acid using fluorescence detector, free bisphosphonate modified amino poly(ethylene glycol)-undecyl mercaptane using fluorescence detector and ELSD, and amino poly(ethylene glycol)-undecyl mercaptane using ELSD

The estimated bisphosphonate content of the polymer as determined from the phosphate assay is 97 ± 2,32 % of the theoretical value, which was quantified as inorganic phosphorus (using ibandronate for the standard curve) after oxidation and complexation with molybdate reagent. This also indicates a successful binding of the phosphate to the polymer and a successful removal of the excess of bisphosphonate by the dialysis.

3.3.6. Binding to hydroxyapatite and gold surface

The final bisphosphonate modified polymer exhibited a high affinity to gold and hydroxyapatite, which was determined by incubation with both substances. Figure 5 shows respective ion-pair HPLC chromatograms (using fluorescence detection) of the final product

before and after incubation with HA or gold. From the chromatograms, it can be concluded that the added polymer is removed completely from the incubation solution, since it is being adsorbed to HA or gold surfaces. For both incubated solutions no remaining peak is detectable, which can be compared with the run of the polymer alone without incubation. The high effectiveness of the removal of the polymer by both gold and HA confirm the presence of functional groups, the free bisphosphonate groups and the presence of thiol group.

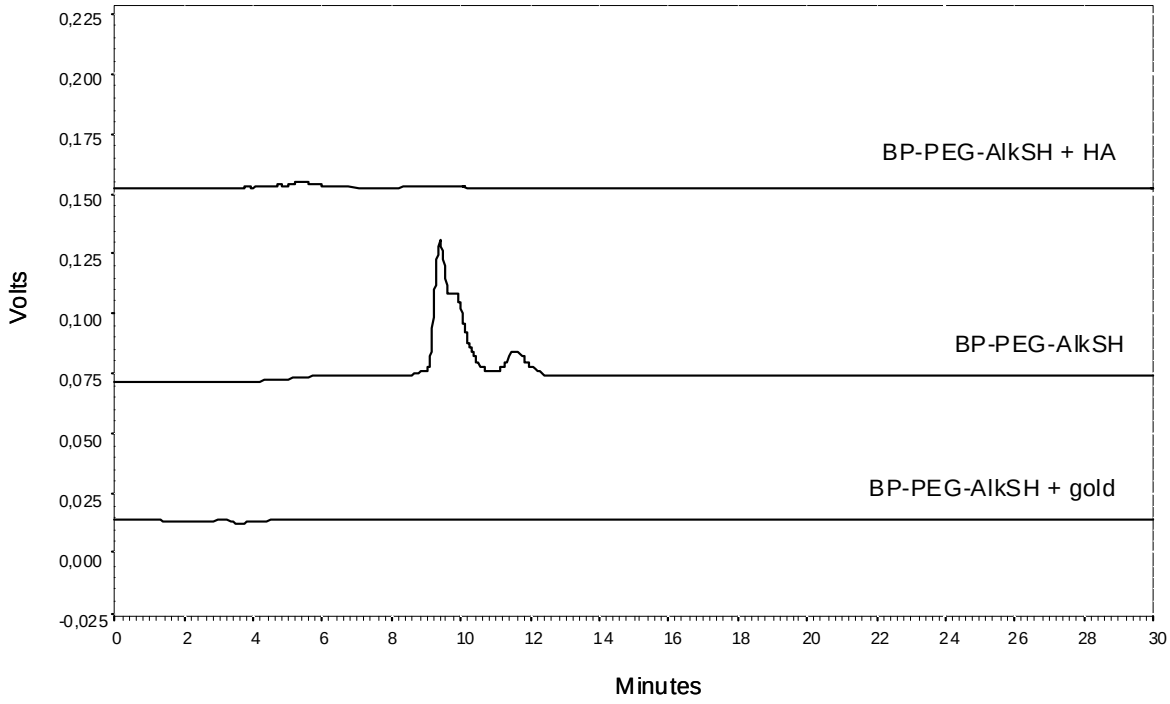

Figure 5: Ion-pair HPLC chromatograms of polymer modified with free bisphosphonate without HA and gold, after incubation with HA or with gold

4. Conclusions:

Bifunctional thioalkylated poly(ethylene glycol) derivatives have been successfully synthesized, which allow both the binding to gold and to hydroxyapatite surfaces. These polymers possess both a high affinity for gold surfaces due to the functionalization of the hydrophilic PEG polymer by a terminal thiol containing alkyl group. The polymer was further conjugated to a bisphosphonate moiety, which is known for its specific affinity to hydroxyapatite contained in bone tissue. Therefore, the synthesized bisphosphonate-modified polymer showed a high binding to the bone mineral hydroxyapatite. The presented data demonstrate that the synthesized bisphosphonate-modified polymers represent a well defined platform for the development of bone targeting drug delivery system based on gold nanoparticles functionalized with the PEG derivatives via the formation of self assembled monolayers. However, further experiments are necessary to optimize the functionalization of the nanoparticles with the synthesized polymers and to optimize the development of particulate-based bone drug delivery system intended for the treatment of bone diseases.

5. References

1. Claudia Fruijtier-Polloth, "Safety assessment on polyethylene glycols (PEGs) and their derivatives as used in cosmetic products," Toxicology **214,** 1-38 (2005).

2. Rob Webster, Eric Didier, Philip Harris, Ned Siegel, Jeanne Stadler, Lorraine Tilbury, and Dennis Smith, "PEGylated proteins: evaluation of their safety in the absence of definitive metabolism studies," Drug Metabolism and Disposition **35,** 9-16 (2007).

3. J. Milton Harris, Nancy E. Martin, and Marlene Modi, "Pegylation. A novel process for modifying pharmacokinetics," Clinical Pharmacokinetics **40,** 539-551 (2001).

4. Natalija Gorochovceva, Ruta Kulbokaite, Remigijus Juskenas, and Ricardas Makuska, "Synthesis and study of chitosan and poly(ethylene glycol) graft copolymers containing triazine moiety," Chemija **15,** 22-27 (2004).

5. M. J. Roberts, M. D. Bentley, and J. M. Harris, "Chemistry for peptide and protein PEGylation," Advanced Drug Delivery Reviews **54,** 459-476 (2002).

6. Olaf Kinstler, Graham Molineux, Michael Treuheit, David Ladd, and Colin Gegg, "Mono-N-terminal poly(ethylene glycol)-protein conjugates," Advanced Drug Delivery Reviews **54,** 477-485 (2002).

7. J. Milton Harris and Robert B. Chess, "Effect of PEGylation on pharmaceuticals," Nature Reviews Drug Discovery **2,** 214-221 (2003).

8. Steve Brocchini, Antony Godwin, Sibu Balan, Ji won Choi, Mire Zloh, and Sunil Shaunak, "Disulfide bridge based PEGylation of proteins," Advanced Drug Delivery Reviews **60,** 3-12 (2008).

9. Jing Li and W. John Kao, "Synthesis of Polyethylene Glycol (PEG) Derivatives and PEGylated-Peptide Biopolymer Conjugates," Biomacromolecules **4,** 1055-1067 (2003).

10. Kelley Britton Keys, Fotios M. Andreopoulos, and Nikolaos A. Peppas, "Poly(ethylene glycol) Star Polymer Hydrogels," Macromolecules **31,** 8149-8156 (1998).

11. N. A. Peppas, K. B. Keys, M. Torres-Lugo, and A. M. Lowman, "Poly(ethylene glycol)-containing hydrogels in drug delivery," Journal of Controlled Release **62,** 81-87 (1999).

12. Robert Knerr, Barbara Weiser, Sigrid Drotleff, Claudia Steinem, and Achim Goepferich, "Measuring cell adhesion on RGD-modified, self-assembled PEG monolayers using the quartz crystal microbalance technique," Macromolecular Bioscience **6,** 827-838 (2006).

13. W. A. Hild, M. Breunig, and A. Goepferich, "Quantum dots - Nano-sized probes for the exploration of cellular and intracellular targeting," European Journal of Pharmaceutics and Biopharmaceutics **68,** 153-168 (2008).

14. Takehiko Ishii, Yuka Sunaga, Hidenori Otsuka, Yukio Nagasaki, and Kazunori Kataoka, "Preparation of water soluble CdS quantum dots stabilized by functional poly(ethyleneglycol) and its application for bioassay," Journal of Photopolymer Science and Technology **17,** 95-98 (2004).

15. Hidenori Otsuka, Yukio Nagasaki, and Kazunori Kataoka, "PEGylated nanoparticles for biological and pharmaceutical applications," Advanced Drug Delivery Reviews **55,** 403-419 (2003).

16. C. Vericat, M. E. Vela, G. A. Benitez, J. A. M. Gago, X. Torrelles, and R. C. Salvarezza, "Surface characterization of sulfur and alkanethiol self-assembled monolayers on Au(111)," Journal of Physics: Condensed Matter **18,** R867-R900 (2006).

17. L. Dreesen, Y. Sartenaer, A. Peremans, P. A. Thiry, C. Humbert, J. Grugier, and J. Marchand-Brynaert, "Synthesis and characterization of aromatic self-assembled monolayers containing methylene and ethylene glycol entities by means of sum-frequency generation spectroscopy," Thin Solid Films **500,** 268-277 (2006).

18. Abraham Ulman, "Formation and Structure of Self-Assembled Monolayers," Chemical Reviews (Washington, D. C.) **96,** 1533-1554 (1996).

19. Lawrence H. Dubois and Ralph G. Nuzzo, "Synthesis, structure, and properties of model organic surfaces," Annual Review of Physical Chemistry **43,** 437-463 (1992).

20. Ralph G. Nuzzo, Lawrence H. Dubois, and David L. Allara, "Fundamental studies of microscopic wetting on organic surfaces. 1. Formation and structural characterization of a self-consistent series of polyfunctional organic monolayers," Journal of the American Chemical Society **112,** 558-569 (1990).

21. Marc D. Porter, Thomas B. Bright, David L. Allara, and Christopher E. D. Chidsey, "Spontaneously organized molecular assemblies. 4. Structural characterization of n-alkyl thiol monolayers on gold by optical ellipsometry, infrared spectroscopy, and electrochemistry," Journal of the American Chemical Society **109,** 3559-3568 (1987).

22. Colin D. Bain, E. Barry Troughton, Yu Tai Tao, Joseph Evall, George M. Whitesides, and Ralph G. Nuzzo, "Formation of monolayer films by the spontaneous assembly of organic thiols from solution onto gold," Journal of the American Chemical Society **111,** 321-335 (1989).

23. R. L. C. Wang, H. J. Kreuzer, and M. Grunze, "Molecular Conformation and Solvation of Oligo(ethylene glycol)-Terminated Self-Assembled Monolayers," Journal of Physical Chemistry B **101,** 9767-9773 (1997).

24. Boru Zhu, Thomas Eurell, Rico Gunawan, and Deborah Leckband, "Chain-length dependence of the protein and cell resistance of oligo(ethylene glycol)-terminated self-assembled monolayers on gold," Journal of Biomedical Materials Research **56,** 406-416 (2001).

25. Soumya R. Benhabbour, Heather Sheardown, and Alex Adronov, "Cell adhesion and proliferation on hydrophilic dendritically modified surfaces," Biomaterials **29,** 4177-4186 (2008).

26. Vivechana Dixit, Jeroen Van den Bossche, Debra M. Sherman, David H. Thompson, and Ronald P. Andres, "Synthesis and Grafting of Thioctic Acid-PEG-Folate Conjugates onto Au Nanoparticles for Selective Targeting of Folate Receptor-Positive Tumor Cells," Bioconjugate Chem. **17,** 603-609 (2006).

27. Jamie M. Bergen, Horst A. von Recum, Thomas T. Goodman, Archna P. Massey, and Suzie H. Pun, "Gold nanoparticles as a versatile platform for optimizing physicochemical parameters for targeted drug delivery," Macromolecular Bioscience **6,** 506-516 (2006).

28. Hasan Uludag, "Bisphosphonates as a foundation of drug delivery to bone," Current Pharmaceutical Design **8,** 1929-1944 (2002).

29. Anke J. Roelofs, Keith Thompson, Sharon Gordon, and Michael J. Rogers, "Molecular Mechanisms of Action of Bisphosphonates: current Status," Clinical Cancer Research **12,** 6222s-6230s (2006).

30. Sung Wook Choi and Jung Hyun Kim, "Design of surface-modified poly(d,l-lactide-co-glycolide) nanoparticles for targeted drug delivery to bone," Journal of Controlled Release **122,** 24-30 (2007).

31. Sebastien A. Gittens, Keith Bagnall, John R. Matyas, Raimar Lobenberg, and Hasan Uludag, "Imparting bone mineral affinity to osteogenic proteins through heparin-bisphosphonate conjugates," Journal of Controlled Release **98,** 255-268 (2004).

32. Sebastien A. Gittens, Pavel I. Kitov, John R. Matyas, Raimar Loebenberg, and Hasan Uludag, "Impact of Tether Length on Bone Mineral Affinity of Protein-Bisphosphonate Conjugates," Pharmaceutical Research **21,** 608-616 (2004).

33. Sebastien A. Gittens, John R. Matyas, Ronald F. Zernicke, and Hasan Uludag, "Imparting bone affinity to glycoproteins through the conjugation of bisphosphonates," Pharmaceutical Research **20,** 978-987 (2003).

34. Sebastien A. Gittens, Geeti Bansal, Cezary Kucharski, Mark Borden, and Hasan Uludag, "Imparting mineral affinity to fetuin by bisphosphonate conjugation: a comparison of three bisphosphonate conjugation schemes," Molecular Pharmaceutics **2,** 392-406 (2005).

35. Hasan Uludag and Jennifer Yang, "Targeting Systemically Administered Proteins to Bone by Bisphosphonate Conjugation," Biotechnology Progress **18,** 604-611 (2002).

36. Hasan Uludag, Niki Kousinioris, Tiejun Gao, and Darko Kantoci, "Bisphosphonate Conjugation to Proteins as a Means To Impart Bone Affinity," Biotechnology Progress **16,** 258-267 (2000).

37. Fazle Hosain, Richard P. Spencer, Helene M. Couthon, and Georges L. Sturtz, "Targeted delivery of antineoplastic agent to bone: Biodistribution studies of technetium-99m-labeled gem-bisphosphonate conjugate of methotrexate," Journal of Nuclear Medicine **37,** 105-107 (1996).

38. H. Hirabayashi, T. Takahashi, J. Fujisaki, T. Masunaga, S. Sato, J. Hiroi, Y. Tokunaga, S. Kimura, and T. Hata, "Bone-specific delivery and sustained release of diclofenac, a non-steroidal anti-inflammatory drug, via bisphosphonic prodrug based on the Osteotropic Drug Delivery System (ODDS)," Journal of Controlled Release **70,** 183-191 (2001).

39. Dong Wang, Scott Miller, Monika Sima, Pavla Kopeckova, and Jindrich Kopecek, "Synthesis and Evaluation of Water-Soluble Polymeric Bone-Targeted Drug Delivery Systems," Bioconjugate Chem. **14,** 853-859 (2003).

40. Geeti Bansal, Sebastien A. Gittens, and Hasan Uludag, "A di(bisphosphonic acid) for protein coupling and targeting to bone," Journal of Pharmaceutical Sciences **93,** 2788-2799 (2004).

41. Charles R. Degenhardt and Don C. Burdsall, "Synthesis of ethenylidenebis(phosphonic acid) and its tetraalkyl esters," Journal of Organic Chemistry **51,** 3488-3490 (1986).

42. Zan Xie, Ye Jiang, and Di Qun Zhang, "Simple analysis of four bisphosphonates simultaneously by reverse phase liquid chromatography using n-amylamine as volatile ion-pairing agent," Journal of Chromatography, A **1104,** 173-178 (2006).

43. T. C. Schmidt, M. Petersmann, L. Kaminski, V. Loew, and G. Stork, "Analysis of aminobenzoic acid in wastewater from a former ammunition plant with HPLC and combined diode array and fluorescence detection," Fresenius' Journal of Analytical Chemistry **357,** 121-126 (1997).

44. Masayuki Yokoyama, Teruo Okano, Yasuhisa Sakurai, Akira Kikuchi, Nobuyuki Ohsako, Yukio Nagasaki, and Kazunori Kataoka, "Synthesis of poly(ethylene oxide) with heterobifunctional reactive groups at its terminals by an anionic initiator," Bioconjugate Chem. **3,** 275-276 (1992).

45. Joerg K. Tessmar, Antonios G. Mikos, and Achim Goepferich, "Amine-Reactive Biodegradable Diblock Copolymers," Biomacromolecules **3,** 194-200 (2002).

46. Pierre Oudet Charles Mioskowski Luc Lebeau, "Synthesis of New Phospholipids Linked to Steroid-Hormone Derivatives Designed for Two-Dimensional Crystallization of Proteins," Helvetica Chimica Acta **74,** 1697-1706 (1991).

47. Sidney Udenfriend, Stanley Stein, Peter Boehlen, Wallace Dairman, Willy Leimgruber, and Manfred Weigele, "Fluorescamine. Reagent for assay of amino acids, peptides, proteins, and primary amines in the picomole range," Science (Washington, DC, United States) **178,** 871-872 (1972).

48. Byron Ballou, B. Christoffer Lagerholm, Lauren A. Ernst, Marcel P. Bruchez, and Alan S. Waggoner, "Noninvasive imaging of quantum dots in mice," Bioconjug Chem **15,** 79-86 (2004).

49. P. T. Daley-Yates, L. A. Gifford, and C. R. Hoggarth, "Assay of 1-hydroxy-3-aminopropylidene-1,1-bisphosphonate and related bisphosphonates in human urine and plasma by high-performance ion chromatography," J Chromatogr **490,** 329-338 (1989).

50. Yukio Hirai, Norimasa Yoza, and Shigeru Ohashi, "Flow injection analysis of inorganic polyphosphates," Analytica Chimica Acta **115,** 269-277 (1980).

51. Matthew B. Murphy, Jeffrey D. Hartgerink, Achim Goepferich, and Antonios G. Mikos, "Synthesis and in Vitro Hydroxyapatite Binding of Peptides Conjugated to Calcium-Binding Moieties," Biomacromolecules **8,** 2237-2243 (2007).

52. Kianoush Motesharei and David C. Myles, "Molecular Recognition on Functionalized Self-Assembled Monolayers of Alkanethiols on Gold," Journal of the American Chemical Society **120,** 7328-7336 (1998).

53. Dariusz Witt, Rafal Klajn, Piotr Barski, and Bartosz A. Grzybowski, "Applications, properties and synthesis of w-functionalized n-alkanethiols and disulfides - the building blocks of self-assembled monolayers," Current Organic Chemistry **8,** 1763-1797 (2004).

54. Hong Cai and C. K. Lim, "Comparison of HPLC, capillary electrophoretic and direct spectrofluorimetric methods for the determination of temoporfin-poly(ethylene glycol) conjugates in plasma," Analyst (Cambridge, United Kingdom) **123,** 2243-2245 (1998).

55. Sufeng Zhang, Jennifer E. I. Wright, Natali Ozber, and Hasan Uludag, "The interaction of cationic polymers and their bisphosphonate derivatives with hydroxyapatite," Macromolecular Bioscience **7,** 656-670 (2007).

56. Y. Jiang, X. Q. Zhang, and Z. R. Xu, "Analysis of zoledronic acid and its related substances by ion-pair RP-LC," Chromatographia **60,** 405-409 (2004).

Chapter 3

Optimization of the Synthesis of Thioalkylated Poly(ethylene glycol) Derivatives

Gamal Zayed[1], Jörg Teßar[1], Achim Göperich[1]

[1]Department of Pharmaceutical Technology, University of Regensburg

1. Introduction

For the successful coating of the gold nanoparticles, polymers are needed, which have defined functionalities on both sides of the molecule, which are the binding sites for the gold nanoparticles and at the same time the intended functionalities at the end of the PEG polymer.

The PEGylated thioalkyl polymers intended for the surface modification were previously already synthesized in our group [1], but their functionalities were not always well defined. The reactions were mainly done in solid support making the purification steps always possible by rinsing the used gold for the surface modification of quartz crystals (solid support). The applied rinsing scheme was used in order to remove excess of reagents or non bound molecules of byproducts, e.g. not bearing the thiolated alkyl chain, which is necessary for the binding of gold. In order to coat nanoparticles this cleaning procedure is not applicable, so an optimized synthesis had to be developed. In order to compare the possible reaction procedure, a retrosynthetic analysis was applied, which can further highlight the differences of the two applied synthesis schemes.

1.1. Retrosynthetic analysis of poly(ethylene glycol)-undecyl mercaptane

The desired polymeric compounds are heterobifunctional PEG derivatives consisting of an alkanethiol part and attached PEG chains, also bearing certain functionalities. Based on the published papers on these heterobifunctional PEG derivatives [1] and known facts such as the solubility of the used compounds, a retrosynthetic scheme can been created to depict the different possible synthetic pathways for the preparation of the poly(ethylene glycol)-undecyl mercaptane derivatives (Figure 1). Due to the two main new linkages (A and B), there are two possible ways to prepare these PEG derivatives: for the first one (Route I), each part (the aliphatic thiol part and the PEG chain) is synthesized separately and then finally linked to obtain the target molecule. For the second route (Route II), the aliphatic part is reacted first with PEG chain and afterwards the thiol group is attached to the aliphatic part.

For the different routes a careful protection of the functional groups is necessary to obtain defined products, which are necessary for the intended coating of the gold nanoparticles. Especially during the Williamson ether synthesis the reaction with the thiol has to be prevented in order to maintain the gold binding functionality.

Based on literature data, the second method seemed to be more common and also more versatile, as the stepwise modification also allows exchanging the chemical functionalities. The proposed retrosynthetic schemes were applied to different poly(ethylene

glycol)$_{2000}$-undecyl mercaptane derivatives, which are expected to chemically form stable and also protein resistant coatings for gold nanoparticles and also bear the ability being further functionalized with targeting moieties. The structures of the desired compounds are illustrated in Figures 1 and 2 (compound I and II) together with a short description of the necessary synthetic steps using the two different synthetic routes.

<table>
<tr><td>Route I</td><td>1) Addition of the thioacetate to 11-bromo-1-undecene (Linkage A)
⇨ Removal of acetic acid
⇨ Protection of the thiol group in order to avoid side reaction
2) Williamson ether synthesis with monomethoxy poly(ethylene glycol) (Linkage B)
⇨ Removal of thiol protection group</td></tr>
<tr><td></td><td> 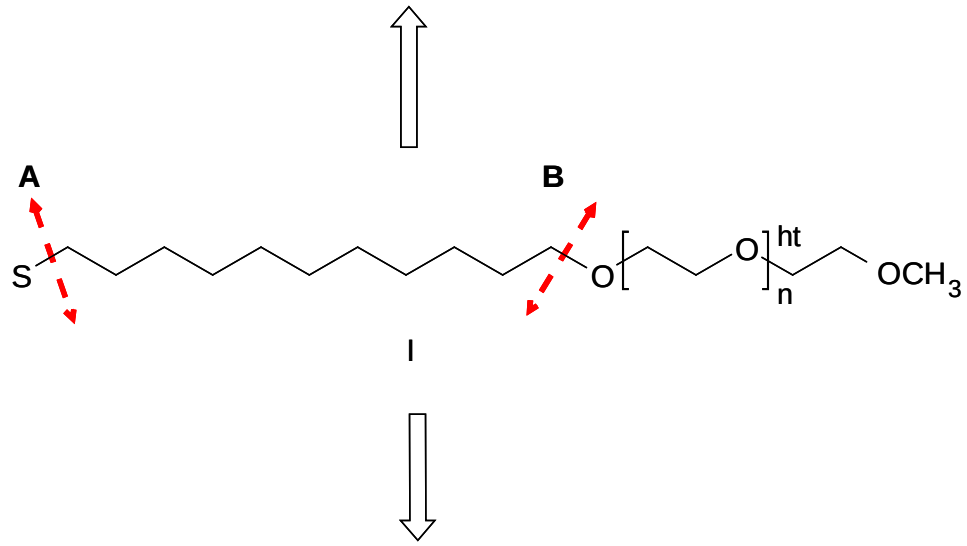

I</td></tr>
<tr><td>Route II</td><td>1) Williamson Ether synthesis with monomethoxy poly(ethylene glycol) and 11-bromo-1-undecene (Linkage B)
2) Addition of the thioacetate to the unsaturated double bond (Linkage A)
⇨ Removal of acetic acid</td></tr>
</table>

Figure 1: Retrosynthesis of methoxy poly(ethylene glycol)-undecyl mercaptane

1) Addition of the thioacetate to 11-bromo-1-undecene (Linkage A)
   ⇨ Removal of acetic acid
   ⇨ Protection of the thiol group in order to avoid side reaction
2) Williamson ether synthesis with protected amino poly(ethylene glycol) (Linkage B)
   ⇨ Removal of thiol and amino protection group

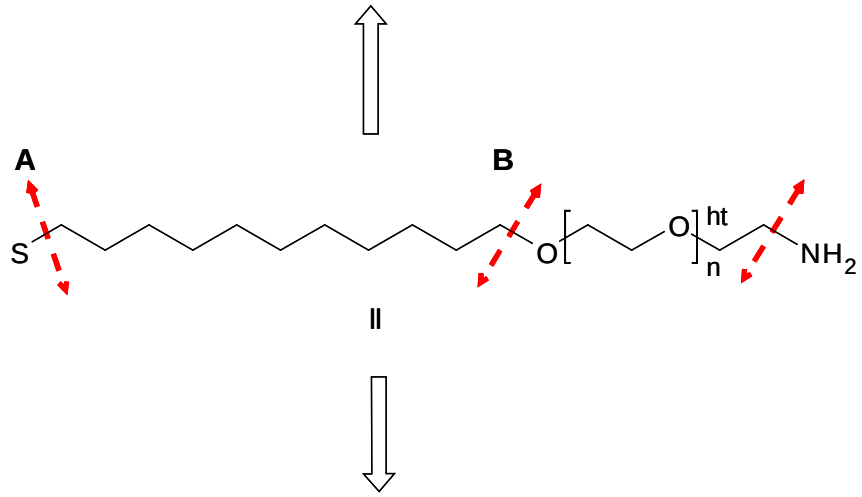

1) Williamson Ether synthesis with protected amino poly(ethylene glycol) and 11-bromo-1-undecene (Linkage B)
2) Addition of the thioacetate to the unsaturated double bond (Linkage A)
   ⇨ Removal of acetic acid and amino protection group

Figure 2: Retrosynthesis of amino poly(ethylene glycol)-undecyl mercaptane

For both synthetic routes several critical reaction steps had to be considered, which will be explained briefly in the following paragraphs.

Step 1: Deprotection of thiol and amine group functionalities

Because of the thiol group's sensitivity against oxidation to the corresponding disulfide, its deprotection is usually performed as the final step during synthesis. Many different parameters should be considered for the selection of the appropriate deprotection strategy, which generally can be carried out in alkaline as well as in acidic medium. Strong alkaline conditions must be avoided because the ethylene glycol chains are unstable in strong alkaline media and consequently can be cleaved yielding shorter polymer chains [2]. Due to this possible side reaction, the chosen method of deprotection was either mild acidic or mild basic conditions. Both of the two methods can be applied to S-acetyl or S-benzyl derivatives. However, the acidic conditions are more preferred, since basic conditions may even more promote the formation of disulfides. Additionally, in case of the amino poly(ethylene glycol)-

undecyl mercaptane the mild acidic conditions would deprotect the thiol and the amine groups in one reaction step.

Step 2: Introduction of thiol group.

Aliphatic thiol groups can be introduced using a protected form of sulfur either by radically initiated addition of thioacetic acid or benzyl mercaptane to terminal n-alkenes [3] or alternatively by nucleophilic substitution of sulfur nucleophiles with corresponding primary alkyl halides [4]. Although the synthetic routes starting from of alkenes or alkyl halides are nearly similar, the preparation of thiols from alkenes usually gives better yields and higher purities. On the other hand, terminal-alkene substrates are difficult to be obtained chemically or from the supplier and are more expensive than corresponding alkyl halides [5]. Addition of thioacetic acid [6], thiobenzoic acid [7] and 3-mercaptopropionic acid [8] to terminal alkenes in the presence of benzoyl peroxide or AIBN follows anti-Markonikov rule and therefore the desired protected terminal thiols are obtained in high yields (above 80-90%). The mild conditions for the introduction and subsequent deprotection are the main advantages of this method [5].

Step 3: Williamson ether synthesis

For both PEG derivatives, the newly formed alkyl ether (Bond B) can be obtained by addition of methoxy terminated poly(ethylene glycol) or protected amino poly(ethylene glycol) to either a dihaloalkane (X-$(CH_2)_n$-X) or to a terminal haloalkene. In case of using the dihaloalkane, the reaction of both halogen atoms may occur and subsequently both ends of the aliphatic chain might be PEGylated, giving rise to a mixture of mono-PEGylated and di-PEGylated alkane which can be further used only after extensive purification. In case of the haloalkene, there is only the possibility for one reaction to take place, which is through nucleophilic substitution of the terminal halogen atom by the PEG anion. The double bond on the other side of the haloalkene is inert towards a nucleophilic substitution and consequently doesn't need protection. Furthermore the double bond is a very convenient precursor for the thiol group as already explained before. For the ether formation a strong base is required in order to activate the hydroxyl terminus of the PEG chain by converting it into the conjugated base (PEG anion or PEG alkoxide). This conjugated base can then react with the haloalkene through nucleophilic substitution of the halogen atom. Different bases such as sodium hydride and sodium hydroxide have been applied in order to obtain the active conjugated base. Excess of haloalkene (3-4 folds) should be applied, to obtain as much as possible conversion of the PEG chains, which would be the most difficult compounds to separate from each other [9-11].

Step 4: Protection of the amino group of poly(ethylene glycol)-monoamine

Di-(t-butyl) dicarbonate (di-BOC) is usually used as amine protecting group because during cleavage of the protecting groups it also produces stable tertiary carbocation and can be removed under mild acidic conditions. The BOC protection of the amines usually takes place in alkaline medium in order to selectively protect amines and leave hydroxyl groups free, which are needed for the following ether synthesis (Figure 3) [12].

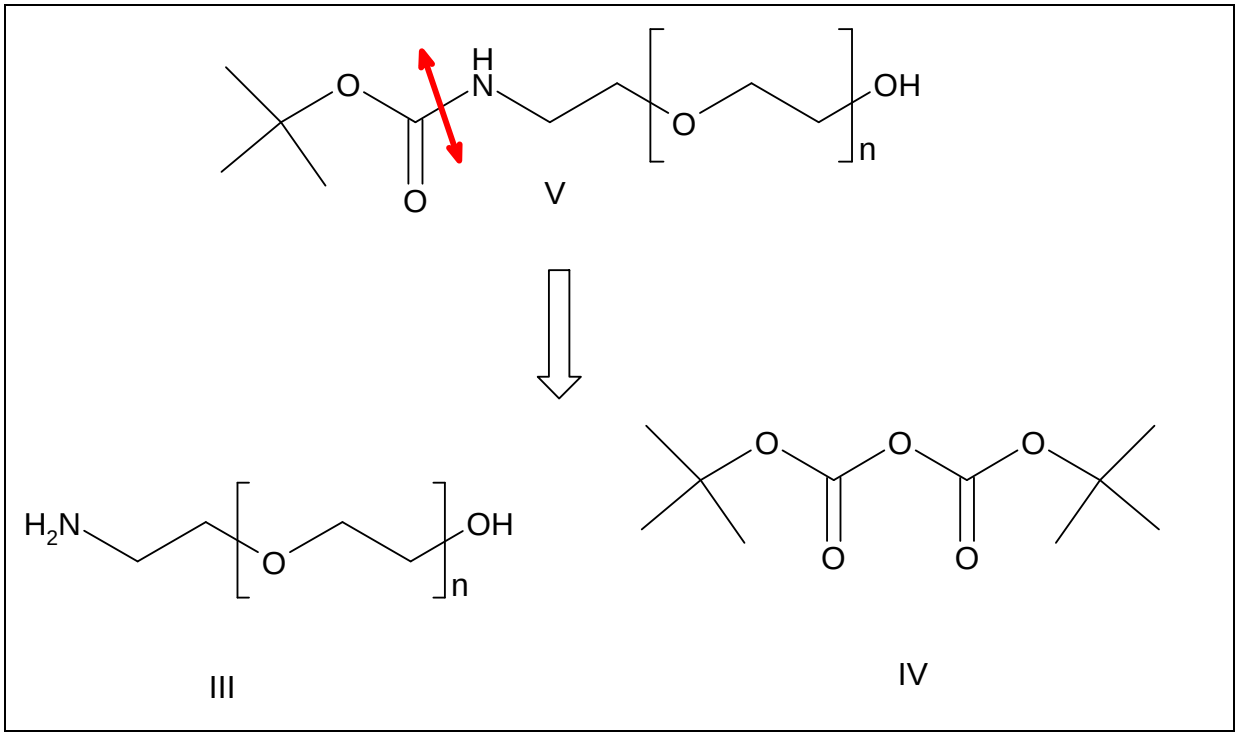

Figure 3: Retrosynthesis scheme of BOC-Protected amino poly(ethylene glycol)

1.2. Retrosynthesis of bisphosphonate-modified amino poly(ethylene glycol)-undecyl mercaptane

From the retrosynthetic point of view, conjugation of the bisphosphonate compound to amino poly(ethylene glycol)-undecyl mercaptane can be done by two synthetic pathways, either using the organic soluble ester form or the water soluble free form of the bisphosphonate. Since the free form of the bisphosphonate is highly hydrophilic and insoluble in organic medium, EDC/NHS chemistry needs to be applied for the conjugation. The optimal conditions for the reaction with the water soluble EDC is a slightly acidic buffer solution in order to obtain stable NHS-esters of bisphosphonate [13-16]. However, under these conditions the amine will be protonated and loose much of its chemical reactivity. Alternatively, the reaction can be carried out in non aqueous medium applying the DCC/NHS principle. In this case the unhydrolyzed bisphosphonate will react with DCC and NHS to form the active esters,

which subsequently react very rapidly with the primary amine group of amino poly(ethylene glycol)-undecyl mercaptane, yielding the unhydrolyzed bisphosphonate-conjugated polymer [17,18]. Hydrolysis of the ester form of the bisphosphonate-conjugated PEG can be done using acidic hydrolysis with concentrated HCl or 30% HBr in acetic acid. However, these strong conditions, usually result at the same time in the cleavage of the amide bond connecting the PEG chain and bisphosphonate molecule or eventually also the breakdown of the PEG chain [19-21]. Alternatively, this hydrolysis can be done using reagents from peptide synthesis, which can perform the quantitative dealkylation of the bisphosphonate ester under mild conditions, e.g. an excess of bromotrimethylsilane followed by methanolsis of the resulting trimethylsily ester [22-25]. The retrosynthetic analysis toward the synthesis of the desired compounds is depicted in Figure 4.

Route I	1) Conjugation of the protected ester of phosphonic acid with the poly(ethylene glycol) using DCC and NHS chemistry in organic medium 2) Cleavage of the phosphonic acid ester groups
	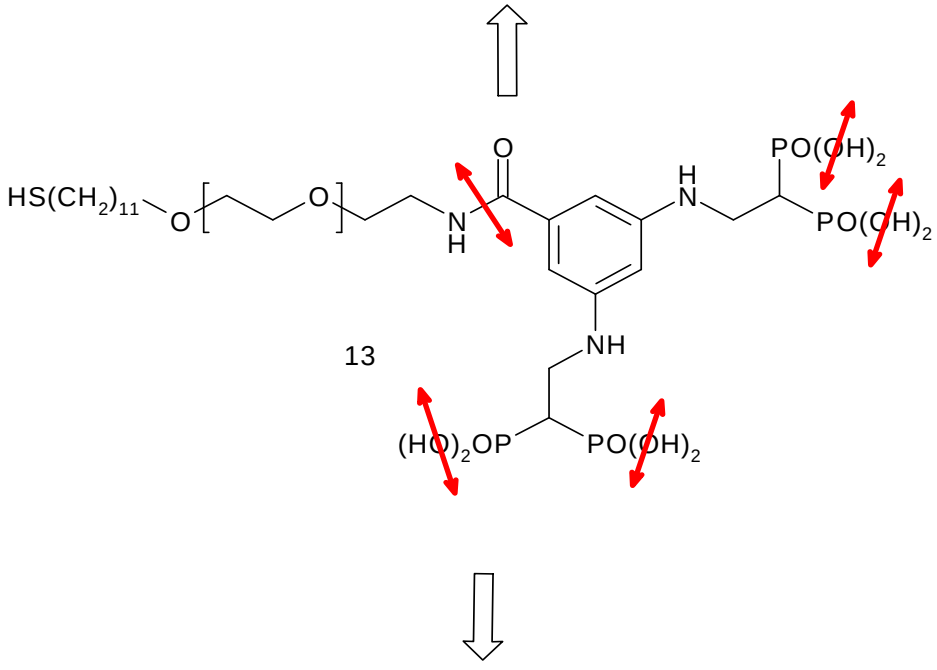
Route II	Conjugation of the phosphonic acid compound with the poly(ethylene glycol) using EDC chemistry in aqueous medium

Figure 4: Retrosynthesis of bisphosphonate modified poly(ethylene glycol)-undecylmercaptane

2. Materials

11-bromo-1-undecene, dibenzoyl peroxide, thioacetic acid (TAA), acetyl chloride, sodium sulphate, 2-chlorotrityl chloride, sodium hydride (NaH), sodium hydroxide (NaOH), sodium borate decahydrate, methoxy poly(ethylene glycol) 2000 (mPEG), ethylene oxide gas (EO), potassium bis(trimethylsilyl) amide, α,α´ azoisobutyronitril (AIBN), di(tert-butyl)dicarbonate (di-BOC), tetramethylsilane (TMS), potassium hydroxide (KOH), 4-phenylspiro[furan-2(3),1'-phthalan]-3,3`-dione (fluorescamine), N-hydroxyl succinimide (NHS), N,N\-dicyclohexyl cardodiimide (DCC), bromotrimethylsilane. DEAE-sephadex A25, dialysis tubing molecular weight cutoff (MWCO) 1000 Da. Toluene, methanol, hexane, chloroform, 1,4-dioxane, acetone, methanol, acetonitrile, diethyl ether, tetrahydrofuran (THF), methylene chloride, sodium sulphate, hydrochloric acid, sulfuric acid, acetic acid, sodium acetate, ammonium carbonate, zinc powder, ammonium heptamolybdate tetrahydrate, diethyl ether, ascorbic acid and hydroxyapatite (HA) were purchased from Merck (Darmstadt, Germany). Deuterated chloroform was from Deutero GmbH (Kastellaun, Germany). 3,5-di(tetraethyl ethylamino-2,2-bisphosphonate)benzoic acid and 3,5-di(ethylamino-2,2-bisphosphono) benzoic acid were synthesized according to the reported method [26]. Ibandronate was supplied from Boehringer (Mannheim, Germany).

3. Methods

3.1. Synthesis of methoxy poly(ethylene glycol)-undecyl mercaptane

3.1.1. Route I (previously reported method)

In this method the two main parts of the polymer, the thioalkylated part and the PEG chain, were separately synthesized and then liked together.

a. Synthesis of 11-bromo-undecylmercaptane

The alkanethiol residue consisting of 11 carbon atoms and a terminal thiol group was synthesized from 11-bromo-1-undecene, 5 ml of thioacetic acid and 75 mg of dibenzoyl peroxide were dissolved in 100 ml of dry toluene and heated at 80 ^{o}C for three hours in order to start the radical formation for the addition of the thioacetate to produce bromoundecyl thioacetate ester. Methanolic HCl prepared by slow addition of 20 ml of acetyl chloride to 200 ml of cooled degassed methanol was then used to cleave the acetate from the intermediate after evaporation of toluene. The obtained product is commonly extracted using hexane, which is then washed with water and finally dried using sodium sulphate, before evaporation

of the solvent, yielding the liquid product, which can easily be characterized using NMR [27,28].

b. Protection of the thiol group of 11-bromo-1-undecanethiol

The subsequently necessary protection of the free thiol is performed by reacting 11-bomo-undecyl mercaptane with 2-chlorotrityl chloride, which is an effective protecting group for mercaptane. 4 g of the 11-bromoundecyl mercaptane and 4.7 g of 2-chorotrityl chloride were dissolved in chloroform and stirred overnight at room temperature. The chloroform was finally evaporated and the protected thiol was characterized by NMR [29,30].

c. Williamson ether synthesis of methoxy poly(ethylene glycol)-undecyl mercaptane

For the final conjugation with the polymer, 4 g (2 mmol) of methoxy poly(ethylene glycol) were dissolved in 100 ml of dry dioxane and 240 mg (10 mmol) of sodium hydride were added and stirred for one hour for a complete deprotonation of the terminal alcohol. Then, 5.7 g (10 mmol) of the protected 11-bromo-undecyl mercaptane were added and thee reaction mixture was stirred for 24 hours at room temperature. The solution was filtered after addition of 5 ml methanol (to quench excess sodium hydride) and then the solvent was evaporated under vacuum. The obtained product was purified by repeated precipitation in 200 ml cold diethyl ether and finally dried. For the deprotection, 3 g of the PEG with the protected thiol group were dissolved in 20 ml of methanol containing 200 mg iodine and the solution was stirred at room temperature for one day. After evaporation of the methanol, the residue was dissolved in water and excess of iodine was removed using an ion exchange resin [31]. After evaporation of water, the produced polymer was purified by repeated precipitation in cooled diethyl ether and finally characterized by HPLC and NMR.

3.1.2. Route II for the synthesis of methoxy poly(ethylene glycol)-undecyl mercaptane

a. Synthesis of methoxy poly(ethylene glycol)-1-undecene

- *Using 50% aqueous sodium hydroxide*

The synthesis was carried out according to a procedure described by Prime et al. [32] (Scheme 1), 4 g (2 mmol) of methoxy poly(ethylene glycol) (**1**) were melted then 0.5 ml of a 50% aqueous solution of sodium hydroxide were added and the obtained mixture was heated to 110 °C in an oil bath for 30 minutes. Subsequently, 2.0 ml of 11-bromo-1-undecene (**2**) were added and the reaction mixture was kept at that temperature under stirring overnight. At the end of reaction, the mixture was dissolved in toluene (50 ml) and filtered to remove formed inorganic salts (NaOH and NaBr). After evaporation of toluene, the obtained polymer

residue was dissolved in acetone and precipitated in cooled ether, collected, dried and characterized by HPLC and NMR [33].

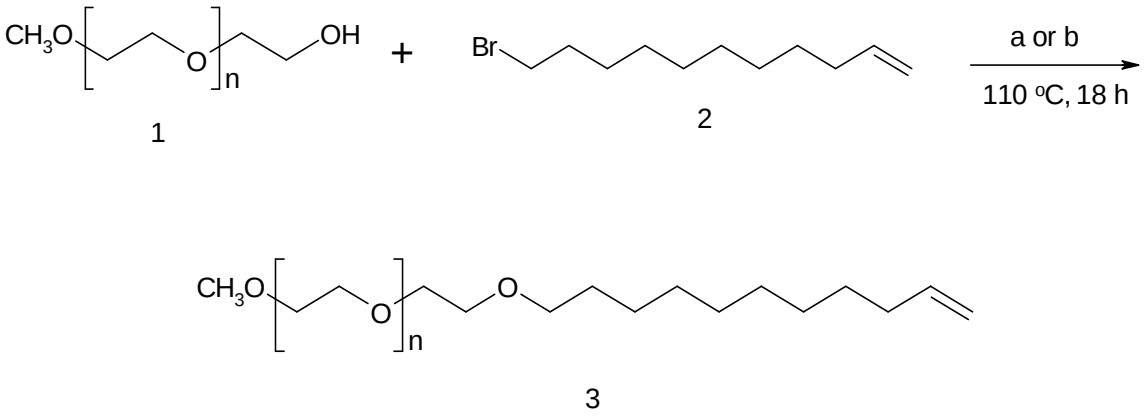

a: Aqueous NaOH (50%), b: NaH

Scheme 1: Synthesis of methoxy poly(ethylene glycol)-1-undecene

• *Using sodium hydride powder*

Alternatively, 4 g (2 mmol) of methoxy poly(ethylene glycol) (**1**) were melted, then different amounts of sodium hydride were added and the mixture was allowed to react at 110 °C in an oil bath for 30 minutes. After the evolving of hydrogen stopped, 2.0 ml of the 11-bromoundecne were added and the reaction was continued for 24 hours at this temperature. After quenching excess sodium hydride with methanol, the added excess of methanol was evaporated, the residue was dissolved again in toluene and filtered to remove inorganic salts. After evaporation of toluene, the residue was dissolved in the least amount of acetone and precipitated again in ice cooled diethyl ether. The polymer product was collected by filtration, dried under vacuum and finally analyzed by NMR and HPLC [34].

b. Addition of thioacetic acid to methoxy poly(ethylene glycol)-1-undecene

For the addition of the thiol functionality, 4.2 g of methoxy poly(ethylene glycol)-1-undecene (**3**) were dissolved in dry methanol, thioacetic acid and α,α´ azoisobutyronitrile (AIBN) were added and the mixture was refluxed under argon atmosphere to give methoxy poly(ethylene glycol)-undecane thioester (**4**) according to Scheme 2. The concentrations of thioacetic acid and AIBN as well as the reaction time have been varied to give the highest possible conversion of the thiol group [35].

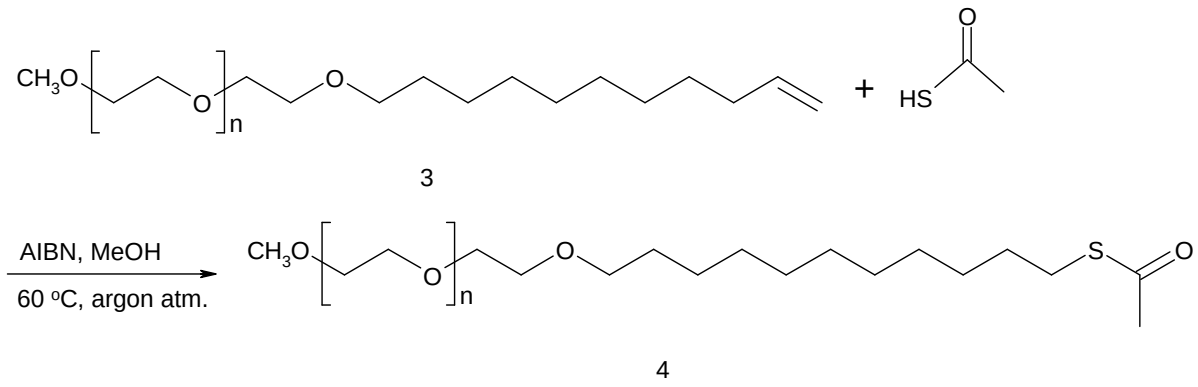

Scheme 2: Synthesis of methoxy poly(ethylene glycol)-undecane thioester

c. Hydrolysis of methoxy poly(ethylene glycol)-undecane thioester

Subsequently, the obtained thioester was hydrolyzed to the free thiol as described before. HCl in MeOH was added to the thioester of the polymer and the reaction mixture was refluxed overnight (Scheme 3). After evaporation of the solvent, the thioalkylated polymer was purified by repeated precipitation in cooled diethyl ether.

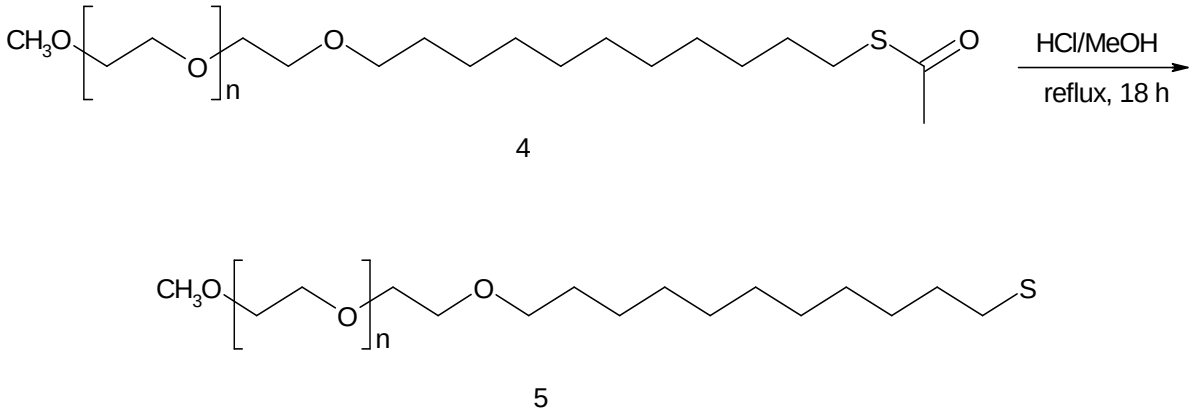

Scheme 3: Acidic hydrolysis of methoxy poly(ethylene glycol)-undecane thioester to methoxy poly(ethylene glycol)-undecyl mercaptane

3.2. Synthesis of amino poly(ethylene glycol)-undecyl mercaptane

3.2.1. Synthesis of poly(ethylene glycol) monoamine (PEG-NH_2).

Poly(ethylene glycol) monoamine (**6**) was synthesized according to the Scheme 4. About 25 g of ethylene oxide gas (EO) were condensed in 150 ml of dried THF (dried by molecular sieve) cooled to -79 ^oC using dry ice in methanol, then 25 ml of 0.5% potassium bis(trimethylsilyl) amide solution in toluene were added. After stirring the solution for 36 hours at room temperature, the solution was concentrated under vacuum until a viscous polymer was obtained. To obtain the pure polymer product, the viscous liquid was dissolved

in methylene chloride, centrifuged to remove any undissolved impurities and finally precipitated in ice cooled diethyl ether for several times. The precipitated product was collected by filtration and vacuum dried for two days [36].

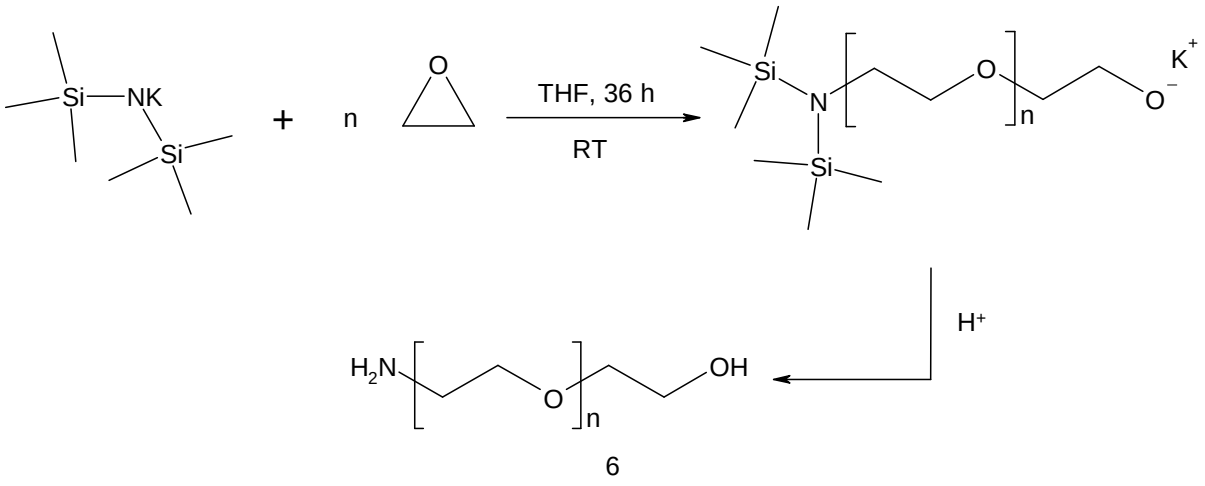

6

Scheme 4: Synthesis of poly(ethylene glycol) monoamine

3.2.2. Protection of the terminal primary amine group

Before application to the Williamson ether synthesis, the amino group has to be protected as described before to avoid the alkylation of the amine. Therefore, 5 g (2.5 mmol) of the synthesized PEG-NH_2 and 600 mg of potassium hydroxide were dissolved in 15 ml of water and the solution was cooled down to 0 °C in an ice bath. 0.6 or 2.750 g of the di(tert-butyl)dicarbonate (2.75 or 12.5 mmol, 1.1 and 5 molar equivalents respectively) were dissolved separately in 15 ml of dioxane and added dropwise to the aqueous cooled solutions of PEG-NH_2. The obtained reaction mixtures were stirred at 0 °C for four hours, and finally allowed to warm to room temperature while stirring overnight (Scheme 5). After the evaporation of the solvent, the residues were dissolved again in acetone, filtered to remove insoluble salt (KOH) and the solid protected polymers (PEG-NH-BOC) were obtained by precipitation in ice cold diethyl ether. The obtained protected PEG-NH_2 (**7**) was dried under vacuum and analyzed [12,37,38].

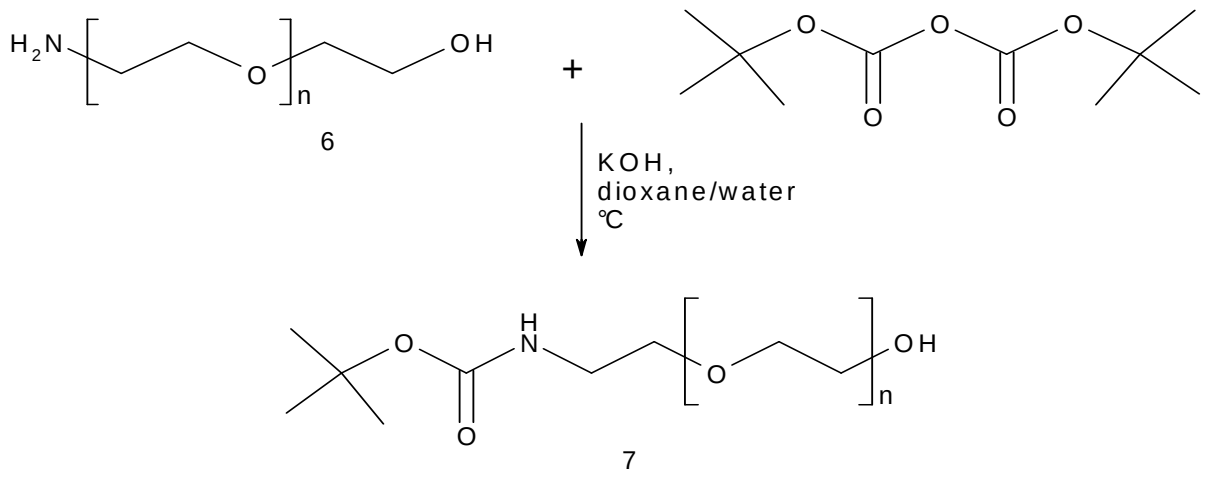

Scheme 5: Synthesis of BOC-protected amino poly(ethylene glycol)

3.2.3. Determination of free amine groups using the fluorescamine assay

In order to quantify the success of the protection, the free amine groups of the polymers were quantified using fluorescamine. A standard curve for HO-PEG-NH_2 was obtained according to the following procedure, 600 µl of a fluorescamine solution (10 mg in 100 ml acetone) were added to 1400 µl of borate buffer (50 mM, pH 8.5) containing different concentrations of the synthesized PEG-NH_2 (5, 10, 15, 20, 25 and 50 µM). The solutions were then allowed to react at room temperature for 5 minutes, after which the fluorescence intensity was measured at 390 nm excitation and 475nm emission wavelengths. Subsequently, the amount of free amine in the protected polymer was determined by adding the same amount of fluorescamine to borate buffer containing 25 µM of the protected amino PEG, which was measured as described before.

3.2.4. Synthesis of BOC-protected amino poly(ethylene glycol)-1-undecene

BOC-protected poly(ethylene glycol) monoamine (compound **7**) was reacted with an excess of 11-bormo-1-undecene (**2**) using sodium hydride as described before for the synthesis of methoxy poly(ethylene glycol)-1-undecene similar to Scheme 1.

3.2.5. Addition of thioacetic acid to the terminal double bond of the BOC-protected amino poly(ethylene glycol)-1-undecene.

The reaction between thioacetic acid and BOC-protected amino poly(ethylene glycol)-1-undecene (**8**) was conducted similar to that described before for mPEG-Undecene. BOC-protected amino poly(ethylene glycol)-1-undecane thioacetate ester (**9**) was obtained as in Scheme 6. The subsequent hydrolysis of the thioester was performed as described for the methoxy derivative. However, during this step also the BOC protecting group is cleaved yielding the final polymer product (**10**), which commonly dimerizes forming the

corresponding disulfide. For an extended purification and removal of byproducts, the amino poly(ethylene glycol)-undecyl mercaptane was dissolved in 50 ml dichloromethane and washed several times with 25 ml water containing 400 mg sodium bicarbonate in separating funnel. Afterwards, the organic layer was dried by sodium sulfate and the polymer was obtained again by precipitation in cold diethyl ether and investigated by ^{1}H-NMR, HPLC and MALDI-ToF.

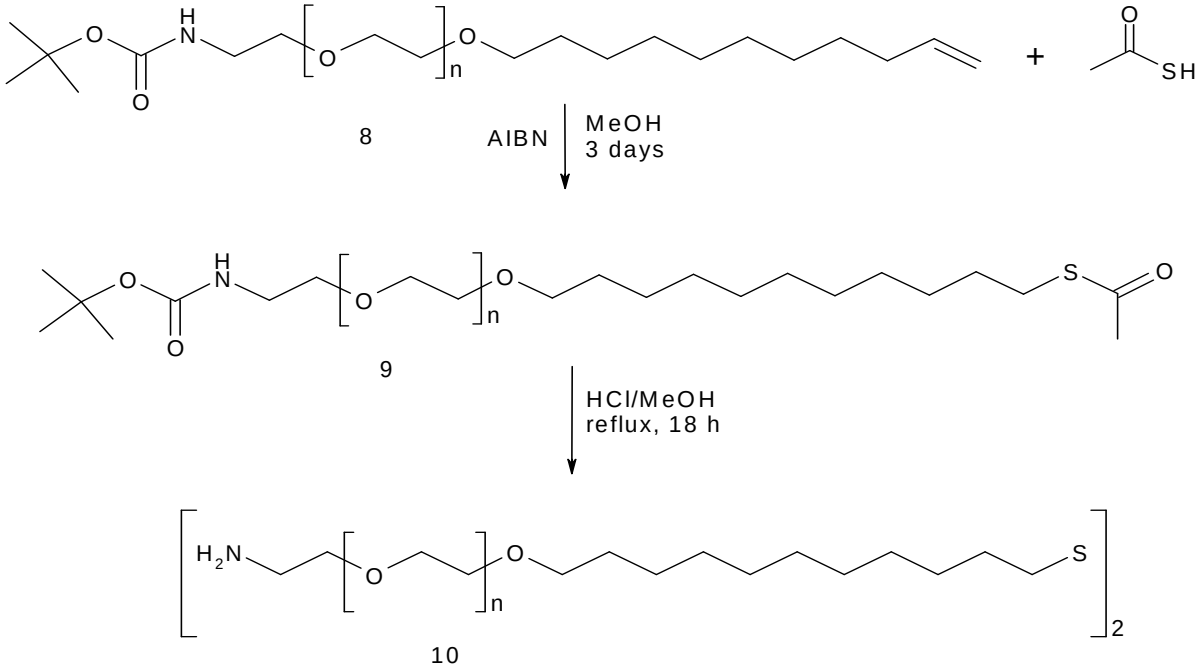

Scheme 6: Synthesis of BOC-protected amino poly(ethylene glycol)-1-undecane thioacetate ester and amino poly(ethylene glycol)-undecyl mercaptane

3.3. Synthesis of bisphosphonate-modified amino poly(ethylene glycol)-undecyl mercaptane

The bisphosphonate-modified polymer was synthesized using the above described synthesis schemes in aqueous and organic media, however, only the organic route yielded a successful product. For this reaction, 3,5-di(tetraethyl ethylamino-2,2-bisphosphonate)benzoic was dissolved in dry dioxane and different amounts of N-hydroxyl succinimide (NHS) and N,N‘-dicyclohexyl carbodiimide (DCC) were added and reacted for 2 hours at room temperature. Subsequently, amino poly(ethylene glycol)-undecyl mercaptane was added and allowed to bind for different times to yield the polymer modified with the unhydrolyzed bisphosphonate (**12**) (Scheme 7). At the end of the reaction, the mixture was centrifuged to remove the formed byproduct (dicyclohexylurea), and the solvent dioxane was finally evaporated. The obtained viscous residue was then dissolved in a minimum amount of

acetone, precipitated in ice cooled diethyl ether, collected, dried and analyzed. The free bisphosphonate containing compound was obtained by hydrolysis of compound **12** using bromotrimethylsilane followed by methanolsis to give the free bisphosphonate-modified polymer (**13**) [26].

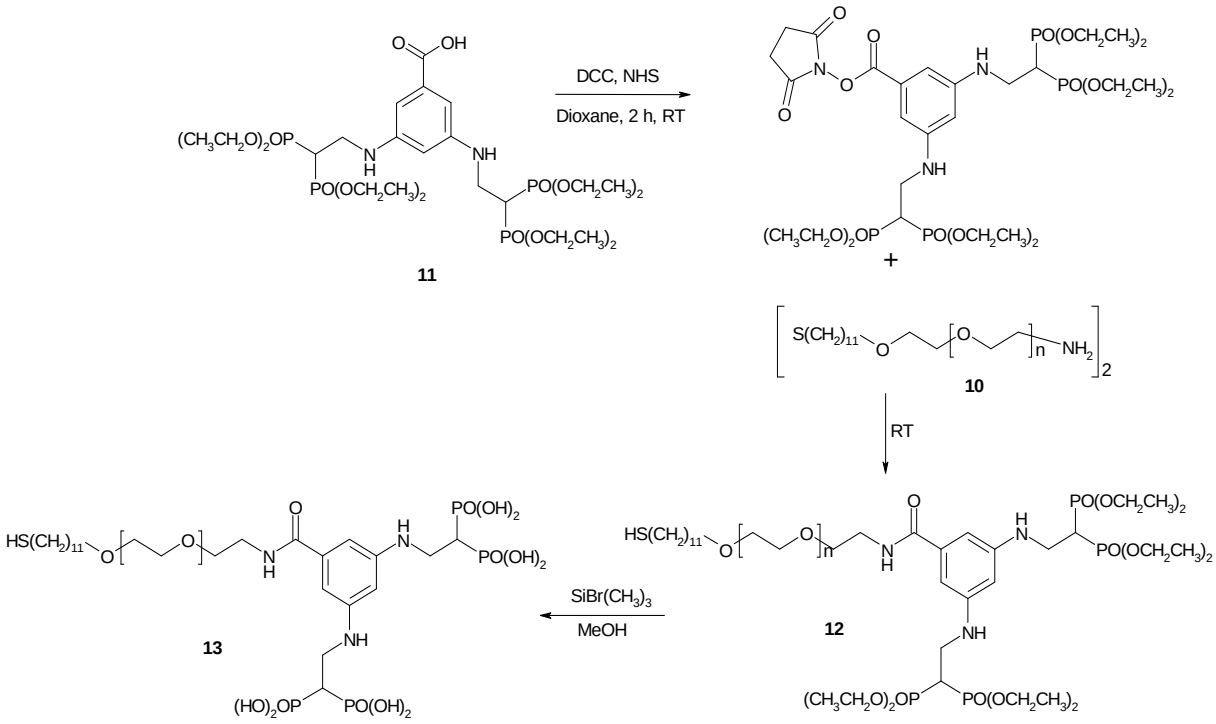

Scheme 7: Synthesis of bisphosphonate-modified poly(ethylene glycol)-undecyl mercaptane

The free bisphosphonate-modified polymer was further purified using an anion exchange column DEAE-sephadex A25. Therefore, 2 g of the sepharose were swollen in 0.2 M acetate buffer of pH=4 for two days. Then the obtained polymer was dissolved in acetate buffer and added to the sepharose while stirring the mixture at room temperature. Unbound impurities were then removed by filtration and subsequently the polymer was eluted by exchanging the buffer to basic 0.2 M ammonium carbonate buffer (pH 8.5). This washing step was repeated 2-3 times to completely elute the polymer. The buffer salt ammonium carbonate was subsequently removed by freeze drying and dialysis of the initially freeze dried polymer for 48 hours against deionized water using dialysis tubes of 1 kDa cutoff.

3.4 Analysis of the Synthesized Polymers

3.4.1. ^{1}H-NMR analysis

^{1}H-NMR (nuclear magnetic resonance spectroscopy) spectra were recorded on a Bruker Avance 600 spectrometer (Bruker Biospin, Rheinstetten, Germany). For the measurement, the polymer samples were dissolved in deuterated chloroform and TMS was used as internal standard.

3.4.2. HPLC analysis

High pressure liquid chromatography (HPLC) analysis was done using a setup consisting of a DGU-14A degasser, LC-10-AT pump, SIL-10 AD autosampler, RF-10A XL fluorescence detector, SPD-10A VP UV-Vis detector and a SCL-10A VP system controller all from Shimadzu, Duisburg, Germany).

HPLC of the synthesized polymers was performed under the following conditions. A linear gradient of 20% to 100% solvent B (90% acetonitrile in water) in solvent A (10% acetonitrile in water) over 30 minutes was applied as mobile phase at a flow rate of 1 ml/min. 50 µl samples (5 mg/ml) were separated at 40 °C using a combination of a PL-RPS guard column and an analytical column (PL-RPS 300 Å, 5 µm). The samples were detected by a low temperature evaporative light scattering (ELSD) detector (Method I) [39].

Ion-pair chromatography of the free bisphosphonate containing samples was performed on a standard C_{18} column (25 cm × 4,6 mm I.D., 5 µm, Supleco, Deisenhofen, Germany). Here, the mobile phase used was a mixture of 18 mM *n*-amylamine aqueous solution (adjusted to pH 7.0 with acetic acid) and acetonitrile (95:5, v/v). The flow rate was 1 ml/min and the experiments done at room temperature (Method II) [40,41].

3.4.3. Mass Spectrometry of the Polymers (MALDI-ToF MS)

Matrix assisted laser desorption/ionization mass spectrometry (MALDI-ToF) was performed on a HP G2030A spectrometer in positive mode. The polymers were analyzed in the range of 0-6000 m/z, data were averaged from about 150 laser shot per spectrum using indoleacrylic acid dissolved in THF (0.15 mg/ml) as matrix. The samples were prepared on the target by depositing 1 µl of a mixture of matrix solution and polymer solution (1 mg/ml) (3:1).

3.4.4. Determination of bisphosphonate content of the modified-polymer

Quantitative determination of the bisphosphonate incorporated in the polymer was performed after oxidation of the bisphosphonate to orthophosphate and the subsequent reaction with molybdenum-ascorbate reagent to yield a phosphomolybdate complex, which

can be detected at 820 nm. Pure ibandronate was used as standard for the construction of the calibration curve [42-44].

3.4.5. Determination of PEG concentration in the synthesized polymer

Additionally, a spectrophotometric method for the quantitative determination of PEG concentrations was used based on the absorbance measurement of fluorescein dye after partitioning into an aqueous two-phase system containing PEG in the upper phase and ammonium sulfate in the lower phase. The decrease of fluorescein absorbance in the lower phase here is directly proportional to the PEG concentration. To 300 µl of ammonium sulfate (31% w/v in 0.5 M acetate buffer pH 5 containing 77 µM fluorescein), 40 µl of the respective PEG samples are added. The samples are allowed to settle in dark for 30 minutes at room temperature before measuring the absorbance at 475 nm using a 96-well plate reader. PEG solutions of known concentration are used for the construction of standard curve [45].

4. Results and Discussion

4.1. Synthesis of methoxy poly(ethylene glycol)-undecyl mercaptane

4.1.1. Route I

Using the already described method for the PEG synthesis as described by Knerr et al. [1], methoxy poly(ethylene glycol)-undecyl mercaptane and amino poly(ethylene glycol)-undecyl mercaptane were synthesized by first thiolating the alkene and later forming the ether link.

a. Synthesis of 11-bromo-undecylmercaptane

11-bromo-1-undecene was reacted with thioacetic acid in the presence of dibenzoyl peroxide using a radical mediated addition to the double bond, which followed the anti-Marconikov rule and gave acetate protected thiol derivative (11-bromoundecyl thioacetate ester). The ^{1}H-NMR spectrum of this intermediate is characterized by the following signals; δ_H: 3.4 (t, 2H, $BrCH_2$-), 2.85 (t, 2H, -CH_2S-), 2.3 (s. 3H, CH_3COS-), 1.2-1.9 (m, 18H, the remaining protons of the aliphatic part), which allowed to quantify the amount of conversion to the thioacetate of almost 90%.

To obtain the free 11-bromoundecyl mercaptane, the intermediate was refluxed with degassed methanolic HCl overnight. ^{1}H-NMR spectrum of the mercaptane is presented in Figure 5 and it is characterized by the representative signals for the alkyl protons neighboring the brome and the mercaptyl group; δ_H: 3.4 (t, 2 H), 2.55 (m, 2 H), and 1.9-1,2 (m, 18 H).

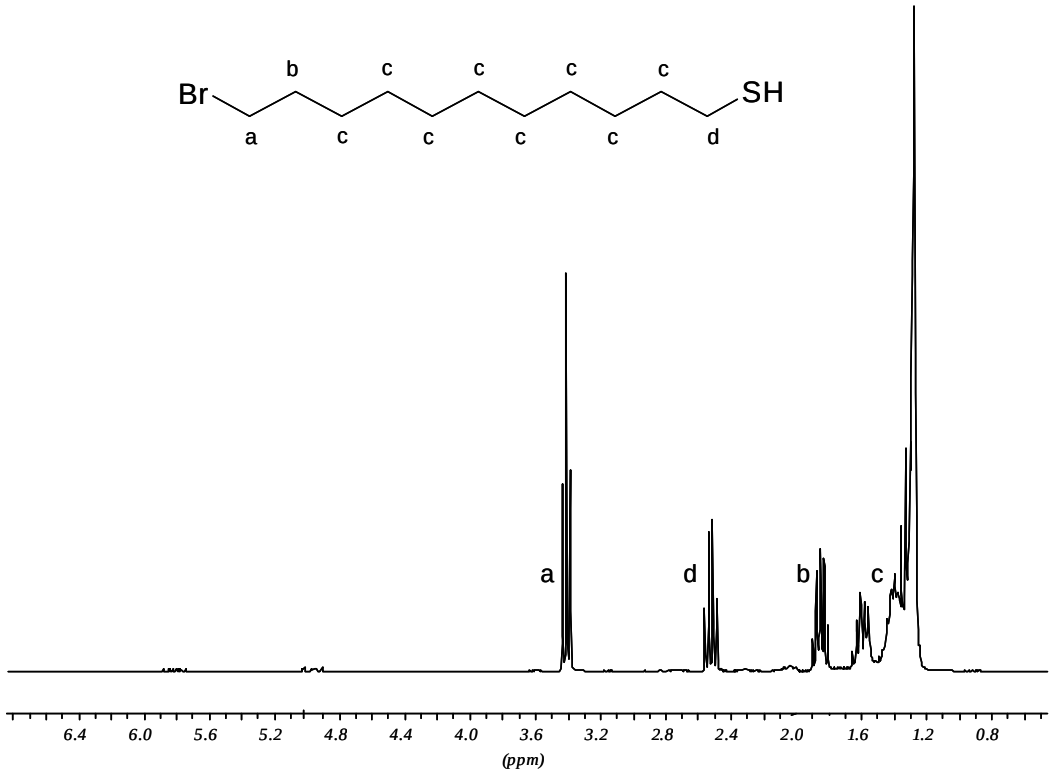

Figure 5: ^{1}H-NMR spectrum of 11-bromoundecyl mercaptane

b. Protection of the thiol group of 11-bromo-1-undecanethiol

Because of the high reactivity and to avoid byproducts, the thiol group needs to be protected before the further reaction with PEG chain. Otherwise, the thiol group would participate in the reaction and a modification of the alkanethiol part would occur from both ends with PEG chains, which also would prevent the attachment of the polymer to gold surfaces. The protection was performed by reacting the 11-bromoundecyl mercaptane with 2-chlorotrityl in chloroform. This reaction produced 11-bromoundecyl-(2-chloro trityl) sulfide [29], which is characterized by the following ^{1}H-NMP signals; δ_H: 6.7-8.1 (m, 14 H), 3.41 (t, 2 H), 1.98 (t, 2 H), and 1.9-1,2 (m, 18 H).

c. Williamson ether synthesis of methoxy poly(ethylene glycol)-undecyl mercaptane

For the subsequent Williamson ether synthesis, the hydroxyl group of methoxy poly(ethylene glycol) was reacted with the protected 11-bromoundecyl mercaptane in the presence of sodium hydride to form the new ether bond between the aliphatic part and the PEG chain. Sodium hydride firstly reacts with the hydroxyl group of the PEG forming the respective alkoxide. This alkoxide acts then as powerful nucleophilic reagent with the alkyl halide and results in the ether formation [46].

The ^{1}H-NMR of the thioalkylated methoxy poly(ethylene glycol) after cleavage of the thiol protection group with iodine is presented below in Figure 6, the obtained spectrum is

characterized by the following signals; δ_H: 3.8-3.8 (m, 180 H), 3.3 (s, 3 H), 2.00 (t, 1 H) and 1.85-1.2 (m, 6 H).

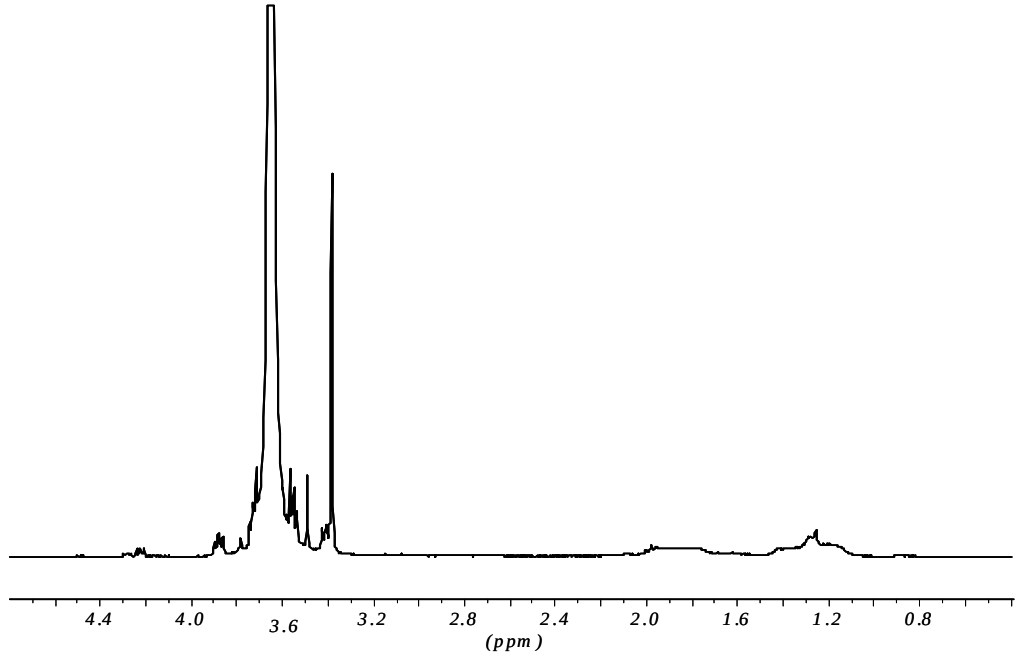

Figure 6: ^{1}H-NMR spectrum of methoxy poly(ethylene glycol)-undecyl mercaptane synthesized by route I

The expected integrals for the complete conversion of the PEG to alkylated PEG, however, should be 182, 3, 0, and 16 protons, respectively. While there was no obvious correlation between the expected and measured integrals, the signal of the methylene group adjacent to the SH group ($\delta_{theo.}$ = 2.55 ppm) was completely missing as shown in Figure 6.

In order to characterize the obtained product, HPLC analysis of the polymer was performed on the reversed phase polymer column (Method I) as presented in Figure 7. Here the observed retention time of the main peak for the synthesized polymer did not differ much from the educt methoxy poly(ethylene glycol), which indicates that only little conversion of the PEG was obtained, which is visible at the later occurring peak at 20 min in the chromatogram B. In order to improve the conversion, the reaction conditions were changed several times, but no significant improvement was achieved, which was attributed to the fact that no big excess of mPEG could be used. When excess mPEG are used to PEGylate all the used thioalkylated part, a mixture of thioalkylated PEG and mPEG will be obtained, which is very difficult to be separated from each other giving rise to a purification problem. As the polymers for the modification of colloids can't be purified using the adsorption step, which was done in the earlier publication, an improved method had to be developed to solve the problem.

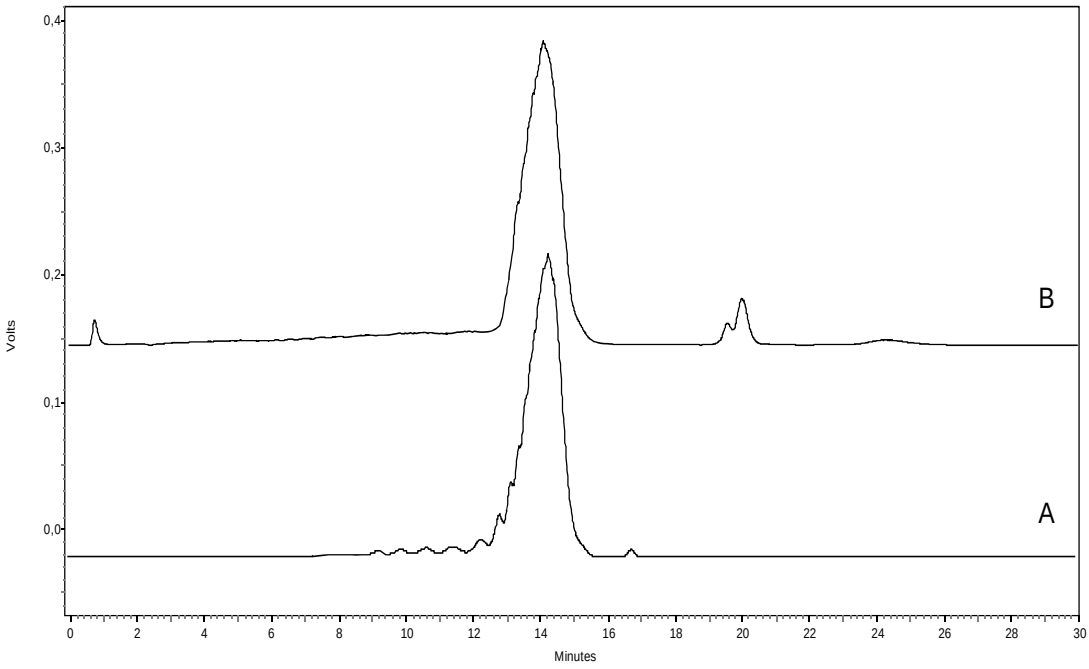

Figure 7: HPLC chromatograms of mPEG (A) and mPEG-AlkSH synthesized by route I (B)

4.1.2. Route II for synthesis of methoxy poly(ethylene glycol)-undecyl mercaptane

The improved synthesis route was based on the following steps:

(1) Reaction of 11-bromo-1-undecene with methoxy poly(ethylene glycol) using highly concentrated base to produces polymer-alkene product

(2) Addition of thioacetic acid to the terminal double bond of the polymer-alkene intermediate using α,α´-azoisobutyronitril (AIBN) to produce the thioacetate

(3) Hydrolysis of the thioester by methanolic HCl to obtain the desired thioalkylated polymer.

a-Synthesis of methoxy poly(ethylene glycol)-1-undecene

I - Using Sodium Hydroxide as base

Methoxy poly(ethylene glycol) was reacted first with 11-bromo-1-undecene using aqueous 50% sodium hydroxide solution as base. Therefore the sodium hydroxide solution was added to the melted PEG and allowed to react for 30 minutes at 110 °C. The formed mPEG alkoxide reacted with the alkyl bromide by nucleophilic displacement of the bromine leaving group forming the methoxy poly(ethylene glycol)-1-undecene as described in Scheme 1 [47]. The double bond of 11-bromo-1-undecene, as convenient precursor of the later introduced thiol, does not need any protection, because it is inert towards nucleophilic substitution [5]. The ^{1}H-NMR spectrum of the obtained intermediate (**3**) (Scheme 1) is characterized by the following signals; δ_H: 5.9-5.7 (m, 1 H) CH of the double bond, 5.05-4.9

(t, 2 H) CH_2 of the double bond, 3.85-3.53 (m, 180 H) protons of the PEG part, 3.49-340 (m, 2 H) CH_2O of the alkene part, 3.38 (s, 3 H) methoxy group of mPEG, 2.10-2.0 (m, 2 H) CH_2 adjacent to the double bond, 1.65-1.25 (m, 14 H) residual protons of the alkene part. The obtained integrals agreed with the expected values, indicating that every mPEG molecule is attached to one molecule of alkene part (i.e 100% conversion).

The HPLC chromatogram of the obtained product is compared to that of mPEG in Figure 8. The chromatogram of mPEG is characterized by a single peak eluting at 15 minutes (chromatogram A). Modification of mPEG with 11-bromoundecne using both investigated bases produced compounds eluting significantly later at about 20 minutes, which can be attributed to the attachment of the lipophilic alkyl chain (chromatogram B and C).

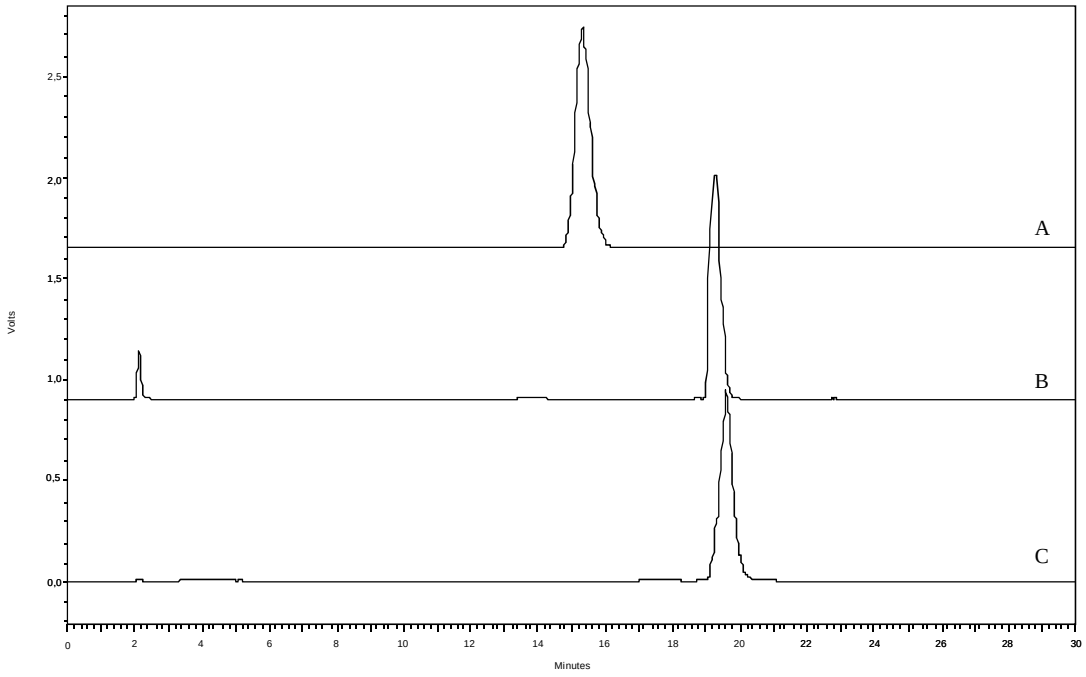

Figure 8: HPLC chromatograms of mPEG (A), mPEG-undecene prepared by sodium hydroxide (B) and mPEG-undecene prepared by sodium hydride (C)

II - Using sodium hydride powder as base

The synthesis of the mPEG-undecene (**3**) was additionally investigated using sodium hydride powder instead of the aqueous sodium hydroxide. The exchange was performed in order to ensure the stability of poly(ethylene glycol), which can eventually be hydrolyzed in strong alkaline media to shorter PEG chains [2], and furthermore the reaction scheme known from literature had to be adapted in order to conjugate the alkene to the BOC protected amino PEG, which would be sensitive to water due to its contained urethane group. Consequently, the reaction was carried in absence of added water.

The ^{1}H-NMR spectrum of the obtained product is presented in Figure 9 and exhibited no differences to the spectrum obtained with sodium hydroxide catalysis, also the obtained integrals are in good agreement with the expected theoretical values. A similar agreement was obtained also for the HPLC analysis, which was already described above.

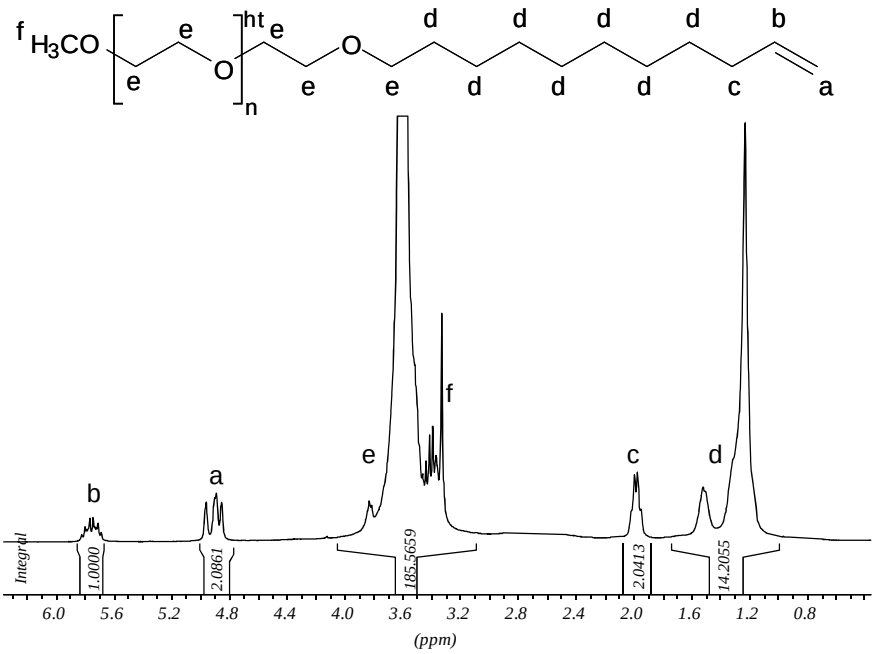

Figure 9: ^{1}H-NMR spectrum of methoxy poly(ethylene glycol)-1-undecene

b. Addition of thioacetic acid to the terminal double bond to form the thioester

Thioacetic acid was used as the most common and versatile reagent for the free radical addition of thiol precursor to terminal alkenes. It is inexpensive and can be easily deprotected to the free thiol. The conversion of the terminal double bond of mPEG-undecene into mPEG-undecane thioester was carried out by radical addition of thioacetic acid under reflux in methanol in the presence of azoisobutyronitrile (AIBN) as radical initiator.

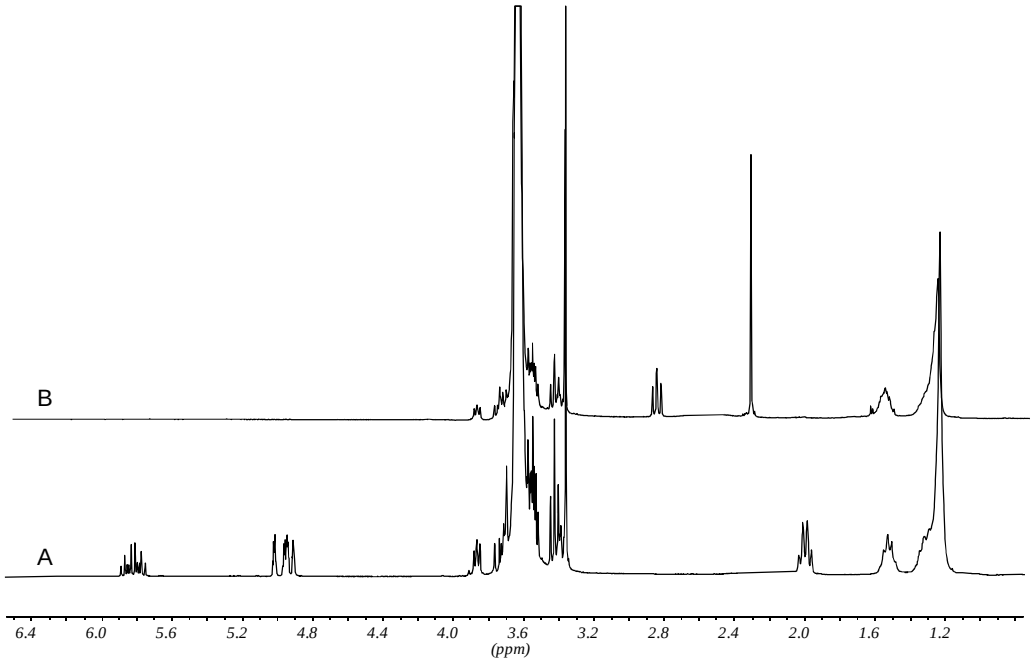

Figure 10: ^{1}H-NMR spectrum of methoxy poly(ethylene glycol)-1-undecene (A) and methoxy poly(ethylene glycol)-1-undecane thioacetate ester (B)

The addition of thioacetic acid was followed via ^{1}H-NMR by monitoring the disappearance of the signals of the double bond at 5.8 ppm (m, 1H, $CH{=}CH_2$) and 5.0 ppm (t, 2H, $CH_2{=}CH$) as well as the signal of the adjacent methylene group at 2.0 ppm (m, 2H, $CH_2CH{=}$) (Figure 10, spectrum A). The ongoing reaction was, furthermore, characterized by the appearance of new signals at approximately 2.85 ppm for the methylene triplet in neighborhood of the thioester and at 2.3 ppm a singlet corresponding to the acetate end group (Figure 10, spectrum B) [48]. The conversion was investigated at different concentrations of thioacetic acid and AIBN as well as after different reaction times as shown in Table 1. 100% addition of thioacetic acid to the double bond was obtained by a 1.5 molar equivalent of AIBN, 12 molar equivalent of thioacetic acid and a reaction time of 72 hours under reflux in 20 ml dry methanol. Similar results were obtained by Oliveira et al. [49], who found that the addition of thioacetic acid to the double bond was increased by increasing the concentration of the radical initiator AIBN.

Table 1: Effects of different concentrations of thioacetic acid and AIBN as well as the reaction time on amount of thioacetate ester produced in methanol

AIBN (molar equivalent)	TAA (molar equivalent)	Conversion %
0.1[1]	2	25
0.5[1]	4	35
1.0[2]	8	80
1.5[2]	12	100

[1] reaction time = 48 hours

[2] reaction time = 72 hours

c. Hydrolysis of methoxy poly(ethylene glycol)-1-undecane thioester

Because the thiol group is rather sensitive and easily oxidized to the disulfide, its deprotection is usually the final step of the synthesis. Hydrolysis of the thioester can be done in acidic or basic conditions. In case of alkaline condition, a significant level of disulfide is obtained. In order to avoid too much disulfide formation, hydrolysis was performed under acidic conditions and with inert gas to reduce the amount of oxygen [5]. The stability of the ether linkages allowed the hydrolysis of mPEG-undecane thioester to be carried out with methanolic hydrochloric acid (HCl/MeOH) to produce the deprotected mPEG-undecyl mercaptane polymer. The ^{1}H-NMR spectrum of methoxy poly(ethylene glycol)-undecyl mercaptane (Figure 11) is characterized by the following signals; δ_H: 3.8-3.5 (m, 180 H), 3.45 (t, 2H), 3.35 (s, 3H), 2.7-2.45 (tt, 2H) and 1.8-1.2 (m, 18H) corresponding to the PEG chain, methylene group of the aliphatic part adjacent to newly formed ether bond, methoxy group of the PEG chain, methylene group adjacent to thiol group and the remaining protons of the aliphatic part, respectively.

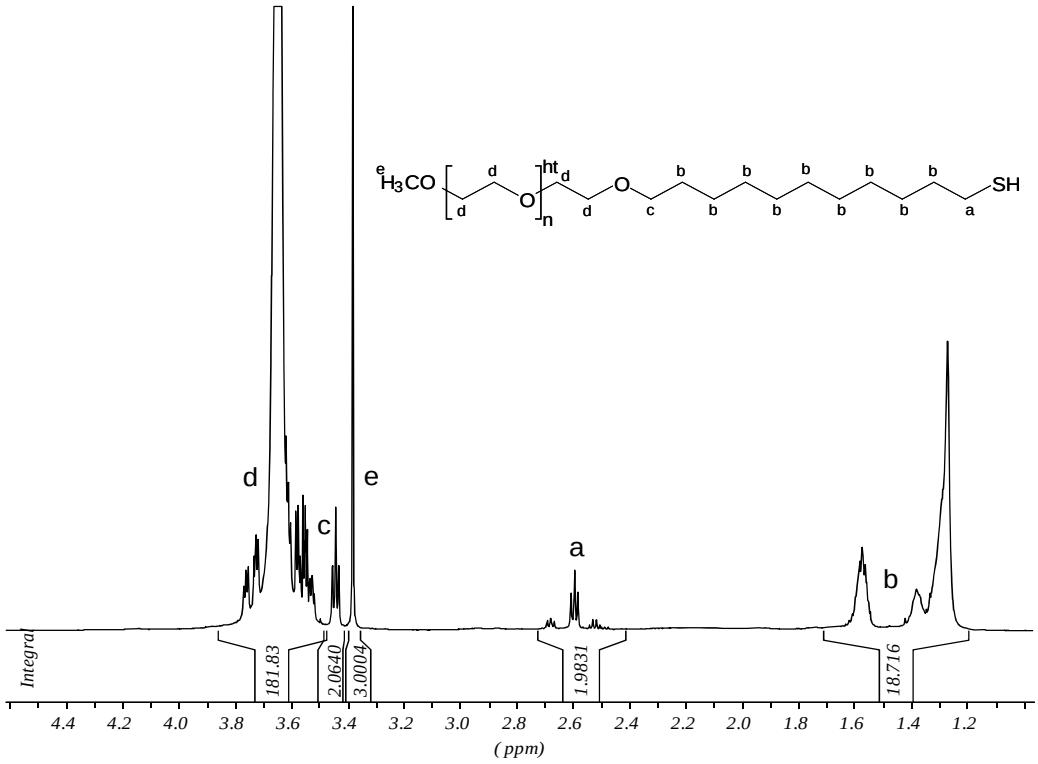

Figure 11: [1]H-NMR spectrum of methoxy poly(ethylene glycol)-undecyl mercaptane

Besides [1]H-NMR, HPLC analysis of the methoxy poly(ethylene glycol)-undecyl mercaptane was performed to compare it with the educt methoxy poly(ethylene glycol) (Figure 12). The chromatogram of the polymer modified with the thioalkyl chain (chromatogram B) is characterized by two peaks at 19 and 22 minutes, which correspond to the reduced form of the polymer (mPEG-AlkSH monomer, 19min) and the respective oxidized form ((mPEG-AlkS)$_2$ dimer, 22min). The chosen column was here separating the two synthesized compounds and the PEG according the lipophilicity (C18-material) and additionally according their size (size exclusion). The attachment of aliphatic part to the mPEG chain results in an increased hydrophobicity and the still occurring dimerization by oxygen increases the molecular weight of the product, yielding the typical double peak for these compounds, which were already observed by Knerr et al. [50] and which can be removed using reducing agents just before the chromatography.

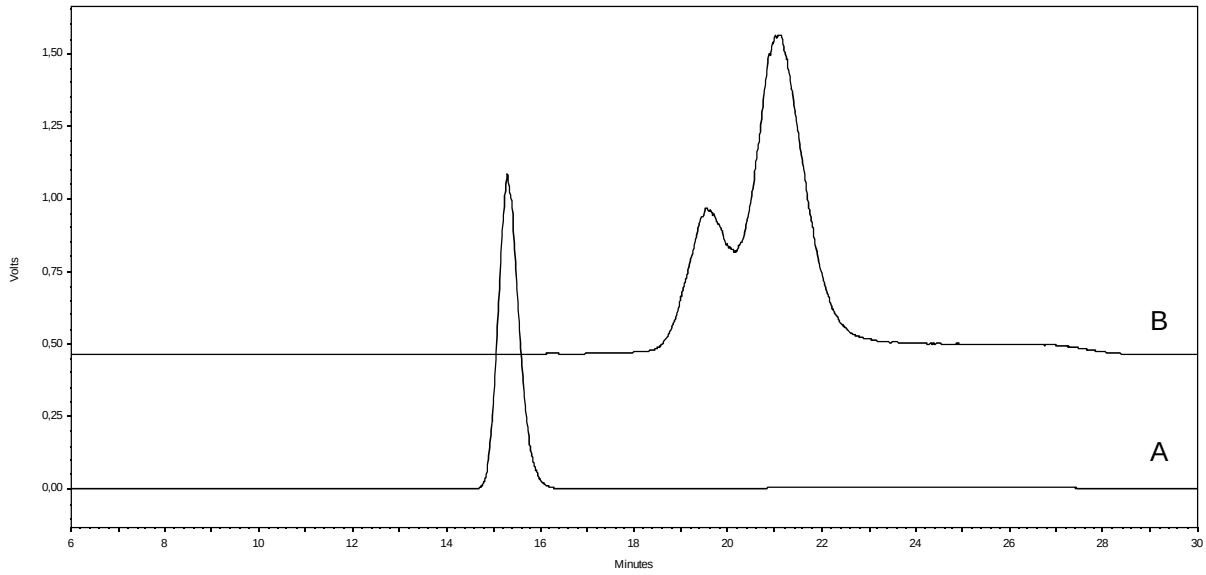

Figure 12: HPLC chromatograms of methoxy poly(ethylene glycol) (A) and methoxy poly(ethylene glycol)-undecyl mercaptane (B)

4.2. Synthesis of amino poly(ethylene glycol)-undecyl mercaptane

4.2.1. Synthesis of poly(ethylene glycol) monoamine

Bifunctional polymer, poly(ethylene glycol) monoamine with a molecular weight of about 2000 Da, was synthesized by ring opening polymerization of ethylene oxide using potassium bis(trimethylsilyl) amide. Due to the absence of the internal standard of the methoxy group in mPEG, the number average molecular weight was determined after modification with trifluoroacetic acid anhydride (TFAA). The ^{1}H-NMR spectra of the synthesized polymers are depicted in Figure 13. The ^{1}H-NMR confirmed the structure of HO-PEG-NH_2, which is characterized by two signals, one signal at δ_H: 2.95-2.80 ppm corresponding to the two protons adjacent to the amino group (NH_2CH_2-), and a second large peak at δ_H: 3.9-3.4 ppm corresponding to protons of the PEG chain. The number average molecular weight was calculated using the NMR integrals according to a method described by Tessmar et al. [51] for the molecular weight determination of HO-PEG-NH_2 and NH_2-PEG-PLA. The number average molecular weight was calculated after acylation of the amine and hydroxyl groups with TFAA. The protons of the ethylene unit neighboring the hydroxyl group were shifted from δ_H: 3.6 ppm to δ_H: 4.4 ppm, and as well the protons adjacent to amino group (2.95-2.8 ppm) shifted up field to the same position of the main PEG protons at 3.9-3.4 ppm due to formation of the amide link. The integrals of the polymer signals before and after reacting with trifluoroacetic acid anhydride are listed in Table 2. Based on these values, the average molecular weight of the polymer was calculated to be about 1990 Da.

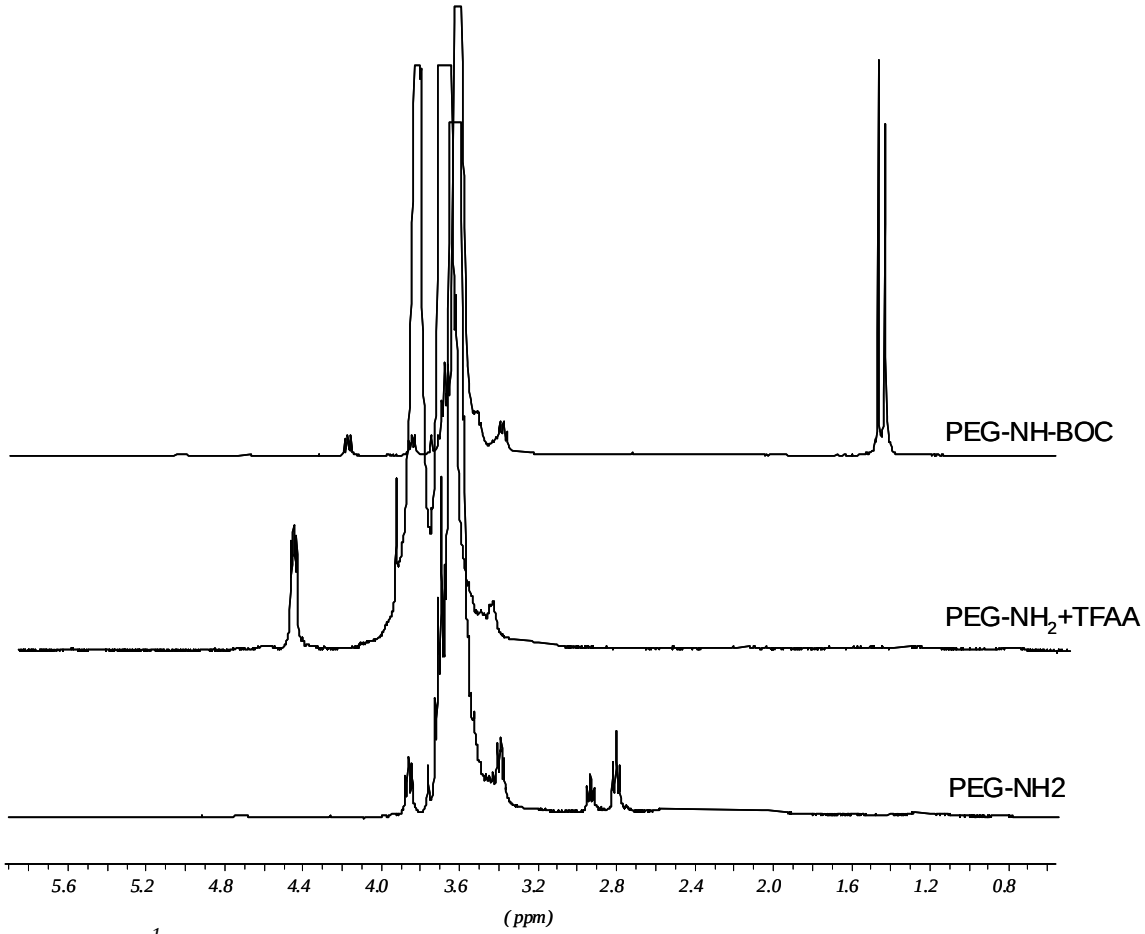

Figure 13: ^{1}H-NMR spectra of amino poly(ethylene glycol) (PEG-NH_2), amino poly(ethylene glycol) + trifluoroacetic acid (PEG-NH_2+TFAA) and amino poly(ethylene glycol) protected with BOC (PEG-NH-BOC)

Table 2: Chemical shifts and integrals of the above NMR spectra

Chemical shift (ppm)	Signals integration		
	HO-PEG-NH_2	HO-PEG-NH_2 + TFAA	HO-PEG-NH-BOC
1.3-1.4	0.00	0.00	8.61
2.8-2.95	2.00	0.00	0.00
3.4-3.9	179.99	181.0	179.5
4.1-4.2	0.00	0.00	2.05
4.4-4.5	0.00	2.00	0.00

In order to confirm the molecular weight calculation, MALDI-ToF was performed, which also showed the size distribution of the obtained polymer (Figure 14). The mass spectrum of the HO-PEG-NH_2 showed the molecular weight distribution with the typical repeat units of 44 Da and a Gaussian distribution. The peak maximum was observed at the

molecular weight of 2038 Da. The number of monomers (n) for this polymer can be calculated to be about 46 repeat units (2038/44 ≈ 46), which agrees well with the data obtained by ^{1}H-NMR, since 46 ethylene units would carry 46*4 = 184 protons [52,53].

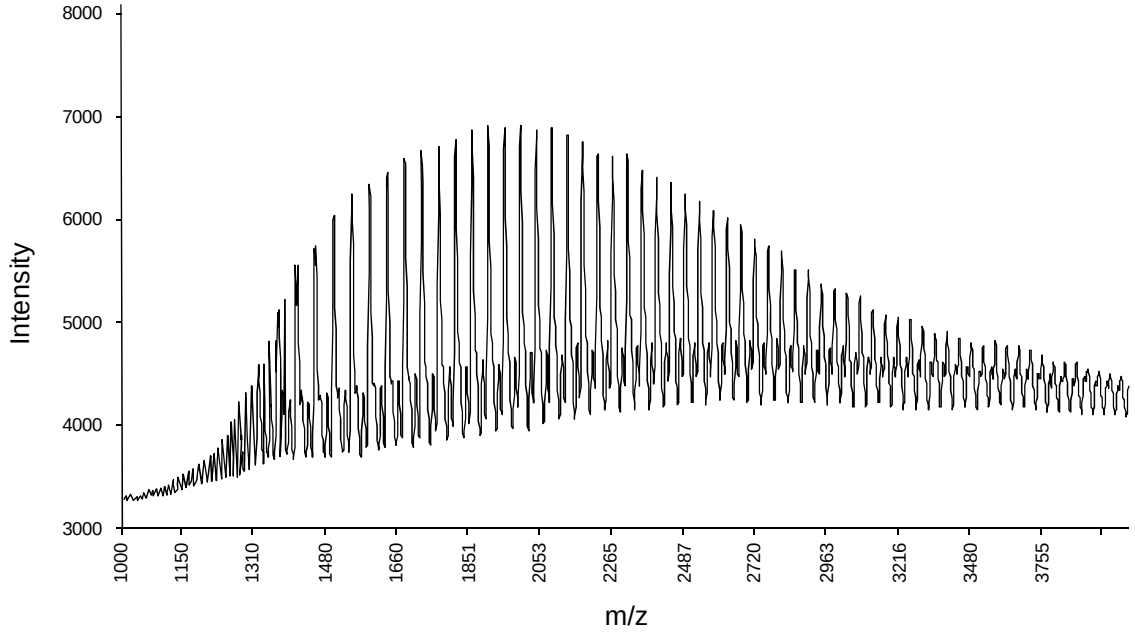

Figure 14: MALDI-ToF mass spectrum of synthesized amino poly(ethylene glycol)

After characterization of the obtained polymer, the terminal amino group had to be protected to avoid alkylation of both ends. The primary amine group was protected by reacting amino PEG with di(tert-butyl)dicarbonate (di-BOC). The reaction was carried out under alkaline conditions and low temperature in a dioxane/water mixture to allow selective protection of the amino group since the ester formed on the hydroxyl group would be immediately cleaved [12,54]. The ^{1}H-NMR spectrum of the protected polymer (HO-PEG-NH-BOC), using 1.1 molar equivalent of BOC, is displayed in Figure 13 with the integrals in Table 2. The characteristic signals of the spectrum appear at δ_H: 3.9-3.4 ppm for the PEG chain and 1.4-1.3 ppm for the BOC group. Similarly as for the TFAA modification the PEG protons adjacent to the amine are shifted up field to 4.2-4.1 ppm due to formation of the urethane with BOC.

A quantification of the successful protection was carried out by fluorescamine assay of the primary amine. Fluorescamine reacts rapidly and in high sensitivity with primary amines to form a fluorophor with an excitation wavelength of 390 nm and an emission wavelength of 475 nm. The obtained fluorescence intensity is proportional to the primary amine concentration, stable over several hours, and excess reagent is hydrolyzed within minutes [55-

58]. Since the fluorescence of the conjugate is dependent on the amine, a standard curve was recorded for the HO-PEG-NH_2 with fluorescamine in borate buffer.

Based on the standard curve, the amounts of free amine in HO-PEG-NH_2 after protection using different concentrations of BOC (1.1 and 5 molar equivalents) were found to be less than 1% (Figure 15) indicating the successful protection of the primary amine of PEG by using this method with both BOC concentrations.

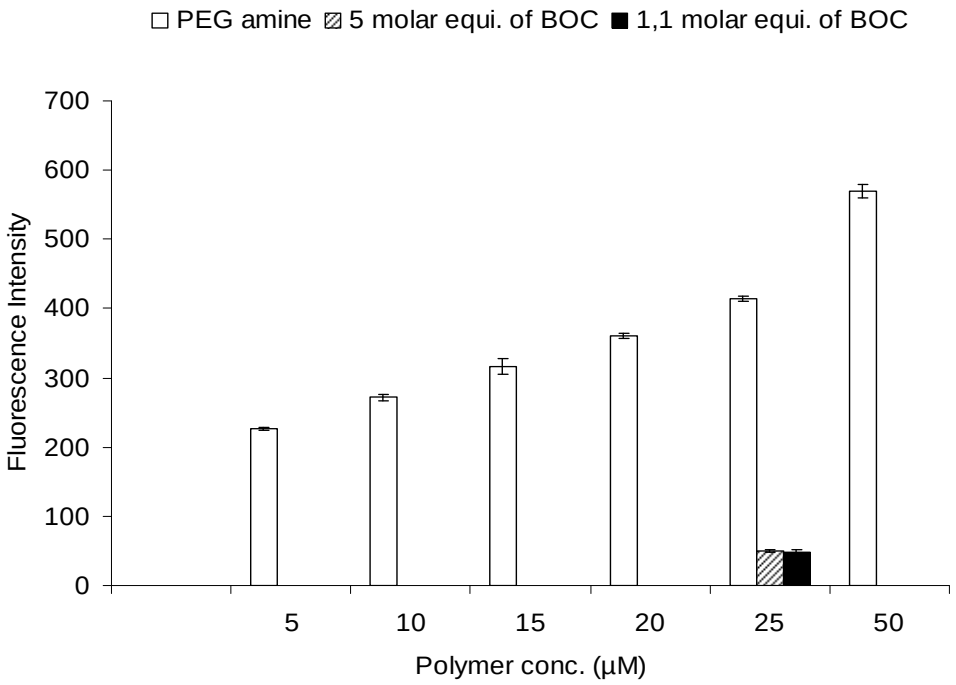

Figure 15: Fluorescence intensity after reaction of different concentrations of HO-PEG-NH_2 and BOC protected HO-PEG-NH_2 using 1.1 and 5 molar equivalents with fluorescamine

4.2.2. Synthesis of BOC-protected amino poly(ethylene glycol)-1-undecene

BOC protected amino PEG was subsequently reacted with 11-bromo-1-undecene using sodium hydride as already described to avoid the presence of water, the reaction was carried out as described for the synthesis of methoxy poly(ethylene glycol)-1-undecene. The ^{1}H-NMR spectrum of the obtained BOC-NH-PEG-undecene is presented in Figure 16. The spectrum again shows the characteristic signals of both the aliphatic part and the protected amino PEG chain, located at δ_H: 5.9-5.8 (m, 1 H), 5.05-4.9 (t, 2 H), 4.2 (m, 2 H), 3.9-3.3 (m, 180 H), 2.0 (m, 2H) and 1.8-1.2 ppm (m, 23 H). The integrals of these signals agreed well with the theoretical values and indicated that the reaction took place only on the hydroxyl end of the polymer.

Figure 16: H-NMR spectrum of BOC protected amino poly(ethylene glycol)-1-undecene

The HPLC chromatogram of BOC-NH-PEG-1-undecene compared to HO-PEG-NH_2 is presented in Figure 17 (chromatogram A and B). The peak of amino poly(ethylene glycol) is detected at a retention time of 14 minutes (chromatogram A), while BOC protected amino poly(ethylene glycol)-1-undecene eluted later at about 20 minutes (chromatogram B) due to the attachment of two hydrophobic moieties, BOC group and the alkene chain.

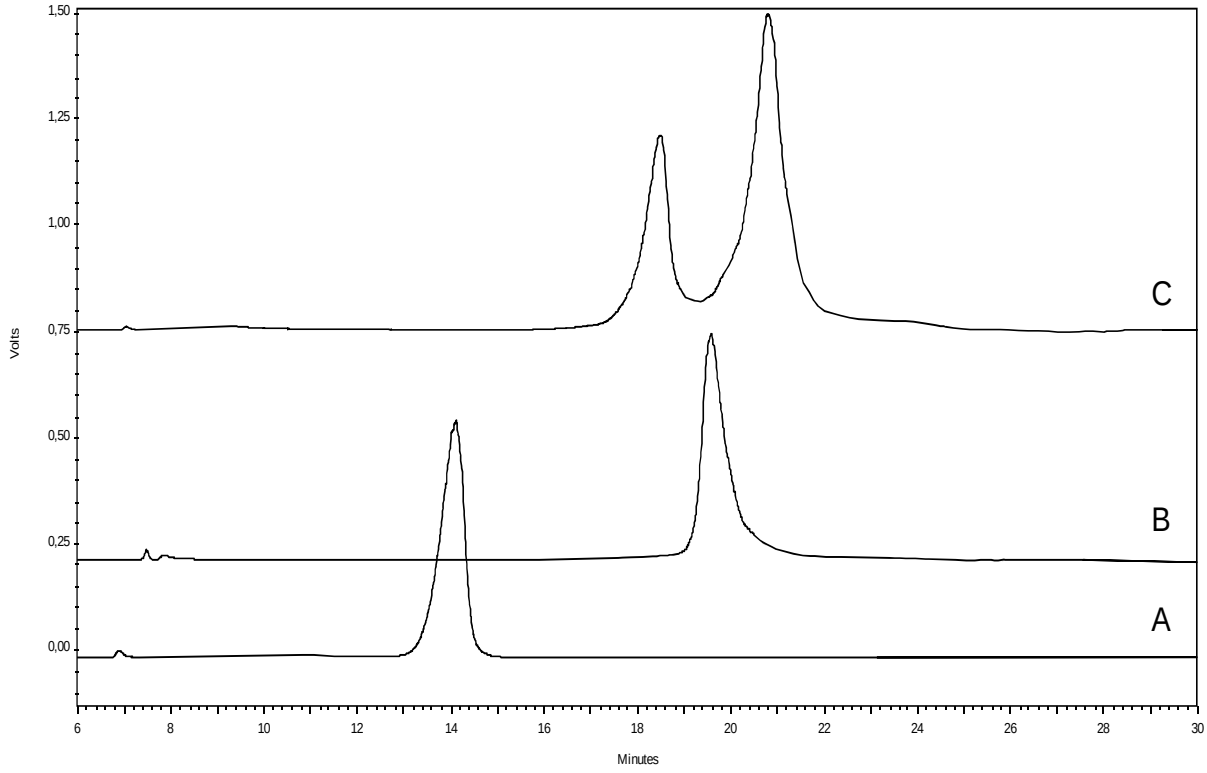

Figure 17: HPLC of amino poly(ethylene glycol) (A), BOC protected amino poly(ethylene glycol)-1-undecene (B), and amino poly(ethylene glycol)-undecyl mercaptane (C)

4.2.3. Addition of thioacetic acid to the terminal double bond

The addition of thioacetic acid to the terminal double bond yielded the thioacetate ester of the BOC protected amino PEG-undecane. Figure 18 shows the ^{1}H-NMR spectrum of the produced thioacetate ester with no signs of the educts double bond and the newly introduced appeared acetate's signals (δ_H: 4.2-4.1 ppm (t, 2H, protons adjacent to the urethane bond), 3.9-3.4 ppm (m, 182 H), 2.8 ppm (t, 2 H), 2.3 ppm (s, 3 H) and 1.8-1.2 ppm (m, 27 H)).

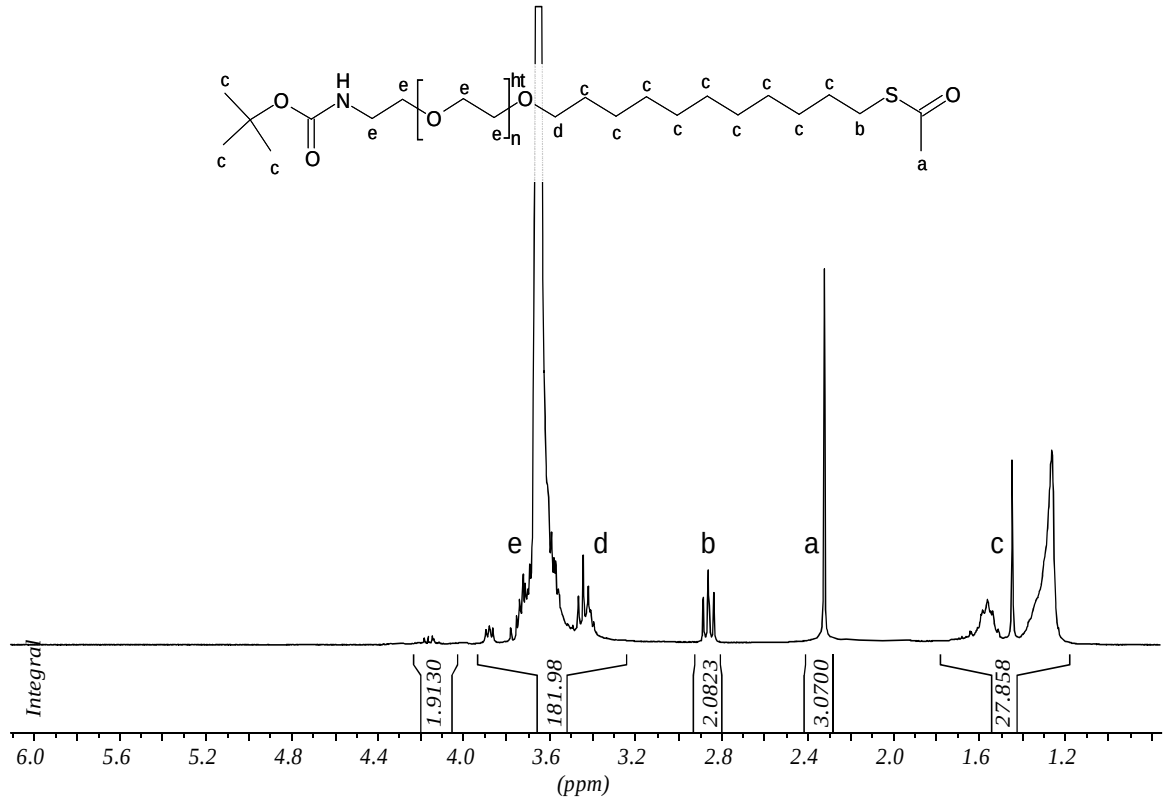

Figure 18: H-NMR spectrum of BOC protected amino poly(ethylene glycol)-1-undecene thioacetate ester

4.2.4. Hydrolysis of BOC-protected amino poly(ethylene glycol)-undecane thioester

The last step, the hydrolysis of thioacetate ester and deprotection of the amino group, was done in methanolic HCl, which hydrolyzes both the ester and the BOC protecting group, yielding amino poly(ethylene glycol)-undecyl mercaptane [5,38,59]. The added washing step was performed to deprotonate the amine for further modification. The ^{1}H-NMR spectrum showed the signals of the alkanethiol part and PEG chain with the characteristic signals (δ_H: 3.9-3.4 ppm (m, 182 H, protons of PEG chain), 2.9-2.8 ppm (t, 2 H, protons adjacent to amino group), 2.55 ppm (t, 2 H, protons adjacent to thiol group) and 1.8-1.2 ppm (m, 16 H)). HPLC analysis of the finished polymer is presented in Figure 17 (chromatogram C). The chromatogram is characterized again by two peaks as for the mPEG derivative; the first peak related to the reduced form (free thiol) eluted at about 18 minutes and the second peak related to the oxidized form (disulfide form) eluted at 21 minutes.

4.3. Synthesis of bisphosphonate-modified amino poly(ethylene glycol)-undecyl mercaptane

The conjugation of the poly(ethylene glycol) amine was investigated in aqueous and organic medium. However, in water the conjugation was not successful due to side reactions with the phosphonic acid and the low reactivity of the amine. In organic solvent the carboxyl group of unhydrolyzed bisphosphonate (compound **11**) was first activated by DCC and NHS to form the active ester, which then reacted with the amine group of the polymer forming a stable amide bond (Scheme 7) [60]. Figure 19 shows the HPLC chromatograms of the polymer before (chromatogram A) and after (chromatogram C) conjugation to bisphosphonate compared to bisphosphonate alone (chromatogram B). The chromatogram of the unmodified polymer shows the characteristic peak of the oxidized form of the polymer at 20 minutes, while the relative hydrophilic and smaller bisphosphonate is characterized by a peak at approximately 8 minutes. After attachment to the polymer a new peak is resulting, which is eluted at about 15 minutes.

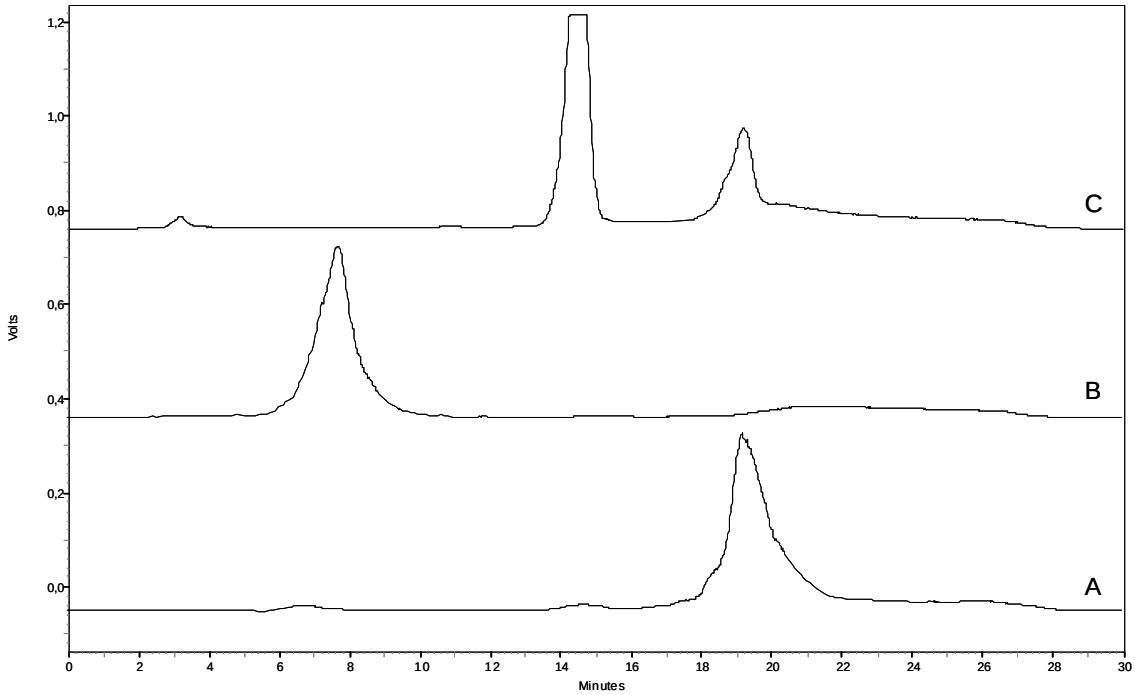

Figure 19: HPLC chromatograms of amino poly(ethylene glycol)-undecyl mercaptane (A), 3,5-di(tetraethyl ethylamino-2,2-bisphosphonate)benzoic (B) and the product (C)

Due to the slow reaction of the bisphosphonate ester with the polymer, the effect of the reaction time on the conversion was investigated. Increasing the reaction time from 24 hours to 48 hours resulted in further decrease of the amount of the unreacted polymer, while increased reaction time did not reduce this amount much more, most likely due to the

deactivation of the activated bisphosphonate. For further investigations a reaction time of 48 hours was, therefore, considered to be optimal.

Similar experiments were carried out to investigate the effect of the molar ratio of bisphosphonate to polymer on the percent conversion. The highest conversion was obtained for the 2 molar equivalents of bisphosphonate to amino poly(ethylene glycol)-undecyl mercaptane. The final dealkylation of the tetraethyl ester of bisphosphonate-modified polymer was done using bromotrimethylsilane under mild conditions and produced the free bisphosphonate modified-polymer [61,62].

4.3.1. Determination of bisphosphonate concentration in the modified-polymer

In order to quantify the amount of bisphosphonate conjugated to the polymer, a sensitive spectrophotometric method for its determination was established according to Daley-Yates [42], which depends on oxidation of bisphosphonate to orthophosphate with ammonium persulfate and the subsequent formation of a colored complex with molybdenum-ascorbate reagent (λ_{abs}=820 nm). The chosen method had a wide linearity range up to 500 µg/ml phosphate with 10 ng/ml a determination limit [43,44]. A standard curve of a commercial bisphosphonate (ibandronate) was used for calibration. Quantification of the amount of incorporated phosphate in the polymer was performed according the similar procedure as for the standard and showed that about 95 ± 3.6 % of the theoretical amount of phosphorus were incorporated in the polymer, which indicates the successful modification with the bisphosphonate group.

4.3.2. Determination of PEG concentration in the synthesized polymers

The chosen method to quantify PEG was based on the measurement of the decrease of fluorescein absorbance in an aqueous two phase system with PEG acting as a phase transfer catalyst. This indirect method of quantification is know from literature and allows to detect PEG concentrations as low as 0.1 µM [45]. Serial dilutions of methoxy poly(ethylene glycol) (mPEG) and the synthesized amino poly(ethylene glycol) (PEG-NH_2) were added to the fluorescein solution and the alteration of absorbance was measured. A direct relation between the PEG concentration and the absorbance difference of fluorescein was observed (increasing PEG concentrations led to increase in the absorbance differences) as indicated in Figure 20.

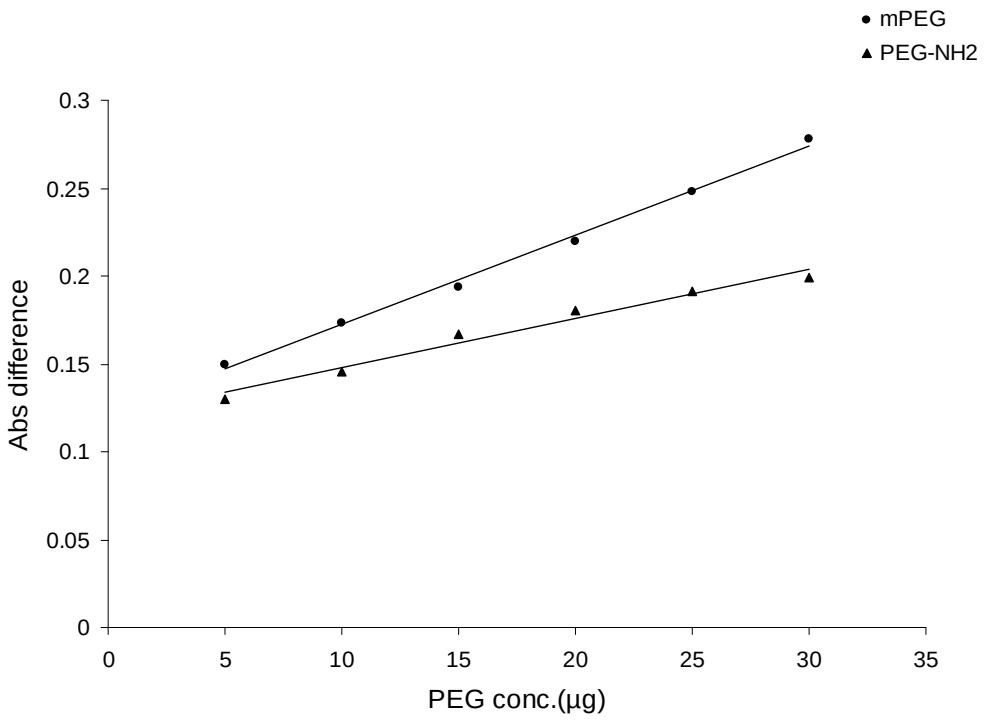

Figure 20: Determination of methoxy poly(ethylene glycol) 2000 (mPEG), R = 0.998, and amino poly(ethylene glycol) 2000 (PEG-NH_2), R = 0.988, by fluorescein

In case of the synthesized thioalkylated polymers, methoxy poly(ethylene glycol)-undecyl mercaptane (mPEG-AlkSH) and amino poly(ethylene glycol)-undecyl mercaptane (NH_2-PEG-AlkSH), the determination could not be performed as indicated in Figure 21, which was attributed to the interference of the thioalkylated parts of the polymers with the phase transfer of fluorescein. Consequently an accurate determination of the PEG content could not be performed and the polymer had to be further investigated according to its functionality as already described in chapter 2.

A) R = -0.205

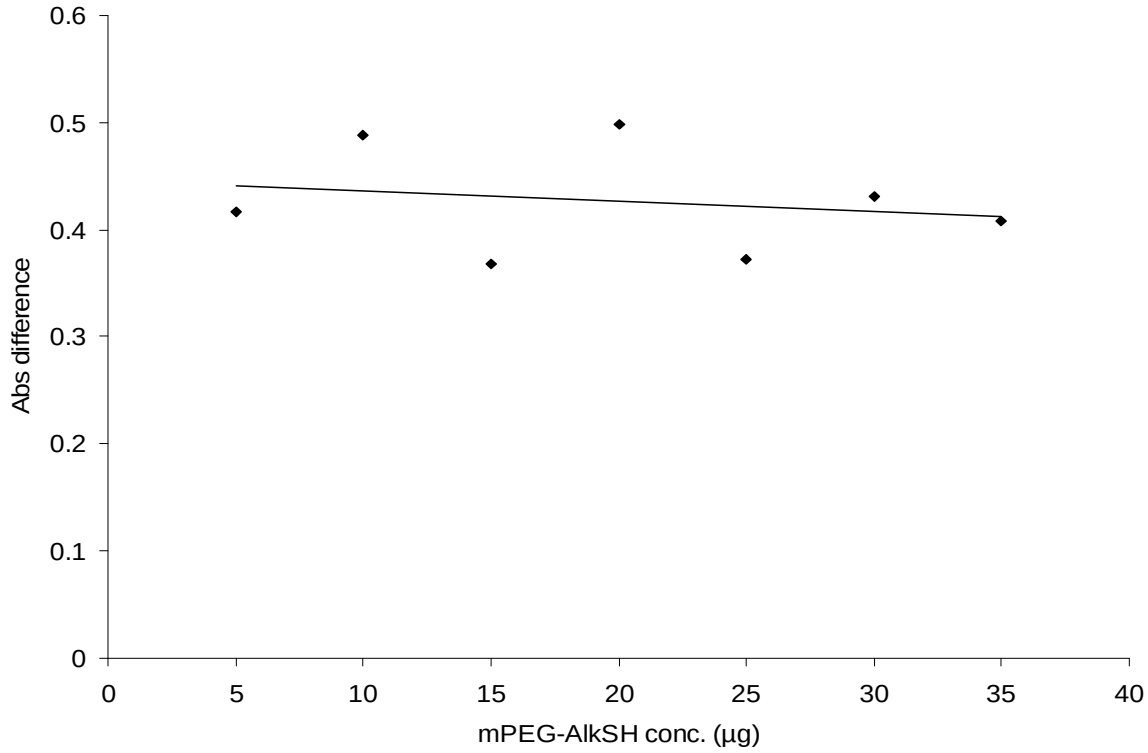

B) R = 0.798

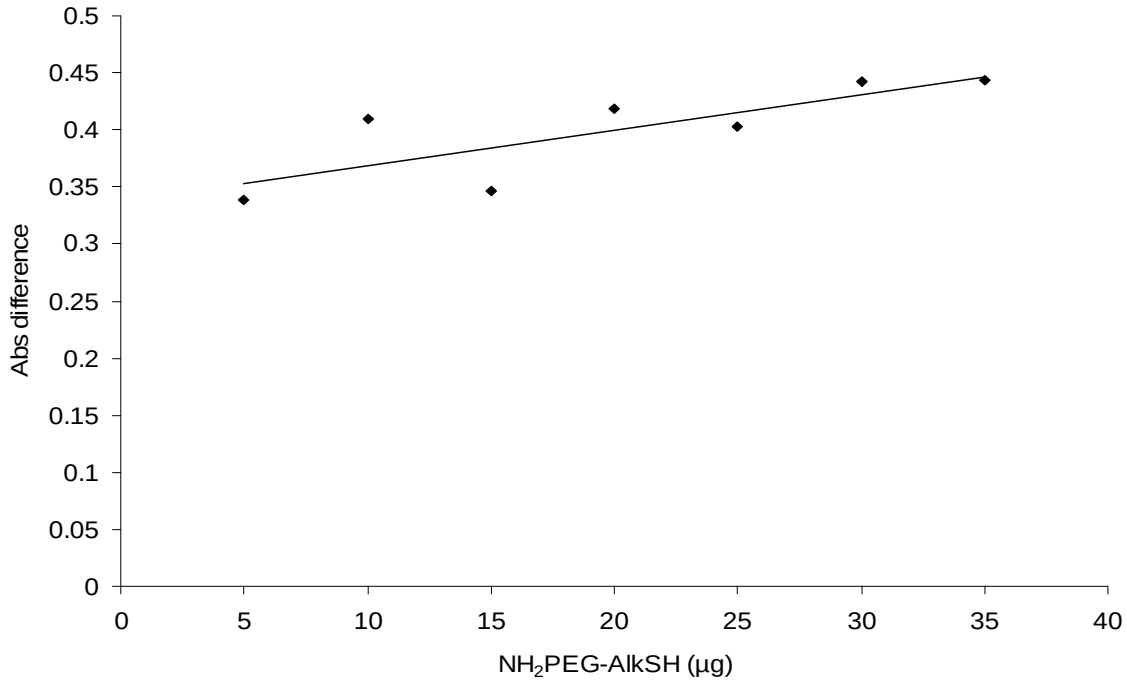

Figure 21: Quantitative determination of methoxy (A) and amino (B) poly(ethylene glycol)-undecyl mercaptane with no observed fluorescence changes

5. Conclusions

The synthesis of polymers used for the later modification of gold nanoparticles was thoroughly optimized in order to have defined substances for the coating of the surfaces. The already described synthesis was lacking the necessary purity in order to be sure of the surface composition of the later obtained nanoparticles. The synthesis schemes were optimized to achieve high conversions, which were done by using an excess of the easier to remove reagents, and also the following purification was performed making use either of the unique solubility of PEG or the high negative charges of the bisphosphonate group. By applying these optimization steps, high conversions were achieved and the polymers were obtained with very high purities. Since they are mainly used for the surface modification of small nanoparticles, the amounts synthesized were sufficient, but for a commercial application of the polymer an improvement of the yields without sacrificing the amounts of conversion would be further necessary.

6. References

1. Robert Knerr, Sigrid Drotleff, Claudia Steinem, and A. Goepferich, "Self-assembling PEG Derivatives for Protein-repellant Biomimetic Model Surfaces on Gold," Biomaterialien **7,** 12-20 (2006).

2. Neville Boden, Richard J. Bushby, Steven Clarkson, Stephen D. Evans, Peter F. Knowles, and Andrew Marsh, "The design and synthesis of simple molecular tethers for binding biomembranes to a gold surface," Tetrahedron **53,** 10939-10952 (1997).

3. Marcio C. S. de Mattos and Rafael Berrelho Bernini, "The reaction of (R)-limonene with S-thioacids," Journal of the Brazilian Chemical Society **18,** 1068-1072 (2007).

4. C. Naud, P. Calas, H. Blancou, and A. Commeyras, "Synthesis of terminally perfluorinated long-chain alkanethiols, sulfides and disulfides from the corresponding halides," Journal of Fluorine Chemistry **104,** 173-183 (2000).

5. Dariusz Witt, Rafal Klajn, Piotr Barski, and Bartosz A. Grzybowski, "Applications, properties and synthesis of w-functionalized n-alkanethiols and disulfides - the building blocks of self-assembled monolayers," Current Organic Chemistry **8,** 1763-1797 (2004).

6. Carmichael Roberts, Christopher S. Chen, Milan Mrksich, Valerie Martichonok, Donald E. Ingber, and George M. Whitesides, "Using mixed self-assembled monolayers presenting RGD and (EG)3OH groups to characterize long-term attachment of bovine capillary endothelial cells to surfaces," Journal of the American Chemical Society **120,** 6548-6555 (1998).

7. S. Kanagasabapathy, A. Sudalai, and B. C. Benicewicz, "Montmorillonite K 10-catalyzed regioselective addition of thiols and thiobenzoic acids onto olefins: an efficient synthesis of dithiocarboxylic esters," Tetrahedron Letters **42,** 3791-3794 (2001).

8. Hyunsoo Han and Kim D. Janda, "A soluble polymer-bound approach to the Sharpless catalytic asymmetric dihydroxylation (AD) reaction: preparation and application of a [(DHQD)2PHAL-PEG-OMe) ligand," Tetrahedron Letters **38,** 1527-1530 (1997).

9. Saleh A. Ahmed and Mutsuo Tanaka, "Synthesis of oligo(ethylene glycol) toward 44-mer," J Org Chem **71,** 9884-9886 (2006).

10. Siu Choon Ng, Tong Sun, and Hardy S. O. Chan, "Chiral discrimination of enantiomers with a self-assembled monolayer of functionalized b-cyclodextrins on Au surfaces," Tetrahedron Letters **43,** 2863-2866 (2002).

11. Christie A. Canaria, Jeffrey O. Smith, C. J. Yu, Scott E. Fraser, and Rusty Lansford, "New syntheses for 11-(mercaptoundecyl)triethylene glycol and mercaptododecyltriethyleneoxy biotin amide," Tetrahedron Letters **46,** 4813-4816 (2005).

12. Pierre Oudet Charles Mioskowski Luc Lebeau, "Synthesis of New Phospholipids Linked to Steroid-Hormone Derivatives Designed for Two-Dimensional Crystallization of Proteins," Helvetica Chimica Acta **74,** 1697-1706 (1991).

13. Geeti Bansal, Jennifer E. I. Wright, Cezary Kucharski, and Hasan Uludag, "A dendritic tetra(bisphosphonic acid) for improved targeting of proteins to bone," Angewandte Chemie, International Edition **44,** 3710-3714 (2005).

14. Sebastien A. Gittens, Geeti Bansal, Cezary Kucharski, Mark Borden, and Hasan Uludag, "Imparting mineral affinity to fetuin by bisphosphonate conjugation: a comparison of three bisphosphonate conjugation schemes," Molecular Pharmaceutics **2,** 392-406 (2005).

15. Eva Kynclova, Elisabeth Elsner, Andreas Kopf, Gerhard Hawa, Thomas Schalkhammer, and Fritz Pittner, "Novel method for coupling of poly(ethyleneglycol) to carboxylic acid moieties of proteins," Journal of Molecular Recognition **9,** 644-651 (1996).

16. G. Mattson, E. Conklin, S. Desai, G. Nielander, M. D. Savage, and S. Morgensen, "A practical approach to crosslinking," Molecular Biology Reports **17,** 167-183 (1993).

17. Gianfranco Pasut, Fabiana Canal, Lisa Dalla Via, Silvia Arpicco, Francesco M. Veronese, and Oddone Schiavon, "Antitumoral activity of PEG-gemcitabine prodrugs targeted by folic acid," Journal of Controlled Release **127,** 239-248 (2008).

18. Kyung Chul Cho, Sun Hwa Kim, Ji Hoon Jeong, and Tae Gwan Park, "Folate receptor-mediated gene delivery using folate-poly(ethylene glycol)-poly(L-lysine) conjugate," Macromolecular Bioscience **5,** 512-519 (2005).

19. Marc Lecouvey and Yves Leroux, "Synthesis of 1-hydroxy-1,1-bisphosphonates," Heteroatom Chemistry **11,** 556-561 (2000).

20. Vojtech Kubicek, Jakub Rudovsky, Jan Kotek, Petr Hermann, Luce Vander Elst, Robert N. Muller, Zvonimir I. Kolar, Hubert Th Wolterbeek, Joop A. Peters, and Ivan Lukes, "A Bisphosphonate Monoamide Analogue of DOTA: A Potential Agent for Bone Targeting," Journal of the American Chemical Society **127,** 16477-16485 (2005).

21. A. J. Kresge, P. H. Fitzgerald, and Y. Chiang, "Position of protonation and mechanism of hydrolysis of simple amides," Journal of the American Chemical Society **96,** 4698-4699 (1974).

22. Jean Pierre Haelters, Helene Couthon-Gourves, Alan Le Goff, Gaelle Simon, Bernard Corbel, and Paul Alain Jaffres, "Synthesis of functionalized alkoxyalkylidene gem-bisphosphonates," Tetrahedron **64,** 6537-6543 (2008).

23. Kumar R. Bhushan, Eiichi Tanaka, and John V. Frangioni, "Synthesis of conjugatable bisphosphonates for molecular imaging of large animals," Angewandte Chemie, International Edition **46,** 7969-7971 (2007).

24. M. J. Phillips, P. Duncanson, K. Wilson, J. A. Darr, D. V. Griffiths, and I. Rehman, "Surface modification of bioceramics by grafting of tailored allyl phosphonic acid," Advances in Applied Ceramics **104,** 261-267 (2005).

25. Frank W. Foss, Ashley H. Snyder, Michael D. Davis, Michael Rouse, Mark D. Okusa, Kevin R. Lynch, and Timothy L. Macdonald, "Synthesis and biological evaluation of g-aminophosphonates as potent, subtype-selective sphingosine 1-phosphate receptor agonists and antagonists," Bioorganic & Medicinal Chemistry **15,** 663-677 (2007).

26. Geeti Bansal, Sebastien A. Gittens, and Hasan Uludag, "A di(bisphosphonic acid) for protein coupling and targeting to bone," Journal of Pharmaceutical Sciences **93,** 2788-2799 (2004).

27. Harri Salo, Andrei Guzaev, and Harri Loennberg, "Disulfide-Tethered Solid Supports for Synthesis of Photoluminescent Oligonucleotide Conjugates: Hydrolytic Stability and Labeling on the Support," Bioconjugate Chem. **9,** 365-371 (1998).

28. Colin D. Bain, E. Barry Troughton, Yu Tai Tao, Joseph Evall, George M. Whitesides, and Ralph G. Nuzzo, "Formation of monolayer films by the spontaneous assembly of organic thiols from solution onto gold," Journal of the American Chemical Society **111,** 321-335 (1989).

29. S. Mourtas, D. Gatos, V. Kalaitzi, C. Katakalou, and K. Barlos, "S-4-Methoxytrityl mercapto acids: synthesis and application," Tetrahedron Letters **42,** 6965-6967 (2001).

30. Benjamin T. Houseman and Milan Mrksich, "Efficient Solid-Phase Synthesis of Peptide-Substituted Alkanethiols for the Preparation of Substrates That Support the Adhesion of Cells," Journal of Organic Chemistry **63,** 7552-7555 (1998).

31. Alena Braunova, Michal Pechar, Richard Laga, and Karel Ulbrich, "Hydrolytically and reductively degradable high-molecular-weight poly(ethylene glycol)s," Macromolecular Chemistry and Physics **208,** 2642-2653 (2007).

32. Kevin L. Prime and George M. Whitesides, "Adsorption of proteins onto surfaces containing end-attached oligo(ethylene oxide): a model system using self-assembled monolayers," Journal of the American Chemical Society **115,** 10714-10721 (1993).

33. Kuk Ro Yoon, Ok Ja Yoon, Young Shik Chi, and Insung S. Choi, "Uniform grafting of poly(1,5-dioxepan-2-one) by surface-initiated, ring-opening polymerization," Macromolecular Research **14,** 205-208 (2006).

34. Li Ping Zhu, Bao Ku Zhu, Li Xu, Yong Xiang Feng, and You Yi Xu, "Synthesis of amphiphilic poly(phthalazinone ether sulfone ketone)-graft-poly(ethylene glycol) graft copolymers via Williamson etherification," Journal of Applied Polymer Science **104,** 2973-2979 (2007).

35. Jose A. Camerano, Miguel A. Casado, Miguel A. Ciriano, Cristina Tejel, and Luis A. Oro, "Peripheral SH-functionalisation of carbosilane dendrimers including the synthesis of the model compound dimethylbis(propanethiol)silane and their interaction with rhodium complexes," Dalton Transactions 3092-3100 (2005).

36. Masayuki Yokoyama, Teruo Okano, Yasuhisa Sakurai, Akira Kikuchi, Nobuyuki Ohsako, Yukio Nagasaki, and Kazunori Kataoka, "Synthesis of poly(ethylene oxide) with heterobifunctional reactive groups at its terminals by an anionic initiator," Bioconjugate Chem. **3,** 275-276 (1992).

37. L. Dreesen, Y. Sartenaer, A. Peremans, P. A. Thiry, C. Humbert, J. Grugier, and J. Marchand-Brynaert, "Synthesis and characterization of aromatic self-assembled monolayers containing methylene and ethylene glycol entities by means of sum-frequency generation spectroscopy," Thin Solid Films **500,** 268-277 (2006).

38. Guillaume Clave, Herve Boutal, Antoine Hoang, Francois Perraut, Herve Volland, Pierre Yves Renard, and Anthony Romieu, "A novel heterotrifunctional peptide-based cross-linking reagent for facile access to bioconjugates. Applications to peptide fluorescent labelling and immobilisation," Organic & Biomolecular Chemistry **6,** 3065-3078 (2008).

39. Min Liu, Cao Xie, Wen Xu, and Weiyue Lu, "Separation of polyethylene glycols and their amino-substituted derivatives by high-performance gel filtration chromatography at low ionic strength with refractive index detection," Journal of Chromatography, A **1046,** 121-126 (2004).

40. Zan Xie, Ye Jiang, and Di Qun Zhang, "Simple analysis of four bisphosphonates simultaneously by reverse phase liquid chromatography using n-amylamine as volatile ion-pairing agent," Journal of Chromatography, A **1104,** 173-178 (2006).

41. T. C. Schmidt, M. Petersmann, L. Kaminski, V. Loew, and G. Stork, "Analysis of aminobenzoic acid in wastewater from a former ammunition plant with HPLC and combined diode array and fluorescence detection," Fresenius' Journal of Analytical Chemistry **357,** 121-126 (1997).

42. P. T. Daley-Yates, L. A. Gifford, and C. R. Hoggarth, "Assay of 1-hydroxy-3-aminopropylidene-1,1-bisphosphonate and related bisphosphonates in human urine and plasma by high-performance ion chromatography," J Chromatogr **490,** 329-338 (1989).

43. Constantinos K. Zacharis and Paraskevas D. Tzanavaras, "Determination of bisphosphonate active pharmaceutical ingredients in pharmaceuticals and biological material: a review of analytical methods," Journal of Pharmaceutical and Biomedical Analysis **48,** 483-496 (2008).

44. Sufeng Zhang, Jennifer E. I. Wright, Natali Ozber, and Hasan Uludag, "The interaction of cationic polymers and their bisphosphonate derivatives with hydroxyapatite," Macromolecular Bioscience **7,** 656-670 (2007).

45. Claude Guermant, Jeanne Brygier, Danielle Baeyens-Volant, Michelle Nijs, Jean Vincentelli, Claudine Paul, and Yvan Looze, "Quantitative determination of polyethylene glycol based upon its salting out and partitioning of a dye into the resulting aqueous two-phase system," Analytical Biochemistry **230,** 254-258 (1995).

46. Jane Y. Park, Metin H. Acar, Ariya Akthakul, William Kuhlman, and Anne M. Mayes, "Polysulfone-graft-poly(ethylene glycol) graft copolymers for surface modification of polysulfone membranes," Biomaterials **27,** 856-865 (2006).

47. Lutz Schmitt, Markus Ludwig, Hermann E. Gaub, and Robert Tampe, "A metal-chelating microscopy tip as a new toolbox for single-molecule experiments by atomic force microscopy," Biophysical Journal **78,** 3275-3285 (2000).

48. Benoit Gadenne, Ibrahim Yildiz, Matteo Amelia, Flavio Ciesa, Andrea Secchi, Arturo Arduini, Alberto Credi, and Francisco M. Raymo, "Luminescence quenching in supramolecular assemblies of quantum dots and bipyridinium dications," Journal of Materials Chemistry **18,** 2022-2027 (2008).

49. Marcia G. Oliveira, Bluma G. Soares, Claudia M. F. Santos, Milton F. Diniz, and Rita C. L. Dutra, "Mercapto-modified copolymers in copolymer blends. Part 1. Functionalization of EPDM with mercapto groups and its use in NBR/EPDM blends," Macromolecular Rapid Communications **20,** 526-531 (1999).

50. Robert Knerr, Barbara Weiser, Sigrid Drotleff, Claudia Steinem, and Achim Goepferich, "Measuring cell adhesion on RGD-modified, self-assembled PEG monolayers using the quartz crystal microbalance technique," Macromolecular Bioscience **6,** 827-838 (2006).

51. Joerg K. Tessmar, Antonios G. Mikos, and Achim Goepferich, "Amine-Reactive Biodegradable Diblock Copolymers," Biomacromolecules **3,** 194-200 (2002).

52. H. J. Raeder and W. Schrepp, "MALDI-TOF mass spectrometry in the analysis of synthetic polymers," Acta Polymerica **49,** 272-293 (1998).

53. R. N. Jagtap and A. H. Ambre, "Overview literature on matrix assisted laser desorption ionization mass spectroscopy (MALDI MS): Basics and its applications in characterizing polymeric materials," Bulletin of Materials Science **28,** 515-528 (2005).

54. S. Mohapatra, S. K. Mallick, T. K. Maiti, S. K. Ghosh, and P. Pramanik, "Synthesis of highly stable folic acid conjugated magnetite nanoparticles for targeting cancer cells," Nanotechnology **18,** 385102-1-385102/9 (2007).

55. Tjasa Bantan-Polak, Miki Kassai, and Kathryn B. Grant, "A comparison of fluorescamine and naphthalene-2,3-dicarboxaldehyde fluorogenic reagents for microplate-based detection of amino acids," Analytical Biochemistry **297,** 128-136 (2001).

56. Shukuan Li, Zhijian Yang, Xinghua Sun, Yuying Tan, Shigeo Yagi, and Robert M. Hoffman, "A simultaneous colorimetric assay of free and protein-coupled polyethylene glycol," Analytical Biochemistry **313,** 335-337 (2003).

57. S. Jill Stocks, Andrew J. M. Jones, Charles W. Ramey, and Donald E. Brooks, "A fluorometric assay of the degree of modification of protein primary amines with polyethylene glycol," Analytical Biochemistry **154,** 232-234 (1986).

58. Juan C. Stockert, Alfonso Blazquez, Sergio Galaz, and Angeles Juarranz, "A mechanism for the fluorogenic reaction of amino groups with fluorescamine and MDPF," Acta Histochemica **110,** 333-340 (2008).

59. S. W. Garrett, O. R. Davies, D. A. Milroy, P. J. Wood, C. W. Pouton, and M. D. Threadgill, "Synthesis and characterization of polyamine-poly(ethylene glycol) constructs for DNA binding and gene delivery," Bioorganic & Medicinal Chemistry **8,** 1779-1797 (2000).

60. Katja Riebeseel, Elfi Biedermann, Roland Loeser, Norbert Breiter, Ralf Hanselmann, Rolf Muelhaupt, Clemens Unger, and Felix Kratz, "Polyethylene Glycol Conjugates of Methotrexate Varying in Their Molecular Weight from MW 750 to MW 40000: Synthesis, Characterization, and Structure-Activity Relationships in Vitro and in Vivo," Bioconjugate Chem. **13,** 773-785 (2002).

61. Sebastien A. Gittens, Geeti Bansal, Ronald F. Zernicke, and Hasan Uludag, "Designing proteins for bone targeting," Advanced Drug Delivery Reviews **57,** 1011-1036 (2005).

62. Rotem Erez, Sharon Ebner, Bernard Attali, and Doron Shabat, "Chemotherapeutic bone-targeted bisphosphonate prodrugs with hydrolytic mode of activation," Bioorganic & Medicinal Chemistry Letters **18,** 816-820 (2008).

Chapter 4

Preparation, Stabilization and Surface Functionalization of Gold Nanoparticles

Gamal Zayed[1], Jörg Teßar[1], Achim Göpferich[1]

[1]Department of Pharmaceutical Technology, University of Regensburg

1. Introduction

Colloidal gold consists of sub-micrometer-sized particles of gold usually dispersed in water. The synthesis of gold nanoparticles (GNPs) has received considerable attention and a lot of different synthetic procedures have been described to obtain gold nanoparticles in different sizes, shapes, and dispersion media (either aqueous or non aqueous). Controlling the size, shape and structure of gold nanoparticles is technologically important because of the strong relation between these parameters and the resulting properties, such as the interaction with light, which is valuable for many applications of gold nanoparticles [1-5].

Aqueous gold nanoparticles dispersions are the most common especially for biomedical and biological applications. The simplest method of preparation is based on the reduction of aqueous hydrogen tetrachloroaurate solution by trisodium citrate. In this method, citrate anions have a dual function; in the beginning they act as the reducing agent to reduce Au^{+3} to Au^{0}. Later they also act as a stabilizing agent for the nanoparticle dispersion by forming a charged layer of citrate anions on the surface of the formed particles [6]. The mechanism of citrate reduction of gold chloride salts to form gold nanoparticles occurs through a multi-step process [7]. The initial step is the oxidation of citrate ions to produce dicarboxy acetone:

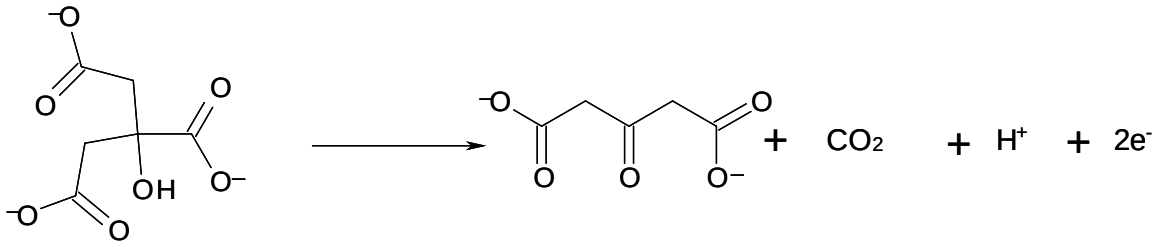

The second step is the reduction of auric (gold III) salt to aurous (gold I) salt:

$$AuCl_3 + 2e^- \longrightarrow AuCl + 2Cl^-$$

The third step is the disproportionation of the different aurous species to gold atoms where three gold I chloride combine together to produce elemental gold and one molecule of auric chloride. The gold atoms serve as nucleation sites for the growth of gold nanoparticles [8].

$$3AuCl \longrightarrow 2\,Au^0 + AuCl_3$$

$$n\,Au^0 \longrightarrow (Au^0)_n$$

The further growth of the nanoparticles is dependent on the ratios of the reactants, temperature and also the stirring rate, and can therefore be used to control the sizes of the obtained particles [9]. The finally obtained particles then posses a surface consisting of excess of citrate, which renders the particles negatively charged and consequently well disperses in the reaction medium.

Subsequently, the surface of the citrate-stabilized gold nanoparticles demands a further protection in order to increase the aggregation stability. For this task, self assembled monolayers (SAMs) on gold provide a versatile tool to protect and stabilize gold nanoparticles by separating the metal core from the surrounding environment, in order to prevent occurring particle growth and reversible agglomeration [10]. Poly(ethylene glycol) (PEG) derivatives here have been widely used to coat and stabilize gold nanoparticles, because they are hydrophilic, water soluble, biocompatible and also resistant to unspecific protein adsorption due to the steric stabilization of the PEG chains [11-14].

Many different research papers describe the useful application of similarly functionalized gold nanoparticles. Yoshimoto et al. [15], for example, reported the preparation of PEGylated GNPs, which were intended to be used as high-performance photothermal agents in photothermal therapy (PTT). Gold nanoparticles can also be applied as X-ray contrast agent with absorption properties that overcome some limitations of traditional agents due to their particulate character [16]. They appear to be non-toxic and enable higher and longer imaging times than currently possible using standard iodine-based agents [17]. A very recent study showed the successful use of antibody-conjugated PEGylated gold nanoparticles to label human cancer tissue that has been surgically resected from patients. The study takes the advantages of strong optical scattering of gold nanoparticles to image the actual distribution of the tumor and its stomal tissue with a simple darkfield microscope. Since the used gold nanoparticle-antibody conjugates are effectively stabilized by heterofunctional PEG molecules, they are highly stable under the biological conditions and unbound particles can be rinsed away quantitatively when the incubated tissue doesn’t contain the targeted antigen [18].

The objectives of this chapter are to describe the preparation of stable gold nanoparticles with sizes suitable for the intravenous administration and the optimization of their synthesis. Furthermore, the effect of subsequent surface modifications by PEGylation using methoxy and amino terminated poly(ethylene glycol)-undecyl mercaptane on particle properties, such as size, zeta potential and dispersion stability, were analyzed in the presence of electrolytes and proteins, which normally lead to significant aggregation of only citrate stabilized particles.

2. Experimental

2.1. Materials and Methods

Hydrogen tetrachloroaurate tri-hydrate ($HAuCl_4.3H_2O$), methoxy poly(ethylene glycol) 2000, ultrafilteration tubes (50,000Da MWCO), and bovine serum albumin were purchased from Sigma-Aldrich Chemical Company (Steinheim, Germany). Trisodium citrate, sodium chloride, nitric acid, hydrochloric acid were purchased from Merck (Darmstadt, Germany). Methoxy poly(ethylene glycol)-undecyl mercaptane (mPEG-AlkSH), amino poly(ethylene glycol)-undecyl mercaptane (NH_2PEG-AlkSH) were synthesized as described in chapter 2. All glassware was thoroughly washed with freshly prepared aqua regia (HCl: HNO3 = 3:1), extensively rinsed with Millipore water several times and oven-dried at 150 ^oC for 2-3 h before use. All solutions were filtered through 0.22 µm membrane filter (Corning Incorporated, Corning NY 14832, Germany) before use.

2.2. Preparation of gold nanoparticles

Gold nanoparticles (GNPs) were synthesized in one step aqueous preparation, in which hydrogen tetrachloroaurate was brought to boiling and reduced by rapid addition of sodium citrate. 100 ml water containing different concentrations of $HAuCl_4.3H_2O$ was heated until boiling under reflux, and then 1 ml aqueous solution of tri-sodium citrate trihydrate solution was added rapidly. Boiling and stirring were continued for 20 minutes. After that, the heating mantle was removed and the solution was stirred until it was cooled down to room temperature. Stock solutions of the gold salt (1%) and trisodium citrate (170 mg/ml) were prepared using Millipore water and were filtered through 0.22 µm membrane filter. Different volumes of the above mentioned solutions were applied in order to investigate the effect of citrate/gold ratio on the size of the obtained nanoparticles. The produced nanoparticles were characterized by UV-Vis spectroscopy, size and zeta potential measurements using photon correlation spectroscopy [19].

2.3. Characterization of the prepared gold nanoparticles

2.3.1. UV-visible spectroscopy of the prepared nanoparticles

Ultraviolet-visible light absorption spectra of the citrate-stabilized and the PEG-coated GNPs were taken at room temperature using a spectrophotometer (Uvikon-941, Kontron Instrument, Germany).

2.3.2. Size and zeta potential measurements by photon correlation spectroscopy (PCS)

The size distributions and the zeta potentials of the synthesized gold nanoparticles before and after polymer coating were analyzed by photon correlation spectroscopy (PCS) using a Zetasizer 3000 HAS (Malvern, Instruments GmbH, Germany). For a typical measurement 300 µl of GNPs were added to 3 ml of Millipore water immediately before measuring their size and zeta potential. The refractive index and the viscosity of water were used for the calculation of the results.

2.3.3. Determination of nanoparticle concentrations by ICP-OES

The actual concentration and consequently also the number of gold nanoparticles per volume after synthesis were determined by using inductively coupled plasma-optical emission spectroscopy (ICP-OES). Defined volumes of the nanoparticle dispersion were dissolved in aqua regia, more precisely diluted with Millipore water and the obtained samples were directly analyzed by ICP-OES (Horiba Jobin Yvon, 70P, S+S, Munich, Germany). The gold content of the dissolved particles was determined from a calibration curve constructed from different concentration, from 10 to 100 ppm, of hydrogen tetrachloroaurate tri-hydrate [20].

2.3.4. Stabilization and surface-functionalization of gold nanoparticles

Citrate stabilized GNPs were used without modification and after coating with either methoxy poly(ethylene glycol)-undecyl mercaptane (mPEG-AlkSH) or amino poly(ethylene glycol)-undecyl mercaptane (NH_2PEG-AlkSH). Different amounts of the two polymers, 1-5 µg per ml of the nanoparticles dispersion, were added to the nanoparticles to study the effect of coating on their size and also to determine the necessary concentration for a complete surface coating. The mixture was incubated while permanently stirring at room temperature for one day to allow sufficient exchange of citrate anions on the particle surface. The excess of unbound polymers was removed by several times ultracentrifugation using ultrafiltration tubes having molecular weight cut-off (MWCO) of 50.000 Da. The effect of surface coating of the particles was observed for their UV-Vis absorption, particle size and zeta potential.

a. Testing the dispersion stability of the surface-functionalized nanoparticles

In order to test the dispersion stability at high electrolyte concentration, the gold nanoparticles were incubated with 300 µl of 5 M NaCl for 2 ml of particle dispersion. The measured changes in UV-Vis absorbance, size and zeta potential of nanoparticles were used as indicators for their stability [21-23].

b. Interaction of surface-functionalized nanoparticles with proteins (BSA and bovine serum)

The interaction of citrate stabilized, methoxy and amino PEG coated gold nanoparticles with BSA (200 µg per ml of colloidal solution) and serum (10% v/v) was studied to investigate the effect of the different surface properties of the nanoparticles on protein adsorption. The particle samples were incubated with proteins over night at room temperature while permanently shaking the flasks. The interaction of the gold nanoparticles and proteins was monitored by UV-Vis spectroscopy, size determination and zeta potential measurement [23].

3. Results and Discussion

3.1. Preparation and characterization of gold nanoparticles

3.1.1. Effect of citrate concentrations on the size of the produced nanoparticles

The size of the nanoparticles prepared by the reduction of gold salt normally depends on a number of parameters, such as the type of reducing agent and the initial concentration of the metal precursor. The type of reducing agent determines the rate of nucleation and subsequently the particle growth: a slow reduction produces large particles, while fast reduction usually produces smaller particles [24]. The chosen synthesis of gold nanoparticles by citrate reduction represents a good model system for the production of GNPs in context of this thesis, because of its simplicity and reproducibility. After addition of trisodium citrate to the boiling solution of the gold salt, a bluish color appeared, indicating the formation of gold nuclei. A few minutes later, the solution turned brilliant deep red due to the formation of the nanoparticles. The deep red color of gold nanoparticles in water is due to the strong light absorption in the visible region due to the oscillation of surface electrons after exposure to light, a phenomenon characteristic for metallic nanoparticles called surface plasmon resonance (SPR). This general phenomenon of metallic particles depends mainly on their size, shape, composition and dielectric environment [25,26]. The obtained size and size distribution of the gold nanoparticles are very important parameters, which determine their physical and chemical properties. In order to prepare gold nanoparticles suitable for intravenous administration, different concentrations of trisodium citrate were used. By increasing the citrate to gold ratio from 3 to 34 the sizes of the particles were reduced from 145 ± 17 nm to 38 ± 1.5 nm. Table 1 shows the effect of the amounts of the used citrate on the size and UV-Vis absorption spectra of gold nanoparticles. Using a weight ratio of citrate to gold of 3, the average size of the obtained nanoparticles was 145 nm, as determined by photon correlation

spectroscopy, and the corresponding surface plasmon resonance (SPR) band in the UV-Vis spectrum was 533 nm. In case of a citrate to gold ratio of 17 the obtained particle sizes were 91 nm and λ_{max} of SPR was 530 nm. Increasing the ratio of citrate to gold to 34, the size of the obtained GNPs was 38 nm with a λ_{max} of the SPR of 524 nm. Consequently, lower concentrations of sodium citrate resulted in a smaller number of nuclei and so more gold atoms aggregate per particles, which results in the increase of the average particles diameter [6]. The obtained results are in good agreement with many results reported in literature [27-30].

Furthermore, different batches of gold nanoparticles were prepared using the highest concentration of sodium citrate (citrate/gold = 34), from these experiments gold nanoparticles with similar sizes and acceptable polydispersity indices (Table 2) were obtained each time indicating high reproducibility of the citrate reduction for the preparation of gold nanoparticles. Figure 1 shows the measured size distributions of different batches of as-prepared gold nanoparticles. The obtained nanoparticles show a quite narrow monomodal size distribution with only one peak observed in the size distribution curve (Figure 1). The average diameter of different batches of as-prepared gold nanoparticles is about 36.7 ± 1.7 nm [31,32].

Table 1: Effect of the amounts of sodium citrate on the size and the Surface Plasmon Resonance (SPR) of the synthesized gold nanoparticles

$HAuCl_4.3H_2O$ (mg)	Trisodium citrate dihydrate (mg)	Citrate/Gold ratio	Size (nm)	SPR maximum (nm)[1]
20	60	3	145 ±17	533
10	170	17	91 ±14	530
5	170	34	38 ± 1.5	524

[1] Size is determined by PCS

Table 2: Size and polydispersity index of different batches of gold nanoparticles

Batch	Mean size (nm)	S.D	Polydispersity index
B1	38.8	2.132	0.336
B2	34.9	0.589	0.486
B3	35.8	1.617	0.252
B4	37.2	0.954	0.495
Mean ± SD	36.7 ± 1.7	-	0.392 ± 0.118

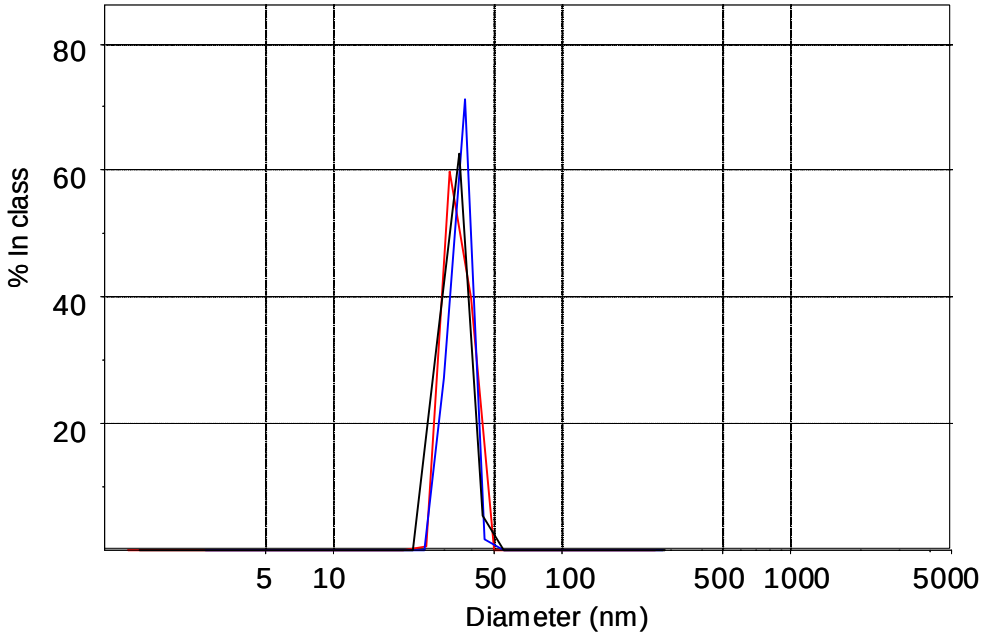

Figure 1: Size distribution of different batches of synthesized gold nanoparticles

3.1.2. Determination of the nanoparticles concentrations

The gold content of the nanoparticles from different batches was analyzed by ICP-OES. The results indicated that almost all the added gold was converted to gold nanoparticles, which shows that the reduction of $HAuCl_4.3H_2O$ by sodium citrate is about 100% completed under the above mentioned conditions. For further calculations of the actual number of gold nanoparticles per ml, the determined concentration and the size of the obtained nanoparticles were used.

3.2. Stabilization and surface-functionalization of gold nanoparticles

Citrate-stabilized gold nanoparticles are typical hydrophobic colloids carrying a large excess of negative surface charges and consequently they are only stable in very low ionic

strength solutions, where the adsorbed charges are still able to prevent the close contact between individual particles. Due to this properties, gold nanoparticles are thermodynamically very unstable and consequently require special stabilization [33]. It is therefore especially important to modify their surfaces in order to increase the colloidal stability also in physiological fluids. To this end, thiol chemistry has been widely applied due to the high affinity of sulfur to gold surfaces with chemical species ranging from small molecules to larger biomacromolecules and also polymers [13].

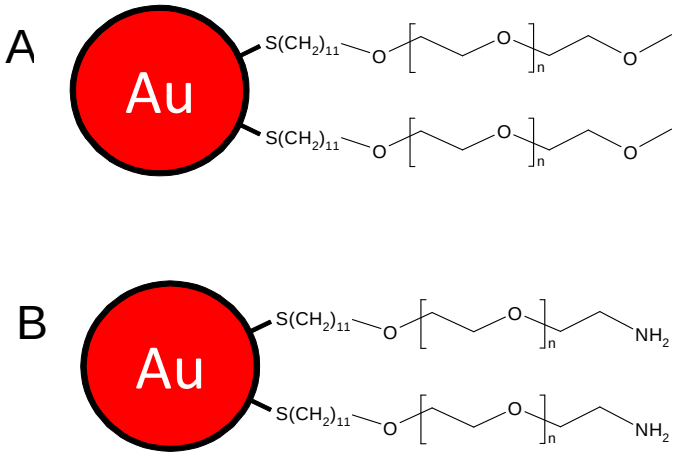

Figure 2: Surface stabilization and functionalization of gold nanoparticles with mPEG-AlkSH (A) and with NH_2PEG-AlkSH (B)

The surface of the produced gold nanoparticles was subsequently stabilized and further functionalized by methoxy poly(ethylene glycol)-undecyl mercaptane (mPEG-AlkSH) and amino poly(ethylene glycol)-undecyl mercaptane (NH_2PEG-AlkSH) as depicted in Figure 2. Different concentrations of the respective polymers ranging from 1-5 µg per 1 ml of the colloidal solution from one batch have been used. Figure 3 shows the observed effects of the concentration of mPEG-AlkSH and NH_2PEG-AlkSH on the size of the coated nanoparticles compared to the effect of non thioalkylated mPEG. Addition of 1 µg of mPEG-AlkSH to 1 ml of nanoparticle solution (containing $7*10^{10}$ particles) resulted in an increase of the average particles size from 38.8 to 43.6 nm as measured with photon correlation spectroscopy. Further increasing the concentration to the double concentration (2µg/ml) increased the size slightly to 44.2 nm. Further increase did not affect the size of GNPs anymore, which indicates that a sufficient amount of polymer was provided to completely coat the available nanoparticle surfaces. In case of H_2NPEG-AlkSH, applying 1 µg/ml increased the measured size to 45.54 nm. While further increasing the concentration more than 1 µg/ml did not result in any further

increase of the size. Addition of different concentrations of pure mPEG to GNPs solution did not result in any increase of the particle size, since mPEG can't bind to gold surfaces due to the lack of thiol functionalities. The increase of particle size after addition of mPEG-AlkSH and NH_2PEG-AlkSH on the other hand can be attributed to a single layer coating of the particle surfaces with the added polymers, which both contain thiolated alkyl chains with a strong affinity to gold surfaces suitable to form self assembled monolayers on gold via the sulfur-gold bond [34].

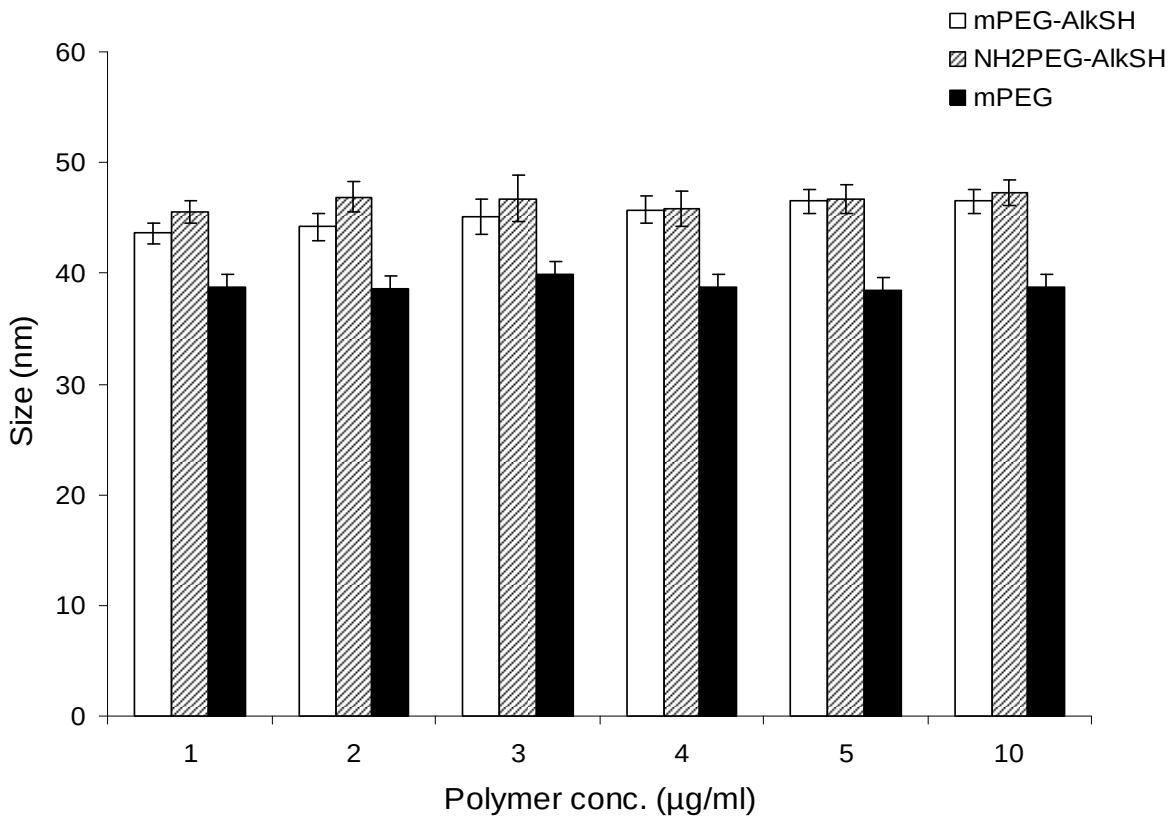

Figure 3: Effect of different concentrations of mPEG, mPEG-AlkSH and NH_2PEG-AlkSH on the size of gold nanoparticles

Figure 4 shows the measured size distribution of gold nanoparticles before and after coating with polymers as determined by photon correlation spectroscopy. The size of the mPEG-AlkSH coated gold nanoparticles is generally larger than those of uncoated nanoparticles, with an obvious shift of the particle size distribution peak to larger sizes, but nevertheless the nanoparticles still have the same narrow size distribution and low polydispersity index and no signs of the formation of larger sized aggregates.

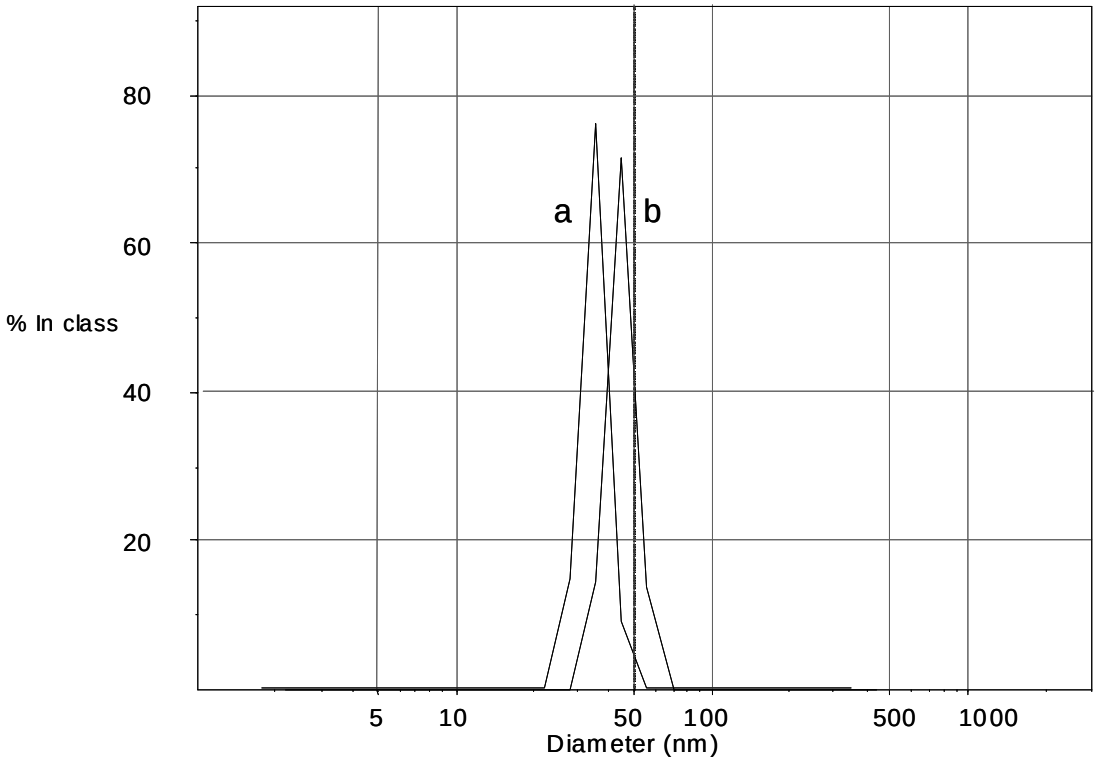

Figure 4: Size distribution of citrate-stabilized gold nanoparticles (a) and mPEG-AlkSH-coated gold nanoparticles (b)

The surface charge plays an important role for the stability of nanoparticles. Therefore, the zeta potential of gold nanoparticles was measured before and after coating with polymers (Figure 5). The zeta potential of citrate stabilized nanoparticles was determined to be -47.3 ± 5.5 mV, while the zeta potential of mPEG-AlkSH coated nanoparticles increased to be about -20 mV. This observation is attributed to the shielding effect (screening of some of the negative charges on the particle surfaces) of the neutral PEG chains attached to nanoparticle surface and also to the occurring replacement of most of the adsorbed citrate anions on the particle surfaces. The measured zeta potential of NH_2PEG-AlkSH-coated gold nanoparticles is almost neutral most likely due to the presence of amine groups, which can be protonated and become positively charged, leading to the formation of only slightly negative or neutral nanoparticles [23,35,36].

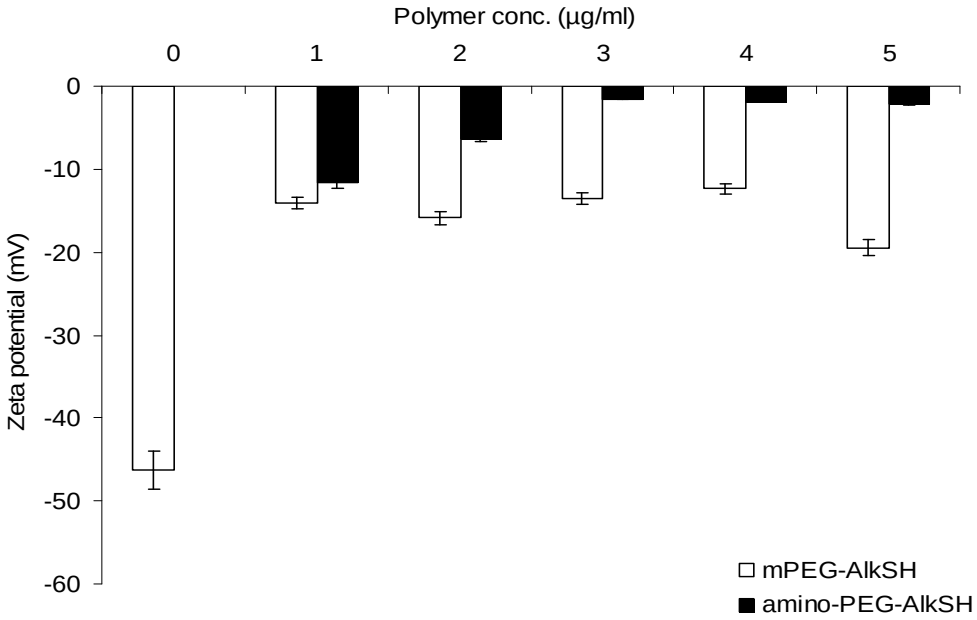

Figure 5: Effect of different concentrations of mPEG-AlkSH and NH_2PEG-AlkSH on the zeta potential of gold nanoparticles

3.3. Purification of gold nanoparticles from excess polymer

Removal of the excess of unbound polymers from the coated nanoparticle dispersion is one essential step before further application of nanoparticles due to possible interactions of the free PEG with the conducted measurements. In order to investigate the purification, an excess of mPEG-AlkSH (5 µg/ml) was added to the nanoparticle dispersion to ensure complete coating of the particles. The remaining free fraction (unbound to the surface) was removed by ultrafiltration at 750 g for 20 minutes using ultrafiltration tubes (molecular weight cut-off (MWCO), 50 kDa), which retain only the nanoparticles and allow the free polymer to pass with the filtrate. After four cycles of ultrafiltration, no further free polymers were detected via iodine-assay in the filtrate, indicating a complete removal of the unbound polymers. The zeta potential (surface charge), size and size distribution of the gold nanoparticles were measured before and after ultrafiltration to investigate the impact of the purification process on the resulting properties of nanoparticles. Figure 6 shows the sizes of GNPs coated with mPEG-AlkSH before and after ultrafiltration compared to the size of merely citrate-stabilized GNPs. Ultrafiltration had no detectable effect on the size of GNPs as shown in Figure 6. In contrast, the zeta potential of the coated particles was increased from -31.5 ± 6.1 to -18.2 ± 7.0 mV after four cycles of ultrafiltration (Figure 7), which could be attributed to the removal of still present citrate anions adsorbed on the particles surface during the purification process.

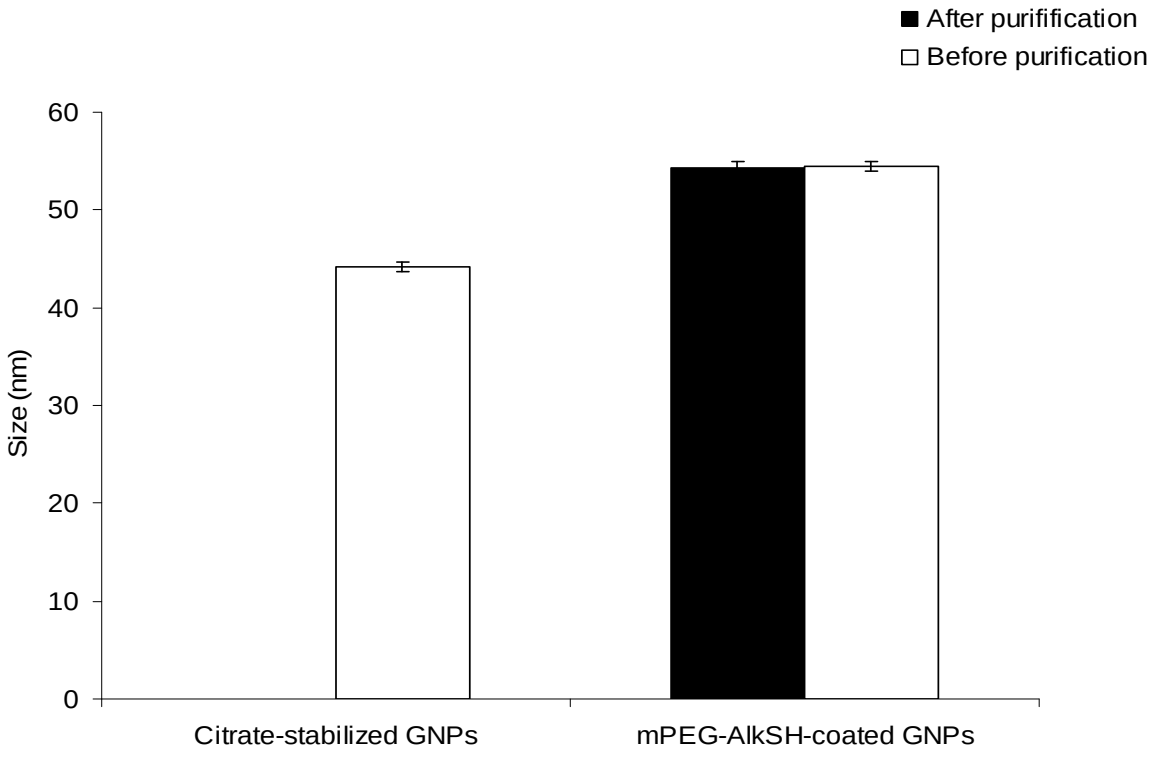

Figure 6: Effect of ultrafiltration on the size gold nanoparticles coated with mPEG-AlkSH

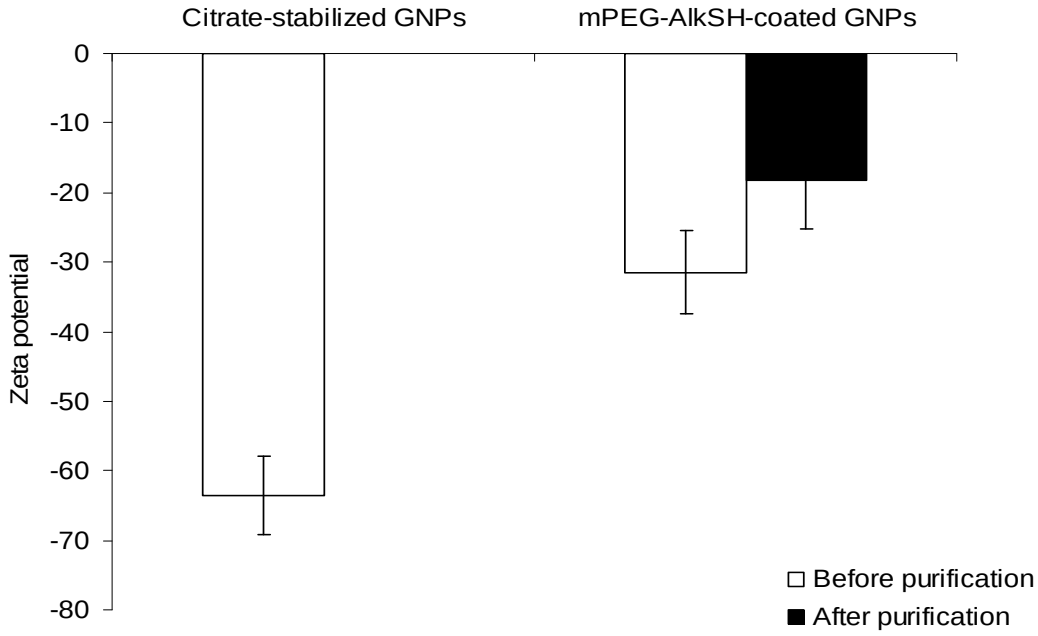

Figure 7: Effect of ultrafiltration on the zeta potential of gold nanoparticles coated with mPEG-AlkSH

3.4. Dispersion stability of surface-functionalized gold nanoparticle

Dispersion stability of unfunctionalized nanoparticles is mediated via the electrostatic repulsion of their charged surfaces, lacks of the sufficient surface charge or the absence of other stabilizing agents will always lead to particle aggregation and subsequent precipitation once a certain size of the aggregates is reached. The reduction of gold salts by sodium citrate produces nanoparticles with an excess of citrate anions adsorbed to the particle surfaces creating sufficient surfaces charge that stabilize the particle dispersion [37]. The aggregation of the nanoparticles is characterized by particle increase observed with photon correlation spectroscopy and a shift of the maximum absorbance peak to longer wave lengths. This red shift of aggregated gold nanoparticles thereby arises from the formation of absorption bands of the extinction spectrum at long wave length. These additional absorption bands are caused by electric dipole-dipole interactions and coupling between plasmons of neighbouring particles inside the aggregates, under the prerequisite that the interparticle distances inside the aggregates are smaller than the respective particle diameters [38]. Upon addition of sodium chloride to the merely citrate-stabilized GNPs, the color of gold colloids gradually changed from red to blue followed by appearance of a new very broad absorption band in the UV-Vis spectrum above 700 nm (Figure 8c) indicating the occurrence of aggregation [39,40]. The very rapid aggregation of citrate-stabilized nanoparticles by sodium chloride is due to the shielding of the negative charge and the subsequent reduction of the electrostatic repulsion between the individual particles, which allows the particles to clump together [25,41]. However, when NaCl was added to the PEG-coated GNPs, the plasmon bands were not affected (Figure 8a and 8b), because the surface PEGylated GNPs are not mainly stabilized by electrostatic repulsion, but they are stabilized by the steric repulsion of the uncharged hydrophilic polymers attached to their surfaces [42,43].

In order to characterize the aggregation, particle size measurements are often used, to facilitate the understanding of the aggregation processes. In addition, the apparent size mainly affects the biological application of nanoparticles by destroying their biocompatibility [44]. Figure 9 for example shows the effect of NaCl (5M) addition on the size, determined by photon correlation spectroscopy, of PEG-coated and uncoated (citrate-stabilized) gold nanoparticles. Sodium chloride induced a large size increase of the citrate-stabilized GNPs most likely due to agglomeration of the non-sufficiently shielded nanoparticles [45]. On the other hand, the size of mPEG-AlkSH and NH_2PEG-AlkSH coated GNPs did not show any size increase after sodium chloride addition due their stabilization by the polymer coating.

These results are additionally confirmed by the UV-Vis spectroscopy (Figure 8), similar results were also reported by Nagasaki et al. [13,46].

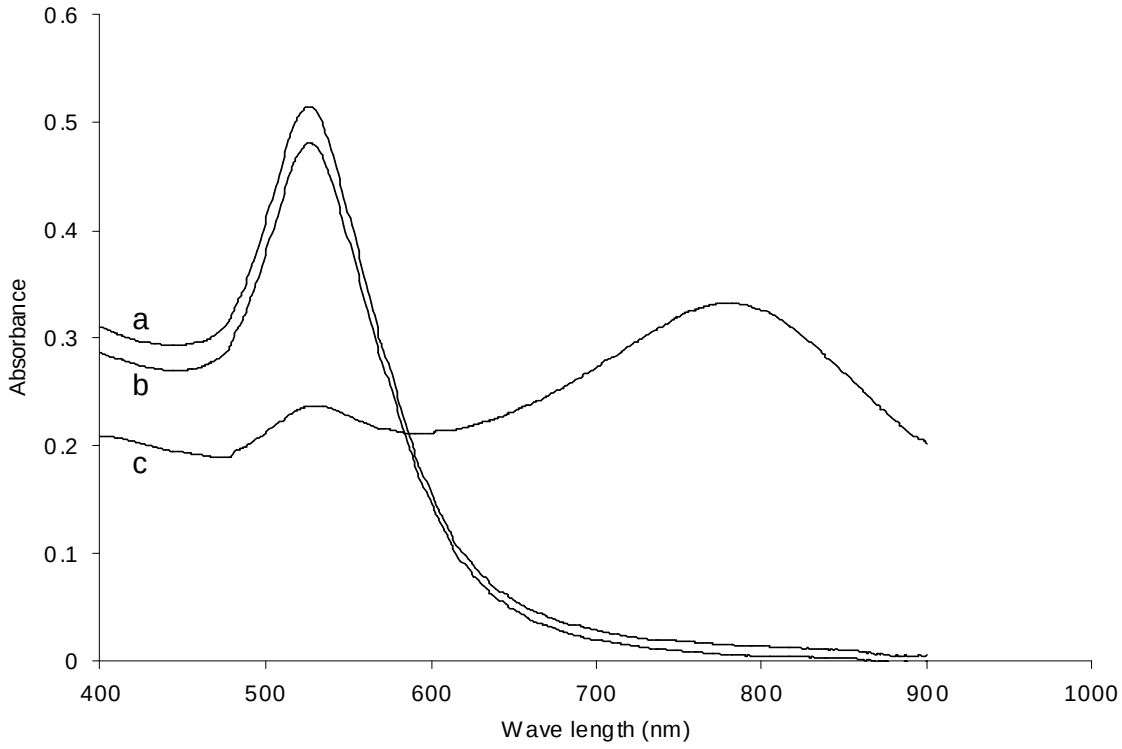

Figure 8: Effect of sodium chloride on the UV-Vis spectra of mPEG-AlkSH-coated GNPs (a), NH_2PEG-AlkSH-coated GNPs (b) and citrate-stabilized GNPs (c)

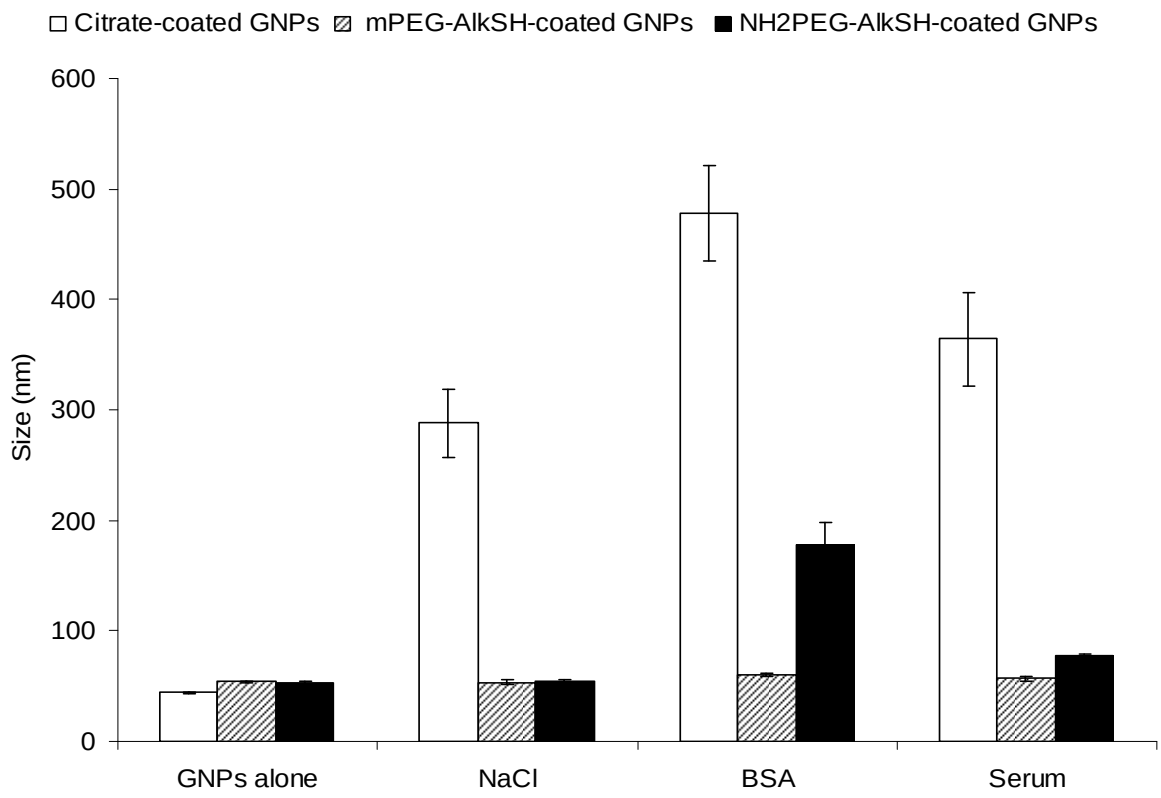

Figure 9: Effect of sodium chloride, BSA and 10% v/v bovine serum on the size of mPEG-AlkSH-coated GNPs, NH_2PEG-AlkSH-coated GNPs and citrate-stabilized GNPs)

The effect of sodium chloride on the zeta potential of the gold nanoparticles is depicted in Figure 10. A pronounced increase of the zeta potential is observed for the citrate-stabilized gold nanoparticles after addition of sodium chloride, which demonstrated the shielding and the occurring neutralization of some of the surface charges. The slightly positive zeta potential observed after addition of sodium chloride to PEG-coated GNPs may be attributed to the adsorption of some sodium cations to the PEG chains and for the amino PEG derivative also a certain amount of charged amine groups may be present.

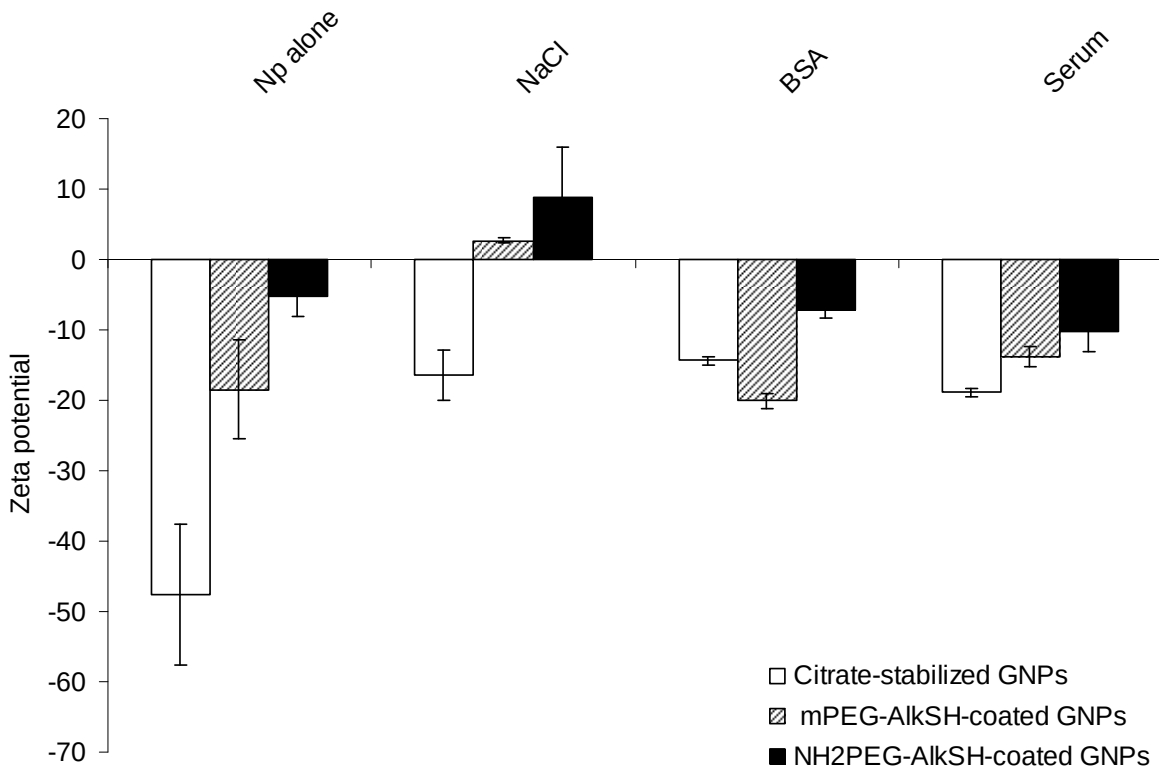

Figure 10: Effect of sodium chloride, BSA and 10% v/v serum on the zeta potential of mPEG-AlkSH-coated GNPs, NH_2PEG-AlkSH-coated GNPs and citrate-stabilized GNPs)

3.5. Interaction of the surface functionalized gold nanoparticles with proteins (BSA and bovine serum)

For a further evaluation of the suitability of the particles for intravenous administration, the stability of the particles was investigated in presence of different proteins, which are present in body fluids. The interaction of the prepared gold nanoparticles either coated or only citrate-stabilized with bovine serum albumin (BSA), the most abundant protein in the plasma, and bovine serum was studied. Citrate-stabilized GNPs used for this investigation rapidly aggregated after addition of bovine serum albumin (BSA) and serum, which is indicated by the disappearance of the characteristic surface plasmon resonance peak in the UV spectrum, in case of BSA, (Figure 11) or by appearance of a new wide absorption band at wave lengths above 650 nm as in case of serum (Figure 12). The large size increase of the citrate-stabilized GNPs induced by the addition of BSA and serum, as shown by photon correlation spectroscopy measurements (Figure 9) furthermore confirms the instability. The observations could be attributed to the interaction of cysteine groups of the added proteins with the GNPs, or the shielding of the negative surface charges by extensive protein adsorption on the particle surface, which then also may induce the further formation of aggregates in the dispersion. In contrast to the bare particles, the spectra of polymer-protected

GNPs are either not affected (in case of mPEG-AlkSH coated GNPs) or show only a slight increase in the size (in case of NH_2-PEG-AlkSH-coated GNPs) by addition of BSA and serum. The slight size increase of NH_2PEG-AlkSH-coated GNPs can be attributed to the occurring interaction of the exposed protonated amino groups with negatively charged carboxylate groups on the added proteins, which may lead to a partial protein coating of the particles [47]. The protein resistance (i.e. the stability) of PEG-coated GNPs is a consequence of the present interfacial water layer, which prevents a direct contact between the lipophilic particle surface and the added proteins [48].

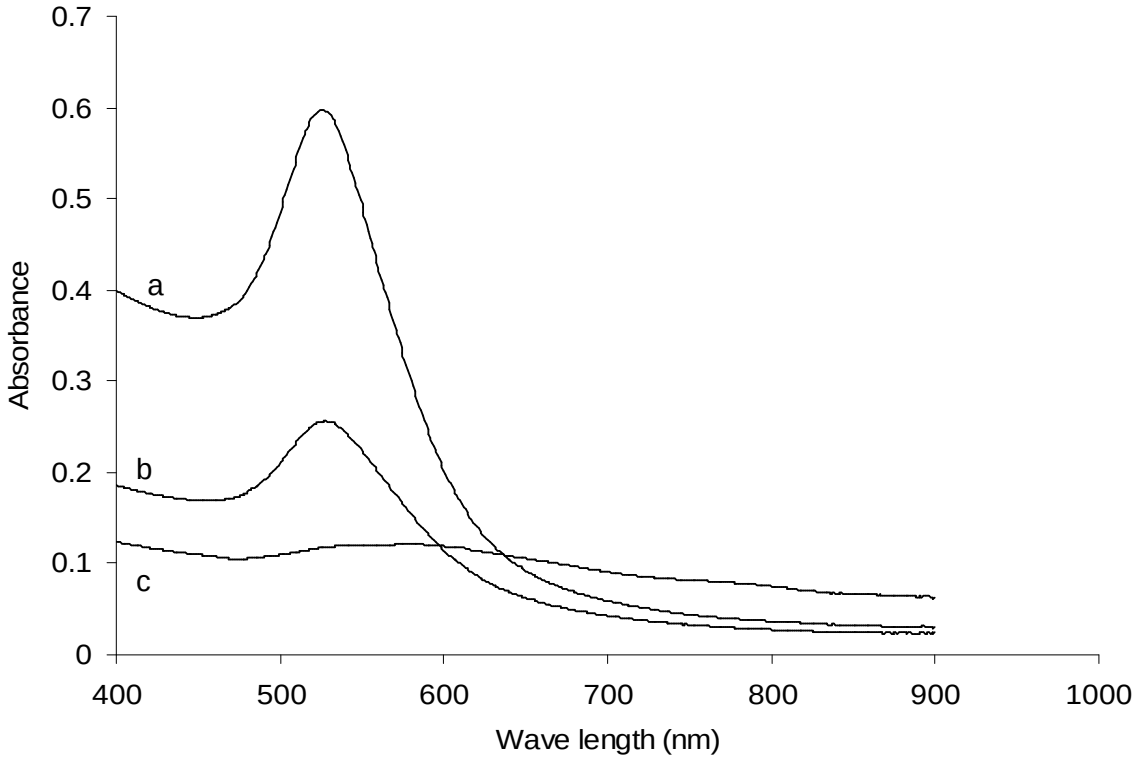

Figure 11: Effect of BSA on the UV-Vis spectra of mPEG-AlkSH-coated GNPs (a), NH_2PEG-AlkSH-coated GNPs (b) and citrate-stabilized GNPs (c)

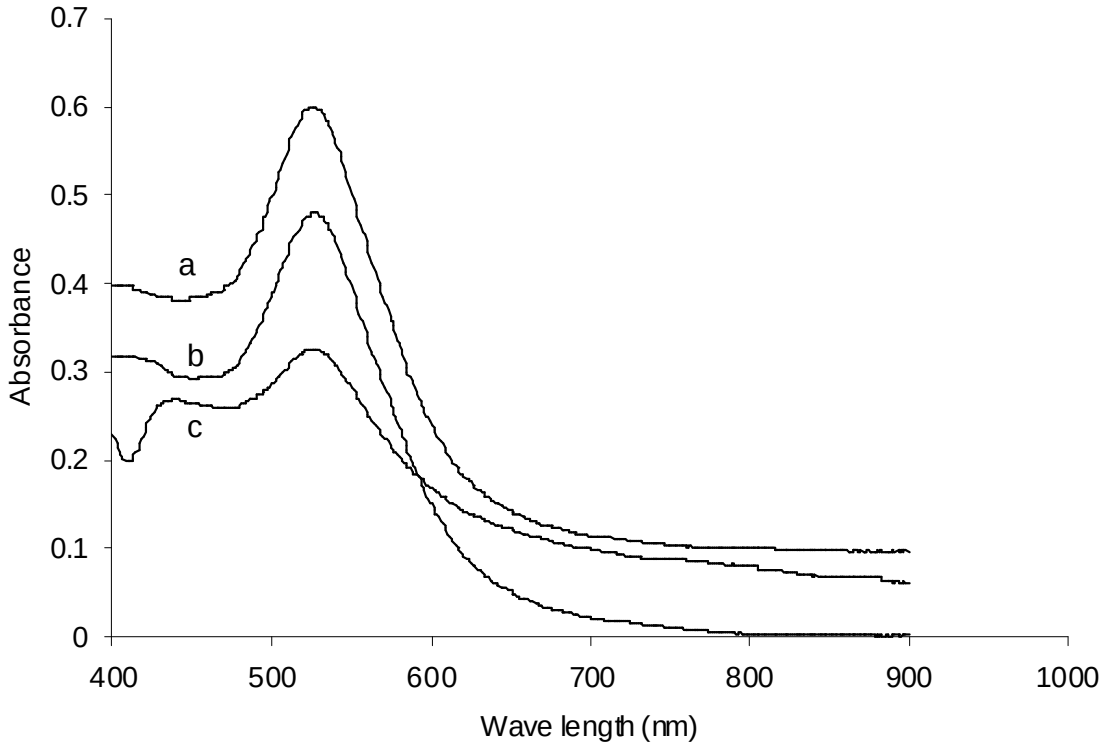

Figure 12: Effect of bovine serum on the UV-Vis spectra of mPEG-AlkSH-coated GNPs (a), NH_2PEG-AlkSH-coated GNPs (b) and citrate-stabilized GNPs (c)

4. Conclusion

Uniform gold nanoparticles were prepared in aqueous solutions by sodium citrate reduction of $HAuCl_4.3H_2O$. The obtained sizes and size distribution as well as the measured surface plasmon resonance of the prepared nanoparticles was strongly influenced by the gold/citrate ratio and could be optimized to produce reproducibly sufficiently small particles. The surface functionalization and further stabilization of the gold nanoparticles was achieved using the heterobifunctional thioalkylated poly(ethylene glycol) derivatives, which were already described in this thesis and which are well known to form well ordered and packed self assembled monolayers on gold surface. The size of the accordingly modified particles slightly increased, while there was also a pronounced increase of the zeta potential observed after the PEGylation of the particles. The finally obtained PEG-coated gold nanoparticles showed a significantly enhanced stability in the presence of electrolyte and proteins.

In conclusion the here presented nanoparticles provide a valuable tool for further modifications on the incorporated terminal amine group, which allows further binding or attachment of biomolecules or other moieties to the particles. The obtained particles then can be used for in vitro or in vivo studies due to their excellent stability in biological fluids.

5. References

1. Benjamin Wiley, Yugang Sun, Jingyi Chen, Hu Cang, Zhi Yuan Li, Xingde Li, and Younan Xia, "Shape-controlled synthesis of silver and gold nanostructures," MRS Bulletin **30,** 356-361 (2005).

2. Gen Tsutsui, Shujuan Huang, Hiroyuki Sakaue, Shoso Shingubara, and Takayuki Takahagi, "Well-size-controlled colloidal gold nanoparticles dispersed in organic solvents," Japanese Journal of Applied Physics, Part 1: Regular Papers, Short Notes & Review Papers **40,** 346-349 (2001).

3. Xianmao Lu, Hsing Yu Tuan, Brian A. Korgel, and Younan Xia, "Facile synthesis of gold nanoparticles with narrow size distribution by using AuCl or AuBr as the precursor," Chemistry--A European Journal **14,** 1584-1591 (2008).

4. Saikat Mandal, P. R. Selvakannan, Sumant Phadtare, Renu Pasricha, and Murali Sastry, "Synthesis of a stable gold hydrosol by the reduction of chloroaurate ions by the amino acid, aspartic acid," Proceedings - Indian Academy of Sciences, Chemical Sciences **114,** 513-520 (2002).

5. Chen Hsun Weng, Chih Chia Huang, Chen Sheng Yeh, Huan Yao Lei, and Gwo Bin Lee, "Synthesis of hexagonal gold nanoparticles using a microfluidic reaction system," Journal of Micromechanics and Microengineering **18,** 035019-1-035019/8 (2008).

6. Xiaohui Ji, Xiangning Song, Jun Li, Yubai Bai, Wensheng Yang, and Xiaogang Peng, "Size Control of Gold Nanocrystals in Citrate Reduction: The Third Role of Citrate," Journal of the American Chemical Society **129,** 13939-13948 (2007).

7. Sanjeev Kumar, K. S. Gandhi, and R. Kumar, "Modeling of formation of gold nanoparticles by citrate method," Industrial & Engineering Chemistry Research **46,** 3128-3136 (2007).

8. Susie Eustis, Hsan Yin Hsu, and Mostafa A. El Sayed, "Gold Nanoparticle Formation from Photochemical Reduction of Au3+ by Continuous Excitation in Colloidal Solutions. A Proposed Molecular Mechanism," Journal of Physical Chemistry B **109,** 4811-4815 (2005).

9. Chen Li Chiang, Meng Bor Hsu, and Long Biao Lai, "Control of nucleation and growth of gold nanoparticles in AOT/Span80/isooctane mixed reverse micelles," Journal of Solid State Chemistry **177,** 3891-3895 (2004).

10. La ongnuan Srisombat, Joon Seo Park, Shishan Zhang, and T. Randall Lee, "Preparation, Characterization, and Chemical Stability of Gold Nanoparticles Coated with Mono-, Bis-, and Tris-Chelating Alkanethiols," Langmuir **24,** 7750-7754 (2008).

11. Fajun Zhang, Maximilian W. A. Skoda, Robert M. J. Jacobs, Stefan Zorn, Richard A. Martin, Christopher M. Martin, Graham F. Clark, Guenter Goerigk, and Frank Schreiber, "Gold nanoparticles decorated with oligo(ethylene glycol) thiols: protein resistance and colloidal stability," Journal of Physical Chemistry A **111,** 12229-12237 (2007).

12. Kazuhiro Matsuura, Kohji Ohno, Shigehiro Kagaya, and Hiromi Kitano, "Carboxybetaine polymer-protected gold nanoparticles: high dispersion stability and

resistance against non-specific adsorption of proteins," Macromolecular Chemistry and Physics **208,** 862-873 (2007).

13. Daisuke Miyamoto, Motoi Oishi, Keiji Kojima, Keitaro Yoshimoto, and Yukio Nagasaki, "Completely Dispersible PEGylated Gold Nanoparticles under Physiological Conditions: Modification of Gold Nanoparticles with Precisely Controlled PEG-b-polyamine," Langmuir **24,** 5010-5017 (2008).

14. Hidenori Otsuka, Yukio Nagasaki, and Kazunori Kataoka, "PEGylated nanoparticles for biological and pharmaceutical applications," Advanced Drug Delivery Reviews **55,** 403-419 (2003).

15. Keitaro Yoshimoto, Yuki Hoshino, Takehiko Ishii, and Yukio Nagasaki, "Binding enhancement of antigen-functionalized PEGylated gold nanoparticles onto antibody-immobilized surface by increasing the functionalized antigen using a-sulfanyl-w-amino-PEG," Chemical Communications (Cambridge, United Kingdom) 5369-5371 (2008).

16. Chenjie Xu, Glenn A. Tung, and Shouheng Sun, "Size and Concentration Effect of Gold Nanoparticles on X-ray Attenuation As Measured on Computed Tomography," Chemistry of Materials ACS (2008).

17. J. F. Hainfeld, D. N. Slatkin, T. M. Focella, and H. M. Smilowitz, "Gold nanoparticles: a new X-ray contrast agent," British Journal of Radiology **79,** 248-253 (2006).

18. Wolfgang Eck, Gary Craig, Aruna Sigdel, Gerd Ritter, Lloyd J. Old, Laura Tang, Murray F. Brennan, Peter J. Allen, and Michael D. Mason, "PEGylated Gold Nanoparticles Conjugated to Monoclonal F19 Antibodies as Targeted Labeling Agents for Human Pancreatic Carcinoma Tissue," ACS Nano **2,** 2263-2272 (2008).

19. Alexander Tkachenko, Huan Xie, Stefan Franzen, and Daniel L. Feldheim, "Assembly and characterization of biomolecule-gold nanoparticle conjugates and their use in intracellular imaging," Methods in Molecular Biology (Totowa, NJ, United States) **303,** 85-99 (2005).

20. Andy Scheffer, Carsten Engelhard, Michael Sperling, and Wolfgang Buscher, "ICP-MS as a new tool for the determination of gold nanoparticles in bioanalytical applications," Analytical and Bioanalytical Chemistry **390,** 249-252 (2008).

21. Jamie M. Bergen, Horst A. von Recum, Thomas T. Goodman, Archna P. Massey, and Suzie H. Pun, "Gold nanoparticles as a versatile platform for optimizing physicochemical parameters for targeted drug delivery," Macromolecular Bioscience **6,** 506-516 (2006).

22. Changsheng Shan, Fenghua Li, Fuyu Yuan, Guifu Yang, Li Niu, and Qiang Zhang, "Size-controlled synthesis of monodispersed gold nanoparticles stabilized by polyelectrolyte-functionalized ionic liquid," Nanotechnology **19,** 285601-1-285601/6 (2008).

23. Chang Hai Wang, Chi Jen Liu, Cheng Liang Wang, Tzu En Hua, Judy M. Obliosca, K. H. Lee, Y. Hwu, Chung Shi Yang, Ru Shi Liu, Hong Ming Lin, Jung Ho Je, and G. Margaritondo, "Optimizing the size and surface properties of polyethylene glycol (PEG)-gold nanoparticles by intense X-ray irradiation," Journal of Physics D: Applied Physics **41,** 195301-1-195301/8 (2008).

24. Tony Azzam and Adi Eisenberg, "Monolayer-protected gold nanoparticles by the self-assembly of micellar poly(ethylene oxide)-b-poly(e-caprolactone) block copolymer," Langmuir **23,** 2126-2132 (2007).

25. Gang Wang and Wenfang Sun, "Optical Limiting of Gold Nanoparticle Aggregates Induced by Electrolytes," Journal of Physical Chemistry B **110,** 20901-20905 (2006).

26. Marie Christine Daniel and Didier Astruc, "Gold Nanoparticles: Assembly, Supramolecular Chemistry, Quantum-Size-Related Properties, and Applications toward Biology, Catalysis, and Nanotechnology," Chemical Reviews (Washington, DC, United States) **104,** 293-346 (2004).

27. Yali Liu, Keith B. Male, Pierre Bouvrette, and John H. T. Luong, "Control of the Size and Distribution of Gold Nanoparticles by Unmodified Cyclodextrins," Chemistry of Materials **15,** 4172-4180 (2003).

28. Andrew N. Shipway, Eugenii Katz, and Itamar Willner, "Nanoparticle arrays on surfaces for electronic, optical, and sensor applications," ChemPhysChem **1,** 18-52 (2000).

29. You Qiu He, Shao Pu Liu, Ling Kong, and Zhong Fang Liu, "A study on the sizes and concentrations of gold nanoparticles by spectra of absorption, resonance Rayleigh scattering and resonance non-linear scattering," Spectrochimica Acta, Part A: Molecular and Biomolecular Spectroscopy **61A,** 2861-2866 (2005).

30. Smritimoy Pramanik, Paltu Banerjee, Arindam Sarkar, and Subhash Chandra Bhattacharya, "Size-dependent interaction of gold nanoparticles with transport protein: A spectroscopic study," Journal of Luminescence **128,** 1969-1974 (2008).

31. Susumu Inasawa, Masakazu Sugiyama, and Yukio Yamaguchi, "Bimodal Size Distribution of Gold Nanoparticles under Picosecond Laser Pulses," Journal of Physical Chemistry B **109,** 9404-9410 (2005).

32. Nimai C. Nayak and Kwanwoo Shin, "Human serum albumin mediated self-assembly of gold nanoparticles into hollow spheres," Nanotechnology **19,** 265603-1-265603/4 (2008).

33. L. A. Dykman and V. A. Bogatyrev, "Gold nanoparticles: preparation, functionalisation and applications in biochemistry and immunochemistry," Russian Chemical Reviews **76,** 181-194 (2007).

34. Ralph A. Sperling, Pilar Rivera Gil, Feng Zhang, Marco Zanella, and Wolfgang J. Parak, "Biological applications of gold nanoparticles," Chemical Society Reviews **37,** 1896-1908 (2008).

35. Raymond M. Schiffelers and Gert Storm, "ICS-283: a system for targeted intravenous delivery of siRNA," Expert Opinion on Drug Delivery **3,** 445-454 (2006).

36. Devika R. Bhumkar, Hrushikesh M. Joshi, Murali Sastry, and Varsha B. Pokharkar, "Chitosan Reduced Gold Nanoparticles as Novel Carriers for Transmucosal Delivery of Insulin," Pharmaceutical Research **24,** 1415-1426 (2007).

37. Thaddeus J. Norman, Jr., Christian D. Grant, Donny Magana, Jin Z. Zhang, Jun Liu, Daliang Cao, Frank Bridges, and Anthony Van Buuren, "Near Infrared Optical Absorption of Gold Nanoparticle Aggregates," Journal of Physical Chemistry B **106,** 7005-7012 (2002).

38. Soonwoo Chah, Matthew R. Hammond, and Richard N. Zare, "Gold nanoparticles as a colorimetric sensor for protein conformational changes," Chemistry & Biology **12,** 323-328 (2005).

39. C. Burns, W. U. Spendel, S. Puckett, and G. E. Pacey, "Solution ionic strength effect on gold nanoparticle solution color transition," Talanta **69,** 873-876 (2006).

40. Layal L. Rouhana, Jad A. Jaber, and Joseph B. Schlenoff, "Aggregation-Resistant Water-Soluble Gold Nanoparticles," Langmuir **23,** 12799-12801 (2007).

41. Santosh Aryal, K. C. R. Bahadur, Narayan Bhattarai, Chul Ki Kim, and Hak Yong Kim, "Study of electrolyte induced aggregation of gold nanoparticles capped by amino acids," Journal of Colloid and Interface Science **299,** 191-197 (2006).

42. Claire Mangeney, Fabien Ferrage, Isabelle Aujard, Valerie Marchi-Artzner, Ludovic Jullien, Olivier Ouari, El Djouhar Rekaie, Andre Laschewsky, Inger Vikholm, and Janusz W. Sadowski, "Synthesis and Properties of Water-Soluble Gold Colloids Covalently Derivatized with Neutral Polymer Monolayers," Journal of the American Chemical Society **124,** 5811-5821 (2002).

43. Muriel K. Corbierre, Neil S. Cameron, and R. Bruce Lennox, "Polymer-stabilized gold nanoparticles with high grafting densities," Langmuir **20,** 2867-2873 (2004).

44. Mahesh D. Chavanpatil, Ayman Khdair, Yogesh Patil, Hitesh Handa, Guangzhao Mao, and Jayanth Panyam, "Polymer-surfactant nanoparticles for sustained release of water-soluble drugs," Journal of Pharmaceutical Sciences **96,** 3379-3389 (2007).

45. Ruxandra Gref, Gregory Miralles, and Edith Dellacherie, "Polyoxyethylene-coated nanospheres: effect of coating on zeta potential and phagocytosis," Polymer International **48,** 251-256 (1999).

46. Yukio Nagasaki, "Polyethylene glycol-b-polyamine stabilized bionanoparticles for nanodiagnostics and nanotherapy," Chemistry Letters **37,** 564-569 (2008).

47. Soo Hyeon Lee, Ki Hyun Bae, Sun Hwa Kim, Kyu Ri Lee, and Tae Gwan Park, "Amine-functionalized gold nanoparticles as non-cytotoxic and efficient intracellular siRNA delivery carriers," International Journal of Pharmaceutics **364,** 94-101 (2008).

48. R. L. C. Wang, H. J. Kreuzer, and M. Grunze, "Molecular Conformation and Solvation of Oligo(ethylene glycol)-Terminated Self-Assembled Monolayers," Journal of Physical Chemistry B **101,** 9767-9773 (1997).

Chapter 5

Polymer Coated Gold Nanoparticles for Bone Targeting via Hydroxyapatite Binding

Gamal Zayed[1], Achim Göpferich[1], Jörg Teßmar[1]

[1]Department of Pharmaceutical Technology, University of Regensburg,
93040 Regensburg, Germany

to be submitted

Keywords: bifunctional polymers, poly(ethylene glycol), gold surface modification, drug targeting, bisphosphonate, hydroxyapatite

Abstract

Gold nanoparticles (GNPs) possess a great potential as model systems for particulate drug delivery due to their ease of production, low toxicity and also the high stability of the noble metal in biological fluids. Due to their unique surface chemistry they can be used as building platform for stable self assembled monolayers of thioalkylated polyethylene glycols with different surface functionalities. In order to functionalize particles, bisphosphonate and methoxy modified poly(ethylene glycol)-undecyl mercaptane (BP-PEG-AlkSH and mPEG-AlkSH) were mixed in different ratios and used to coat gold nanoparticles. The investigations showed that the polymer coated nanoparticles slightly increased in size as determined by PCS, but no significant changes were observed with TEM due to the low contrast of the polymer layer. The surface charge and UV-Vis absorption spectra of the particles were also only slightly changed, indicating well separated particles and a successful replacement of the citrate coating by the polymers. The polymer-coated nanoparticles were stable in different media (5M NaCl, 200 µg/ml BSA and 10% v/v serum), indicating a strong binding of polymers. Bisphosphonate coated particles were furthermore incubated with porous hydroxyapatite ceramics (Endobon®, Biomet) and it was observed that their adsorption to the apatite was dependent on the content of bisphosphonate in the particle surfaces and the adsorption was not affected by calcium ions or proteins added to the media.

In conclusion, the bisphosphonate modified GNPs showed a very good stability, reduced protein adsorption, and a high affinity to hydroxyapatite, which makes them extremely useful for the investigation of the in-vivo bone targeting of gold particles.

1. Introduction

In recent years, a lot of effort was devoted towards the preparation of targeted drug delivery system based on nanoparticles. Many delivery vehicles have been designed based on nanomaterials, such as dendrimers [1,2], nanorods [3], polymeric nanoparticles [4], liposomes [5], nanotubes [6] and metallic nanoparticles [7,8].

Among metallic nanoparticles, gold nanoparticles (GNPs) represent a perfect nanoscale agent, since it has been used for a wide range of biomedical and pharmaceutical applications [9]. These comprise drug delivery [10-12], tumor therapy [13-16], DNA detection [17-20], sensing of protein and carbohydrates [21,22], tissue engineering [23,24], as well as imaging and diagnosis [25,26]. Wang et al. [27] demonstrated that the combination of anticancer drugs with gold nanoparticles could be used as a novel, convenient agent to sensitively target and label drug-resistant cancer cells. The above mentioned applications of gold nanoparticles take the advantages of the unique properties of GNPs, which include simplicity of preparation, low costs of starting materials, low toxicity, high stability and ease of detection due to the high extinction coefficient in UV-Vis spectrum [28,29].

Surface functionalization of nanoparticles is the key step to target them to specific areas of the body or to allow them to selectively interact with a certain cell or tissue. Nanoparticles have been successfully functionalized with different molecules and have been targeted also to different cells [30,31]. For these approaches, GNPs offer a unique surface chemistry that could be used as platform, on which self assembled monolayers of organic molecules can be formed. Various polymers have been reported to form self assembled monolayer (SAMs) on gold nanoparticle surfaces via either chemisorption or physisorption. Thiolated polyethylene glycols are strongly attached to gold surfaces, due to the high affinity of sulphur to gold, and subsequently protect them from aggregation by steric stabilization of the bulk polymer [32]. The protective shell not only serves for the stabilization of nanoparticles, but can also be used for further functionalization with specific components such as drugs or targeting moieties [33].

Until now, the targeting of nanoparticles to bone has not been achieved to a satisfactory extent and the advantages of such systems would be enormous, since a specific delivery of therapeutic agents can be used to treat diseases ranging from osteoporosis to bone cancer. Therefore, the main goal of this research is the preparation and characterization of gold nanoparticles as model nanoparticles for the investigation of in vitro bone targeting of a nanoparticulate system. In order to prepare a targeted particulate system, citrate-stabilized gold

nanoparticles are functionalized with the previously synthesized thioalkylated poly(ethylene glycol)s. The ability of polymer coating to stabilize the GNPs under different conditions (such as the presence of high concentration of electrolytes or proteins) is studied. To obtain an idea about the bone targeting ability of the bisphosphonate-functionalized GNPs, the hydroxyapatite binding affinity of the prepared GNPs is one of the main objectives of the in vitro experiments. These binding experiments will be used to determine the influences of different conditions on the bone mineral binding affinity of functionalized GNPs.

2. Materials

Hydrogen tetrachloroaurate tri-hydrate ($HAuCl_4.3H_2O$), ultrafiltration tubes (MWCO 50,000 Da), and bovine serum albumin (BSA) were purchased from Sigma-Aldrich Chemical Company (Steinheim, Germany). Tri-sodium citrate di-hydrate, hydrochloric acid, nitric acid, sodium chloride and calcium chloride were purchased from Merck (Darmstadt, Germany). Methoxy poly(ethylene glycol)-undecyl mercaptane (mPEG-AlkSH), bisphosphonate-modified amino poly(ethylene glycol)-undecyl mercaptane (BP-PEG-AlkSH), endobone granules (Endobone®, Merck, Darmstadt). All glassware was thoroughly washed with freshly prepared aqua regia (HCl: HNO_3 = 3:1), extensively rinsed with Millipore water several times and oven-dried at 150 °C for 2-3 h before use. All used solutions filtered through 0.22 µm filter before use.

3. Methods

3.1. Preparation of colloidal gold nanoparticles

Gold nanoparticles (GNPs) were synthesized by citrate reduction of tetrachloroaurate tri-hydrate according to the reports in the literatures with slight modifications [34,35]; citrate stabilized nanoparticles of approximately 40 nm in diameter were obtained using the following conditions, 0.5 ml of 1% $HAuCl_4.3H_2O$ was added to 100 ml of Millipore water in a 250 ml round flask. The solution was heated to reflux under vigorous stirring. 1 ml of water containing 170 mg of tri-sodium citrate was then added rapidly to the boiling solution. The addition of the citrate salt resulted in gradual change of the solution color from pale yellow to pink and finally to deep red. Boiling and stirring was continued for another 20 minutes. After that, the heating jacket was removed and the particle dispersion was gradually cooled under stirring to room temperature.

The obtained colloidal dispersion was then centrifuged at low speed (2500 rpm) for 15 minutes to remove coarse particles.

3.2. Modification of nanoparticle surface with different polymers

Methoxy poly(ethylene glycol)-undecyl mercaptane and the bisphosphonate modified PEG polymer were used to coat the originally citrate stabilized GNPs. Excess amounts of each polymer (5µg/ml) were added to the nanoparticle dispersion to ensure a complete coating of the particle surfaces with polymer. For the preparation of GNPs coated with mixed polymers, a parallel adsorption method of both polymer types was applied. The desired polymers (methoxy poly(ethylene glycol)-undecyl mercaptane and the bisphosphonate modified polymer) were added to the nanoparticle dispersion (total concentration of both polymers; 5µg per one ml of the colloidal solution). For example, 50 µl of the first polymer (1µg/µl) and 50 µl of the second polymer (1µg/µl) were mixed together and added to 20 ml of nanoparticle solution to obtain GNPs coated with 50% of each polymer. The resulting mixture was shaked over night in a horizontal shaker set to 200 rpm at room temperature to allow a complete exchange of the citrate anions with the thiolated polymers on the particle surface. Excess of unbound polymer was subsequently removed by four times of ultrafiltration at 750 g [36].

3.3. Characterization of the prepared nanoparticle

3.3.1. UV-Vis spectroscopy

UV-Vis absorption spectra of the aqueous dispersions of citrate stabilized and coated nanoparticles were recorded using spectrophotometer (Uvikon-941, Kontron Instrument, Germany).

3.3.2. Particle size analysis and zeta potential measurements

The medium size, size distribution and the zeta potential of the prepared gold nanoparticles were analyzed by photon correlation spectroscopy using a Zetasizer 3000 HAS (Malvern, Instruments GmbH, Germany). 300 µl of the initial GNP dispersions were added to 3 ml of Millipore water immediately before measuring their size and zeta potential at room temperature. The refractive index and the viscosity of water were used for calculation of the results. The photon correlation spectroscopy measurements were used to calculate the average particle size and their polydispersity index (PI), as dimensionless measure for the broadness of the size distribution [37].

3.3.3. TEM imaging of the nanoparticles

10 µl of the nanoparticle samples were dropped on copper grids (Plano Formvar/Carbon films on 400 mesh grids, 3.05 mm diameter) and dried at room temperature overnight before taking transmission electron microscopy (TEM) images (Zeiss EM 10 C/CR, Germany).

3.3.4. Determination of nanoparticles concentration by ICP

1 ml of the nanoparticle dispersions was treated with the equal volume of aqua regia to dissolve the nanoparticles in order to determine the concentration of elemental gold using inductively coupled plasma optical emission spectroscopy (ICP-OES) (Horiba Jobin Yvon, 70P, S+S, Munich, Germany). The gold concentration was calculated using a standard curve constructed from different concentration of hydrogen tetrachloroaurate tri-hydrate [38].

3.3.5. Dispersion stability of GNPs

High ionic strength salt solution (5 M NaCl), bovine serum albumin (BSA, 200µg/ml) and bovine serum (10% v/v) were added to the particles to test the dispersion stability of coated GNPs in comparison with citrate-stabilized nanoparticles. The stability of the colloidal dispersions was monitored by size determination, zeta potential measurement and by changes in the UV-Vis spectra of nanoparticle dispersions [39,40].

3.3.6. Adsorption of bisphosphonate functionalized gold nanoparticles to endobone

Different concentrations of gold nanoparticles functionalized with different amounts of bisphosphonate contained in the coating were used to study the adsorption behavior of GNP-BP to hydroxyapatite granules (Endobone®) compared to nanoparticles coated with only methoxy poly(ethylene glycol)-undecyl mercaptane. 3 ml of the colloidal dispersions were added to 0.5 g of Endobone granules (size; 2.85-5.6 mm) and incubated for different time intervals at room temperature on a horizontal shaker set to 200 rpm. The percentage of nanoparticles adsorbed to the hydroxyapatite was calculated from the following equation (Equation 1):

$$\%Adsorbed = \frac{Abs_{before} - Abs_{after}}{Abs_{before}} \cdot 100\ \% \qquad \text{(Equation 1)}$$

ABS_{before}: absorbance of nanoparticles at λ_{max} before incubation

ABS_{after}: absorbance of nanoparticles at λ_{max} after incubation

The amount of gold nanoparticles (µmol) adsorbed per m^2 on endobone granules (Q) was determined applying equation 2 [41].

$$Q = \frac{(C_i - C_{eq}) \cdot V}{W \cdot S} \qquad \text{(Equation 2)}$$

Q: amount adsorbed per of gold nanoparticles per m^2 on endobone granules.

C_i: initial concentration of nanoparticles (µmol/L).

C_{eq}: equilibrium concentration of nanoparticles (µmol/L).

V: volume of the solution (3 ml).

W: weight of endobone granules

S: specific surface area of endobone granules (0.1 m^2/g) [42].

Furthermore, the binding was studied in the presence of calcium chloride (2,5 mM), BSA (200 µg/ml) and serum (10 % v/v).

4. Results and Discussion

4.1. Preparation and characterization of gold nanoparticles

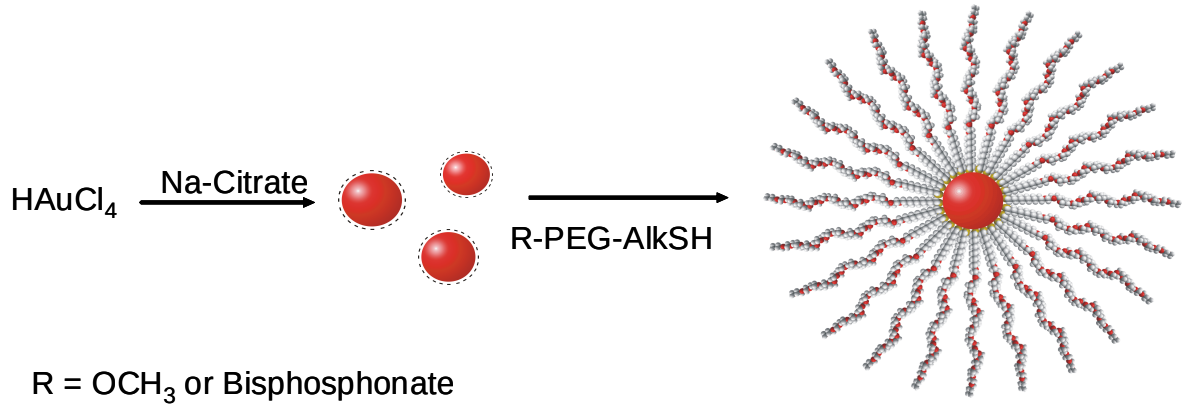

Figure 1: Diagram representing the synthesis of gold nanoparticle

Monodisperse GNPs were prepared by the reduction of $HAuCl_4 \cdot 3H_2O$ solution using tri-sodium citrate as reducing agent as presented in Figure 1. The prepared GNPs were obtained with ruby red color. The formation of the nanoparticles was followed using the UV-Vis spectrum, which shows the characteristic surface plasmon resonance (SPR) at about 524 nm (Figure 2). From the narrow peak of the citrate stabilized GNPs at 524 nm it can be concluded that these particles are well dispersed and the size of the obtained particles (bare GNPs) is about 40 nm [43]. After coating of the particles with synthesized polymers, the SPR at 524 exhibited a red shift of approximately 8 nm relative to the uncoated GNPs [44]. The observed red shift may be attributed to a change of the refractive index of the environment surrounding the nanoparticles as result of attached polymer layer around the particles, which is also an indication of the successful coating of nanoparticles with the polymers [45,46].

The gold content of the GNPs after synthesis was measured by ICP-OES. The determined concentrations of gold showed that nearly all the added gold in the flasks (2.5 mg) was converted to nanoparticles. The number of nanoparticles per ml was calculated based on the ICP measurement and the TEM images and it was found to be about $7*10^{10}$ particles/ml [47,48].

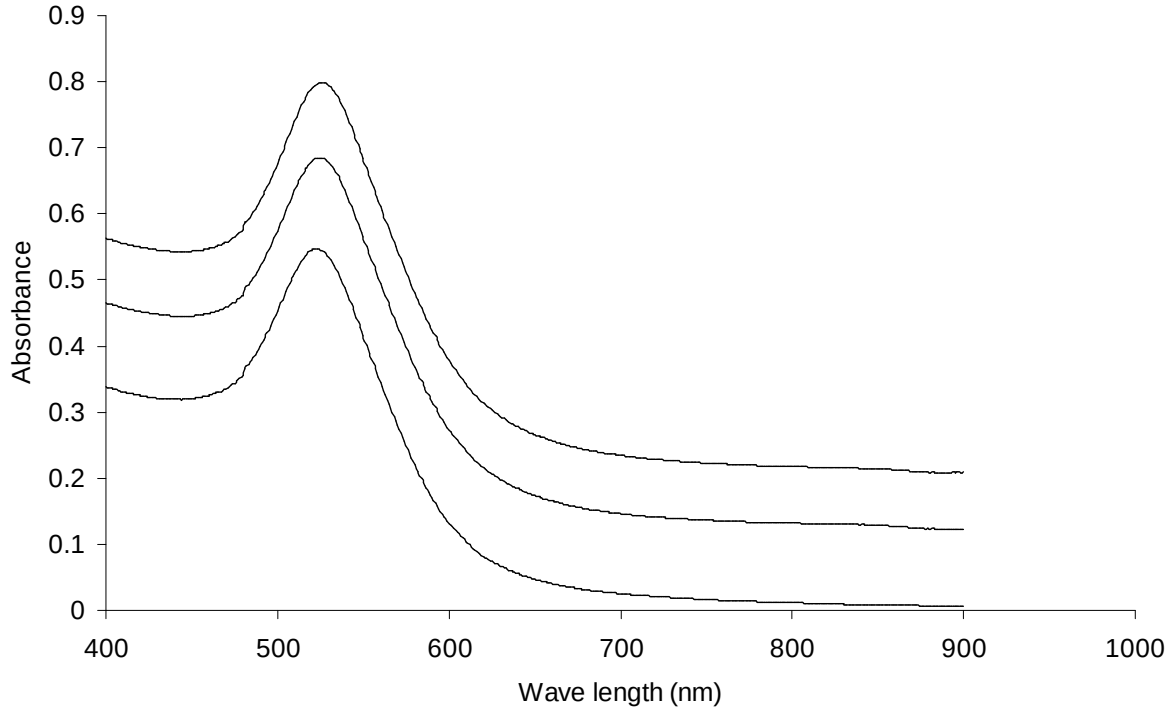

Figure 2: UV-Vis absorption spectra of citrate stabilized and coated gold nanoparticles; mPEG-AlkSH, BP-PEG-AlkSH and citrate coated GNPs (from top to bottom)

Several methods are applied to characterize particles, especially in terms of size, but none of them is generally fully satisfactory. Therefore, a combination of at least two methods, one of which should be a microscopic is highly recommended [49]. The sizes of different preparations of GNPs were determined by photon correlation spectroscopy are listed in Table 1. The sizes of different citrate stabilized gold nanoparticle preparations (1-4 preparations) range from 38.6 ± 0.153 to 46.1 ± 1.12 nm with acceptable polydispersity indices (less than 0.6) [12,37]. Modification of the nanoparticles with thiol containing polymers increased the hydrodynamic sizes as expected due to formation of a PEG monolayer around the nanoparticles. The measured size increases of the GNPs range from 7 to 12 nm. Consequently, the thickness of the polymer layer on the gold nanoparticle was between 3.5 to 6 nm, which agrees well with the results reported in the literatures [40,50].

Table 1: Sizes, polydispersity indices (PI) and zeta potentials of different batches of citrate stabilized and polymers coated GNPs determined by photon correlation spectroscopy

Gold nanoparticle preparations	Hydrodynamic size by PCS (nm)	Poly. Index (PI)	Zeta potential (mV)
Citrate coated GNPs 1	46.1 ± 1.12	0.479 ± 0.0.68	-48.7 ± 5.1
Citrate coated GNPs 2	44.2 ± 0.436	0.543 ± 0.055	-46.0 ± 4.5
Citrate coated GNPs 3	38.6 ± 0.153	0.416 ± 0.08	-47.7 ± 3.2
Citrate coated GNPs 4	41.8 ± 1.03	0.395 ± 0.018	-51.9 ± 8.9
1 coated with mPEG-AlkSH	57.3 ± 3.11	0.426 ± 0.061	-19.4 ± 6.1
2 coated with NH_2PEG-AlkSH	55.5 ± 1.39	0.578 ± 0.005	-2.1 ± 5.3
3 coated with BP-PEG-AlkSH	45.2 ± 1.1	0.465 ± 0.014	-44.6 ± 7.1

To further characterize the morphology and to verify the size of the prepared nanoparticles, imaging by transition electron microscopy (TEM) was applied. The obtained citrate stabilized GNPs are spherical, all smaller than about 100 nm and well-separated from each other when dried on the coated copper grid (Figure 3A). Upon examination of the nanoparticles with higher magnifications it was found that most of the synthesized nanoparticles are spherical

with only few of them exhibiting a slight polygonal shape (Figure 3B). The TEM images revealed no difference in the morphology and the appearance between bare and polymer coated nanoparticles, most likely due to the weak contrast of the polymer shell, which consequently is not visible in the micrographs (Figures 3B, 3C and 3D). The measured size differences range from 7 to 14 nm (between the coated and uncoated GNPs), which is a reasonable size of the polymeric coat of the nanoparticles. Furthermore, these observations also indicate that the integrity of GNPs is not affected by modifying the particles with the used polymers [46].

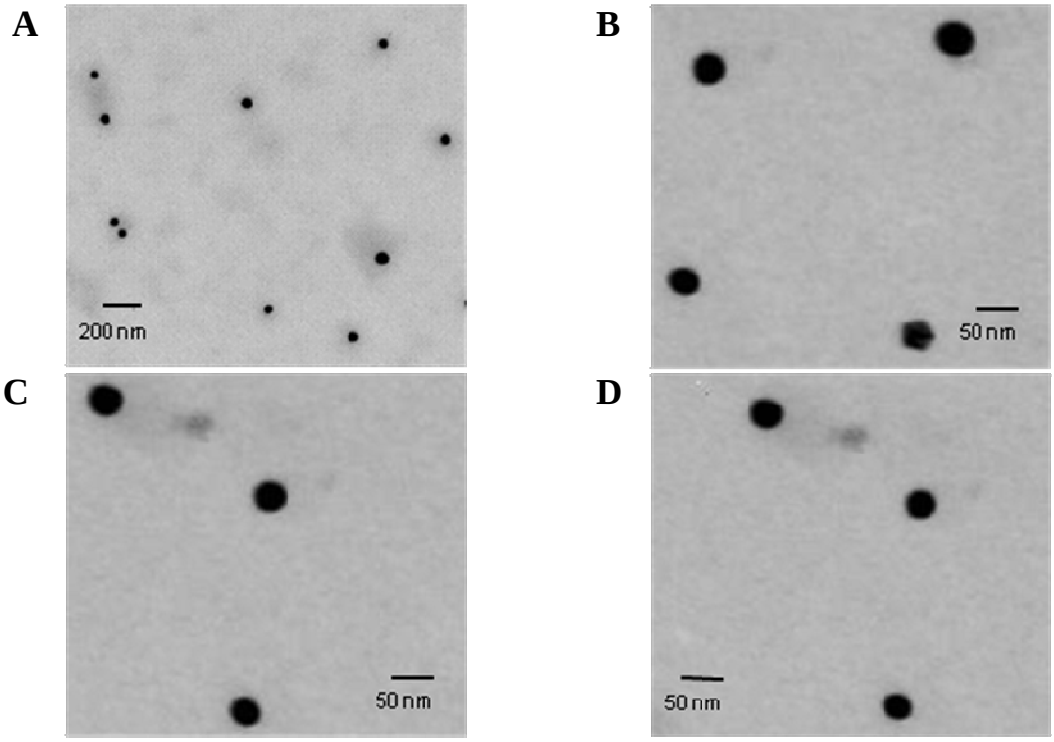

Figure 3: TEM images of the prepared GNPs; citrate stabilized GNPs (A and B), mPEG-AlkSH coated (C) and BP-PEG-AlkSH coated (D)

The surface charges of different gold nanoparticle preparations are listed in Table 1. The zeta potential measurements show that the surface charge of bare (citrate stabilized) GNPs is negative with approximately -48.5 ± 5.5 mV, which is attributed to the adsorption of the negative citrate anions to the particle surface during their synthesis. For dispersed particles the measured surface charge plays an important role for their stability. It is known from the literature that aggregation is very unlikely for charged particles with optimum zeta potentials ($\xi > 30$ mV) due to electrostatic repulsion forces between similarly charged particles [51]. Consequently the

charged particles are kept dispersed, because the double layer repulsion caused by the charges is counteracting the attractive van der Waal forces between two identical gold spheres [52].

Coating of citrate stabilized GNPs with mPEG-AlkSH resulted in an increase of the zeta potential from about -48.7 ± 5.1 to about -19.4 ± 6.1 due to the substitution of some the citrate anions adsorbed on the particle surface by the thiol groups of the polymer [53]. However, the PEG-coated gold nanoparticles were still well dispersed and stabilized, but instead of the electrostatic repulsion due to the steric repulsion of the polymer chains attached to the particle surfaces [54]. For the bisphosphonate-modified GNPs on the other side a high negatively charged particle surface was observed with zeta potentials similar to that of citrate stabilized GNPs (Table 1), which is explained by the presence of additional anionic bisphosphonate groups on the particle surface [55,56].

4.2. Dispersion stability of GNPs

For the biological applications of GNPs, the stability of different GNP preparations was investigated in the presence of high ionic strength media and in the presence of proteins (BSA and bovine serum). The addition of 5 M NaCl to bare GNPs resulted in a rapid aggregation of the nanoparticle monitored by drastic change of their color from ruby red to violet and finally to a colorless solution due to the resulting precipitation of the nanoparticles. The characteristic surface plasmon resonance disappeared and a new broad peak at much higher wave lengths (above 600 nm) was observed due to the formation of larger gold aggregates (Figure 4). The instability of citrate coated GNPs in the presence of high concentrations of NaCl could also be monitored by a large increase of the hydrodynamic size as measured by photon correlation spectroscopy (Figure 5). The GNP aggregation induced by addition of NaCl is due to the reduction of the electrostatic repulsion between surface-charged nanoparticles caused by the added sodium and chloride ions and consequently the decreasing distance between the particles favoring the interaction via van der Waals forces [57,58]. Polymer-coated GNPs on the other hand are not affected by NaCl, as shown in Figure 4 and 5, because they are not stabilized by the surface charge but by the steric repulsion effect of the polymer chains [39].

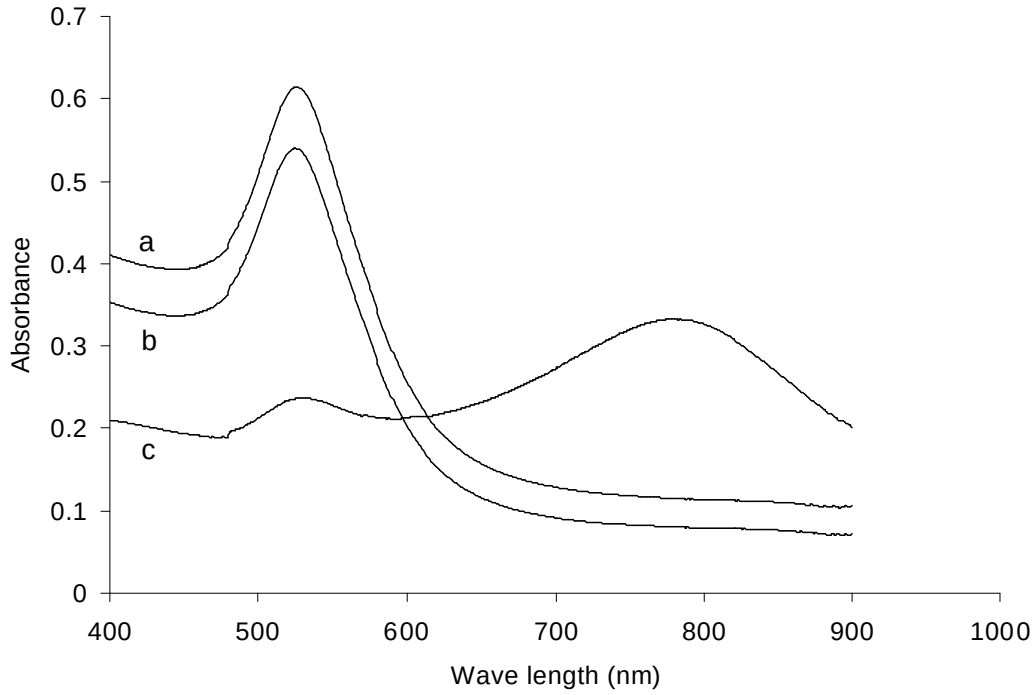

Figure 4: Effect of NaCl on the UV-Vis absorption spectra of mPEG-AlkSH (a), BP-PEG-AlkSH (b) and citrate (c) coated gold nanoparticles

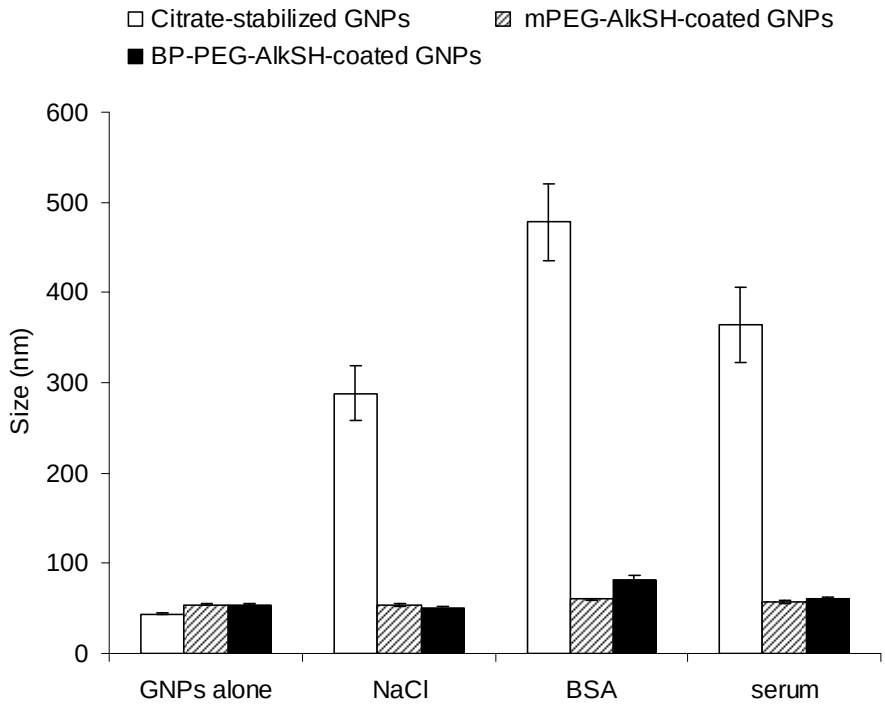

Figure 5: Size of GNPs before and after coating with polymers and the effect of addition of NaCl, BSA and 10% bovine serum on the on the size of coated and citrate stabilized GNPs

Similarly to the sodium chloride addition, citrate-coated GNPs rapidly aggregated after addition of bovine serum albumin (BSA) and also serum, which can be demonstrated by the disappearance of the characteristic surface plasmon resonance (Figure 6 and 7) and by their large size increase as shown by photon correlation spectroscopy measurements (Figure 5). These observations could be attributed to specific interactions of cysteine residues of the added proteins and GNPs or most likely to the adsorption of proteins on the nanoparticles, which both yields a shielding of the negative charges of the GNPs and the subsequent aggregation. In contrast, polymer-protected GNPs are either not affected at all (in case of mPEG-AlkSH coated GNPs) or show only a slight size increase (in case of BP-PEG-AlkSH coated GNPs) by addition of BSA and serum. The protein resistance (i.e. the stability) of PEG-coated GNPs is a consequence of the high stability of the interfacial water layer, which prevents direct contact between the particle surface and the proteins [59]. The slight increase in particle size after addition of BSA and serum to nanoparticles coated with BP-PEG-AlkSH (Figure 5) can be attributed to the presence of

negative charges of the bisphosphonate groups, which can interact with positively charged groups of the proteins.

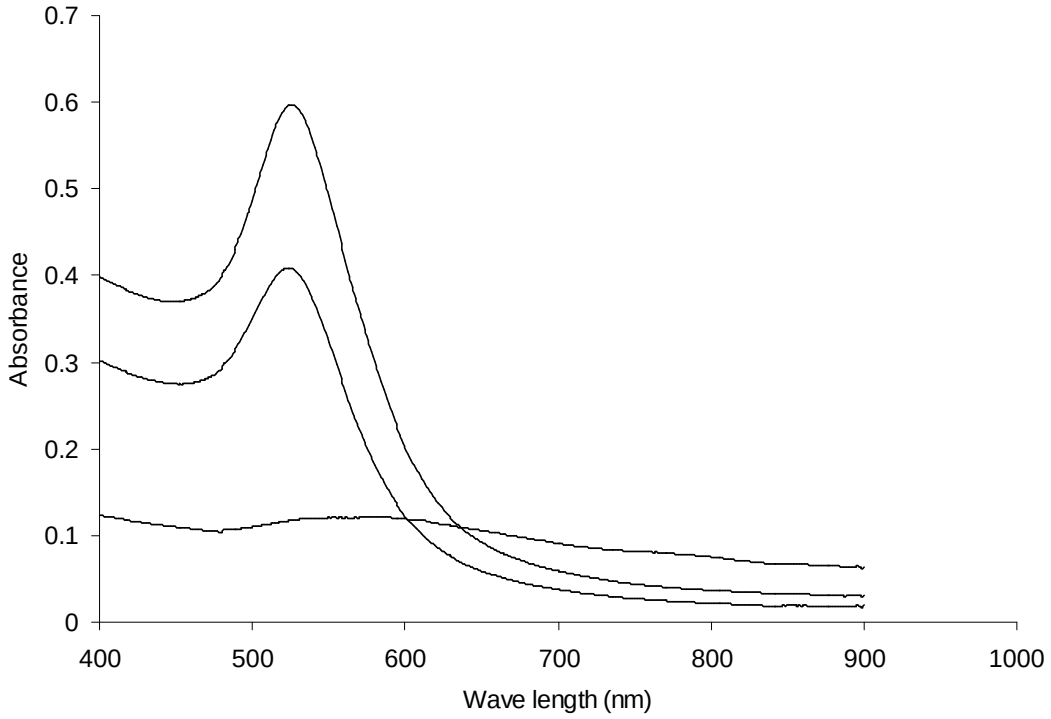

Figure 6: Effect of BSA on the UV-Vis absorption spectra of mPEG-AlkSH coated GNPs, BP-PEG-AlkSH coated GNPs and citrate coated gold nanoparticles (from top to down)

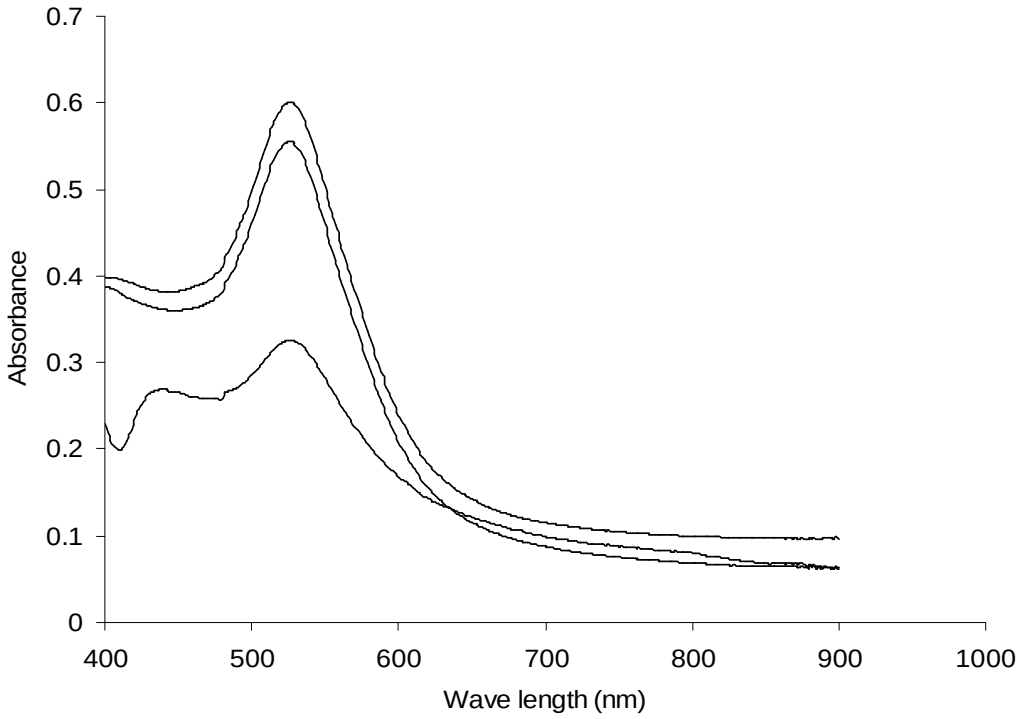

Figure 7: Effect of bovine serum (10 % v/v) on the UV-Vis absorption spectra of mPEG-AlkSH, BP-PEG-AlkSH and citrate coated gold nanoparticles (from top to bottom)

4.3. Adsorption of gold nanoparticles to hydroxyapatite

The adsorption of bisphosphonate modified GNPs (GNPs-BP) to hydroxyapatite was studied to evaluate the affinity of surface-modified gold nanoparticles to bone mineral. For this study endobone was used as a porous hydroxyapatite ceramic produced by sintering of bovine bone and it consequently can be used as model of bone, because it is the major constituent of the natural bone besides the protein [42]. The hydroxyapatite binding of GNPs modified with different amounts of bisphosphonate in the polymer layer was compared with the binding of GNPs coated with 100% of mPEG-AlkSH (0% bisphosphonate). The results showed that increasing the amount of binding ligand for the hydroxyapatite surface (bisphosphonate) led to increasing amounts of GNPs adsorbed to hydroxyapatite as depicted in Figure 8.

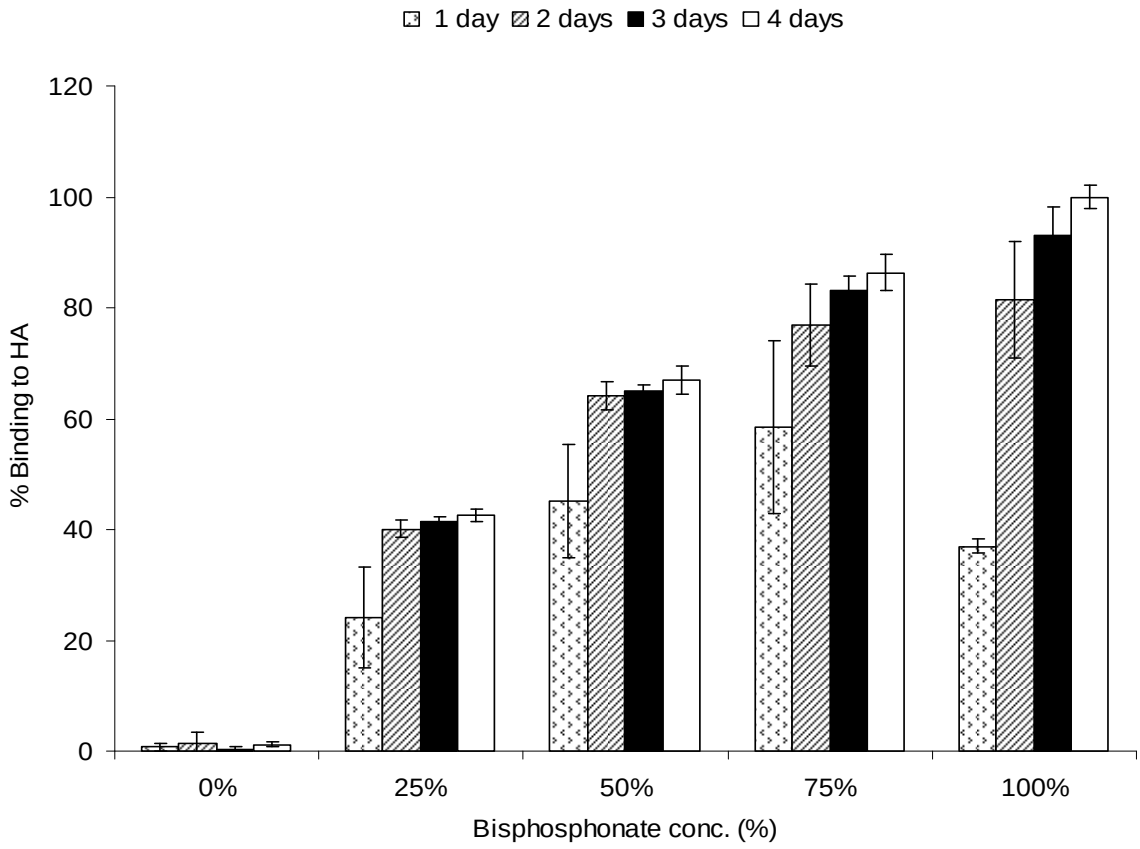

Figure 8: Hydroxyapatite binding of GNPs modified with different amounts of bisphosphonate (e.g, 75% means that GNPs are coated with 75% BP-PEG-AlkSH and 25% mPEG-AlkSH)

GNPs modified with 0% Bp (100% mPEG-AlkSH) showed no affinity to hydroxyapatite, while about 25% of the initially added GNPs modified with 25% BP (75% mPEG-AlkSH) adsorbed to hydroxyapatite within 24 hours. This adsorbed amount increased to about 40% after 48 hours with no further increase in the adsorbed amount by shaking for longer time (up to 4 days). The bound amounts of particles modified with 50% bisphosphonate were about 45% after one day and reached 64% after two days. The adsorbed amounts of GNPs modified with 75% and 100% bisphosphonate were 58% and 37% after one day, and 76% and 81% after two days and reached 86% and 100% after four days respectively. The steady increase in the adsorbed amounts with increasing concentration of bisphosphonate in the particle surface can be explained by the higher hydroxyapatite affinity of GNPs containing more bisphosphonate in their surface. The relatively long time (about two days) to establish the equilibrium between the adsorbed and free particles can be attributed to the necessary diffusion of the particles within the large volume of

the dispersion medium and the necessary penetration into the macro and micro pores of endobone granules on the bottom of the flasks to reach the adsorption sites. Similar results are obtained by many other authors who studied the binding of nanoparticles to hydroxyapatite [55,60].

Since it is well known that bisphosphonate strongly binds to divalent ions, such as calcium [61], the binding assay of bisphosphonate-modified GNPs was repeated in presence of calcium chloride to explore effect of calcium ions on the affinity of the nanoparticles. The used calcium concentration was 2.5 mM, which is the physiological concentration present in blood serum. The binding affinity of 100% bisphosphonate-modified GNPs to hydroxyapatite in the presence and absence of calcium chloride is depicted in Figure 9. It could be observed that there is no difference in the binding of nanoparticles either in presence or absence of calcium. This indicates that the binding affinity of particles to hydroxyapatite is not affected by the presence of calcium ions in the colloidal solution.

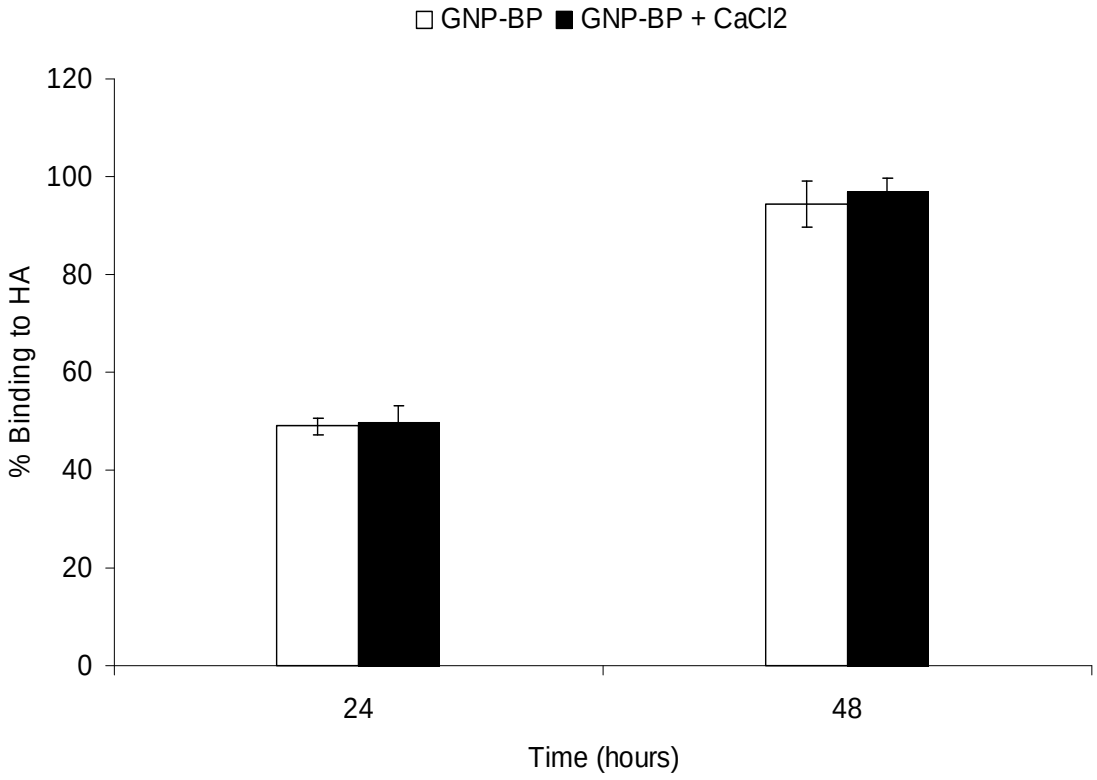

Figure 9: Effect of calcium chloride on the hydroxyapatite binding of bisphosphonate-modified GNPs

Furthermore, the in-vitro binding of bisphosphonate-modified GNPs was carried out in presence of BSA (200 µg/ml) and serum (10% v/v) to determine, if the interaction of bisphosphonate with these proteins compromises the binding to hydroxyapatite. The results of these experiments are presented in Figure 10, which shows that the binding affinity of nanoparticles to hydroxyapatite is not affected by the presence of BSA or serum. The obtained data indicate that the bisphosphonate-modified GNPs are stable and the observed interaction of particles and proteins, especially BSA (Figure 5), does not influence their bone mineral affinity.

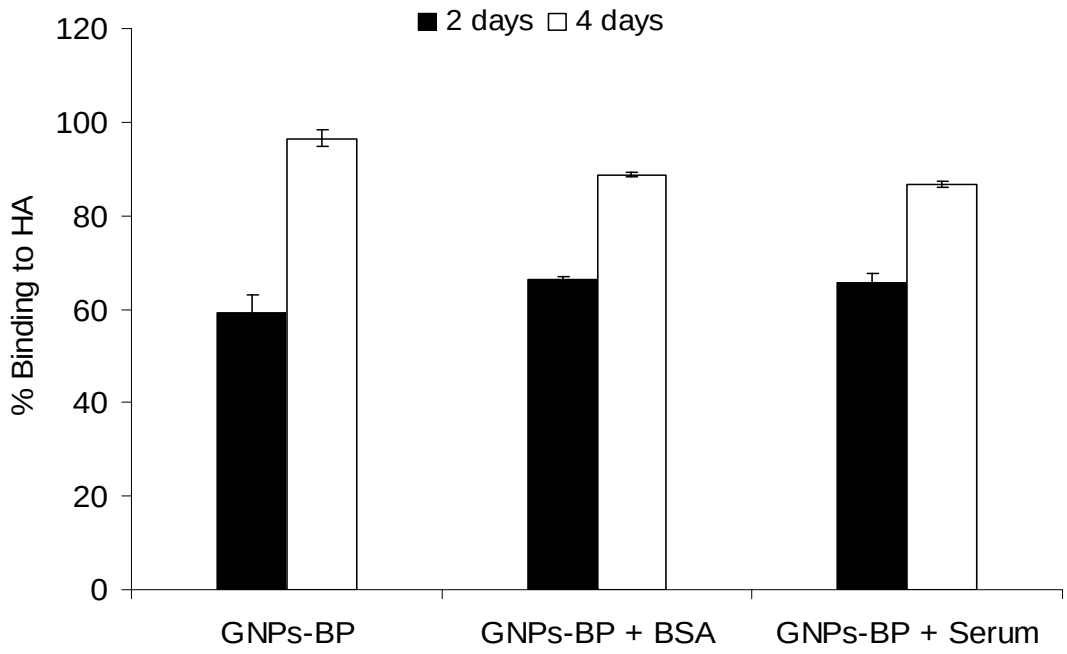

Figure 10: Effect of BSA (200 µg/ml) and bovine serum (10% v/v) on the binding of bisphosphonate-modified GNPs to hydroxyapatite

5. Conclusions

In conclusion, it could be shown that the synthesized polymers, methoxy poly(ethylene glycol)-undecyl mercaptane and the bisphosphonate derivative, are suitable to functionalize gold nanoparticles prepared by citrate reduction. The obtained particles were characterized with respect to size, surface charges and dispersion stability. The polymer modified GNPs showed an enhanced stability against aggregation in different solutions such as high ionic strength NaCl solutions, as well as solutions containing BSA and serum.

Furthermore, the modification of the particles with bisphosphonate modified polymers allowed the preparation of particles with high affinity and strong binding to hydroxyapatite. The binding affinity to bone mineral could be adjusted by increasing the amount of bisphosphonate (targeting ligand) on the particle surfaces. Furthermore, it was demonstrated that the binding is not affected by present calcium ions as well as in presence of proteins.

Based on the conducted in vitro studies, bisphosphonate-functionalized GNPs seem to be a promising model for the investigation of the in vivo bone targeting of nanoparticles. An adjustment of the binding affinity can be achieved by changing the amounts of immobilized bisphosphonate modified polymers. An exchange for other suitable ligands allows using the nanoparticle system also for other targets and the possible exploration for other applications than bone.

6. References

1. Anil K. Patri, Jolanta F. Kukowska-Latallo, and James R. Baker, "Targeted drug delivery with dendrimers: Comparison of the release kinetics of covalently conjugated drug and non-covalent drug inclusion complex," Advanced Drug Delivery Reviews **57,** 2203-2214 (2005).

2. Jolanta F. Kukowska-Latallo, Kimberly A. Candido, Zhengyi Cao, Shraddha S. Nigavekar, Istvan J. Majoros, Thommey P. Thomas, Lajos P. Balogh, Mohamed K. Khan, and James R. Baker, Jr., "Nanoparticle targeting of anticancer drug improves therapeutic response in animal model of human epithelial cancer," Cancer Res **65,** 5317-5324 (2005).

3. Megan E. Pearce, Jessica B. Melanko, and Aliasger K. Salem, "Multifunctional Nanorods for Biomedical Applications," Pharmaceutical Research **24,** 2335-2352 (2007).

4. Lilian E. van Vlerken and Mansoor M. Amiji, "Multi-functional polymeric nanoparticles for tumour-targeted drug delivery," Expert Opinion on Drug Delivery **3,** 205-216 (2006).

5. Eric Forssen and Michael Willis, "Ligand-targeted liposomes," Advanced Drug Delivery Reviews **29,** 249-271 (1998).

6. Jessica B. Melanko, Megan E. Pearce, and Aliasger K. Salem, "Nanotubes, nanorods, nanofibers, and fullerenes for nanoscale drug delivery," Biotechnology: Pharmaceutical Aspects **10,** 105-127 (2009).

7. Stuart C. McBain, Humphrey H. P. Yiu, and Jon Dobson, "Magnetic nanoparticles for gene and drug delivery," International Journal of Nanomedicine **3,** 169-180 (2008).

8. Stephen Hanessian, Justyna A. Grzyb, Feride Cengelli, and Lucienne Juillerat-Jeanneret, "Synthesis of chemically functionalized superparamagnetic nanoparticles as delivery vectors for chemotherapeutic drugs," Bioorganic & Medicinal Chemistry **16,** 2921-2931 (2008).

9. O. V. Salata, "Applications of nanoparticles in biology and medicine," Journal of Nanobiotechnology **2,** No (2004).

10. Ximei Qian, Xiang Hong Peng, Dominic O. Ansari, Qiqin Yin-Goen, Georgia Z. Chen, Dong M. Shin, Lily Yang, Andrew N. Young, May D. Wang, and Shuming Nie, "In vivo tumor targeting and spectroscopic detection with surface-enhanced Raman nanoparticle tags," Nature Biotechnology **26,** 83-90 (2008).

11. Yanli Liu and Stefan Franzen, "Factors Determining the Efficacy of Nuclear Delivery of Antisense Oligonucleotides by Gold Nanoparticles," Bioconjugate Chem. **19,** 1009-1016 (2008).

12. Giulio F. Paciotti, Lonnie Myer, David Weinreich, Dan Goia, Nicolae Pavel, Richard E. McLaughlin, and Lawrence Tamarkin, "Colloidal gold: a novel nanoparticle vector for tumor directed drug delivery," Drug delivery **11,** 169-183 (2004).

13. Priyabrata Mukherjee, Resham Bhattacharya, Nancy Bone, Yean K. Lee, Chitta Ranjan Patra, Shanfeng Wang, Lichun Lu, Charla Secreto, Pataki C. Banerjee, Michael J. Yaszemski, Neil

E. Kay, and Debabrata Mukhopadhyay, "Potential therapeutic application of gold nanoparticles in B-chronic lymphocytic leukemia (BCLL): enhancing apoptosis," Journal of Nanobiotechnology **5,** No (2007).

14. Rachana K. Visaria, Robert J. Griffin, Brent W. Williams, Emad S. Ebbini, Giulio F. Paciotti, Chang W. Song, and John C. Bischof, "Enhancement of tumor thermal therapy using gold nanoparticle-assisted tumor necrosis factor-a delivery," Molecular Cancer Therapeutics **5,** 1014-1020 (2006).

15. Rachana Visaria, John C. Bischof, Melissa Loren, Brent Williams, Emad Ebbini, Giulio Paciotti, and Robert Griffin, "Nanotherapeutics for enhancing thermal therapy of cancer," Int J Hyperthermia **23,** 501-511 (2007).

16. Yu Hung Chen, Chiau Yuang Tsai, Pon Yu Huang, Meng Ya Chang, Pai Chiao Cheng, Chen Hsi Chou, Dong Hwang Chen, Chrong Reen Wang, Ai Li Shiau, and Chao Liang Wu, "Methotrexate Conjugated to Gold Nanoparticles Inhibits Tumor Growth in a Syngeneic Lung Tumor Model," Molecular Pharmaceutics **4,** 713-722 (2007).

17. L. B. Nie, Y. Yang, S. Li, and N. Y. He, "Enhanced DNA detection based on the amplification of gold nanoparticles using quartz crystal microbalance," Nanotechnology **18,** 305501-1-305501/5 (2007).

18. Grit Festag, Andrea Steinbrueck, Andreas Wolff, Andrea Csaki, Robert Moeller, and Wolfgang Fritzsche, "Optimization of gold nanoparticles-based DNA detection for microarrays," Journal of Fluorescence **15,** 161-170 (2005).

19. Joong H. Kim, R. August Estabrook, Gary Braun, Briana R. Lee, and Norbert O. Reich, "Specific and sensitive detection of nucleic acids and RNases using gold nanoparticle-RNA-fluorescent dye conjugates," Chemical Communications (Cambridge, United Kingdom) 4342-4344 (2007).

20. C. Shad Thaxton, Dimitra G. Georganopoulou, and Chad A. Mirkin, "Gold nanoparticle probes for the detection of nucleic acid targets," Clinica Chimica Acta **363,** 120-126 (2006).

21. Charng Sheng Tsai, Ting Bin Yu, and Chao Tsen Chen, "Gold nanoparticle-based competitive colorimetric assay for detection of protein-protein interactions," Chemical Communications (Cambridge, United Kingdom) 4273-4275 (2005).

22. Kadir Aslan, Jian Zhang, Joseph R. Lakowicz, and Chris D. Geddes, "Saccharide sensing using gold and silver nanoparticles - A review," Journal of Fluorescence **14,** 391-400 (2004).

23. J. Ma, Huifen Wong, L. B. Kong, and K. W. Peng, "Biomimetic processing of nanocrystallite bioactive apatite coating on titanium," Nanotechnology **14,** 619-623 (2003).

24. Agustin De La Isla, Witold Brostow, Bernard Bujard, Miriam Estevez, J. Rogelio Rodriguez, Susana Vargas, and Victor M. Castano, "Nanohybrid scratch resistant coatings for teeth and bone viscoelasticity manifested in tribology," Materials Research Innovations **7,** 110-114 (2003).

25. Chenjie Xu, Glenn A. Tung, and Shouheng Sun, "Size and Concentration Effect of Gold Nanoparticles on X-ray Attenuation As Measured on Computed Tomography," Chemistry of Materials ACS (2008).

26. J. F. Hainfeld, D. N. Slatkin, T. M. Focella, and H. M. Smilowitz, "Gold nanoparticles: a new X-ray contrast agent," British Journal of Radiology **79,** 248-253 (2006).

27. Jingyuan Li, Xuemei Wang, Chunxia Wang, Baoan Chen, Yongyuan Dai, Renyun Zhang, Min Song, Gang Lv, and Degang Fu, "The enhancement effect of gold nanoparticles in drug delivery and as biomarkers of drug-resistant cancer cells," ChemMedChem **2,** 374-378 (2007).

28. Catherine M. Goodman, Catherine D. McCusker, Tuna Yilmaz, and Vincent M. Rotello, "Toxicity of Gold Nanoparticles Functionalized with Cationic and Anionic Side Chains," Bioconjugate Chem. **15,** 897-900 (2004).

29. Jun Shan and Heikki Tenhu, "Recent advances in polymer protected gold nanoparticles: synthesis, properties and applications," Chemical Communications (Cambridge, United Kingdom) 4580-4598 (2007).

30. Ralph Weissleder, Kimberly Kelly, Eric Yi Sun, Timur Shtatland, and Lee Josephson, "Cell-specific targeting of nanoparticles by multivalent attachment of small molecules," Nature Biotechnology **23,** 1418-1423 (2005).

31. Xiangyang Shi, Suhe Wang, Sasha Meshinchi, Mary E. Van Antwerp, Xiangdong Bi, Inhan Lee, and James R. Baker, Jr., "Dendrimer-entrapped gold nanoparticles as a platform for cancer-cell targeting and imaging," Small **3,** 1245-1252 (2007).

32. Hidenori Otsuka, Yoshitsugu Akiyama, Yukio Nagasaki, and Kazunori Kataoka, "Quantitative and reversible lectin-induced association of gold nanoparticles modified with a-lactosyl-w-mercapto-poly(ethylene glycol)," Journal of the American Chemical Society **123,** 8226-8230 (2001).

33. A. H. Lu, E. L. Salabas, and F. Schueth, "Magnetic nanoparticles: synthesis, protection, functionalization, and application," Angewandte Chemie, International Edition **46,** 1222-1244 (2007).

34. G. Frens, "Controlled nucleation for the regulation of the particle size in monodisperse gold suspensions," Nature (London), Physical Science **241,** 20-22 (1973).

35. Katherine C. Grabar, R. Griffith Freeman, Michael B. Hommer, and Michael J. Natan, "Preparation and Characterization of Au Colloid Monolayers," Analytical Chemistry **67,** 735-743 (1995).

36. Yanli Liu, Mathew K. Shipton, Joseph Ryan, Eric D. Kaufman, Stefan Franzen, and Daniel L. Feldheim, "Synthesis, Stability, and Cellular Internalization of Gold Nanoparticles Containing Mixed Peptide-Poly(ethylene glycol) Monolayers," Analytical Chemistry **79,** 2221-2229 (2007).

37. M. Rahimnejad, M. Jahanshahi, and G. D. Najafpour, "Production of biological nanoparticles from bovine serum albumin for drug delivery," African Journal of Biotechnology **5,** 1918-1923 (2006).

38. Andy Scheffer, Carsten Engelhard, Michael Sperling, and Wolfgang Buscher, "ICP-MS as a new tool for the determination of gold nanoparticles in bioanalytical applications," Analytical and Bioanalytical Chemistry **390,** 249-252 (2008).

39. Claire Mangeney, Fabien Ferrage, Isabelle Aujard, Valerie Marchi-Artzner, Ludovic Jullien, Olivier Ouari, El Djouhar Rekaie, Andre Laschewsky, Inger Vikholm, and Janusz W. Sadowski, "Synthesis and Properties of Water-Soluble Gold Colloids Covalently Derivatized with Neutral Polymer Monolayers," Journal of the American Chemical Society **124,** 5811-5821 (2002).

40. Seiji Takae, Yoshitsugu Akiyama, Hidenori Otsuka, Teisaku Nakamura, Yukio Nagasaki, and Kazunori Kataoka, "Ligand density effect on biorecognition by PEGylated gold nanoparticles: regulated interaction of RCA120 lectin with lactose installed to the distal end of tethered PEG strands on gold surface," Biomacromolecules **6,** 818-824 (2005).

41. N. Bouropoulos and J. Moradian-Oldak, "Analysis of hydroxyapatite surface coverage by amelogenin nanospheres following the langmuir model for protein adsorption," Calcified Tissue International **72,** 599-603 (2003).

42. S. Joschek, B. Nies, R. Krotz, and A. Gopferich, "Chemical and physicochemical characterization of porous hydroxyapatite ceramics made of natural bone," Biomaterials **21,** 1645-1658 (2000).

43. Wolfgang Haiss, Nguyen T. K. Thanh, Jenny Aveyard, and David G. Fernig, "Determination of Size and Concentration of Gold Nanoparticles from UV-Vis Spectra," Analytical Chemistry (Washington, DC, United States) **79,** 4215-4221 (2007).

44. Zul Merican, Tara L. Schiller, Craig J. Hawker, Peter M. Fredericks, and Idriss Blakey, "Self-assembly and encoding of polymer-stabilized gold nanoparticles with surface-enhanced Raman reporter molecules," Langmuir **23,** 10539-10545 (2007).

45. Dirk Eck, Christiane A. Helm, Norman J. Wagner, and Abraham Vaynberg, "Plasmon Resonance Measurements of the Adsorption and Adsorption Kinetics of a Biopolymer onto Gold Nanocolloids. [Erratum to document cited in CA134:213208]," Langmuir **23,** 9522 (2007).

46. Vivechana Dixit, Jeroen Van den Bossche, Debra M. Sherman, David H. Thompson, and Ronald P. Andres, "Synthesis and Grafting of Thioctic Acid-PEG-Folate Conjugates onto Au Nanoparticles for Selective Targeting of Folate Receptor-Positive Tumor Cells," Bioconjugate Chem. **17,** 603-609 (2006).

47. S. L. Cumberland and G. F. Strouse, "Analysis of the Nature of Oxyanion Adsorption on Gold Nanomaterial Surfaces," Langmuir **18,** 269-276 (2002).

48. Xiong Liu, Mark Atwater, Jinhai Wang, and Qun Huo, "Extinction coefficient of gold nanoparticles with different sizes and different capping ligands," Colloids and Surfaces, B: Biointerfaces **58,** 3-7 (2007).

49. Marie Gaumet, Angelica Vargas, Robert Gurny, and Florence Delie, "Nanoparticles for drug delivery: The need for precision in reporting particle size parameters," European Journal of Pharmaceutics and Biopharmaceutics **69,** 1-9 (2008).

50. Boru Zhu, Thomas Eurell, Rico Gunawan, and Deborah Leckband, "Chain-length dependence of the protein and cell resistance of oligo(ethylene glycol)-terminated self-assembled monolayers on gold," Journal of Biomedical Materials Research **56,** 406-416 (2001).

51. Devika R. Bhumkar, Hrushikesh M. Joshi, Murali Sastry, and Varsha B. Pokharkar, "Chitosan Reduced Gold Nanoparticles as Novel Carriers for Transmucosal Delivery of Insulin," Pharmaceutical Research **24,** 1415-1426 (2007).

52. Jingfang Zhou, David A. Beattie, John Ralston, and Rossen Sedev, "Colloid Stability of Thymine-Functionalized Gold Nanoparticles," Langmuir **23,** 12096-12103 (2007).

53. Ruxandra Gref, Gregory Miralles, and Edith Dellacherie, "Polyoxyethylene-coated nanospheres: effect of coating on zeta potential and phagocytosis," Polymer International **48,** 251-256 (1999).

54. Muriel K. Corbierre, Neil S. Cameron, and R. Bruce Lennox, "Polymer-stabilized gold nanoparticles with high grafting densities," Langmuir **20,** 2867-2873 (2004).

55. V. Hengst, C. Oussoren, T. Kissel, and G. Storm, "Bone targeting potential of bisphosphonate-targeted liposomes," International Journal of Pharmaceutics **331,** 224-227 (2007).

56. Saeeda Jaffar, Ki Tae Nam, Ali Khademhosseini, Jia Xing, Robert S. Langer, and Angela M. Belcher, "Layer-by-layer surface modification and patterned electrostatic deposition of quantum dots," Nano Letters **4,** 1421-1425 (2004).

57. Gang Wang and Wenfang Sun, "Optical Limiting of Gold Nanoparticle Aggregates Induced by Electrolytes," Journal of Physical Chemistry B **110,** 20901-20905 (2006).

58. Santosh Aryal, K. C. R. Bahadur, Narayan Bhattarai, Chul Ki Kim, and Hak Yong Kim, "Study of electrolyte induced aggregation of gold nanoparticles capped by amino acids," Journal of Colloid and Interface Science **299,** 191-197 (2006).

59. R. L. C. Wang, H. J. Kreuzer, and M. Grunze, "Molecular Conformation and Solvation of Oligo(ethylene glycol)-Terminated Self-Assembled Monolayers," Journal of Physical Chemistry B **101,** 9767-9773 (1997).

60. Sung Wook Choi and Jung Hyun Kim, "Design of surface-modified poly(d,l-lactide-co-glycolide) nanoparticles for targeted drug delivery to bone," Journal of Controlled Release **122,** 24-30 (2007).

61. Anke J. Roelofs, Keith Thompson, Sharon Gordon, and Michael J. Rogers, "Molecular Mechanisms of Action of Bisphosphonates: current Status," Clinical Cancer Research **12,** 6222s-6230s (2006).

Chapter 6

Targeting of Bisphosphonate-Functionlized Gold Nanoparticles to Bone

Gamal Zayed[1], Jörg Teßamr[1], Claire Vanpouille[2], François Hindré[2], Jean-Pierre Benoit[2], Achim Göpferich[1]

[1]Department of Pharmaceutical Technology, University of Regensburg, 93040 Regensburg, Germany

[2]Université d'Angers, Inserm U646, Angers, France

to be submitted

1. **Introduction**

Over the past years, a lot of research was devoted to the development of targeted nanoparticles for a localized drug delivery, because of the multitude of advantages and further treatment options this kind of therapy would offer. After in vivo administration of colloidal carriers, the biodistribution and interaction of particulate carriers with different cells and tissues largely depends on the particle size and surface properties such as surface charges and surface hydrophilicity [1,2]. Due to this fact we aimed at the production of a versatile model system that allowed for the use of various targeting ligands. It is based on a gold nanoparticulate core and a stabilizing shell consisting of a stabilizing PEG layer with attached ligands suitable for targeting.

Nanoparticles, like all other colloidal carriers, are taken up by the Kupffer cells of the liver or the macrophages of the spleen and blood stream after intravenous administration. Therefore, the liver represents a major obstacle or sink for the efficient targeting of colloidal carriers to specific sites other than reticuloendothelial system (RES). For a successful targeting approach, the most promising strategy is to avoid the uptake of nanoparticles by the RES by steric stabilization of nanoparticles using a hydrophilic polymer layer such as poly(ethylene glycol) (PEG). The presence of PEG on the particle surface decreases opsonin adsorption and thus also of nanoparticle phagocytosis by the liver, which leads consequently to longer circulation half life of such particles in the blood [3-5].

Metallic nanoparticles are not only used as model systems but also for therapeutic applications. They are very attractive due to their size, physical, chemical and surface properties, which include high chemical stability and easy detection. Flexible nanoparticle surface coatings and functionalization can be utilized to increase the blood residence time, reduce nonspecific biodistribution and investigate the targeting to specific tissues or specific cells by using surface immobilized targeting ligands [6]. Melancon and et al. [7], for example, studied the in vitro and in vivo targeting of hollow gold nanoshells for photothermal ablation therapy, which makes use of the high absorptivity of the nanoparticles in order to irradiate targeted tumor tissues. In vivo results showed that antibody-conjugated ^{111}In-labelled particles have the potential to be delivered to specific sites after intravenous administration in mice, which makes them useful as enhancer for the subsequent photothermal treatment.

For this study we chose bone as target tissue, since bone selective delivery of drug-loaded nanoparticles can potentially lead to high local drug concentrations of bone therapeutic agents suitable to fight osteoporosis or bone cancer. This kind of treatment would additionally minimize the distribution of the cytostatic drugs in the whole body and thereby decrease the

systemic toxicity. Several investigations were already conducted to develop bone targeted drug delivery system using bisphosphonates, small chemical entities with very high affinity to the main inorganic component of bone, the bone mineral hydroxyapatite [8-10]. Based on this knowledge Hengst et al. [11] studied the in vitro bone targeting ability of bisphosphonate-conjugated liposomes as nanoparticulate drug delivery system. The obtained results indicated that the bisphosphonate-conjugated liposomes are useful to target the bone mineral hydroxyapatite in vitro. Further investigations in the literature, however, only describe the use of bisphosphonate labeled proteins used for bone targeting, which apparently are much smaller in size than the here investigated nanoparticles [12].

To investigate the bone targeting ability of recently designed gold nanoparticles with high affinity to hydroxyapatite in vitro, bisphosphonate-modified PEGylated gold nanoparticles were intended to be applied intravenously to mice. The study examines the effect of surface functionalization and PEGylation on the pharmacokinetic profile and the resulting distribution of the gold nanoparticles in vivo. Furthermore, the study elucidates the impact of the bisphosphonate density on the particles surface on the in vivo bone targeting of the functionalized gold nanoparticles.

2. Experimental

2.1. Materials

Amino poly(ethylene glycol)-undecyl mercaptane, methoxy poly(ethylene glycol)-undecyl mercaptane and bisphosphonate-modified amino poly(ethylene glycol)-undecyl mercaptane were synthesized as described in chapter 2. Hydrogen tetrachloroaurate trihydrate ($HAuCl_4.3H_2O$), tri-sodium citrate dihydrate, diethylenetriaminepentaacetic (DTPA) dianhydride, triethylamine (TEA), dialysis tubing (MWCO 1000 Da), dialysis tubing (MWCO 3500 Da), ultrafiltration tubes (50,000 Da MWCO), bovine serum albumin (BSA) and tetramethylsilane (TMS) were purchased from Sigma-Aldrich Chemical Company (Steinheim, Germany). Bovine serum, chloroform, calcium chloride, physiological buffer solution, endobone granules, and acetate buffer pH 5.5, were obtained from Merck (Darmstadt, Germany). Deuterated chloroform was from Deutero GmbH (Kastellaun, Germany). Radioactive indium (^{111}In) was obtained from OctreoScan® Kit (Mallinckrodt, Inc.).

2.2. Methods

2.2.1. Synthesis and characterization of DTPA-PEG-AlkSH

Amino poly(ethylene glycol)-undecyl mercaptane DTPA (DTPA-PEG-AlkSH) derivative was prepared from amino poyl(ethylene glycol)-undecyl mercaptane (NH_2-PEG-AlkSH) and diethylenetriaminepentaacetic (DTPA) as following. To the stirred suspension of DTPA dianhydride (1.43 g, 4 mmol) in 40 ml chloroform, TEA (0.81 g, 8 mmol) and amino poly(ethylene glycol)-undecyl mercaptane (NH_2-PEG-AlkSH) (2.2 g, 1 mmol) were added and further stirred at room temperature for 3 h. After the reaction, chloroform and TEA were removed by heating to 65 °C under vacuum. The obtained DTPA-PEG-AlkSH was purified by dialysis against deionized water using dialysis tube (MWCO, 1000), immediately freeze dried and later characterized by ^{1}H-NMR. The synthesis of DTPA-PEG-AlkSH is described in Scheme 1 [13-15].

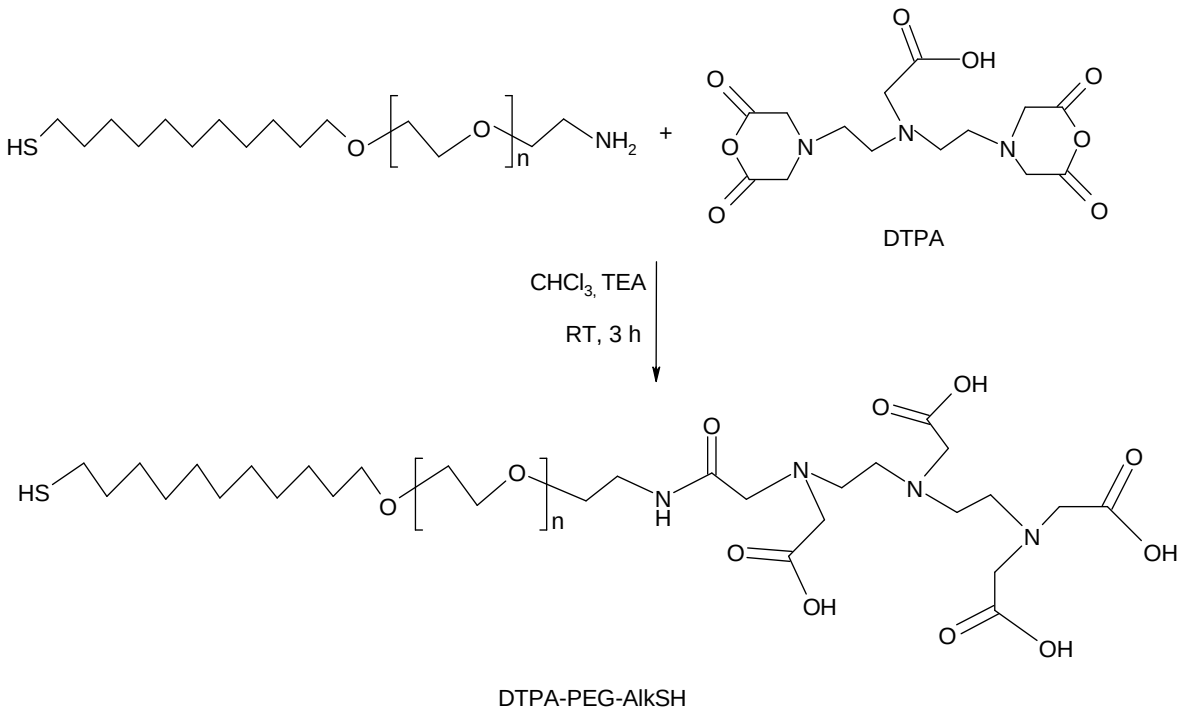

Scheme 1: Synthesis of the amino poly(ethylene glycol)-undecyl mercaptane DTPA derivative

2.2.2. Preparation of gold nanoparticles functionalized with bisphosphonate

Citrate stabilized gold nanoparticles with an average particle size suitable for intravenous administration were synthesized by the reduction of hydrogen tetrachloroaurate tri-hydrate ($HAuCl_4.3H_2O$) using tri-sodium citrate as described in chapter 4. For the subsequent modification of the gold nanoparticle surface, a parallel adsorption method was applied using different combinations of the functionalized polymers. Methoxy poly(ethylene glycol)-undecyl mercaptane, bisphosphonate modified poly(ethylene glycol)-undecyl

mercaptane and DTPA modified poly(ethylene glycol)-undecyl mercaptane were added to the nanoparticle dispersion with a total concentration of 5µg/ml. The amount of DTPA-PEG-AlkSH was kept constantly at 10% of the polymer mixture, while the concentrations of mPEG-AlkSH and BP-PEG-AlkSH were changed to obtain different functionalities of the particles. Three types of gold nanoparticles solutions were prepared from citrate stabilized gold nanoparticles stock solution with a concentration of $7*10^{10}$ particles/ml and with size of 37 nm. *Solution I* (control) which is modified by 10% DTPA-PEG-AlkSH and 90% mPEG-AlkSH, *solution II,* which is modified with 10% DTPA-PEG-AlkSH , 50% mPEG-AlkSH and 40% BP-PEG-AlkSH, and *solution III*, which is modified by modified by 10% DTPA-PEG-AlkSH, 10% mPEG-AlkSH and 80% BP-PEG-AlkSH. Excess polymers were removed by ultrafiltration at 750 g using ultrafiltration tubes.

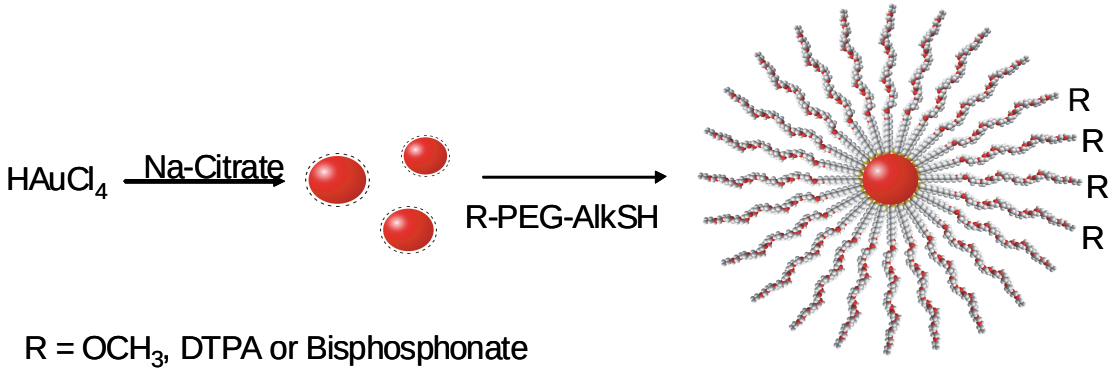

Figure 1: Preparation strategy of surface functionalized gold nanoparticles.

2.3. Characterization of gold nanoparticles

2.3.1. UV-Visible spectroscopy

UV-Vis absorption spectra of aqueous dispersions of the citrate stabilized and polymer coated nanoparticles were recorded using double beam spectrophotometer (Uvikon-941, Kontron Instrument, Germany).

2.3.2. Size distribution and surface charge measurements

Particle size distributions of the gold nanoparticles were determined using the Zetasizer 3000HSA (Malvern Instruments, GmbH, Germany). Nanoparticle dispersions were appropriately diluted with 0.22 µm-filtered Millipore water and size measurements were carried out at a 90° angle with respect to the incident beam. The measurements of the particle surface charges were performed in the standard capillary electrophoresis cell of Zetasizer

3000 HSA (Malvern Instruments, GmbH, Germany), measuring the electrophoritic mobility at 25 °C. Refractive index and viscosity of water were used for the calculation of the results.

2.3.3. TEM imaging of the particles

10 µl of the nanoparticle samples were dropped on graphite coated copper grids and dried at room temperature overnight before taking the images by transmission electron microscopy (TEM) (Zeiss EM 10 C/CR, Germany).

2.3.4. Dispersion stability of nanoparticles

High ionic strength solutions (5M NaCl), bovine serum albumin (BSA, 200µg/ml) and bovine serum (10% v/v) were applied to the test the dispersion stability of coated GNPs in comparison with bare nanoparticles using photon correlation spectroscopy and UV-Vis adsorption spectroscopy.

2.3.5. Determination of nanoparticles concentration by ICP

1 ml nanoparticle dispersion was treated with an equal volume of aqua regia to dissolve the nanoparticles before determining the concentrations of the elemental gold using inductively coupled plasma optical emission spectroscopy (ICP-OES) (Horiba Jobin Yvon, 70P, S+S, Munich, Germany). The concentration was calculated using standard curve constructed by using different concentrations of auric chloride.

2.4. In vitro binding of gold nanoparticles to hydroxyapatite

The bone mineral affinity of *solution I* and *II* compared to that of the control was investigated before carrying out the in vivo studies. 3 ml of the nanoparticle dispersions were added to 0.5 g of the bone mineral hydroxyapatite (Endobone) and shaked on an orbital shaker at 200 rpm at room temperature. The percentages of adsorbed nanoparticles with time were calculated according to equation 1:

$$\%Adsorbed = \frac{Abs_{before} - Abs_{after}}{Abs_{before}} \cdot 100\ \% \quad \text{(Equation 1)}$$

ABS_{before}: is the absorbance of nanoparticles at λ_{max} before shaking with HA

ABS_{after}: is the absorbance of nanoparticles at λ_{max} after shaking with HA

Binding studies in the presence of calcium chloride, BSA and serum were also performed in order to investigate the effect of the presence of electrolytes and proteins on the affinity of the nanoparticles to hydroxyapatite.

2.5. Radiolabelling of gold nanoparticles.

For the accurate in vivo quantitative analysis, gold nanoparticles were labeled with the ^{111}In, which has a half life of 67.3 h. This long half life enables the in vivo detection of the nanoparticles up to 48 h after conjugation and injection of the particles in the animals [7]. 1 ml of gold nanoparticle dispersion ($7*10^{10}$ particles per ml) was added to 3.75 ml of acetate buffer (pH = 5.5) containing 0.8-0.9 MBq of ^{111}In. The mixture was then stirred at room temperature for 15 minutes. Excess of unbound radioactive indium was removed by dialysis for 2 h against physiological buffer using dialysis membrane with a cutoff of 3500 Da.

2.6. Animal biodistribution

The biodistribution experiments were carried out using SWISS male mice weighing between 28 and 34 g (provided by the animal house of the University of Angers) in accordance with the French regulations for animal experiments (law 0189.4 of January 24, 1990). About 100 µl of the dispersions of ^{111}In-labeled gold nanoparticles, with the later determined actual amounts of each solution, were injected intravenously in the tail vein of a mouse under gaseous isoflurane anesthesia. The injected volumes in each mouse would correspond to about $5.6*10^{8}$ particles and $2.5*10^{5}$ cpm of radioactivity. The animals had free access to food and water ad libitum prior to and during the course of the experiments. Four injected mice were sacrificed at specific time points of 15 minutes, 1, 6, 24 and 48 h after the administration of particles. Different organs of each mouse including liver, heart, spleen, lungs, muscles, bone (femur), stomach, small intestine, colon (large intestine), kidneys, urinary bladder, brain, carcass and an accurately weighed sample of blood were taken and placed in scintillation tubes for counting the radioactivity. Additionally, two times three mice were placed in special cages for the collection of urine and faeces samples for the high bisphosphonate carrying particles. The weight of each organ was determined and the corresponding radioactivity in that organ was recorded using a gamma counter (Packard Auto-Gamma 5000 series, Packard Instruments). Tissue concentrations of the nanoparticles were calculated and expressed as percent of the still present injected dose per gram of the respective tissue (% ID/g). The radioactivity still remaining in the tail was also recorded and taken into consideration for the calculation of the total present radioactivity dose in the animals. Blood samples were taken and the concentrations of nanoparticles in correctly weighed blood samples were recorded with time to investigate the pharmacokinetic profile of the injected particles.

2.7. Pharmacokinetic analysis in the blood.

To compare between the different injected nanoparticle solutions, the pharmacokinetic parameters for all types of injected gold nanoparticles such as the area under the curve (AUC), elimination half life ($t_{1/2}$), elimination rate constant (K_{el}) and mean residence time (MRT) were calculated according to the literature [16,17].

3. Results and discussion

3.1. Synthesis and characterization of DTPA-PEG-AlkSH.

Diethylene triaminepentaacetic (DTPA) acid reacted with amino group of amino poly(ethylene glycol)-undecyl mercaptane (NH_2PEG-AlkSH), which resulted in the formation of the DTPA-PEG-AlkSH derivatives. The ^{1}H-NMR spectrum in deuterated chloroform (Figure 1) is characterized by the signals at δ_H: 3.9-3.4 ppm (m, 192 H), 3.2 (s, 8 H), 2.8-2.5 ppm (m, 2 H) and 1.8-1.2 ppm (m, 18 H). The integral of signal at δ_H 3.2 ppm is 7.2 protons, which should be 8 protons. Based on this results, the conversion to product DTPA-PEG-AlkSH was calculated to be about 90%, which agrees well with the results described in the literature [15].

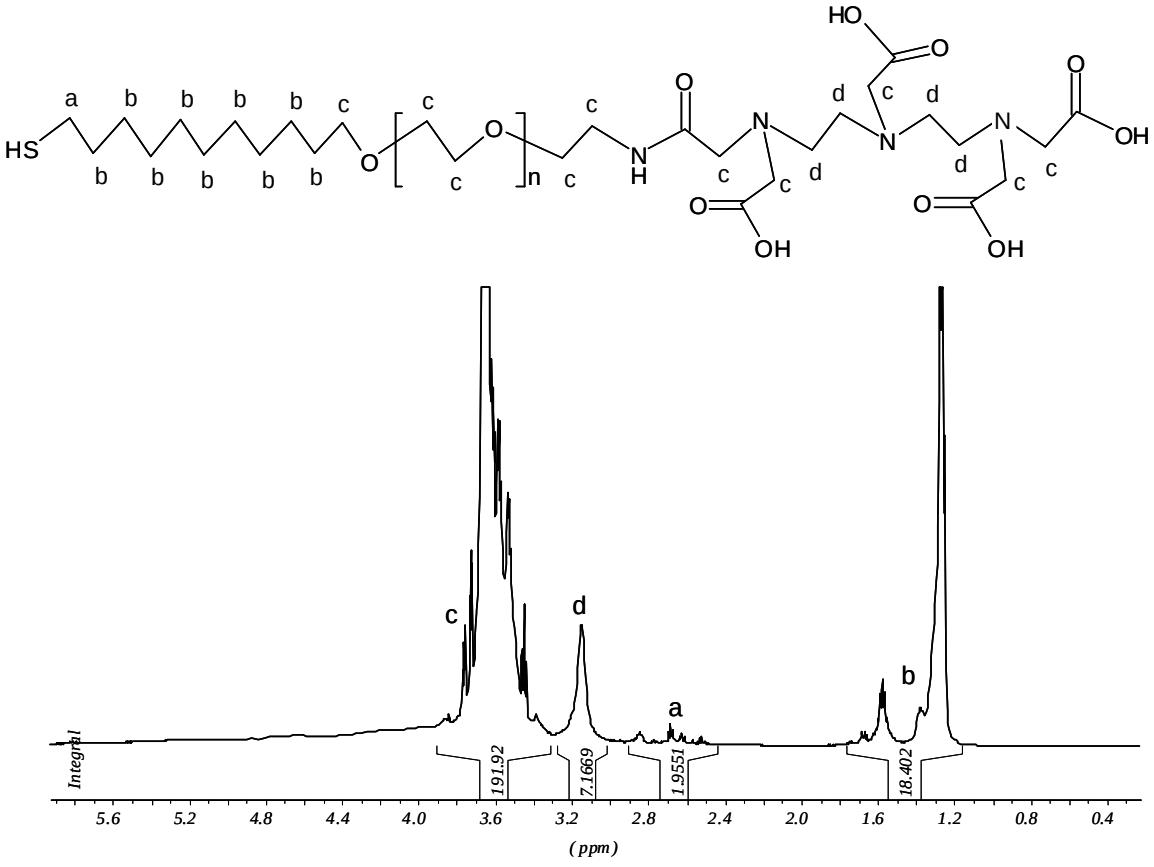

Figure 2: ^{1}H-NMR spectrum of poly(ethylene glycol)-undecyl mercaptane DTPA derivatives

3.2. Preparation and characterization of the bisphosphonate coated gold nanoparticles

3.2.1. Particles sizes and surface charges measurements

Nanoparticles with average particle size in the low nanometer range were synthesized by reducing tetrachloroaurate trihydrate with sodium citrate, a method already described in chapter 4. The formation of the gold nanoparticles is accompanied by a change of the solution color from pale yellow to ruby red. The size of the prepared nanoparticles determined by photon correlation spectroscopy was 37.0 ± 1.5 nm with a polydispersity index (P.I) of 0.495 ± 0.093. The zeta potential of the citrate-stabilized gold nanoparticles out of the synthesis was measured to be about -55.5 ± 13.4 mV (Table 1). This relatively high negative surface charge of nanoparticles is the main cause for the stability of the citrate coated colloidal solution. Coating of the nanoparticles with the mixed polymers resulted in an increase of the size by 12-14 nm due to the hydrophilic polymer coating. The morphology and the surface structure of different samples were investigated by TEM and the obtained results confirmed the size results determined by photon correlation spectroscopy. The coating of nanoparticles with the hydrophilic polymers did not affect the polydispersity index. *Solution I*, which is modified by 10% DTPA-PEG-AlkSH and 90% mPEG-AlkSH showed an increase in the zeta potential from -55.5 mV to -26.3 mV due to replacement of the citrate anions adsorbed on the particles surfaces. While *solution II*, which is modified by 10% DTPA-PEG-AlkSH, 40% BP-PEG-AlkSH and 50% mPEG-AlkSH showed lower increase in the zeta potential (from -55.5 mV to -31.0 mV) due to the incorporation of 40% of the negatively charged bisphosphonate groups within the coating. *Solution III*, which is modified by 10% DTPA-PEG-AlkSH, 80% BP-PEG-AlkSH and 10% mPEG-AlkSH showed the lowest increase in zeta potential (from -55.5 mV to -38.3 mV) due to the incorporation of the highest amount (80%) of bisphosphonate in the coat as shown in Table 1.

Table 1: Size, polydispersity index (P.I) and zeta potential of the citrate-stabilized and polymers- coated gold nanoparticles

	Size (nm)	Polydispersity index (P.I)	Zeta potential (mV)
Citrate stabilized GNPs	37.0 ± 1.51	0.495 ± 0.093	-55.5 ± 13.4
solution I GNPs (coated with 10% DTPA-PEG-AlkSH and 90% mPEG-AlkSH)	48.9 ± 0.53	0.465 ± 0.085	-26.3 ± 7.8
solution II GNPs (coated with 10% DTPA-PEG-AlkSH, 40% BP-PEG-AlkSH and 50% mPEG-AlkSH)	49.5 ± 0.92	0.549 ± 0.012	-31.0 ± 6.8
solution III GNPs (coated with 10% DTPA-PEG-AlkSH, 80% BP-PEG-AlkSH and 10% mPEG-AlkSH)	50.4 ± 1.73	0.561 ± 0.005	-38.3 ± 9.1

3.2.2. UV-Vis absorption spectra

Figure 3 shows the UV-Vis spectra of the bare gold nanoparticles compared with the modified particles of *solution I, II* and *III*. The characteristic surface plasmon resonance (SPR) band of citrate stabilized gold nanoparticles was observed at 522 nm confirming the presence of the spherical nanoparticles. Because the SPR is sensitive to the surface modification of the gold nanoparticles, a slight red shift in the λ_{max} was observed (from 522 nm to 526 nm). The red shift of λ_{max} indicates the disturbance of the electrical double layer present around the nanoparticles by addition of the polymer and confirms their successful attachment (*solution I, II* and *III*) [18].

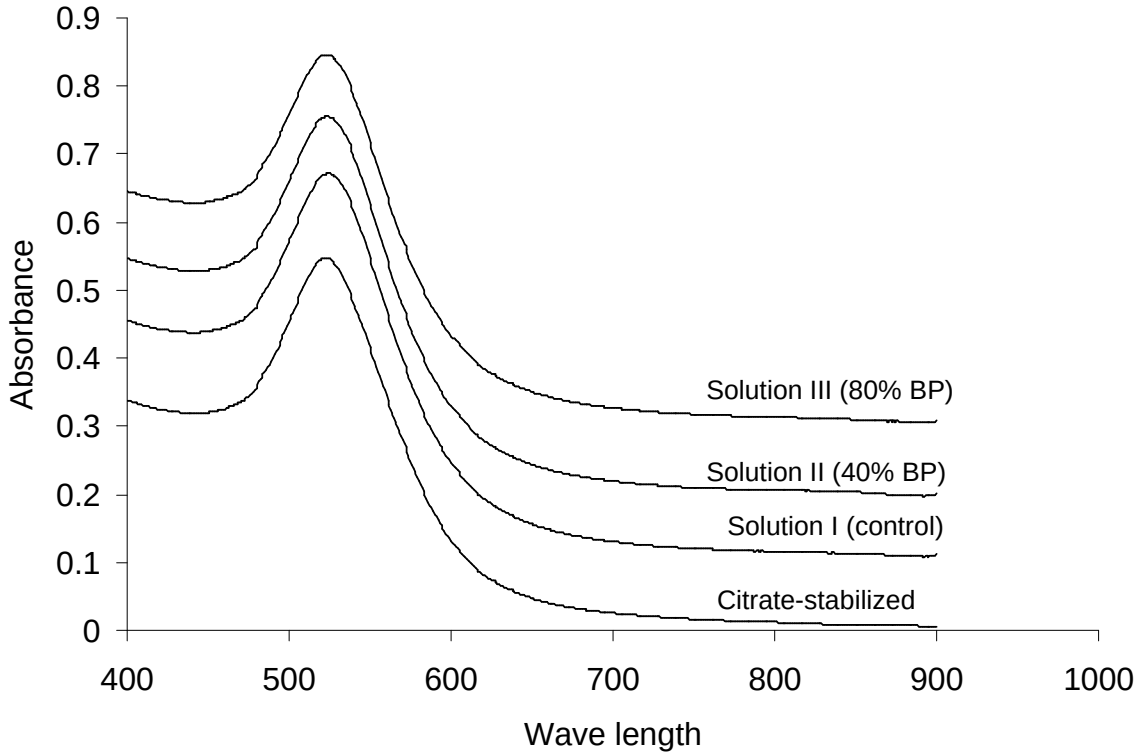

Figure 3: UV-Vis absorption spectra of bare gold nanoparticles, solution I, II and III

3.2.3. Dispersion stability of nanoparticles

As preliminary investigation for the stability of the particles before the in vivo experiments, the stability of *solution I, II* and *III* in comparison to citrate-stabilized gold nanoparticles was tested in the presence of sodium chloride, BSA and bovine serum. Citrate-stabilized gold nanoparticles were significantly more sensitive and are rapidly aggregated to larger particles in the presence of electrolytes (NaCl), BSA and serum. While polymer-coated nanoparticles (*solution I, II* and *III*) are resistant and are not affected by the addition of salt or proteins, due to the presence of a protective layer of polymers around the particle surfaces. These results agreed well with results reported in chapter 4.

3.3. In vitro binding of gold nanoparticles to hydroxapatite

The hydroxyapatite adsorption assay was performed in order to confirm the affinity of surface modified nanoparticles to bone. The bone mineral affinities of the different solutions are presented in Figure 4. About 40% binding of *solution II,* which contains 40% bisphosphonate, was obtained after 2 days of shaking with endobone granules at room temperature compared to only very small amounts (about less than 5%) adsorbed from *solution I,* which contains no bisphosphonate. The bound amounts of *solution III,* which

contains 80% bisphosphonate, were 50% and 80% after 2 and 4 days, respectively. Consequently, the affinity to endobone was increased by increasing the bisphosphonate content on the particles surfaces due to the presence of more binding sites, these results confirms the results reported in the literature [19].

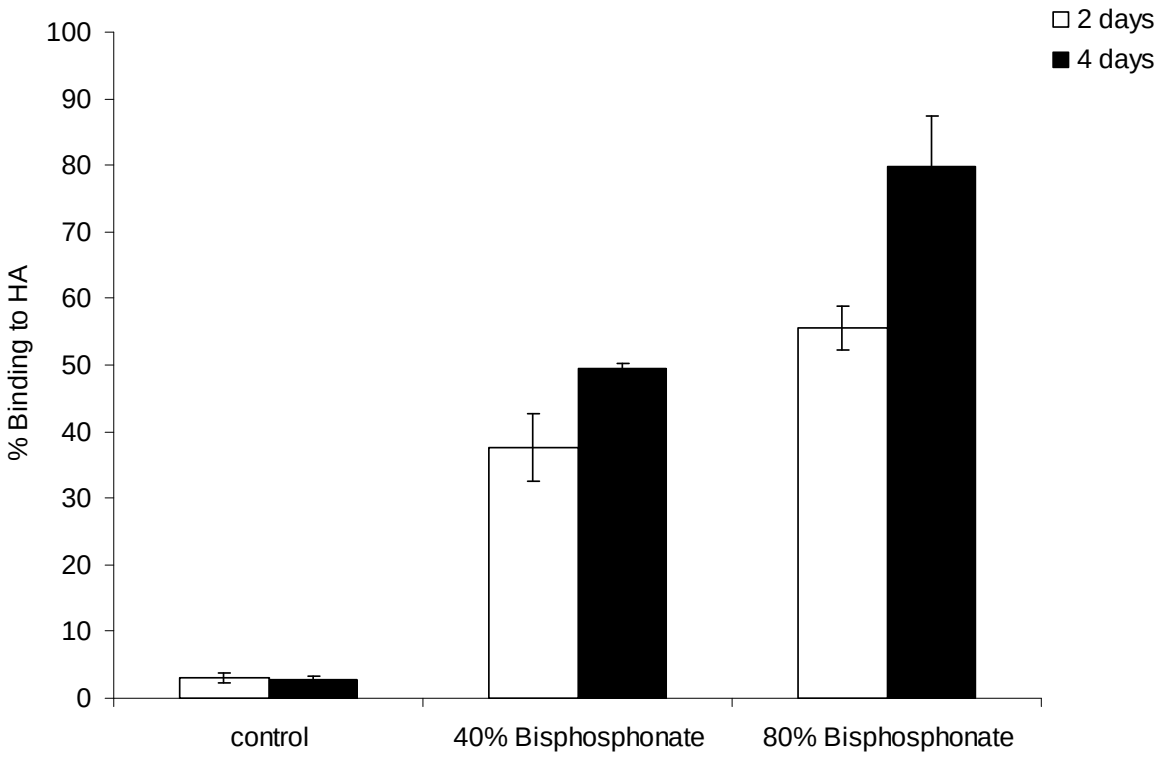

Figure 4: In vitro hydroxyapatite binding affinities of the investigated gold nanoparticle solutions

The effects of BSA, serum and also calcium ions on the binding of gold nanoparticles to hydroxyapatite were also investigated, since the in vivo bone binding is expected to take place in the presence of serum proteins and other cations, such as calcium, which are capable to compete with the bone mineral binding. The obtained results showed that the binding of bisphosphonate-modified gold nanoparticles is not affected by the presence of calcium chloride, BSA and serum as already presented in chapter 5.

3.5. Biodistribution of bisphosphonate-modified gold nanoparticles.

The results of nanoparticles biodistribution at different time points are expressed as percentage of the still present injected dose per gram of the respective tissue (% ID/g) to facilitate the analysis of nanoparticles distribution inside the body. Different tissues were excised at specified time points from the sacrificed animals and the contained radioactivity

was measured. Figure 5 shows the biodistribution of the control gold nanoparticles (*solution I,* without bisphosphonate) in the various tissues at 0.25, 1, 6 and 24 hours after injection. The highest concentration of nanoparticles in the blood was observed at 1 h after injection and the complete distribution in the blood, which were about 20% of ID/g. This concentration decreased to about 10% after 6 h and to about 3% after 24 h. Remarkably, only about 5% ID/g of the injected nanoparticles accumulated in the liver and spleen after 24 h, which consequently means that the injected particles have the ability to avoid the uptake in liver and spleen, which is the usual route for non-shielded nanoparticulate formulations. These results agree well with results observed for other surface PEGylated nanoparticles [5,20-24].

Accumulation of the even not targeted nanoparticles in the bone reached 10% after 24 h. This can however also be attributed to the small weight of the femur. The biodistribution patterns to heart, stomach, small intestine, colon, lung, muscle and brain in addition to liver and spleen did not show substantial accumulation in these organs.

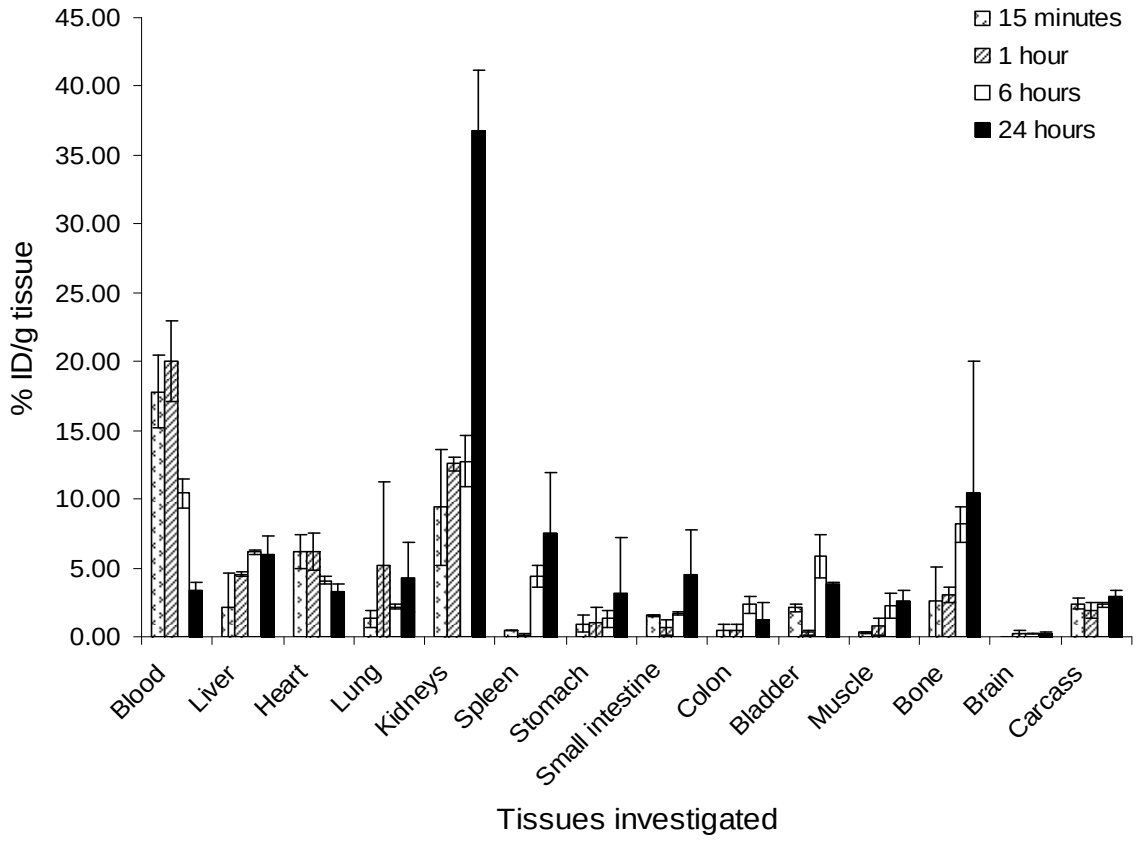

Figure 5: Biodistribution of solution I of gold nanoparticles coated with 0 % bisphosphonate

In contrast, a progressing increase of the radioactivity was observed in the kidneys especially at later time points. The accumulation of the radioactivity in kidneys is

accompanied by a rapid decrease of radioactivity in blood, which indicates the elimination of the ^{111}In-labelled nanoparticles from the systemic circulation and deposition also in the kidneys (Figure 6). This might be explained by an entrapment of the nanoparticles inside the kidneys, because of their relative large size (47 nm) and the hydrophilic coating (due to grafting of PEG to the particles surfaces). The accumulation of radioactivity in the kidneys increases with time, which can be explained by the accumulation of intact nanoparticles and not only the labeled polymers removed from the particles surfaces, because they would be small enough to be excreted via the urine. These results also reflect the high in vivo stability of the thioalkylated PEG-coated gold nanoparticles and support the results from literature [25-27]. The relatively low concentration of nanoparticles in carcass expressed as %ID/g (which refers to the entire body of the animal without the organs and tissues indicated in Figure 5) is mainly attributed to the relative large weight of carcass compared to other tissues and organs. However, if just the injected dose is considered about 50% accumulate in the carcass, which also demonstrates the ability of the particles to extravasate in many tissues.

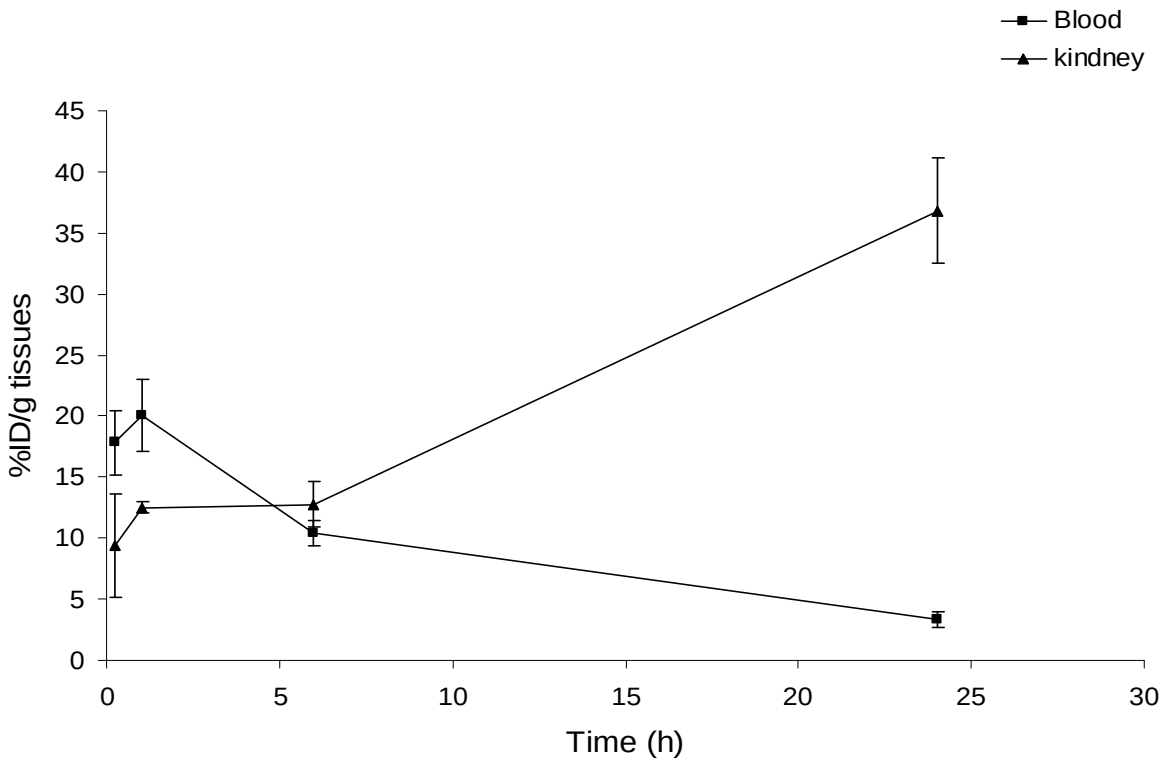

Figure 6: Biodistribution of solution I of gold nanoparticles (control) on the blood and kidney

No large differences were observed for the biodistribution of gold nanoparticles functionalized with 40% bisphosphonate, *solution II* GNPs, (Figure 7). *Solution II* gold nanoparticles showed only a slight increase in the bone accumulation relative to the control,

which eventually could be attributed to the presence of the targeting moiety (bisphosphonate). The insignificant difference of the bone accumulation between the bisphosphonate functionalized and the control GNPs may be due to many different reasons, such as the trapping of many gold nanoparticles in the kidneys, the difficult extravasation of the highly hydrophilic coated gold nanoparticles in the bone, the relative large size of the injected nanoparticles [8,28] or merely the relatively small portion of bone that was used for the investigation in comparison to the remaining bone tissue in the animal (carcass).

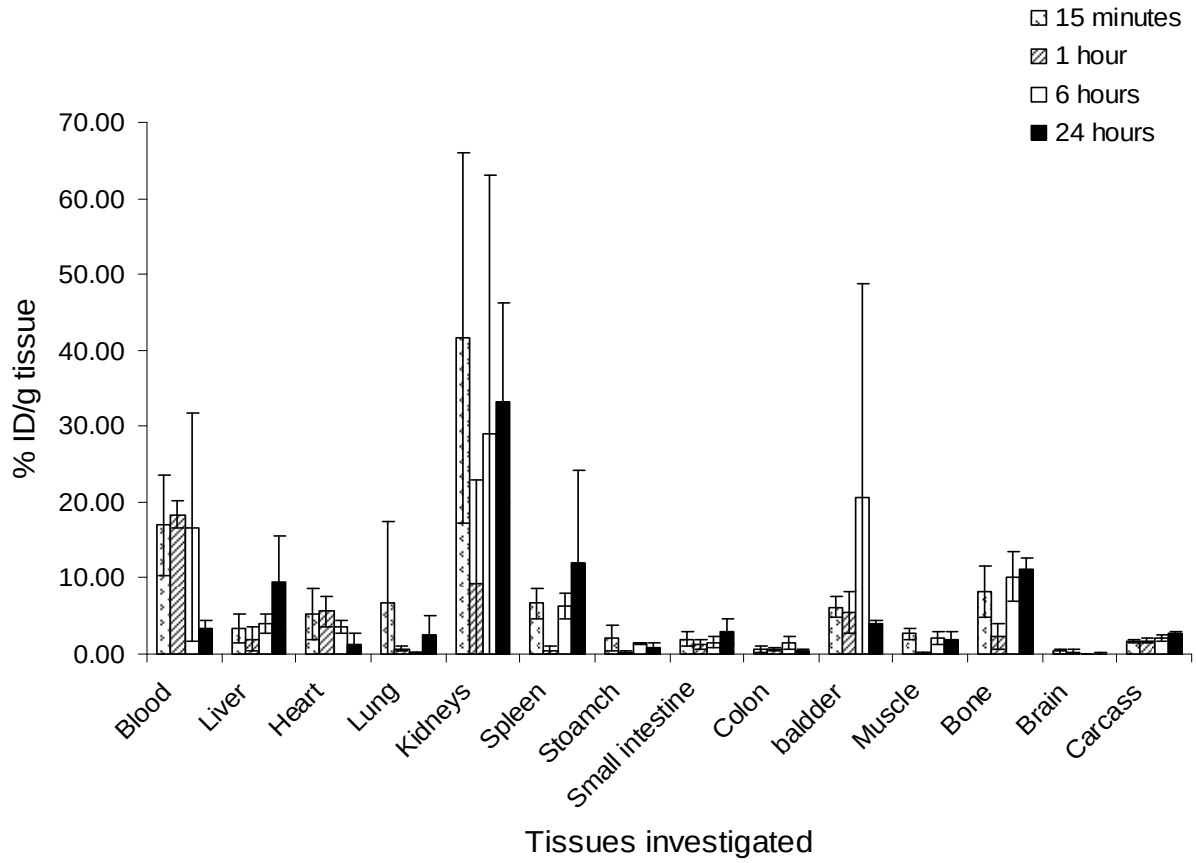

Figure 7: Biodistribution of solution II gold nanoparticles coated with 40% bisphosphonate

The biodistribution of gold nanoparticles functionalized with 80% bisphosphonate (Figure 8) again is quite similar to the biodistribution of *solution II* GNPs (containing 40% of BP, Figure 7) and the control GNPs solution (Figure 5). For an easier comparison, the aimed bone accumulation of the injected colloidal solutions (*solutions I, II* and *III*) is shown in Figure 9. Gold nanoparticles functionalized with the highest BP concentration nevertheless show the highest relative bone accumulation in femur when compared to the other solutions. The bone concentrations of *solution III* after 6 and 24 h, expressed as %ID/g bone, are 17.15 ± 1.79 and 16.41 ± 3.75 respectively compared to 10.14 ± 2.29 and 11.12 ± 1.49 for *solution*

II, and 8.16 ± 1.26 and 10.43 ± 9.64 for *solution I*. These data show that the targeted gold nanoparticles (containing BP) have a tendency to target and accumulate in bone compared to the non-targeted gold nanoparticles. However, the bone concentration of *solution III*, which contains 80% BP on the surface, reached a maximum at 6 h after injection, 17.15 ± 1.79 %ID/g and then decreased again to 16.41 ± 3.75 %ID/g after 24 h and to 12.51 ± 2.6 %ID/g at 48 h, which is not in accordance with the above mentioned properties of bisphosphonates and certainly demands for further investigations.

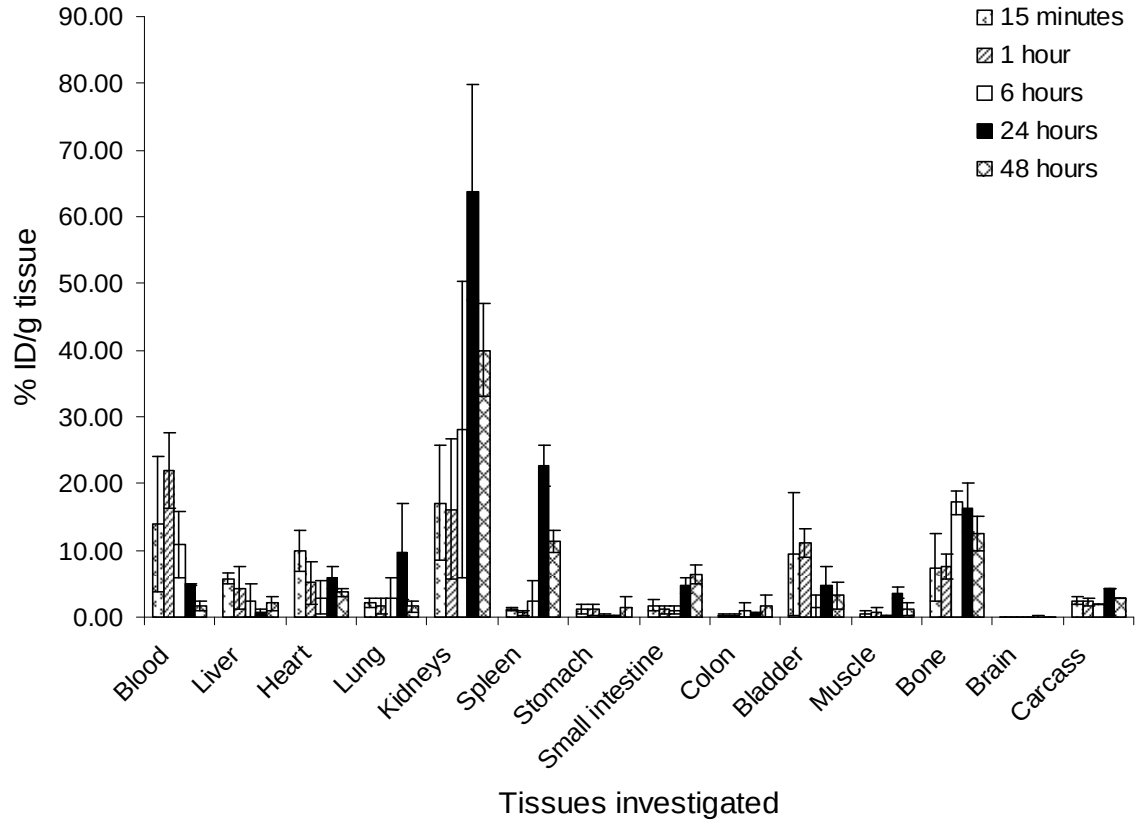

Figure 8: Biodistribution of solution III coated with 80% bisphosphonate.

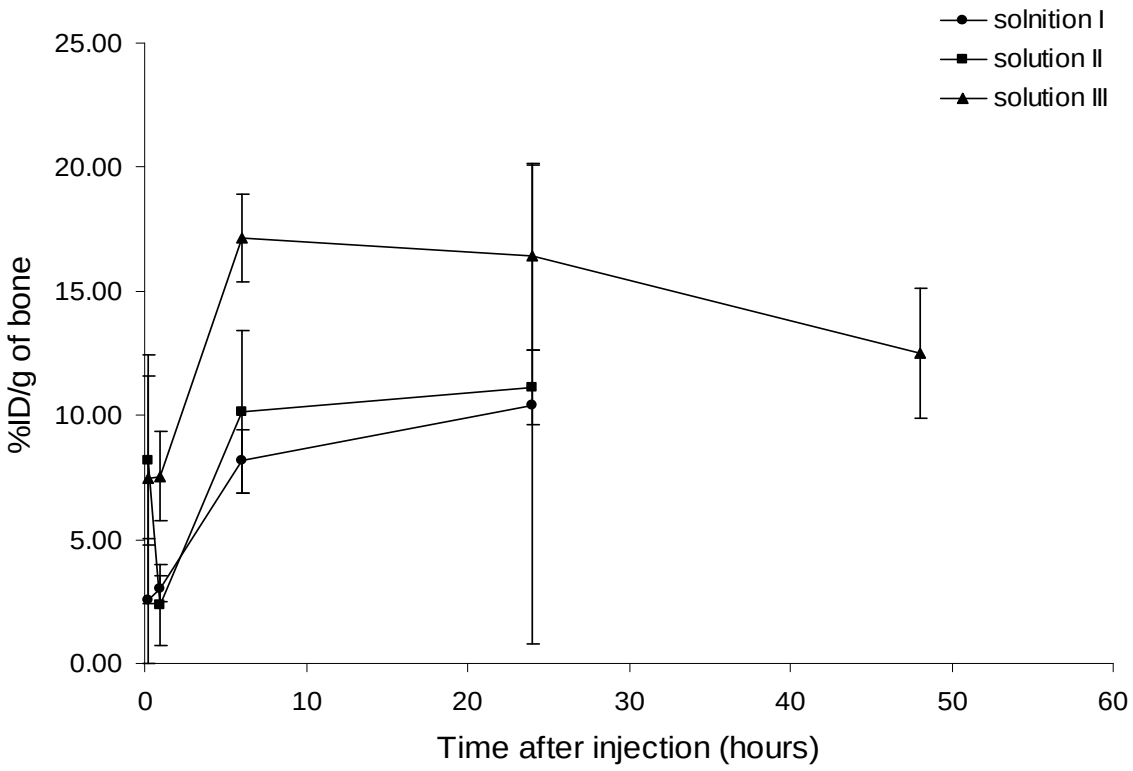

Figure 9: Accumulation of different gold nanoparticles (solutions I, II and III) in bone

3.6. Pharmacokinetic analysis of the tested gold nanoparticles in blood

A non compartmental model was used in order to estimate the pharmacokinetic parameters of the nanoparticle formulations after intravenous injection. Blood concentration-time profiles for the injected nanoparticles are presented in Figure 10 with the calculated parameters summarized in Table 2. For a successful application of the particles as targeted drug delivery system a low elimination rate constant and a long half life in blood is necessary. The determined half life in blood for the three samples are in the following order; *solution III > solution II > solution I*, between 8.96 to 7.25 hours, which are certainly not statistically significant. The relatively long half lives of the investigated gold nanoparticles are due to the surface PEGylation of the nanoparticles, which significantly increases the half lives of nanoparticles as well known form literature [4,5,29,30]. Furthermore, the long circulation half life of nanoparticles helps the particles in vivo to reach their intended target, because the particles need to circulate in blood for a sufficiently long time to have the chance to interact with their specific target cells or tissues [31,32]. In contrast to the here observed behavior, the half life of the non-PEGylated nanoparticles is commonly very short and they rapidly excreted form the blood. Simon et al. [33] studied the circulation half time and body distribution of amine modified polystyrene nanoparticles. They observed that the half lives of the studied

particles are very short and after 30 minutes 60-70% of the 100 nm particles are already accumulated in the liver, which prohibits further reaching of the target organ.

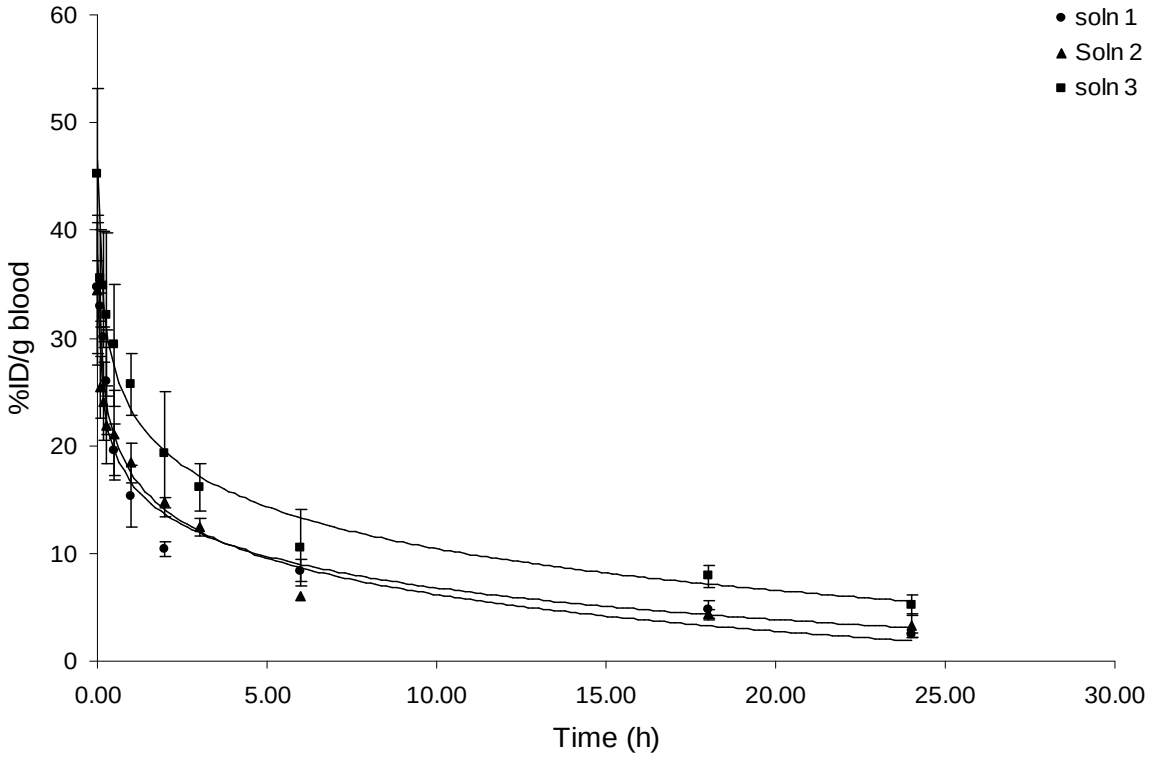

Figure 10: Blood profiles of the gold nanoparticles in blood after intravenous administration

Table 2: Pharmacokinetic parameter of the injected gold nanoparticles

	K_{el} (h^{-1})	$t_{1/2}$ (h)	AUC (ng/g*h)	MRT (h)
Solution 1 (control)	0.0955	7.25	1973.19	8.25
Solution 2 (40% BP)	0.0869	7.97	2040.3	9.45
Solution 3 (80% BP)	0.0773	8.96	3356.56	11.2

5. Conclusions

The presented study revealed that the prepared gold nanoparticles can be successfully stabilized and modified to perform their intended tasks for in vivo experiments. The nanoparticles were synthesized with an appropriately small size and their surfaces were modified with mixtures of polymers, which on the one hand made them inert to high ionic strength or protein solutions, but on the other hand also introduced a high specific affinity to the main bone mineral hydroxyapatite. The conducted in vivo investigations strongly indicated that the functionalized gold nanoparticles showed a minimum uptake by the reticuloendothelial system (liver and spleen) and therefore circulated for very long time in blood. On the other hand the particle also showed a strong tendency to extravasate or distribute to other organs after injection into mice, but the largest accumulation was observed in the kidneys. Also in bone a steady accumulation of the bisphosphonate functionalized nanoparticles was observed in comparison to the control nanoparticles, but further studies have to be conducted here in order to investigate especially the long term fate of the particles in bone.

Acknowledgements

The authors want especially to thank the animalerie house of Angers for the skilful technical support with the animals for the biodistribution study [Service Commun d'Animalerie Hospitalo-Universitaire (S.C.A.H.U.), Pavillon Olivier, Rue Haute de Reculée, 49045 Angers Cedex 01 (France)].

6. References

1. Ganeshchandra Sonavane, Keishiro Tomoda, and Kimiko Makino, "Biodistribution of colloidal gold nanoparticles after intravenous administration: Effect of particle size," Colloids and Surfaces, B: Biointerfaces **66,** 274-280 (2008).

2. Sha Jin and Kaiming Ye, "Nanoparticle-Mediated Drug Delivery and Gene Therapy," Biotechnology Progress **23,** 32-41 (2007).

3. U. Gaur, S. K. Sahoo, T. K. De, P. C. Ghosh, A. Maitra, and P. K. Ghosh, "Biodistribution of fluoresceinated dextran using novel nanoparticles evading reticuloendothelial system," International Journal of Pharmaceutics **202,** 1-10 (2000).

4. Frank Alexis, Eric Pridgen, Linda K. Molnar, and Omid C. Farokhzad, "Factors Affecting the Clearance and Biodistribution of Polymeric Nanoparticles," Molecular Pharmaceutics **5,** 505-515 (2008).

5. Donald E. Owens and Nicholas A. Peppas, "Opsonization, biodistribution, and pharmacokinetics of polymeric nanoparticles," International Journal of Pharmaceutics **307,** 93-102 (2006).

6. Jamie M. Bergen, Horst A. von Recum, Thomas T. Goodman, Archna P. Massey, and Suzie H. Pun, "Gold nanoparticles as a versatile platform for optimizing physicochemical parameters for targeted drug delivery," Macromolecular Bioscience **6,** 506-516 (2006).

7. Marites P. Melancon, Wei Lu, Zhi Yang, Rui Zhang, Zhi Cheng, Andrew M. Elliot, Jason Stafford, Tammy Olson, Jin Z. Zhang, and Chun Li, "In vitro and in vivo targeting of hollow gold nanoshells directed at epidermal growth factor receptor for photothermal ablation therapy," Molecular Cancer Therapeutics **7,** 1730-1739 (2008).

8. Huaizhong Pan, Monika Sima, Pavla Kopeckova, Kuangshi Wu, Songqi Gao, Jihua Liu, Dong Wang, Scott C. Miller, and Jindrich Kopecek, "Biodistribution and Pharmacokinetic Studies of Bone-Targeting N-(2-Hydroxypropyl)methacrylamide Copolymer-Alendronate Conjugates," Molecular Pharmaceutics **5,** 548-558 (2008).

9. Geeti Bansal, Jennifer E. I. Wright, Cezary Kucharski, and Hasan Uludag, "A dendritic tetra(bisphosphonic acid) for improved targeting of proteins to bone," Angewandte Chemie, International Edition **44,** 3710-3714 (2005).

10. Sebastien A. Gittens, Geeti Bansal, Ronald F. Zernicke, and Hasan Uludag, "Designing proteins for bone targeting," Advanced Drug Delivery Reviews **57,** 1011-1036 (2005).

11. V. Hengst, C. Oussoren, T. Kissel, and G. Storm, "Bone targeting potential of bisphosphonate-targeted liposomes. Preparation, characterization and hydroxyapatite binding in vitro," Int J Pharm **331,** 224-227 (2007).

12. Hasan Uludag and Jennifer Yang, "Targeting Systemically Administered Proteins to Bone by Bisphosphonate Conjugation," Biotechnology Progress **18,** 604-611 (2002).

13. X. Wen, Q. P. Wu, Y. Lu, Z. Fan, C. Charnsangavej, S. Wallace, D. Chow, and C. Li, "Poly(ethylene glycol)-conjugated anti-EGF receptor antibody C225 with radiometal chelator attached to the termini of polymer chains," Bioconjug Chem **12,** 545-553 (2001).

14. Xiaoxia Wen, Qing Ping Wu, Shi Ke, Sidney Wallace, Chusilp Charnsangavej, Peng Huang, Dong Liang, Diana Chow, and Chun Li, "Improved Radiolabeling of PEGylated Protein: PEGylated Annexin V for Noninvasive Imaging of Tumor Apoptosis," Cancer Biotherapy & Radiopharmaceuticals **18,** 819-827 (2003).

15. Emiko Nakamura, Kimiko Makino, Teruo Okano, Tatsuhiro Yamamoto, and Masayuki Yokoyama, "A polymeric micelle MRI contrast agent with changeable relaxivity," Journal of Controlled Release **114,** 325-333 (2006).

16. Vanessa Carla Furtado Mosqueira, Philippe Legrand, Jean Louis Morgat, Michel Vert, Evgueni Mysiakine, Ruxandra Gref, Jean Philippe Devissaguet, and Gillian Barratt, "Biodistribution of long-circulating PEG-grafted nanocapsules in mice: effects of PEG chain length and density," Pharmaceutical Research **18,** 1411-1419 (2001).

17. Alf Lamprecht, Jean Louis Saumet, Jerome Roux, and Jean Pierre Benoit, "Lipid nanocarriers as drug delivery system for ibuprofen in pain treatment," International Journal of Pharmaceutics **278,** 407-414 (2004).

18. Priyabrata Mukherjee, Resham Bhattacharya, Nancy Bone, Yean K. Lee, Chitta Ranjan Patra, Shanfeng Wang, Lichun Lu, Charla Secreto, Pataki C. Banerjee, Michael J. Yaszemski, Neil E. Kay, and Debabrata Mukhopadhyay, "Potential therapeutic application of gold nanoparticles in B-chronic lymphocytic leukemia (BCLL): enhancing apoptosis," Journal of Nanobiotechnology **5,** No (2007).

19. Sung Wook Choi and Jung Hyun Kim, "Design of surface-modified poly(d,l-lactide-co-glycolide) nanoparticles for targeted drug delivery to bone," Journal of Controlled Release **122,** 24-30 (2007).

20. Xiaoxiao He, Hailong Nie, Kemin Wang, Weihong Tan, Xu Wu, and Pengfei Zhang, "In Vivo Study of Biodistribution and Urinary Excretion of Surface-Modified Silica Nanoparticles," Analytical Chemistry (Washington, DC, United States) **80,** 9597-9603 (2008).

21. Goldie Kaul and Mansoor Amiji, "Biodistribution and tumor-targeting potential of poly(ethylene glycol)-modified gelatin nanoparticles," Materials Research Society Symposium Proceedings **845,** 229-235 (2005).

22. Sushma Kommareddy and Mansoor Amiji, "Biodistribution and pharmacokinetic analysis of long-circulating thiolated gelatin nanoparticles following systemic administration in breast cancer-bearing mice," Journal of Pharmaceutical Sciences **96,** 397-407 (2006).

23. Takuro Niidome, Masato Yamagata, Yuri Okamoto, Yasuyuki Akiyama, Hironobu Takahashi, Takahito Kawano, Yoshiki Katayama, and Yasuro Niidome, "PEG-modified gold nanorods with a stealth character for in vivo applications," Journal of Controlled Release **114,** 343-347 (2006).

24. Zhuang Liu, Corrine Davis, Weibo Cai, Lina He, Xiaoyuan Chen, and Hongjie Dai, "Circulation and long-term fate of functionalized, biocompatible single-walled carbon nanotubes in mice probed by Raman spectroscopy," Proc Natl Acad Sci U S A **105,** 1410-1415 (2008).

25. Teng Kuang Yeh, Ze Lu, M. Guillaume Wientjes, and Jessie L. S. Au, "Formulating Paclitaxel in Nanoparticles Alters Its Disposition," Pharmaceutical Research **22,** 867-874 (2005).

26. Derek W. Bartlett, Helen Su, Isabel J. Hildebrandt, Wolfgang A. Weber, and Mark E. Davis, "Impact of tumor-specific targeting on the biodistribution and efficacy of siRNA nanoparticles measured by multimodality in vivo imaging," Proceedings of the National Academy of Sciences of the United States of America **104,** 15549-15554 (2007).

27. Hak Soo Choi, Wenhao Liu, Preeti Misra, Eiichi Tanaka, John P. Zimmer, Binil Itty Ipe, Moungi G. Bawendi, and John V. Frangioni, "Renal clearance of quantum dots," Nature Biotechnology **25,** 1165-1170 (2007).

28. Dong Wang, Monika Sima, R. Lee Mosley, Jasmine P. Davda, Nicole Tietze, Scott C. Miller, Peter R. Gwilt, Pavla Kopeckova, and Jindrich Kopecek, "Pharmacokinetic and Biodistribution Studies of a Bone-Targeting Drug Delivery System Based on N-(2-Hydroxypropyl)methacrylamide Copolymers," Molecular Pharmaceutics **3,** 717-725 (2006).

29. J. S. Tan, D. E. Butterfield, C. L. Voycheck, K. D. Caldwell, and J. T. Li, "Surface modification of nanoparticles by PEO/PPO block copolymers to minimize interactions with blood components and prolong blood circulation in rats," Biomaterials **14,** 823-833 (1993).

30. Weibo Cai, Ting Gao, Hao Hong, and Jiangtao Sun, "Application of gold nanoparticles in cancer nanotechnology," Nanotechnology, Science and Applications **1,** 17-31 (2008).

31. Catherine C. Berry and Adam S. G. Curtis, "Functionalisation of magnetic nanoparticles for applications in biomedicine," Journal of Physics D: Applied Physics **36,** R198-R206 (2003).

32. Matti M. van Schooneveld, Esad Vucic, Rolf Koole, Yu Zhou, Joanne Stocks, David P. Cormode, Cheuk Y. Tang, Ronald E. Gordon, Klaas Nicolay, Andries Meijerink, Zahi A. Fayad, and Willem J. M. Mulder, "Improved Biocompatibility and Pharmacokinetics of Silica Nanoparticles by Means of a Lipid Coating: A Multimodality Investigation," Nano Letters **8,** 2517-2525 (2008).

33. Budhi H. Simon, Howard Y. Ando, and and Pardeep Gupta, "Circulation Time and Body Distribution of 14C-Labeled Amino-Modified Polystyrene Nanoparticles in Mice," Journal of Pharmaceutical Sciences **84,** 1249-1253 (1995).

Chapter 7

Summary and Conclusions

1. Summary

In general, the application of custom designed nanoparticles offers many new opportunities to improve existing diagnostic approaches. Some of these systems, furthermore, allow the therapy of hard to treat diseases by novel approaches for a localized delivery with the minimization of undesirable side effects. Consequently, targeted nanoparticles have been applied as label for in vivo imaging, as probes for cellular imaging and also as carriers for therapeutic drug delivery [1]. For the purpose of efficient drug delivery, nanoparticles should be sufficiently stable in vitro and in vivo, highly biocompatible and, most importantly, non-toxic to humans. For the successful application of nanoparticles a suitable surface modification is of utmost importance to acquire particles with the desired properties.

Based on existing knowledge [2], the first aim of this thesis was to synthesize and improve polymers, which can on their one end strongly bind to gold nanoparticle surfaces and at the same time can be modified on the other end with targeting moieties for specific interactions with tissues or cells.

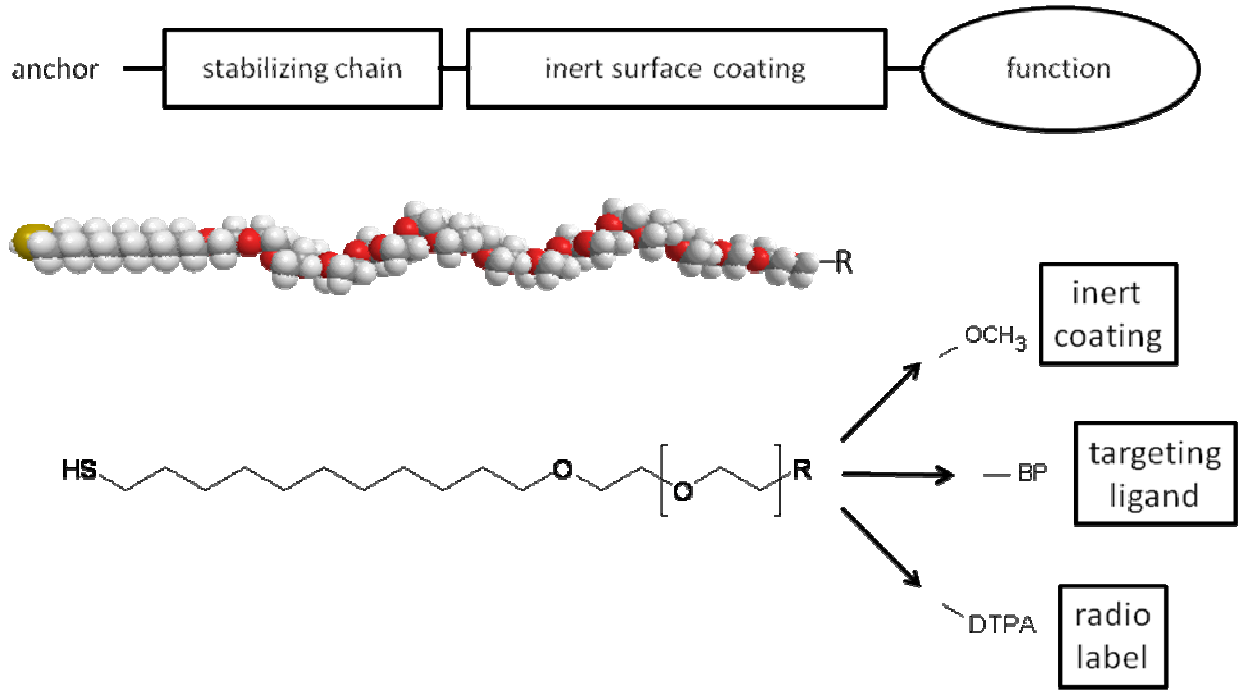

Figure 1: Schematic diagram representing the essential components of the polymer platform used for the modification of the gold particles

The strategy of the polymer development was based on a poly(ethylene glycol) (PEG) backbone, a hydrophilic polymer, which is known to enhance the stability of nanoparticles [3,4], to minimize unspecific proteins adsorption [5], and finally also to increase circulation

half lives of nanoparticles in blood after in vivo administration [6]. For the modification of gold thioalkylated PEG derivatives were synthesized (Figure 1), which anchor to gold surfaces through a stable S-Au bond. In addition to the anchor group, an aliphatic chain was introduced, which is essential to produce a further stabilizing self assembled monolayer on the gold surface due to the hydrophobic attractions between the aliphatic chains [7]. Finally, the PEG chain was terminally derivatized in order to fulfil multiple functions, like an inert surface coating, binding site for radio labels and last but not least the binding site for the targeting ligand.

Synthesis schemes for thioalkylated PEG derivatives were developed and further optimized (**Chapter 2 and 3**) to obtain polymers with a high degree of conversion to ease the later production of the coated particles. Two derivatives were obtained, methoxy poly(ethylene glycol)-undecyl mercaptane (Figure 2a) and amino poly(ethylene glycol)-undecyl mercaptane (Figure 2b). The amine terminated derivative was later further reacted with a custom synthesized bisphosphonate as bone targeting ligand producing a functionalized polymer with a high affinity to the bone mineral hydroxyapatite and also to gold surfaces, which indicated the successful linkage of the thioalkyl chain with PEG and the bisphosphonate [8].

The used bisphosphonate was chosen because of its exceptional high affinity to bone due to two bisphosphonate groups contained in the molecule, and additionally due to the presence of an aromatic ring, which enabled a very sensitive detection of the synthesized polymers. The bisphosphonate was synthesized according to published procedures [9], but it was used at different stages of the reaction, in order to provide compounds, soluble in aqueous and organic medium (Figure 2c, A and B). The finally used polymer was obtained from the reaction of the bisphosphonate ester with the amine terminated polymer and activated using mild hydrolysis of the esters with bromotrimethylsilane (Figure 2d).

Figure 2a: Methoxy poly(ethylene glycol)-undecyl mercaptane

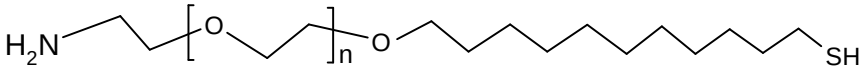

Figure 2b: Amino poly(ethylene glycol)-undecyl mercaptane

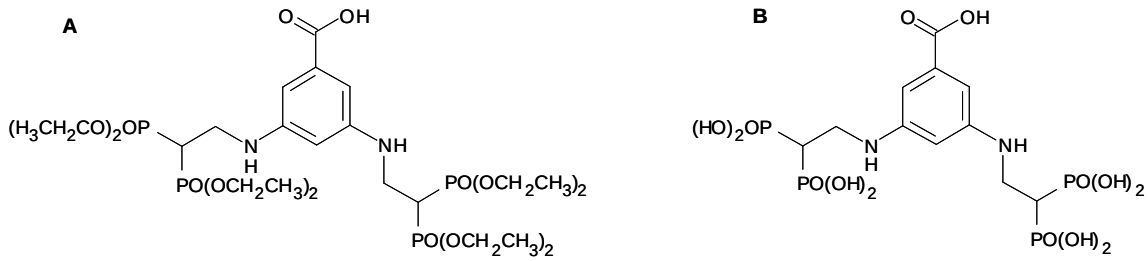

Figure 2c: Bisphosphonates applied for the modification of the polymer:
A) organic soluble derivative and B) water soluble derivative

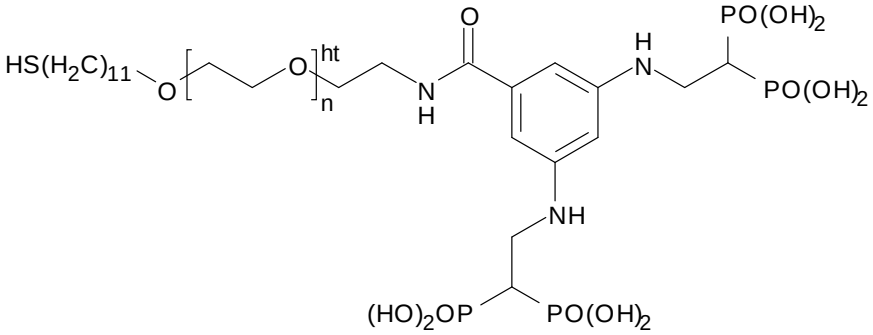

Figure 2d: Bisphosphonate-modified amino poly(ethylene glycol)-undecyl mercaptane

Suitably sized gold nanoparticles dispersed in aqueous medium were prepared by citrate reduction of auric chloride solutions [1]. Different trials were done to obtain nanoparticles, which can be administered intravenously (**Chapter 4**). The prepared nanoparticles were subsequently coated with amino poly(ethylene glycol)-undecyl mercaptane and methoxy poly(ethylene glycol)-undecyl mercaptane and the impact of the polymer coating on important properties of gold nanoparticles, like size and stability in the presence of electrolyte and proteins, was investigated. There was an indirect relation between the amount of added reducing agent (sodium citrate) and the size of the obtained gold nanoparticles, which allowed the adjustment of the particle size. The performed polymer surface modification increased the particle size by a few nanometers and additionally resulted in the formation of nanoparticles, which did not aggregate either by high electrolyte concentrations or proteins in the aqueous medium. In contrast it was demonstrated that citrate-

stabilized GNPs were generally greatly influenced by the addition of sodium chloride, BSA or serum.

The synthesized thioalkylated and targeted polymers (bisphosphonate-modified thioalkylated PEG) were, furthermore, applied to prepare bisphosphonate-functionalized gold nanoparticles (**Chapter 5**). For this preparation citrate stabilized nanoparticles (about 40 nm in diameter) were incubated with different ratios of targeted and inert polymers to allow an exchange of the citrate anions (Figure 3). The coated GNPs showed a slight size increase and greatly enhanced stability in different solutions. The zeta potential of the particles increased by addition of uncharged polymers, but it was similar for the bisphosphonate-coated and citrate-stabilized gold nanoparticles due to the added excess of anionic groups. The hydroxyapatite binding affinity of the particles was studied as a function of surface bisphosphonate amount and could be varied in a wide range with a steady increase with increasing amount of bisphosphonate. Additionally, binding experiments were performed in presence of calcium chloride, BSA and bovine serum to elucidate the effect on the hydroxyapatite affinity, which was not affected by adding any of the added compounds.

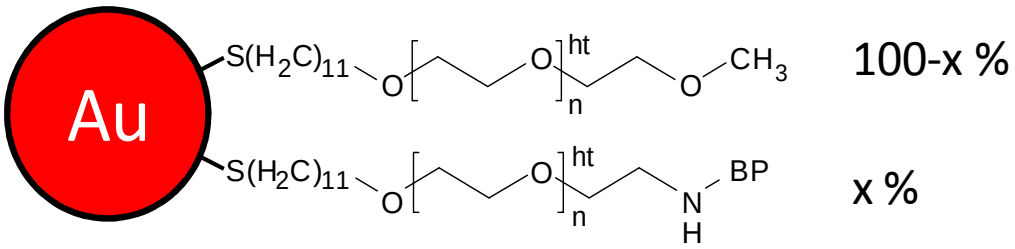

Figure 3: Structure of gold nanoparticles used functionalized with a mixture of mPEG-AlkSH and BP-PEG-AlkSH

To investigate the fate of the nanoparticles in vivo, they were firstly labeled with radioactive indium in order to allow their tracking in vivo. To elucidate the effect of the targeting ligand concentration, nanoparticles containing a low and a high amount (40% or 80%) of bisphosphonate in comparison to control nanoparticles (0% BP) were intravenously administered in mice. The biodistribution to the different organs of the mice and the pharmacokinetic profiles of the injected nanoparticles were determined and compared between the different formulations of the prepared particles (**Chapter 6**). The biodistribution of nanoparticles demonstrated a promising behavior of the targeted and untargeted particles. The nanoparticles exhibited a very long blood circulation time with only minimal uptake by spleen and liver. An enhanced accumulation of the particles was observed in the kidneys,

which probably are suited to trap a fraction of the injected particles in the glomerulus membrane, which certainly necessitates further investigations. On the other hand bone accumulation of the bisphosphonate-functionalized nanoparticles was not largely different from the control nanoparticles, which could be attributed to the very small portion of bone (femur), which was chosen for the distribution study, or to a limited extend of extravasation within the bone. However, the long circulation half lives of the particles makes them a suitable platform for further investigations also of other targeting approaches, especially since the synthesized polymers allow a flexible modification with other suitable ligands, like proteins or eventually antibodies.

2. Conclusions

Heterobifunctional polymers, which can be used for the modification, functionalization and stabilization of gold nanoparticles, were successfully synthesized applying a new synthetic strategy. Highly stable gold nanoparticle dispersions were obtained after coating citrate-stabilized GNPs with the different synthesized polymers, which stabilized the particles by a steric stabilization, which was not affected by the addition of sodium chloride or proteins. The functionalization with bisphosphonates, furthermore, produced nanoparticles with a high affinity to the bone mineral hydroxyapatite, which was not affected by addition of calcium chloride or proteins. Upon intravenous application of the nanoparticles in mice, they circulated for a long time in the blood and were well distributed to many organs and most importantly did not accumulate in liver and spleen, which are common organs of nanoparticle deposition.

The here presented nanoparticle system provides a suitable platform for the investigation of new drug targeting principles. The investigated particles can be prepared using a stable noble metal core for easy detection with electron microscopy, which was coated with an inert polymer layer that, furthermore, provided chemical binding sites for many different ligands using standard carbodiimide chemistry. Due to their small size the particles will extravasate in many different organs, which is essential to make them suitable for the investigation of other targeting principles.

3. References

1. Francesca Porta, Giovanna Speranza, Zeljka Krpetic, Vladimiro Dal Santo, Pierangelo Francescato, and Giorgio Scari, "Gold nanoparticles capped by peptides," Materials Science & Engineering, B: Solid-State Materials for Advanced Technology **140,** 187-194 (2007).

2. Robert Knerr, Sigrid Drotleff, Claudia Steinem, and A. Goepferich, "Self-assembling PEG Derivatives for Protein-repellant Biomimetic Model Surfaces on Gold," Biomaterialien **7,** 12-20 (2006).

3. Daisuke Miyamoto, Motoi Oishi, Keiji Kojima, Keitaro Yoshimoto, and Yukio Nagasaki, "Completely Dispersible PEGylated Gold Nanoparticles under Physiological Conditions: Modification of Gold Nanoparticles with Precisely Controlled PEG-b-polyamine," Langmuir **24,** 5010-5017 (2008).

4. Soo Hyeon Lee, Ki Hyun Bae, Sun Hwa Kim, Kyu Ri Lee, and Tae Gwan Park, "Amine-functionalized gold nanoparticles as non-cytotoxic and efficient intracellular siRNA delivery carriers," International Journal of Pharmaceutics **364,** 94-101 (2008).

5. Jacques Bluemmel, Nadine Perschmann, Daniel Aydin, Jovana Drinjakovic, Thomas Surrey, Monica Lopez-Garcia, Horst Kessler, and Joachim P. Spatz, "Protein repellent properties of covalently attached PEG coatings on nanostructured SiO2-based interfaces," Biomaterials **28,** 4739-4747 (2007).

6. Y. P. Li, Y. Y. Pei, X. Y. Zhang, Z. H. Gu, Z. H. Zhou, W. F. Yuan, J. J. Zhou, J. H. Zhu, and X. J. Gao, "PEGylated PLGA nanoparticles as protein carriers: synthesis, preparation and biodistribution in rats," Journal of Controlled Release **71,** 203-211 (2001).

7. Abraham Ulman, "Formation and Structure of Self-Assembled Monolayers," Chemical Reviews (Washington, D. C.) **96,** 1533-1554 (1996).

8. Sufeng Zhang, Jennifer E. I. Wright, Natali Ozber, and Hasan Uludag, "The interaction of cationic polymers and their bisphosphonate derivatives with hydroxyapatite," Macromolecular Bioscience **7,** 656-670 (2007).

9. Geeti Bansal, Sebastien A. Gittens, and Hasan Uludag, "A di(bisphosphonic acid) for protein coupling and targeting to bone," Journal of Pharmaceutical Sciences **93,** 2788-2799 (2004).

Appendix

1. Abbreviations

^{1}H-NMR	proton nuclear magnetic resonance spectroscopy
%ID	% of injected dose
%ID/g	% of injected dose per gram tissue
λ_{max}	Peak of maximum absorption
ANOVA	analysis of variance
Abs	absorbance
AIBN	α,α´ azoisobutyronitrile
AUC	area under the curve
BBB	blood brain barrier
BOC	di-t-butyl dicarbonate
BP	bisphosphonate
BP-PEG-AlkSH	Bisphosphonate modified poly(ethylene glycol)-undecyl mercaptane
BSA	Bovine serum albumin
$CDCl_3$	deuterated chloroform
CNS	central nervous system
Da	dalton
DCC	N,N\-dicyclohexylcardodiimide
DIC-BP	diclofenac bisphosphonate conjugate
DTPA	diethylenetriaminepentaacetic acid
DTPA-PEG-AlkSH	Diethylenetriaminepentaacetic acid conjugated amino poly(ethylene glycol)-undecyl mercaptane
EDC	1-Ethyl-3-[3-dimethylaminopropyl]carbodiimide hydrochloride
ELSD	evaporative light scattering detector
EO	ethylene oxide gas
EPR	enhanced permeability and retention
ESI-M	electro spray ionization mass spectroscopy
FDA	food and drug administration
GNPs	gold nanoparticles
HA	hydroxyapatite
HCl	hydrochloric acid
HNO_3	nitric acid
HPLC	high pressure liquid chromatography
ICP-OES	inductively coupled plasma-optical emission spectroscopy

IDDM	insulin-dependent diabetes mellitus
IL-1	interleukine-1
IL-6	interleukine-6
K_{el}	elimination rate constant
KOH	potassium hydroxide
L-Asp	L-aspartic acid
L-Glu	L-glutamic acid
MALDI-ToF MS	matrix assisted laser desorption/ionization mass spectrometry
MeOH	methanol
M_p	peak molecular weight
mPEG	poly(ethylene glycol) monomethyl ether
mPEG-AlkSH	methoxy poly(ethylene glycol)-undecyl mercaptane
MRI	magnetic resonance imaging
MRT	mean residence time
MRSA	multiple resistances *staphylococcus aureus*
MS	mass spectroscopy
Mw	molecular weight
MWCO	molecular weight cut-off
NaBr	sodium bromide
NaH	sodium hydride
NaOH	sodium hydroxide
NH_2-PEG-AlkSH	amino poly(ethylene glycol)-undecyl mercaptane
NH_2-PEG-OH	poly(ethylene glycol) monoamine
NHS	N-hydroxysuccinimide
NMR	nuclear magnetic resonance
NPs	nanoparticles
ODDS	osteotropic drug delivery system
PCS	photon correlation spectroscopy
PEG	poly(ethylene glycol)
PEG-AlkSH	poly(ethylene glycol) alkanethiol
PLGA	Poly(lactic-co-glycolic acid)
PPi	inorganic pyrophosphate
PPO	poly(propylene oxide)
PTH	parathyroid hormone

PTT	photothermal therapy
QDs	quantum dots
RES	reticuloendothelial system
RGD	Peptide sequence ARG-GLY-ASP
RP	reversed phase
RP-HPLC	reversed phase high pressure liquid chromatography
RT	room temperature
SAMs	self assembled monolayers
SPIONs	superparamagntic iron oxide nanoparticles
SPR	surface plasmon resonance
$t_{1/2}$	elimination half life
TAA	thioacetic acid
TEA	triethylamine
TEM	transmittance electron microscopy
TFAA	trifluoroacetic acid anhydride
THF	tetrahydrofuran
TMS	tetramethylsilane
TNF	tumor necrosis factor
TsOH	p-toluenesulfonic
UV-Vis	ultraviolet and visible light

2. Curriculum vitae

Name	Gamal Mohamed Soltan Zayed
Date of birth	10.11.1971
Place of birth	Bany-Ady, Assiut, Egypt
Nationality	Egyptian
Martial status	Married

Education and Professional Training:

07.1990	School graduation certificate (Abitur)
09.1990-6.1995	Pharmaceutical course at the Faculty of Pharmacy, Assiut University, Egypt
07.1995-12.1995	Practical education at Al-Aml Pharmacy, Assiut, Egypt
01.1996-02.1997	Pharmacist in Medical service, Egyptian army, Assiut Military Hospital, Assiut, Egypt
03.1997-09.2001	Administrator of Pharmaceutical Technology in the Faculty of Pharmacy, Al-Azhar University Assiut, Egypt
03.1997-09.2001	Master program in Pharmaceutical Sciences, Department of Pharmaceutical Technology, Assiut University, Assiut, Egypt
09.2001	Master Degree of Pharmaceutical Technology, Assiut University, Assiut, Egypt.
10.2001-11.2004	Assistant Lecturer of Pharmaceutical Technology, Al-Azhar University Assiut, Egypt
12.2004-today	PhD program of Pharmaceutical Technology at the Department of Pharmaceutical Technology, Regensburg University, Regensburg, Germany

3. List of Publications

A-Publications:

Gamal Zayed, Achim Göpferich, Jörg Teßmar

"***Synthesis of Bifunctional Polyethylene Glycol Derivatives for Simultaneous Gold Surface Coating and Binding of Hydroxyapatite***"

to be submitted

Gamal Zayed, Achim Göpferich, Jörg Teßmar

*"**Polymer Protected Gold Nanoparticles for Bone Targeting via Hydroxyapatite Binding**"*

to be submitted

B- Conferences Abstracts:

11.10-13.10.2007 DPhG Jahrestagung, Erlangen: *Zayed G., Tessmar J. and Goepferich A.* " **Preparation of Surface Functionalized Gold Nanoparticles**" (*Poster*)

08.10-11.10. 2008 DPhG Jahrestagung, Bonn: *Zayed G., Teßmar J. and Göpferich A.* "**Bisphosphonate-Functionalized Gold Nanoparticles for the Investigation of Bone Targeting**" (*Poster*)

03.10-05.10-2008 Ehrlich 11 2nd World Conference on Magic Bullets, Nürnberg, Germany (2008): *Teßmar J., Zayed G., Hindre F., Benoit J.P., and Göpferich A.* "**Gold Nanoparticles as Model System for the Targeting of Colloids"** (*Poster*)

4. Acknowledgements

The language with all its abundant, plentiful words is helpless to provide me with right words that may explain feelings to all those, who have encouraged and helped me to finish this work.

I wish to express my deepest gratitude to my supervisor and mentor **Professor Dr. Achim Göpferich,** for his keen supervision, continuous support and encouragement. He gave me the chance to join his research team and I am in deep dept of gratitude for his availability and forbearing guidance. I also wish to thank him for spreading friendly and caring atmosphere to the Lab and thus, making it a pleasant place to work at. I appreciate his readiness to support my scholarship and to prepare everything with many mails and correspondence to Egypt.

I think this work was not completed without the great efforts of **Dr. Jörg Teßmar**. I am profoundly grateful towards him for his continuous guidance, encouragements, constructive criticism, valuable comments and discussions. I appreciate the great support made by him during the whole practical work and during the preparation of all reports for the publications and this thesis.

I am very thankful to **Dr. Torsten Blunk** for his permanent interest in my work, valuable discussions and comments during the meetings

I am very grateful to **Dr. Miriam Breunig** for her productive discussions during meetings

I express my deep gratitude to all my former and present colleagues in the Department of Pharmaceutical Technology, they created an atmosphere of companionship and unity making the time spent in Germany unforgettable for me.

Many thanks, especially, go to;

- **Christian Becker** for support he gave to me specially in the beginning of practical work.
- **Angelika Berié** for carrying out the MALDI-ToF analysis of the polymers
- **Ferdinand Brandl** for his continuous and excellent bits&bytes support
- **Dr. Sigrid Grundsteiner** for her help in the synthesis of PEG amine
- **Axel Ehmer** for the help in printing poster for conference presentations
- **Anne Heller** for the preparation of the fixation solution for animal tissues and organs
- **Mathias Henke** for his assistance to solve internet troubles and installation of new programs
- **Wofgang Hild** for the help in the UV-Vis scanning of gold nanoparticle solution
- **Dr. Robert Knerr** for the help in the synthesis of the thioalkylated poly(ethylene glycol)
- **Cornelia Rose** for the analysis of gold nanoparticles by ICP-OES

- **Stefan Rothschenk** for the help in HPLC analysis of the polymers
- **Anna Hezinger** for the imaging of the gold nanoparticles by TEM

In addition I would like to thank all the technical assistants in the department who are **Angelika Berié, Andrea Blaimer**, **Stefan Kolb, Renate Liebl**, and **Edith Schindler** for the support they give to graduate students, starting from all the routine work and assistance during the practical courses through to repair and construction of technical equipments.

My acknowledgement extended also to **Claire Vanpouille** and **Dr. François Hindré**, Inserm U646, Angers, Université d'Angers, France, for the great effort they gave to carry out the in vivo investigations of gold nanoparticles.

Furthermore, I am very grateful to **Dr. Burgermeister** for his support in analyzing the NMR samples and to **Josef kiemaier** for the measurements of ESI-MS samples.

Moreover, I am very thankful to **Lydia Frommer** and **Liane Oettle**, the secretaries of the department. They helped me at all times form the first day for me in Germany, especially in the preparation of the paper work of the thesis.

I would like to say thank you to everybody in the Department of Pharmaceutical Technology for the kind hospitality during my staying in Regensburg.

A lot of thanks to the **Egyptian Government** and Egyptian **Ministry of Higher Education** for financing of my scholarship to study my PhD in Germany. My thanks also go to **Prof**. **Dr. Galal El-Gemeie** and all co-workers in the **Egyptian Cultural Council** in Berlin for their continuous support and help during the time of my scholarship in Germany.

I am very much obliged to my **Family** for their great guidance and support throughout my life and their assistance during my extensive education.

I would like to sincerely thank my wife **Mona** for her patience and support to organize the family, overcome the problems of our children and to plan our everyday life.